THE UNIVERSITY *of* EDINBURGH

Simulation, Testing and Validation of Digital Displacement Hydraulic Power Take-Off for Wave Energy Converters

Sarah Acheson

Engineering Doctorate
Industrial Doctoral Centre for Offshore Renewable Energy
The University of Edinburgh
July 2020

Abstract

Whilst the available global wave power resource is significant at over 2 TW, there has been very little exploitation of it to date for the generation of electricity. This is due in part to the challenge of converting energy from a low speed, high force, variable source to synchronous, grid-quality electricity. The power take-off (PTO) is the subsystem of the wave energy converter (WEC) which carries out this conversion from mechanical to electrical energy.

There are many competing requirements for the design of PTOs, but amongst them are efficiency, load-handling capability, controllability and scalability. The very high ratio of peak-to-mean powers involved means that the system must be able to respond efficiently across a broad load range. Hydraulic systems are a good choice for PTO design as they have very high power densities and are naturally suited to high-force applications. The Quantor is a novel hydraulic WEC PTO concept which combines the quantised PTO of the 'Pelamis' WEC with Digital Displacement (DD) hydraulic pump-motors developed by Artemis Intelligent Power Ltd (AIP). The Quantor should be an efficient PTO that is fully controllable in all four quadrants and is offers power conversion improvements to a broad range of WEC designs.

This project aims to demonstrate the technical feasibility and quantify the performance of the Quantor, using a WEC emulator to test it in representative conditions. First, modelling is carried out of the WEC emulator for design purposes, followed by detailed physical modelling of the envisaged Quantor PTO system. This means the design of the hydraulic circuit can be refined, the control system can be developed and initial efficiency estimates obtained.

After verifying the Quantor in simulation, the WEC hardware-in-the-loop (HIL) emulator and laboratory-scale Quantor system are constructed and commissioned. The WEC emulator system is shown to be a successful test facility for the Quantor PTO. Extensive testing is carried out in both regular and irregular wave conditions and a range of control modes to quantify the performance of the Quantor PTO. The measured input shaft to

generator shaft efficiency exceeds 70% in many cases above a minimum absorbed power threshold. Using the data from testing, efficiency results and a detailed loss breakdown for the Quantor in different operating conditions are produced. The physical model is then validated from this data, in terms of its efficiency and losses. The validated physical model replicates the applied PTO torque and overall efficiency of the Quantor within 5% of the experimental results across the tested power range (approximately 2 to 40 kW of input mechanical power).

After this, a simplified model is produced which replicates the tested PTO torque, efficiency and losses, but can be used to estimate the Quantor performance in various full-scale WEC architectures. This means that reliable PTO performance predictions based on experimental data can be produced for systems other than the laboratory-scale Quantor.

The existence of this Quantor PTO with; the ability to efficiently operate in all four quadrants as demanded by a controller; the availability of a detailed loss breakdown; and the capability to model future system architectures, may provide future opportunities for wave energy developers to design and install commercially successful WECs.

Lay Summary

Due to the problems caused by climate change, we must find alternative sources of energy to fossil fuels. This means we must generate renewable electricity, which will become even more essential as we move towards having more electric transport and heating. Having a broad range of types of renewable electricity (such as solar, wind, geothermal, tidal) means that the electricity supply is more immune to variations in the weather, and that communities in different geographical areas have options for renewable electricity available.

Research has been carried out into wave energy since the 1970s, and many different WECs have been designed. Some prototypes have even been installed in the ocean and successfully generated electricity, such as Pelamis. However, none have reached commercial success so wave energy has not yet become a widely available renewable energy source. This is largely due to the relatively high cost of generating electricity from wave energy. There are several reasons for this, but a major factor is the very high variability in the power transmitted by ocean waves. A WEC must be able to survive very high forces from storm waves, but also generate electricity efficiently even on relatively calm days. The PTO is the part of the WEC which converts mechanical motion caused by the waves into electricity, and must be as efficient as possible as this helps to reduce the cost of the electricity generated. PTOs come in many different forms, such as hydraulic (pressurised oil), electric or pneumatic (pressurised air). This extreme power variability means that the PTO is difficult to design. Usually machinery (e.g. a car engine) is designed for a much smaller range of forces or powers, and has an optimum operating point where it is most efficient, within the chosen power or force range (e.g. in a car 2000 rev per min is often a fuel-efficient engine speed, so the driver changes gear to stay close to this point). However in a wave energy PTO the efficiency must be very high across a huge range of forces (equivalent to a car engine being just as efficient if the car was suddenly 15 times heavier).

A PTO extracts power from the WEC by applying a force to resist the WEC's mechanical

motion, similarly to how a wind turbine extracts power from the wind by slowing the flow of air. The Pelamis PTO was successful because it produced this force using hydraulic cylinders (rams) divided into many chambers. This meant that in large waves with high forces more chambers were used and in small waves fewer chambers were used, but the design meant that the efficiency didn't change too much for different numbers of chambers. This meant that the Pelamis was efficient in both small and large waves. The problem with Pelamis was that every time a chamber was switched on or off, there was a sudden step change in the force applied. This makes it very difficult to design a control strategy which can help the WEC extract more power from the waves, as most control strategies rely on changes in force being smooth.

AIP is a company which develops specialist hydraulic pumps and motors, which are much more efficient and controllable than conventional designs. This is called DD technology. The Quantor PTO is a new type of PTO which combines a DD machine with the technology from the Pelamis. This should mean that the efficiency and ability to handle variable waves are preserved from the Pelamis PTO, but that the DD machine can smooth out the step changes in the forces, so that more control strategies can be used.

The aim of this thesis was to prove that the Quantor works in practice and to measure its performance experimentally. We also wanted to understand in detail the performance of every component, so we can make projections about how a Quantor system in a WEC (which would be larger than what we could build in the laboratory) would perform.

To do this, we carried out extensive mathematical modelling of the Quantor design to understand its behaviour and how to control it. We then built a small but fully-featured Quantor system in the laboratory and tested it using a WEC emulator, which behaved as a WEC would in the sea. After extensive testing, we proved that the Quantor is over 70% efficient in a broad range of conditions, and that it did indeed produce smooth PTO forces. We used the test data to carry out detailed analysis of all the components and the mechanisms by which energy is lost in the system. We then adjusted the mathematical models to match the test data within 5%, so that we have models which actually show the system's real behaviour. We also produced a new model to try and predict how the Quantor might perform if it was a larger system in a WEC in the sea.

Acknowledgements

My deepest thanks must first go to Artemis Intelligent Power Ltd, especially the simulations team, for giving me the opportunity to be part of this tremendous project and patiently teaching me how to be a real engineer. Particular thanks are owed to Daniil Dumnov, Jill MacPherson and Jamie Taylor, who, as well as being delightful to work with, solved myriad problems along the way. Thanks to Win Rampen for his help in finding examiners. Ross Henderson, as well as having many of the ideas which lead to the existence of Quantor, taught me a huge amount from his profound grasp of the Quantor's technical detail.

The support of my supervisors, Mohammad Abusara, Gerasimos Theotokatos and particularly Jonathan Shek, was of great benefit. Jonathan deserves special thanks for wading through my entire thesis and for helping to clarify what to actually write about. David Ingram's advice at several critically challenging points of the last four years was of enormous help.

Thanks to the former employees of Albatern, for introducing me to the world of hydraulics. Many thanks also to my fellow IDCOREans for teaching me Matlab, helping deliver hundreds of presentations and being (mostly) cheerfully in the same boat (especially Calum Kenny).

I would like to profoundly thank Dinner Club for their encouragement, teasing, providing me with interesting things to think about other than Quantor, and of course, for feeding me. Laura Glover deserves special recognition as a goldmine of common sense and the chef of almost all my dinners in the last few months.

Many thanks to my friends at Life Church for their presence, support and prayers through the hurdles of the last three years. Particular thanks to Helen Cope for doing all the hard work of printing, binding and submission on my behalf.

Thank you to Esteban Munch Jones, for remaining level-headed throughout.

Thanks to Chris and Fran, and my parents, for helping me catch my breath, and for giving me the determination to carry on and finish the job.

Here I raise my Ebenezer,
Hither by thy help I've come.

Contents

List of Figures

List of Tables

List of Abbreviations

AIP Artemis Intelligent Power Ltd.

AMC2 Artemis Modular Controller.

AWS Archimedes Wave Swing.

BDC bottom dead centre.

CAN Controller Area Network.

DD Digital Displacement.

DDC Discrete Displacement Cylinder.

DDP Digital Displacement pump.

DDPM Digital Displacement pump motor.

EMA electromechanical actuator.

EMEC European Marine Energy Centre.

EWTEC European Wave and Tidal Energy Conference.

Fd fractional displacement.

FS Full scale.

HIE Highlands and Islands Enterprise.

HIL hardware-in-the-loop.

HPV high pressure valve.

LP low pressure.

LPV low pressure valve.

MAV Motoring Annular Valve.

MIMO multiple-input-multiple-output.

OWC oscillating water column.

P proportional.

PI proportional integral.

PRRV proportional pressure reducer reliever valve.

PTO power take-off.

PV pressure-volume.

PWP Pelamis Wave Power.

SOTA state-of-the-art.

TDC top dead centre.

UoE University of Edinburgh.

WEC wave energy converter.

WES Wave Energy Scotland.

WR1 Wind Rig 1.

Nomenclature

$\ddot{\eta}$	Heave excursion acceleration of WEC
Δp	Differential hydraulic pressure
$\omega_{\dot{WEC}}$	Angular acceleration of WEC
$\dot{\theta}_m$	Angular speed of PTO motors
$\dot{\theta}_{EM}$	Angular velocity of electric motor on test rig
$\dot{\theta}_{rig}$	Rig PTO shaft speed
$\dot{h}$	Velocity of hydraulic cylinders used to calculate geometric flow
$\dot{p}$	Rate of change of oil pressure
$\dot{x}_{WEC}$	Linear velocity of WEC in heave
η	Heave excursion: the difference in heave position between the water surface and the WEC
η_p	Pumping efficiency
$\eta_{AccTrans}$	Efficiency of transient flow path between HP accumulator and chamber
η_{EM}	Efficiency of electric motor
γ	Factor applied in JONSWAP spectral distribution
ω	Shaft angular velocity
ω	Shaft rotational speed
ω_f	Wave angular frequency (in the frequency domain)
ω_{WEC}	Angular velocity of WEC
ρ	Density of water
τ	Shaft torque
τ_{ideal}	Ideal torque from hydraulic machine

τ_{PTO} Applied PTO torque

τ_{PTO} PTO torque

θ_{rig} Measured angular position of rig PTO shaft

θ_{WEC} Angular position of an absorber

A Area of hydraulic actuators used to calculate geometric flow

A_w Waterplane area of WEC

B Oil bulk modulus

c_{PTO} PTO damping coefficient

c_{PTO} PTO damping coefficient

D Displacement of hydraulic machine

F_d Fractional displacement of DD machine

F_e Wave excitation force

F_i Inertia force on WEC

F_r Wave radiation force

F_s Net restoring stiffness force on a WEC

F_{PTO} PTO force

G Unspecified gear ratio

g Gravitational acceleration

G_d Test rig drive gear ratio of 17.4

G_s Gear scaling

G_{PTO} PTO splitter gear ratio on test rig of 40:26

G_{WEC} Gear ratio in WEC

H Wave height of regular waves

h Hydraulic cylinder stroke position

H_s Significant wave height of irregular seas

H_s Significant wave height of irregular waves

I Moment of inertia

I_{PTO} Additional inertia term which may be used for reactive control of a PTO

k_{PTO} PTO spring coefficient

k_{PTO} PTO spring coefficient

$Loss_{AccTrans}$ Energy lost due to transient events between HP accumulator and chamber

m Mass of WEC

N Number of quantised steps

n Polytropic exponent

P Power

p Oil pressure

p_0 Initial pressure

P_{EM} Electrical power output of electric motor

P_{fluid} Fluid power

P_{mech} Mechanical power

Q Oil flow rate

Q_{gain} Gain flow required to change the pressure of PTO actuators

Q_{geo} Geometric flow from PTO actuators

Q_{ideal} Ideal flow from hydraulic machine

Q_{slug} Slug flow

Q_{total} Total flow requirement of Digital Displacement pump motor (DDPM)

r Radius of winch drum in heaving WEC

R_i Intrinsic resistance of PTO

R_m Load resistance

R_{PTO} Generalised PTO load resistance for linear damping

R_{PTO}^{opt} Optimum generalised PTO load resistance for linear damping

T Period of regular waves

T Wave period of regular waves

T_e Energy period of irregular waves

T_e Wave energy period

T_p Wave peak period

V Volume of fluid in PTO actuators

V_0 Initial volume

V_1 Final volume

V_{cham} Volume of PTO actuator chamber

W Work done

X_i Intrinsic reactance of PTO

x_{WEC} WEC heave position

Z_i Intrinsic impedance of WEC

Z_{PTO} Load impedance of PTO

Z_{PTO}^{opt} Optimum load impedance of PTO

Chapter 1

Introduction

1.1 Background and Motivation

The possible impact of the change in levels of carbon dioxide on the global climate was first considered at the end of the 19th century [25]. The connection between the artificial release of carbon dioxide by humans through the burning of fossil fuels and an increase in global temperatures was identified by Callendar a few decades later (although he viewed this positively) [26]. Increasing evidence for the negative impacts of climate change on species, global water resources, agriculture and other important areas has led to a drive on an international level to reduce greenhouse gas emissions in many areas of human activity, including electricity production [27–30]. This has resulted in a gradual migration from fossil fuel-based electricity generation to less carbon-intensive methods such as nuclear power, hydroelectric power, biofuels, solar power, wind power and tidal power. Fossil fuels were used to generate 87.7% of all electricity in the world in 1973 and were still the major source for electricity generation in 2017 at 72.7% [31]. However, in the same period, the global production of electricity increased almost four-fold. To keep reducing the world's reliance on fossil fuel-based electricity production whilst also meeting increasing demand, a broad range of renewable energy technologies is required. Ideally, this would allow all available sustainable energy sources to be harnessed, in a way which improves the security of supply against the variability of each component (e.g. wind) and so that communities in any geographical area have access to affordable sustainable energy. Within this kind of framework, wave energy could provide sustainable energy to coastal communities in many parts of the world, especially those which have limited access to other alternatives such as hydroelectric power or wind power.

The world wave power resource is estimated to be a vast 2.11±0.05 TW [32]. The UK has a total wave energy resource of 230 TW h per year, which is estimated to result in an annual practical resource of 70 TW h, half of which is found in Scotland [33]. As the electrification of heating and transport networks becomes more widespread, the demand for renewable electricity will only increase [34, 35]. As well as being a possible resource for electricity generation, wave energy could also be used for desalination of water [36]. Further discussion of the justification for the exploitation of wave energy can be found in [37, 38].

Despite having all this potential, wave energy has not yet been deployed on a large commercial scale, although many different types and designs of WEC have been proposed [39]. This is due to the many technical challenges involved in converting energy from a random, reversing, high force, low speed resource with very high extreme values to synchronous, grid quality electricity [40]. The subsystem of a WEC which performs this conversion from mechanical motion of the device to electricity is the PTO. The cost of designing, building, installing and maintaining a WEC with an efficient PTO in the harsh and challenging marine environment has restricted the growth of the industry, as it struggles to commercially compete with other electricity sources [39].

PTO design is a core challenge of realising the potential benefits of wave energy, as many of the technical difficulties of constructing a WEC culminate in this single subsystem. The design requirements of a WEC PTO include;

- Efficient instantaneous power absorption over a very broad range of amplitudes and wavelengths (typical peak to mean power ratios are up to 15 to 1 [18]).
- Efficient conversion of variable instantaneous power to steady electrical power [2].
- Ability to handle power transferred at low speeds with high torques [12].
- Responsive four-quadrant controllability [41].
- Fault tolerance [18].
- Storm survivability [12].

This is certainly not a full list of requirements as robustness to the marine environment, reliability, and ease of assembly and maintenance are also necessary to produce a commercially successful PTO i.e. a PTO with an acceptable cost. Many of options have been proposed, including electromagnetic PTOs, pneumatic PTOs and hydraulic PTOs. [39] provides a useful brief comparison of electromagnetic and hydraulic PTOs, and [12]

contains a detailed comparative discussion of several types of transmission. Hydraulic systems are a strong candidate for meeting these requirements, as they are well-suited to applications with high forces and torques [12], even at low speeds. They are also capable of providing energy storage in the form of accumulators, which enables the smoothing out of peaks and troughs in the input power [12, 40]. However, the need for broad-band efficiency and precise four-quadrant controllability is not by conventional hydraulic machines and novel approaches must be used to tackle the challenges of WEC PTOs. Additionally, conventional hydraulic transmissions are capable of providing continuously variable load and flow, but would need to be sized according to the maximum instantaneous power, which would mean that the average exported power would be in a very inefficient operating regime of the transmission [42].

As described, the potential of hydraulic systems to meet the requirements of WEC PTOs is high. To maximise power extraction, an ideal PTO should be capable of applying different control strategies in a way which optimises the coefficients of the PTO inertia, damping and spring terms throughout the varying incident waves [43]. This means that the PTO must be able to both absorb and return energy to the WEC to keep the system in resonance with the waves, whilst still extracting and converting some of it. This is difficult to achieve practically as the system must be capable of reactive power flows. Reactive control was successfully demonstrated with promising efficiencies of 70% for a hydraulic PTO in Pelamis [9], but the 'quantised' PTO response meant that achieving continuous optimum PTO torque, as described in [43], was not possible. However combining the quantising features of Pelamis with the highly efficient, high bandwidth, DD hydraulic pump motors of AIP may produce an efficient PTO with the ability to continually respond with the optimum PTO torque ([13] contains an explanation of DD® technology). This PTO concept is known as the Quantor.

In order to develop and prove that the proposed Quantor system does indeed have the desired full reactive control capability an extensive programme of testing is required. Practically, it is much more straightforward to prove the system in the lab before sea trials. Building a test rig which realistically embodies the inertia and stiffness of a sea-going WEC system should rigorously prove the concept, and allow control gain and stability to be optimised on the rig [20]. This test rig must have full four-quadrant capability to allow the Quantor's reactive control response to be tested. This will also allow components and subsystems to be tested at a realistic range of speeds and torques and permit a 'first run' of system integration, to help smooth out later (seagoing) builds.

1.2 Quantor Hydraulic Power Take-Off

1.2.1 Quantor Concept

The Quantor PTO can be considered as an evolution of the Pelamis PTO. The Pelamis PTO used a novel digital approach to provide a discrete set of net loads from pressurising or not pressurising individual piston areas. This 'quantised' system could approximate continuous control by choosing the number of discrete load steps which were enabled (pressurised) at any one time [42] (see Figure 1.1). This system meant that absorbed power was transferred directly to (and from) the energy storage accumulators, so that instantaneous power absorption was very high and absorbed power was decoupled from average exported power. The PTO demonstrated a wave-to-wire efficiency of over 70% across the power range [7].

However, a disadvantage of this discretised system meant that the PTO could not provide a continuously variable load, which does limit the power absorption [42] and means that many control strategies which could yield power or reliability performance improvements cannot be applied. Adding a further continuously controlled load of the same range as the quantised load steps would make it possible to achieve continuous control across the full load and power range. For this to work, the continuously controlled load must be controlled fast enough to compensate for the step changes in the quantised load [42]. Figure 1.2 shows the idealised Quantor concept combining a quantised system with a continuously controlled load step from a DDPM, producing a smooth PTO load which can follow the ideal demand from the controller.

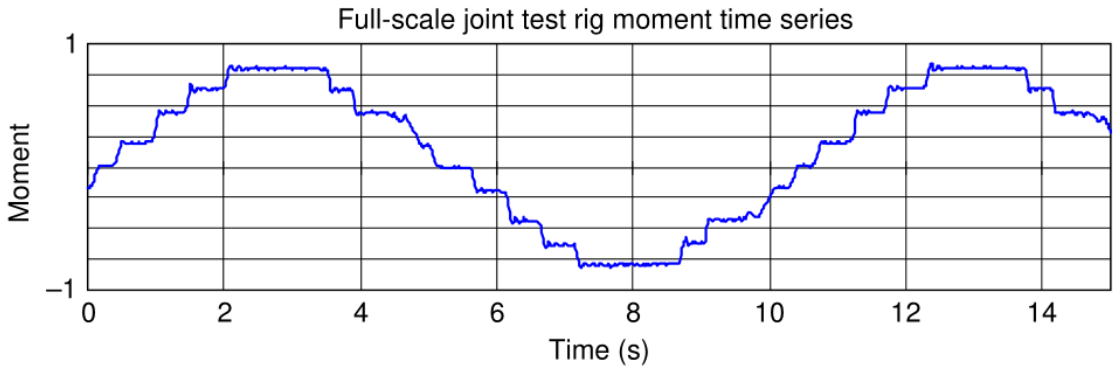

Figure 1.1 *Data from a practical application of the quantisation approach: time series from Pelamis full-scale joint test rig showing quantisation of load under a sinusoidal excitation (moment has been normalised) [1].*

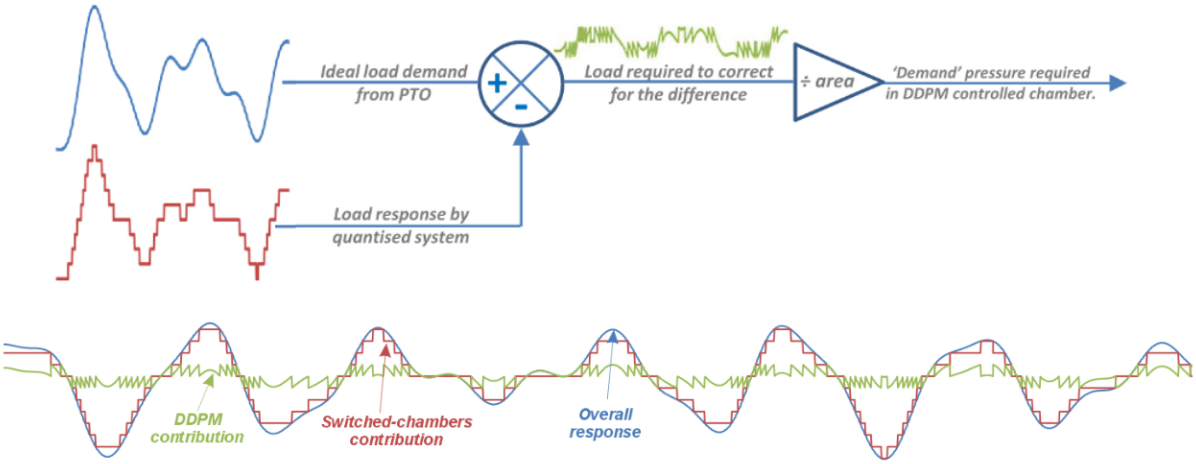

Figure 1.2 *Idealised Quantor concept taken from [2]. The error between the ideal load demand from the PTO (blue) and the load response from the quantised system (red) can be corrected using a DDPM capable of producing a rapidly changing load (green).*

1.2.2 Wave Energy Scotland PTO Development Programme

The development of the Quantor PTO was funded by through the Wave Energy Scotland (WES) PTO programme. WES was formed in 2014 by the Scottish Government under Highlands and Islands Enterprise (HIE). WES aims to ensure that Scotland continues to lead the development of wave energy, through awarding procurement contracts to projects focused on particular subsystems of WECs. These include projects focusing on PTO systems, control systems, materials and novel WEC design. These projects have stages with 'gates' for progressing to the next stage, with funding increasing for higher stage projects. The Quantor PTO has progressed through the Stage 2 round of the WES PTO development programme and recently completed Stage 3, with a funding award of £2.5m over two years. AIP and Quoceant collaborated for both the Stage 2 and Stage 3 projects.

Stage 2 Project

Quoceant and AIP completed a Stage 2 project to verify the technical feasibility of various aspects of the Quantor PTO. The key aim of this initial project was to demonstrate the control and machine functionality to successfully integrate AIP DDPM technology with a Pelamis-like PTO [2]. The purpose of the DDPM in the Quantor is to counteract the force steps from the quantised chambers (or equivalent rotary actuators) so that the final PTO torque varies smoothly. This requires that the DDPM is very responsive to the rapidly varying pressure demand signal and is capable of both producing (when pumping)

and consuming (when motoring) the required flow to compensate for the step changes in torque. This was demonstrated on a test rig at AIP premises as is further explained in Chapter 3.

Stage 3 Project

The key technical aims of the Stage 3 Project, which provided the opportunity for this research were;

1. To construct an in-house PTO test rig that physically emulates the dynamics of a range of WECs.
2. To build, test and quantitatively assess an integrated Quantor PTO system.

There were other objectives in the Stage 3 project such as market research improving the endurance of DD components for small-scale and MW-scale WEC deployments. These will not be discussed in detail here and more information can be found in [44].

Having completed Stage 2, the next logical step was to construct and test a fully integrated Quantor PTO system, with a new PTO test rig which would be capable of representing a range of WEC designs in irregular seas (the WEC emulator). Figure 1.3b shows a schematic of the lab system designed for the project, with the contents of the green box being the outcome of aim 1 and the contents of the yellow box being the outcome of aim 2. The PTO test rig subsystem replaces the WEC in Figure 1.3a above, and a choice of linear or rotary quantised actuators on the WEC is envisaged, with the Quantor PTO using rotary actuators. The switching valves, accumulator, DDPM system and generator in the lab system are identical components to those of the WEC system. This means that the Quantor will be tested at representative speeds and torques for sea deployment, with real inertia and real actuators, which allows many control problems to be solved in the lab. This will resolve many of the physical and control challenges of building and commissioning a PTO in a safe and accessible environment. This WEC emulator may in the future be used by other developers, as no comparable facility currently exists in Scotland.

For both aims 1 and 2, intensive modelling and simulation work was required to select components, to design a control system and to identify potential problems. This was accompanied by mechanical and electrical design activities, before construction and commissioning.

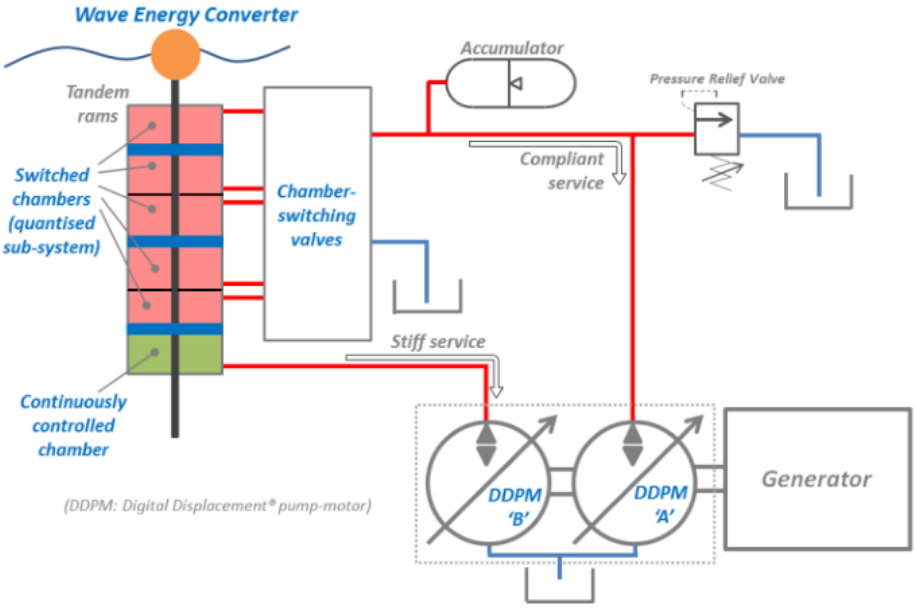

(a) *Schematic of Quantor with single degree-of-freedom WEC [2].*

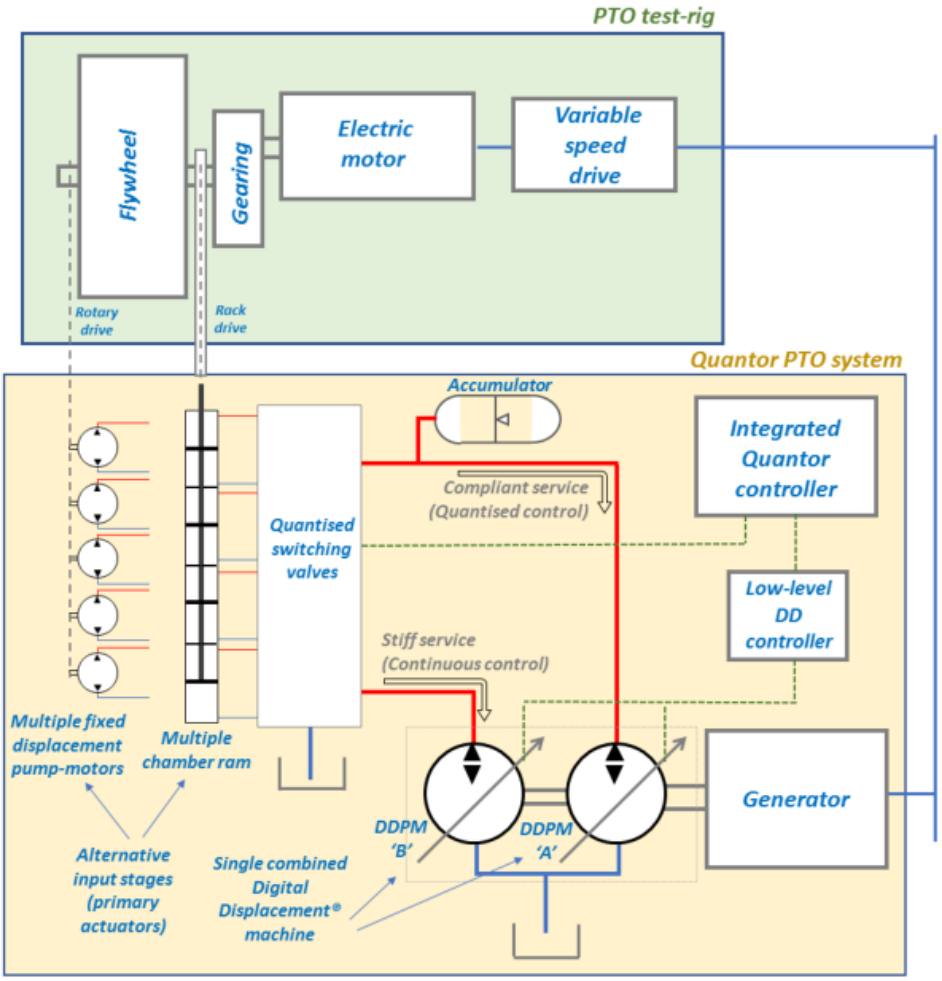

(b) *Schematic of integrated PTO test rig and Quantor [45] system constructed for Stage 3 WES project.*

Figure 1.3 *Schematics of Quantor in WEC and of AIP experimental setup for Stage 2 project shown together for comparison [2].*

1.2.3 Company Backgrounds

Artemis Intelligent Power Ltd

AIP was formed in 1994 as a spin-out from the University of Edinburgh (UoE) to develop novel, efficient and controllable hydraulic machines using DD Technology. The company is now developing DD machines and systems for a broad range of applications, including excavators, trains and industrial applications [46]. In 2018 the Danish company Danfoss acquired a majority share in Artemis to produce and export Digital Displacement pump (DDP)s in volume [47].

AIP's efficient and controllable DDPM machines are highly relevant to wave energy PTO (which was the original application in the minds of the company founders). It is a challenge to make an efficient PTO using conventional hydraulic machines due to their high fixed losses and low efficiency at part load, which is a common operating condition due to the variability of ocean waves [2]. AIP's technology outperforms conventional hydraulics in both of these aspects, as shown in Figure 1.4, so opens up the possibility of making a highly efficient and responsive wave energy PTO.

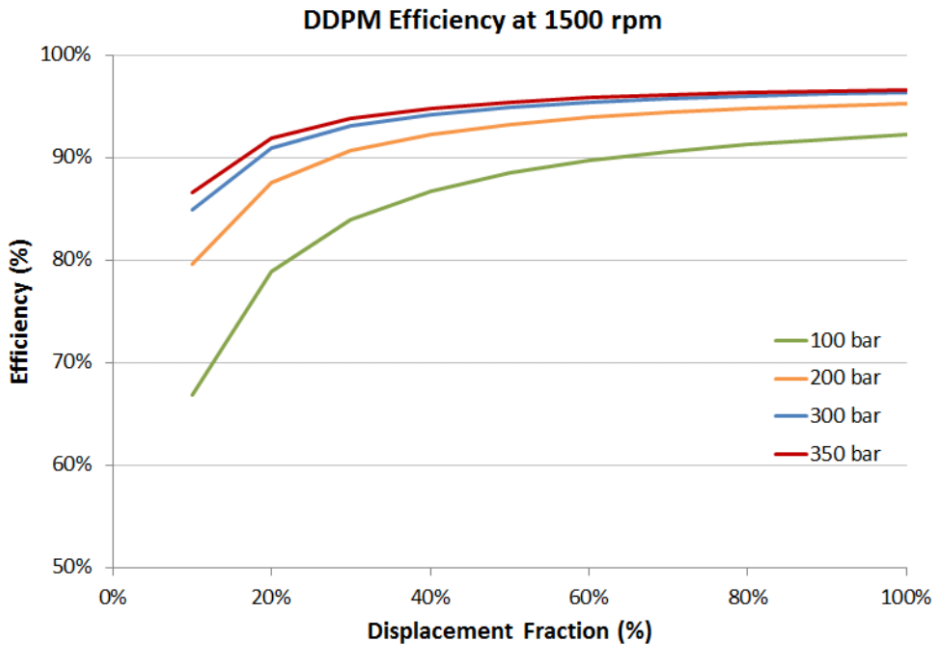

Figure 1.4 *Typical DDPM efficiencies at* 1500 rpm *over a range of displacements [3].*

Quoceant Ltd

Quoceant Ltd was formed after Pelamis Wave Power (PWP) went into administration in 2014 and is made up largely of former PWP team members. The Pelamis wave energy device was tested at the European Marine Energy Centre (EMEC) between 2010 and 2014, generating over 250 MW h of electricity [7]. Quoceant now offers consultancy services to the marine renewables sector on a wide variety of projects [48].

Quoceant's experience of developing the Pelamis PTO has informed the design of the Quantor PTO so that it encompasses potential improvements to the Pelamis system.

1.3 Research Aims

This research tests the hypothesis that; **the Quantor is a highly controllable and efficient PTO system for wave energy conversion that can be representatively tested at laboratory scale to understand full-scale deployments.**

The hypothesis above is broken down into several aims and objectives, relating to its controllability, efficiency and the test methods used. The research aims detailed below are informed by this hypothesis, by the general need for smooth, four-quadrant PTO torque and by the need for robust testing methods to realistically evaluate WEC PTO systems. The aims addressed here are numbered, with the relevant objectives bullet-pointed below;

1. Demonstrate that the Quantor can smoothly follow a PTO torque demand in all four quadrants in representative test conditions
    - Simulate the Quantor's operation in all four quadrants.
    - Design and build a test rig (consisting of a WEC emulator and laboratory-scale Quantor) to test the Quantor's performance in a range of representative conditions.
2. Quantify the Quantor's efficiency and losses in a range of representative test cases
    - Produce a detailed simulation of the Quantor, including its losses.
    - Test isolated Quantor components to measure specific losses.
    - Full Quantor testing on the rig, using a range of regular and irregular waves.
3. Estimate performance of alternative full-scale Quantor architectures
    - Validate Quantor simulation using test results.

- Extend the validated model to full-scale Quantor architectures to evaluate performance.

The project activities will roughly follow a classic research structure of simulation, building a laboratory test system, testing and model validation. Initial simulation will be used to develop a control system, predict the Quantor's four-quadrant behaviour and estimate losses and efficiency (in support of aim 1 and 2). The WEC emulator and lab-scale Quantor will be constructed and the performance results obtained for the full system and for specific components. This should allow aims 1 and 2 to be fulfilled by demonstrating the Quantor's torque control performance as well as giving measurement of the system losses. The subsequent validation of the Quantor model based on the test data will mean that meaningful insight can be gained into Quantor's performance at full-scale. Extending the experimentally validated model of the Quantor to full-scale architectures should produce realistic estimations of the PTO's efficiency, as the losses in the system will be quantified. The quantification of these losses makes possible accurate estimations of the corresponding loss at full-scale, for example, how more powerful PTO actuators would change the system efficiency.

The novelty of this research lies in several different areas:

- The Quantor itself is a novel WEC PTO and therefore any research carried out on this system is new.

- The construction of a test rig with a WEC emulator is a rare research activity hitherto and to the best of the author's knowledge has not previously been done at this power scale with a significant inertia (see Chapter 2).

- Aside from the loss analysis carried out for Pelamis [49] which has remained largely confidential, there are no known cases of WEC PTOs for which a detailed loss breakdown based on real data has been collected.

Since the Quantor is intended to be a versatile and scalable PTO with many potential architectures, the outcomes of this research are not relevant to a single design or even category of WEC but should be applicable across almost the whole WEC design spectrum (with a few particular exceptions such as oscillating water column (OWC)s).

1.4 Outline of the Thesis

Chapter 2 reviews the relevant literature, covering topics such as previous hydraulic WEC PTOs, control strategies for WECs and the development of DD machines.

Chapter 3 discusses the work which was carried out previously on the Quantor as part of the WES Stage 2 PTO project. The Stage 2 Project was carried out prior to the author's involvement at AIP, so this chapter is an extension of the literature review and provides a more specific context to the work discusses in the thesis.

Chapter 4 explains the physics-based model of the Quantor lab system constructed in the design stage and simulated efficiency results and loss results. The simple Simulink modelling carried out for the Stage 2 Project was used as the starting point, and the author greatly extended this to produce a highly detailed Simscape system model with a Simulink controller. This work was done with the supervision and support of AIP and Quoceant staff but carried out by the author.

Chapter 5 describes the laboratory system constructed at AIP premises, comprising a WEC emulator and a scaled Quantor system. The overall design of this was agreed during the Stage 2 project, before the author's involvement. The author did assist with sizing of components such as the electric motor and drive, flywheel and PTO motors.

Chapter 6 describes the key test results obtained for the Quantor system. The final Quantor testing and data analysis were largely carried out by the staff of AIP and Quoceant after the author did much of the initial rig commissioning and control system design.

Chapter 7 describes the use of test data to validate models of individual Quantor components, as the first stage of Quantor loss analysis. This was done by the author, using data gathered by others as described above.

Chapter 8 describes the loss analysis of the Quantor, validation of the full Quantor model using experimental data. Again, this is the author's work, using the test data.

Appendix A describes the production of a simplified model for exploring different Quantor architectures. This was carried out by other AIP and Quoceant staff, based on the validation work done by the author. This is included for the reader's interest, to show how the Quantor could perform in a full-scale sea deployment.

Chapter 2

Literature Review

The Quantor project encompasses a broad range of activities, including hydraulic and mechanical system design, control system design, WEC emulator design, laboratory PTO testing, simulation and model validation. Specific to this thesis are the challenges of designing a test rig to emulate a WEC in irregular seas, modelling of the PTO, testing of the PTO and model validation. The relevant literature is explored below, giving context to the choice of a hydraulic PTO and describing WECs which have been designed in this way, exploring control strategies for WEC PTOs previously proposed by other researchers, explaining the unique hydraulic machine (DDPM) used in this project and finally discussing previous test rigs which have been built to measure the performance of PTOs.

2.1 Types of Power Take-Off

A fundamental challenge of PTO design is that the oscillations of wave energy absorbers are slow, bidirectional and irregular. This means that a PTO requires a complex transmission with a high gearing ratio so that an oscillating absorber can power a generator [12]. Typical approaches include gearing through a pneumatic or hydraulic system, or using a direct drive electrical generator which omits the need for gearing [50].

A great variety of technical approaches to power extraction have been proposed. The options available for power take-off for a particular WEC are very dependent on the operating principle of the WEC, the type of motion selected (linear or rotary) and the physical capacity the WEC has to accommodate a PTO, both in terms of size and mass. Some historical examples are given below, with a brief description of the PTO strategy. This gives an indication of the technical challenge of PTO design and the range of possible

approaches.

What follows in Sections 2.1.1 to 2.1.3 is not an exhaustive list of PTO strategies; for example, water turbine-based PTOs for over-topping devices (such as the WaveDragon) have not been covered, nor have dielectric elastomer PTOs, but these are more unusual choices for a WEC PTO.

2.1.1 Air Turbines for Oscillating Water Columns

The principle of an OWC is that there is a trapped column of air with its base in the sea such that the rise and fall of the waves compresses and expands the air column, which can be used to drive an air turbine connected to a generator [4]. Figure 2.1 shows a diagram of the Limpet OWC device. The attraction of using a air turbines for wave energy conversion is that they can increase the slow wave velocity to the velocities necessary for electrical generator operation by using air ducts and careful foil design [40]. Wells turbines are often chosen for OWCs as they rotate in the same direction even if the air flow is bidirectional [50]. Whilst it is possible to match the impedance of the turbine PTO to the OWC [4], this system will necessarily be tuned to a particular design sea state (due to the fixed dimension of the OWC) and therefore will have limited power absorption in other sea conditions. The possibility of using reactive control to widen the absorption bandwidth of OWCs with Wells turbines has been proposed but the low efficiency of the Wells turbine when acting as a compressor (i.e. supplying reactive power) means that the gains in generated power are very limited [51].

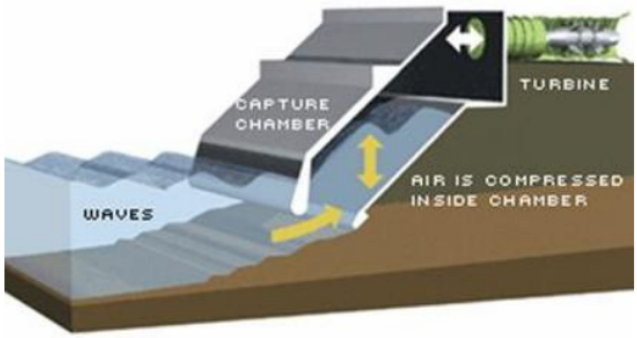

Figure 2.1 *Diagram of Limpet OWC which was installed in Islay in 1999, showing an inclined air column and Wells turbine at the top of the air chamber [4]. Image from [5]*

2.1.2 Direct Drive Electrical Power Take-Off

Rather than using a complex pneumatic or hydraulic system to gear the WEC velocity to the speed of a typical electrical generator, it has been proposed that a new type of electrical machine could be designed which would operate at the same speed as the WEC prime mover, i.e. 2 m/s or less. This would reduce the number of parts needing maintenance, as well as the stages of conversion between absorption and generation [52]. AWS constructed a linear direct drive electrical generator which was 35 m in height with a stroke of 7 m and a maximum linear generator force of 1 MN [6], shown in Figure 2.2. There were problems with the water brakes in this prototype so full power was never reached, but it was shown to generate an average of 24 kW in a sea with a peak power of 240 kW. However, AWS have since abandoned this concept and are exploring alternatives [52].

The design of linear direct-drive generators is very challenging. The low velocity results in large torque and current requirements, which are limited by thermal limits and magnetic saturation in the generator windings [53]. Maintaining air gaps to tolerance with the possible wave loads on the mounting structure would require careful consideration [40]. Rotary direct-drive generators could be possible, in either bidirectional or unidirectional (with a clutch) designs. In both cases the generator must absorb high instantaneous torques as there is no inherent energy storage in the system, meaning that the system must be designed for peak powers much higher than the average power rating. Grid connection via a converter is required to handle the variable speed of these machines [53].

The lack of energy storage in these systems for smoothing of peak powers is a challenging control issue, as well as leading to the over-sizing of machines relative to their average expected operating power, reducing efficiency.

2.1.3 Hydraulic Power Take-Off

Hydraulic systems are intrinsically well-suited to this application as they are capable of handling bidirectional motion, low speeds, high torques, as well as having the capability of storing energy in accumulators, which help smooth the electrical output [1, 40, 50]. [50] notes that the use of high pressure hydraulics can be advantageous to WECs where size and weight is an issue due to the high power density, and the force created by these pressures is significantly greater than those from the best electrical machines. The use of variable displacement hydraulic machines would potentially mean that fixed speed electrical machines could be used, which reduces the need for complex and expensive power electronics when connecting to the grid [53].

Figure 2.2 *Photograph of AWS taken in 2004 at the beginning of the submersion operation. Image from [6]*

Hydraulic PTOs can have either linear or rotary actuators. Hydraulic cylinders, with appropriate sealing, are a good option for PTO inputs. These were used in Pelamis and Wavestar, which are discussed more in Section 2.2. Generally, linear systems in WECs must be treated with caution as extreme waves can cause huge loads forcing cylinders into their end stops, potentially damaging components [50]. Large hydraulic pumps (ideally with variable displacement) could also be used as WEC PTO actuators [40]. Check valves or other hydraulic systems can be used to rectify the flow from the bidirectional input, meaning that downstream equipment need only be unidirectional [50]. Energy storage is another significant benefit of hydraulic systems, in that accumulators can be used to smooth the power output to the generator, reducing the effect of the input variance on the output [50] and reducing the losses in the downstream components [40].

A key issue for hydraulics in wave energy is the part-load efficiency or pumps and motors [40, 50]. The variability of input wave energy is such that a PTO's hydraulic machines would need to be oversized relative to the mean input power to handle very high peak powers. This means that they spend most of their lives operating at part load, away from the maximally efficient operating point [50]. The possible sources of losses in conventional hydraulic machines are detailed in [40]. Whilst hydraulic systems do have many advantages for wave energy, improving the part-load efficiency of hydraulic machines is a critical step for this type of PTO. Of course, the more smoothing of the input power which can be carried out in 'upstream' in the PTO, the less need there is for high part-load efficiency 'downstream'.

2.2 Wave Energy Converters with Hydraulic Power Take-Off

2.2.1 Pelamis

The Pelamis WEC was constructed by PWP and deployed at EMEC's Billia Croo test site between 2004 and 2007, with the follow-up P2 machine installed in Orkney in 2010. Unfortunately, PWP went into administration in 2014 and its assets were bought by WES [54]. The Pelamis was an innovative attenuator-type WEC with a quantised hydraulic PTO. The P2 demonstrated typical wave-to-wire conversion efficiencies of 70% in sea trials [9].

The Pelamis PTO is pictured in Figure 2.3a. The long axis is roughly perpendicular to the oncoming wave crests and energy is extracted from the relative motion of the joints between the bodies. As the segments of the Pelamis move relative to each other, hydraulic cylinders between the joints pump fluid into the PTO. Central to the Pelamis PTO was the application of a discretised approximation to the ideal PTO load, using hydraulic cylinders with multiple chambers which could each be connected to high or low pressure via a control manifold [8]. The pressurisation or depressurisation of individual piston areas according to the control algorithm gave a quantised approximation to fully reactive control. The absorbed power was transferred directly to and from the energy storage accumulators with minimal losses [42]. Figure 2.3b gives a simple overview of the Pelamis PTO. However, the main drawback of this approach is that smooth continuous control is not possible and hysteresis needs to be introduced to prevent limit-cycling around the load steps, which limits power absorption [42].

The development of the Pelamis PTO involved many different processes. As well as a full suite of hydrodynamic models, which were validated using a 1/7th scale model in tank tests, a full-scale model of a single PTO joint was constructed and bench-tested in the lab. More information about the Pelamis test rigs can be found in Section 2.5.1.

The story of the development of the Pelamis and details about its other features are supplied in more detail in [1, 8, 9, 55].

(a)

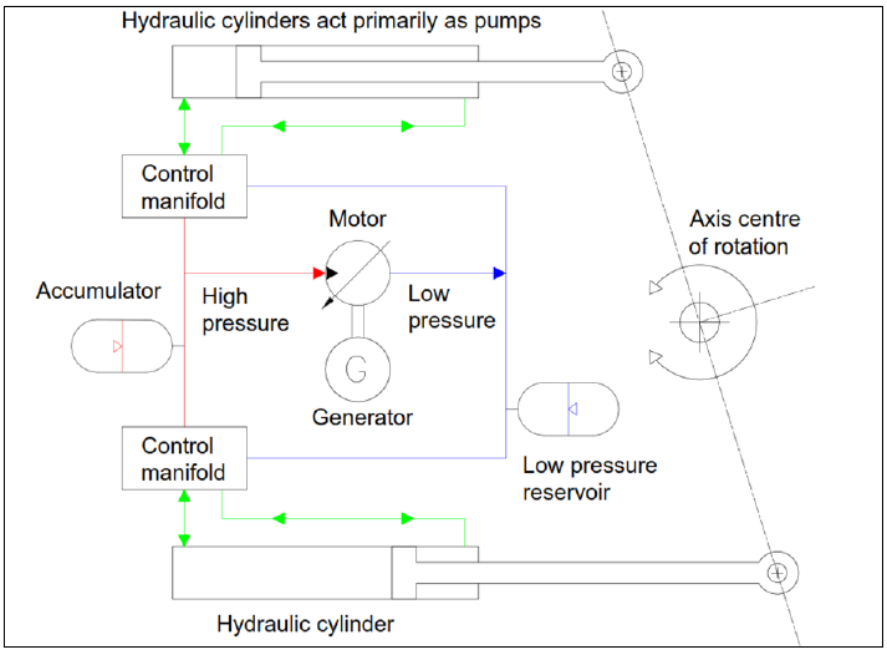

(b)

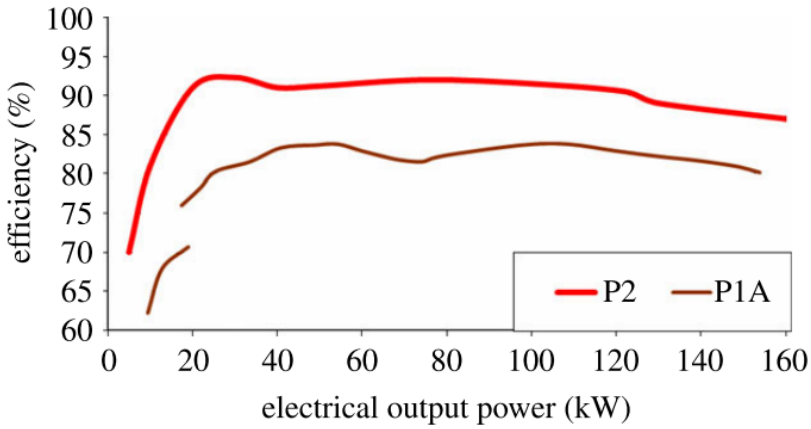

(c)

Figure 2.3 *(a) shows a photo of P2 Pelamis in Orkney [7], (b) is a simple schematic of Pelamis PTO for a single PTO module in a joint [8] and (c) shows the efficiency of two iterations of Pelamis design (P1 and P2)[9]*

2.2.2 Wavestar

The Wavestar is a Danish WEC concept for which a 110 kW prototype was installed in Hanstholm in September 2009 as shown in Figure 2.4. The Wavestar has a hydraulic PTO; the floats move up and down with the motion of the waves and pump hydraulic fluid into a common manifold, which then supplies a hydraulic motor which drives a generator. The aims of this prototype deployment were, among others, to demonstrate the efficiency of the PTO and to check that the measured power absorption was in line with expectations [10]. However, there is little reported data on the actual measured performance of the PTO from these trials.

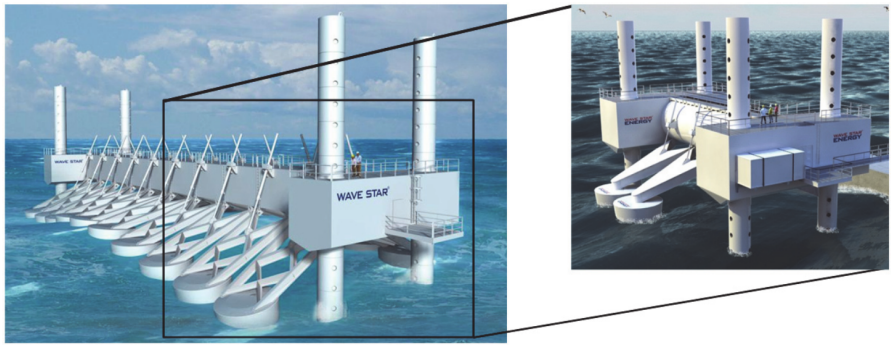

Figure 2.4 *Commercial Wavestar concept on left with 20 floats rated to* 600 kW *and scaled prototype with 2 floats rated to* 110 kW *as installed in Hanstholm [10].*

There are however several studies of the possibility of using alternative architectures for hydraulic PTOs for the Wavestar [11, 12, 56, 57]. The concept most thoroughly reported in the literature is that of the Discrete Displacement Cylinder (DDC), on which extensive modelling [56, 57] and full-scale bench testing has been carried out [11]. This concept shares several operating principles with the Pelamis PTO, in that force control is achieved through discrete variations of pressure and area combinations, using the DDC which has three different cylinder chamber areas built into it. This is illustrated in Figure 2.5.

[57] presents a wave-to-wire model of the full-scale Wavestar with DDC PTO. It seems that this work was done before the DDC bench test and as such does not use a validated model of the DDC. The modelled system seems to perform very well, being capable of a broad range of force control in all four quadrants, handling peak power absorption without compromising efficiency and maintaining efficient performance even in small waves (reported results are efficiencies of over 70% even when at only 15% of load capacity). However it is not apparent how realistic these results are, and the system does not seem to have demonstrated reactive control in an experimental setup (although this did work for a similar system in the Pelamis [9], so four-quadrant control for the

DDC seems entirely feasible). Experimental validation of the DDC simulation results from the bench is presented in [11], but it is not clear how this relates to the broader wave-to-wire model. Further information about bench-testing carried out on the DDC concept is provided in Section 2.5.2.

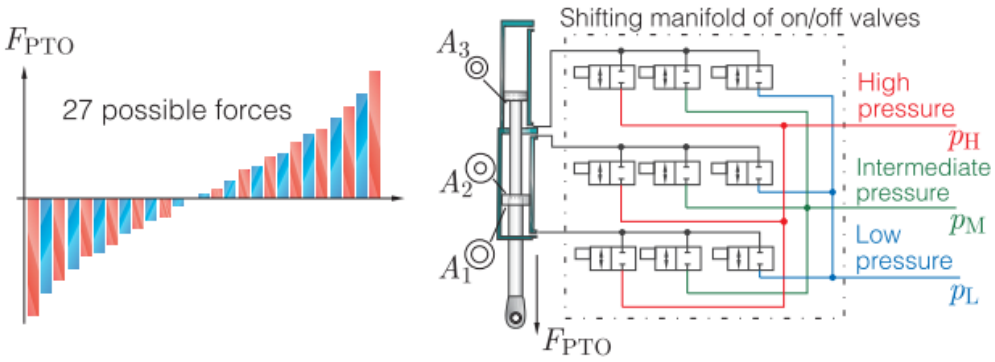

Figure 2.5 *Simplified schematic of proposed Wavestar DDC PTO system [11]*

2.3 Power Take-Off Control Strategies

The design of a control strategy for a WEC PTO is of critical importance to the success of a WEC. A WEC is generally constructed for a particular design sea state (which may relate to a planned deployment site) but this means that its performance is mechanically optimised for a particular wave condition and not for other sea states. Given the variability of ocean waves, a second method apart from mechanical design is needed to optimise WEC performance across more sea states and to reduce the dependence of the power output on a single specific design wave condition. Control strategies can be used to improve power absorption in the design sea state, broaden the range of sea states over which absorption can occur and also protect hardware in extreme load cases. It can also be relatively cost-effective to implement new control architecture compared to other WEC subsystems [58].

2.3.1 Basic Power Extraction

[59] describes a scenario of a semi-submerged sphere moving purely in heave. This provides a useful simple example for looking at the equation of motion of a WEC. The forces on the sphere are:

- Net restoring stiffness force $F_s = \rho g A_w \eta$
  This is the difference between gravitational and buoyancy forces. ρ is the water

density, A_w is the waterplane area, g is gravitational acceleration and η is the heave excursion, i.e. the difference in heave position between the water surface and the buoy.

- Inertia force $F_i = m\ddot{\eta}$
  This is the force due to the mass m of the body moving with acceleration $\ddot{\eta}$.
- Wave excitation force F_e which is the sum of the pressure forces on the body surface.
- Wave radiation force F_r due to the waves radiated by the body.
- PTO force F_{PTO} applied by the PTO hardware according to the demand of the PTO controller.

An equation of motion for heave can then be given [59]

$$F_i + F_r + F_s = F_e + F_{PTO} \tag{2.1}$$

For this expression, the hydrodynamic forces excitation and radiation are approximated by linear theory: motions and wave amplitudes are assumed to be small. The WEC is assumed to be referenced to a rigidly fixed point and mooring forces are ignored. F_{PTO} usually consists of a damping term which extracts real power when applied to the measured velocity of the WEC. Other control terms may be added, as explained below.

Whilst there exists an abundant variety of different WEC designs, with distinct structural features and approaches to power-extraction, the majority of WECs rely on some form of oscillating system with a frequency response to incident waves, and therefore exhibit the behaviour known as resonance [60]. Exceptions to this would include over-topping devices such as the Wave Dragon and the Tapchan [40]. This means that most WECs produce maximum output power when the incident wave period matches the natural period of the device. When resonance is not attained (i.e. when the incoming wave period does not match the natural period of the device), the output energy of the device is reduced. The severity of this reduction depends partially on the natural resonance bandwidth of the WEC: if it is a point-absorber, its resonance bandwidth is very narrow and therefore it is at any given time unlikely to be perfectly in resonance with the waves; however if it is a more horizontally-extended type of device such as an attenuator the resonance frequency bandwidth will be greater [60].

The optimal energy transfer from wave to absorber occurs when the absorber's resonant frequency matches the incident wave frequency [12, 40]. It is possible to shift the frequency

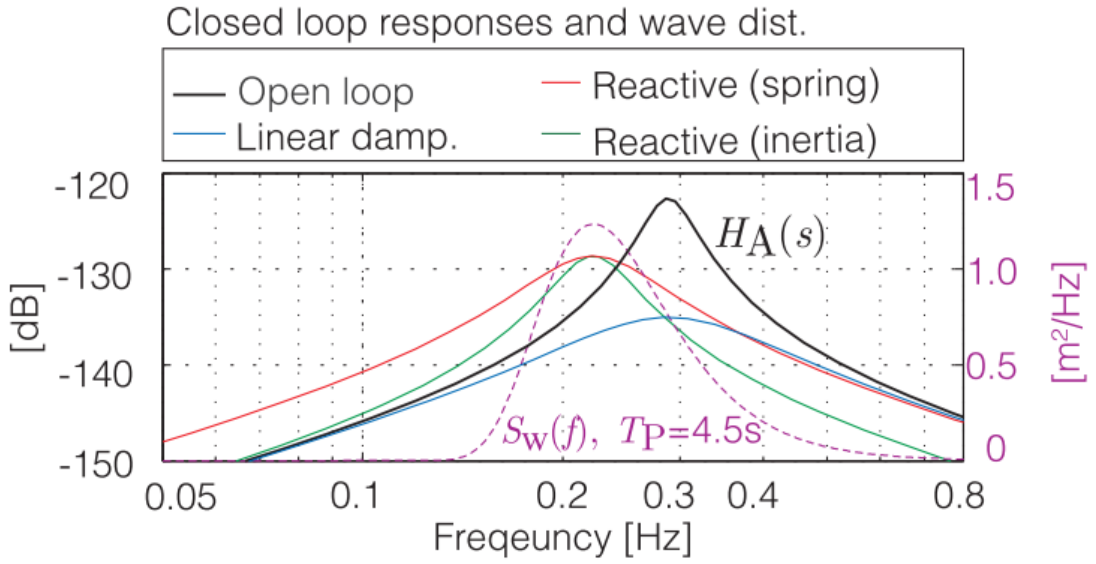

Figure 2.6 *The graph shows the effect of different control strategies on the response of the absorber. $S_W(f)$ shows the wave spectrum for an irregular sea of peak period (T_P) 4.5 s and H_s 1.75 m and H_A shows the absorber response, with different PTO control strategies. Taken from [12]*

response of the absorber by changing the applied PTO torque (τ_{PTO}) based on feedback of the absorber's motion. This shift in frequency response is shown in Figure 2.6 for the reactive (spring) and reactive (inertia) cases. A linear damping case would be mathematically defined by Equation (2.2) where c_{PTO} is the PTO damping coefficient and ω_{WEC} is the angular velocity of an absorber. Note in Figure 2.6 that this does not produce a phase shift in the absorber response.

$$\tau_{PTO} = c_{PTO}\omega_{WEC} \tag{2.2}$$

Equation (2.3) defines the case of reactive control with an additional inertial term, where I_{PTO} is the emulated additional inertia.

$$\tau_{PTO} = c_{PTO}\omega_{WEC} + I_{PTO}\dot{\omega_{WEC}} \tag{2.3}$$

Equation (2.4) defines the case of reactive control with a spring term, where k_{PTO} is the emulated spring constant and θ_{WEC} is the angular position of the absorber.

$$\tau_{PTO} = c_{PTO}\omega_{WEC} + k_{PTO}\theta_{WEC} \tag{2.4}$$

In both these cases of reactive control, the resonant frequency of the absorber has been shifted to match the incident waves. Achieving this practically means that the PTO

must be capable of providing and absorbing reactive power, so that it operates in all four quadrants [12, 61].

Below is a brief overview of the various control strategies discussed in the literature.

Linear Damping

A more general form for the linear damping than Equation (2.2) is given in Equation (2.5) where the resistance R_{PTO} is a coefficient of proportionality.

$$F_{PTO}(t) = -R_{PTO}\dot{\eta}(t) \tag{2.5}$$

According to [62] the optimum load resistance in the frequency domain R_{PTO}^{opt} is given by Equation (2.6) where R_i is the intrinsic resistance and X_i is the intrinsic reactance.

$$R_{PTO}^{opt} = \sqrt{R_i^2(\omega_f) + X_i^2(\omega_f)} \tag{2.6}$$

The further the system is from resonance the larger R_{PTO}^{opt} will need to be to bring the WEC back into resonance.

Complex Conjugate and Reactive Control

Equation (2.4) is a specific example of the general result for maximising the useful absorbed energy for a body oscillating in one mode. A more general discussion is given in [59]. According to [60] the optimum condition occurs when the intrinsic reactance $X_i(\omega_f)$ is cancelled and the load resistance $R_m(\omega_f)$ is equal to the intrinsic resistance $R_i(\omega_f)$. [63] describes two strategies for achieving this, which are called complex conjugate control, and phase and amplitude control. Both of these options require hardware capable of handling reactive power flows and can be generalised together as 'reactive control'.

There are two conditions which must be met to maximise the absorbed power from a regular wave; the WEC velocity must be in phase with the excitation force (which is satisfied in resonance), and the interference between the incident wave and the wave re-radiated must be at its most destructive. These can be considered as conditions for optimum phase and optimum amplitude respectively [60]. These two conditions can be expressed as a single condition described with a complex mechanical impedance (which has units of force divided by velocity). If the system's intrinsic impedance is Z_i then the optimum load impedance Z_{PTO} is the complex conjugate of Z_i, according to Equation (2.7) [59, 60, 63]. This results in the total mechanical reactance being cancelled, hence the term

reactive control.

$$Z_{PTO}^{opt}(\omega_f) = Z_i^*(\omega_f) = (R_i(\omega_f) + iX_i(\omega_f)))^* \tag{2.7}$$

There are some discrepancies of nomenclature in the literature between the terms 'complex-conjugate control' and 'reactive control'. In [60] they are described as equivalent whereas in [40] a distinction is drawn, where full complex conjugate control refers to the full cancellation of spring and inertia as in Equation (2.7), and reactive control refers to any use of a negative spring term to shift the phase response of the WEC, which is similar to the description in [12, 61]. This thesis will follow the pattern set by [40], where complex-conjugate control is the fullest possible realisation of reactive control.

A perfect closed-loop full complex-conjugate controller would be unstable [40, 59]. This could be approximated with advance knowledge of the input, from either a wave buoy in advance of the WEC or a model [64]. However, the challenge of implementing full complex-conjugate control means that reactive control which introduces a phase shift is a much simpler and more appealing option.

When using reactive control, it is possible to reach a situation in which the energy contributing to the mechanical spring to keep the WEC in resonance is much greater than the useful energy being extracted by the damper in the PTO. If the transfer of reactive power is not very efficient, unacceptable additional losses may be incurred attempting to keep the WEC in resonance [40]. Depending on the type of powertrain and hardware used in the WEC this reverse power flow may not be possible. Hydraulic powertrains are a good option for reactive control so long as the machines involved can operate as both pumps and motors [40].

Optimal Velocity Tracking

It is possible to derive an expression for the optimal velocity based on phase and amplitude control, and to treat WEC control as a velocity tracking problem. This can be implemented with a simple proportional (P) or proportional integral (PI) control loop [59]. However the velocity is necessarily tracked by adjusting the applied PTO force and arguably calculating and applying the optimum force is a more direct control strategy, rather than attempting to control a secondary variable.

Model-Predictive Control

[62] describes model-predictive control, where the controller has some short-term future knowledge of the wave excitation force and operates to maximise the power extracted

within this future time window, using a discrete time model of the PTO. The controller can include knowledge of the constraints of the PTO machinery and provide a 'constrained optimum' control. This method requires reactive power capabilities of the PTO hardware, as well as good algorithms for wave prediction, and in the presented results the average reactive power flows required to enforce an optimal WEC motion exceeded the average absorbed power. However, in [62], this was the most effective control strategy in terms of absorbed power in both regular and irregular waves.

Latching

In [65] a small buoy (with a natural period shorter than those of the average incident waves) is controlled using a latching strategy. The aim of this is to bring the absorber velocity and excitation force more closely into phase by latching the absorber in a fixed position until the wave excitation force is in the correct phase, at which point the absorber is released. It is challenging to implement latching control in irregular seas where the optimum time to release the absorber varies wave-by-wave [59], and there is also the issue of mechanically designing some kind of brake to hold the absorber in place when it is subject to large forces [40]. However, there is the advantage that this control strategy does not require reactive power flows, which may make it appealing even though the absorbed power tends to be lower than alternatives [59].

Other Strategies

Many other control strategies are mentioned in the literature. Unlatching is another example which doesn't require reactive power flow. This is the dual of latching control strategies described above but where the natural period of the absorber is longer than that of the energetic part of the spectrum in the location. The absorber moves freely for part of the cycle and the PTO is engaged at a particular velocity [40]. This has similar mechanical challenges to latching due to the sudden change of forces due to the engagement or disengagement of the PTO load. [66] explores maximum power-point tracking using a 'perturb and observe' approach. There are also control strategies which do not just focus on a single absorber but explore how an array of individual WECs can be controlled to maximise absorption [67, 68]. There are also the possibilities of designing control strategies to optimise for variables other than absorbed power, such as LCOE [69]. The author recommends [40], [59] and [58] for more detail on this topic.

2.3.2 Summary of Control Strategy Review

In conclusion, many different control strategies have been proposed throughout the literature. However, most of these have only been implemented in models and not in hardware, often because the control strategies require reactive power flows and not many WECs have been constructed with this capability. Pelamis is an example of a sea-trialled WEC which was able to use reactive power control strategies [9], as is Corpower [70]. However, it seems that there is still a gap between the possible control strategies for optimising power absorption (or other variables) and the real hardware available with the capability to handle four-quadrant highly variable loads whilst producing the desired control force.

2.4 Digital Displacement Pump Motor Technology

DD hydraulic machines are an alternative to conventional variable displacement hydraulic machines which generally rely on swash-plate mechanisms, which have many intrinsic losses [13, 40]. The principle of DD is that the output of a fixed displacement radial pump can be varied by enabling or disabling its cylinders in real time, to meet system demand on a stroke by stroke basis [71]. Each radial piston is connected to a solenoid-controlled poppet valve, which the controller can enable or disable as the cylinder reaches bottom dead centre (BDC), which is the point of the piston's greatest extension i.e. its greatest volume. If an enabling decision is made, the solenoid receives a current pulse which results in a magnetic field around the valve, closing the low pressure (LP) poppet, so that over the following 180° of shaft rotation a pulse of flow (in the form of a half-sinusoid) is pumped to the system [71]. Figure 2.7 shows the fluid flow for a single cylinder through each of the low pressure valve (LPV) and high pressure valve (HPV) for idling and pumping. During the intake stage, for both idling and pumping, the LPV is open to tank as the solenoid has not been magnetised. As the crankshaft rotates from 0° to 180° (BDC) the piston-cylinder assembly (shown in yellow and orange) extends, drawing in flow from tank through the LPV. In an idling situation, the solenoid is not activated and the LPV remains open, so that during the rotation from 180° to 360° where the piston-cylinder assembly is compressing, the fluid is exhausted back to tank through the LPV. When pumping occurs, the solenoid is enabled around BDC, closing the LPV when the piston-cylinder is at its greatest extension. As the crankshaft continues to rotate, the fluid in the piston is compressed and the pressure increases, such that the HPV (which is a simple check valve) opens passively, injecting the pressurised fluid into the high pressure gallery. Once the fluid has left the piston, the HPV passively closes again and the LPV

solenoid is deactivated, connecting the pump to tank again for the next stroke.

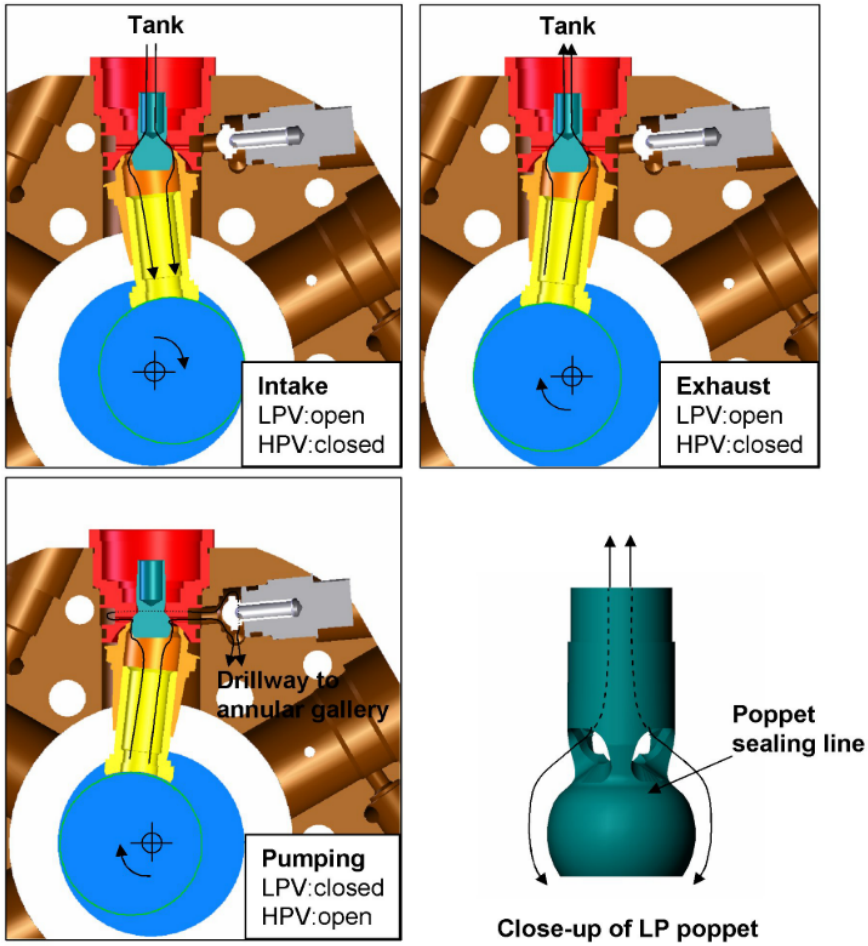

Figure 2.7 *Diagram of fluid flow in idle and pumping conditions for a single cylinder in an early DD pump [13].*

A DD machine typically has multiple cylinders arranged in a radial configuration, as shown in Figure 2.8. A group of cylinders arranged in line in the same axial section is called a bank (Figure 2.8 shows a single bank), and one DD machine may have multiple banks of cylinders and even multiple services (distinct HP outlets). Figure 2.9 shows a DDP with three banks of cylinders.

In addition to DDP machines, Salter and Rampen invented the DDPM, which can both pump and motor. In these machines, the HPV, as well as the LPV, is solenoid controlled. In a motoring stroke, the LPV is closed well after BDC, so that a very brief pumping stroke occurs as the piston approached top dead centre (TDC), pressurising the cylinder. At TDC the HPV is opened and the LPV remains closed, so that fluid from the high pressure gallery enters the chamber, producing torque on the shaft for half a rotation. Shortly before BDC, the HPV closes and the LPV reopens to tank, beginning the cycle

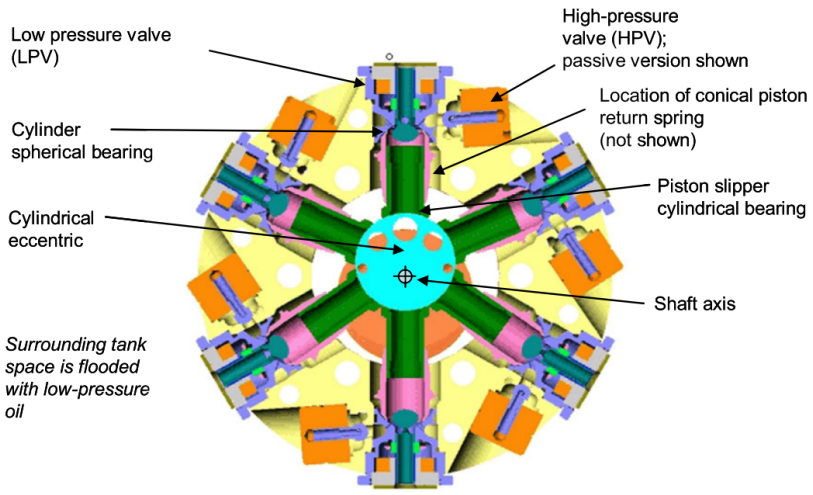

Figure 2.8 *Section of a radial-piston DDP, normal to the crankshaft axis, showing the arrangement of multiple cylinders around the crankshaft in one bank [13].*

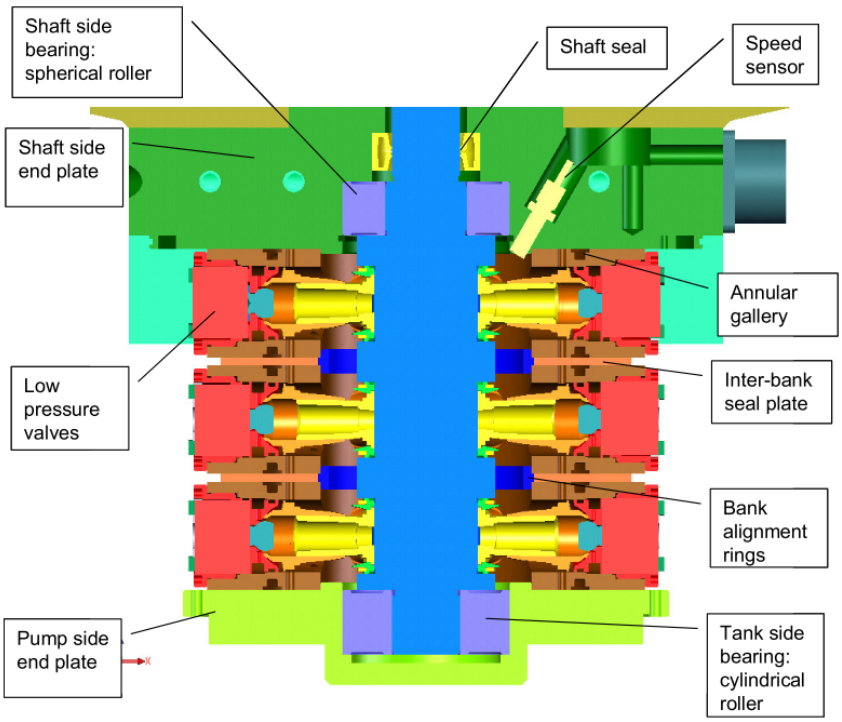

Figure 2.9 *Plan section of a DDP showing arrangement of three banks of cylinders [13].*

again. Figure 2.10 summarises the three different cycles of idling, pumping and motoring.

DD machines demonstrate very good efficiency across a broad range of operating conditions. Figure 2.11 shows measured efficiency results for the 'C2' DDP machine at full displacement, which peaks at 97%. They generally outperform conventional hydraulic machines such as swash-plate pumps quite significantly. Figure 2.12 shows a comparison between the C2 measured data, a simulated model of the C2 and a model of an axial swash-plate pump reconstructed from [14]. At full displacement, the C2 is more efficient across the entire operating map than the conventional pump, with the greatest differences being at low speed with high pressure and at high speed with low pressure. This improvement in efficiency at part load over swash-plate pumps means that DDPM machines are much more promising for hydraulic wave PTOs than conventional machines. Particularly the ability to manage variable flows and variable powers, with a fast response, combined with the ability to control pressure at variable speed make this technology very relevant to wave energy [72].

More detail on the development of DD machines can be found in [13] and [71].

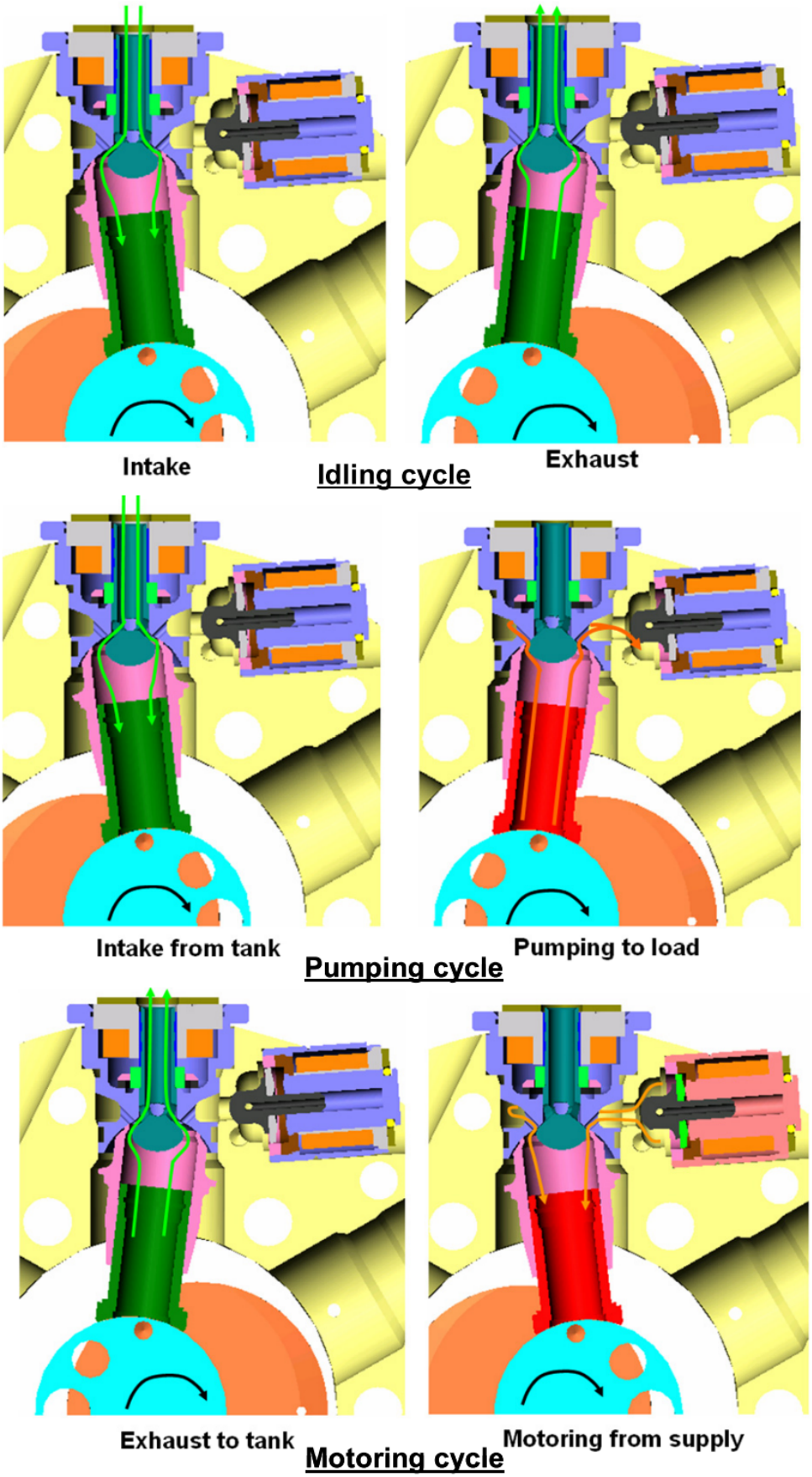

Figure 2.10 *Diagram of fluid flow for idling, pumping and motoring [13].*

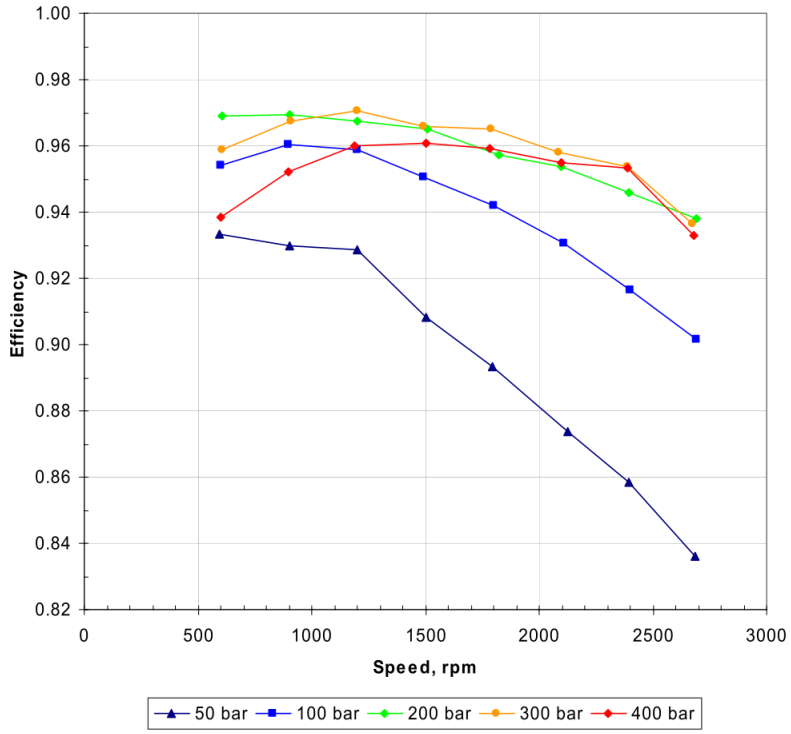

Figure 2.11 *Measured efficiency results at full DDP (known as C2) displacement presented in [13]. Lines are for different pressures, measured in bar*

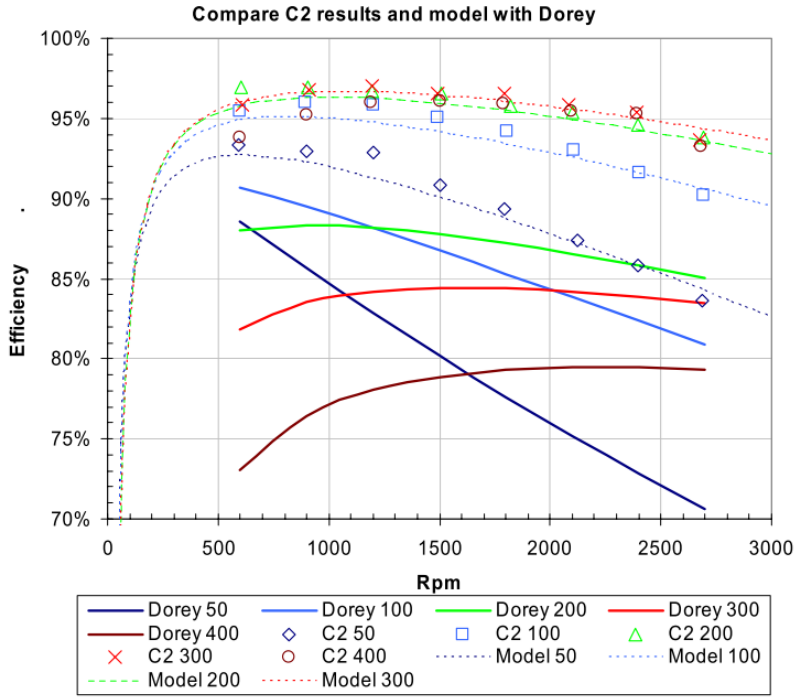

Figure 2.12 *Comparing C2 experimental data (points) with C2 modelled data (dashed) and Dorey's model [14] of an axial piston pump at full displacement [13]. Pressures are given in bar after the name of the model used, e.g. 'Dorey 100' means the Dorey model at* 100 bar.

2.5 Test Rigs for Experimental Testing of Wave Energy Power Take-Off

In terms of previous work test benches for the development of wave energy PTOs, the literature is fairly limited, both in terms of the number of studies in this field, and also the detail to which it is described. This is in contrast to the vast amount of information available on modelling wave energy systems or physical model tank testing. The most relevant work in the field is described below.

2.5.1 Pelamis Test Rigs

In the course of developing the Pelamis WEC, two test rigs were built to test the PTO [1]. One was a 1/7th scale model of the full WEC including a scaled PTO which was tested in a wave tank, and the other was a full-scale model of a single joint, actuated by an accompanying rig.

The 1/7th scale model PTO (shown in Figure 2.13a) was constructed with representative piston areas, control valves and accumulator sizes. Some hydraulic simplification was made as pilot valves could be omitted at this scale. In the dry test rig shown in Figure 2.13c a ball-screw operating under closed-loop control following a wave profile. This was mainly to develop the PTO control algorithm.

After this a single full-scale joint of the Pelamis (shown in Figure 2.13d was built in the lab and a 1 MW hydraulic actuation system was mounted to drive the Pelamis cylinders using a prescribed wave input. This rig was used to measure the primary and secondary transmission efficiency, and to validate simulations.

There is no mention of inertia in the rig, although it seems that, given the scale of the Pelamis WEC (180 m in length [9]), using a representative inertia at full-scale in a lab environment would have been impractical.

2.5.2 Wavestar PTO Cylinder Test Rig

An 840 kN test rig was built at Aalborg University to test a DDC, as shown in Figure 2.14 (capable of maximum forces of 420 kN for the Wavestar PTO [11]. The experimental emphasis appears to have been on effective and rapid switching between different discrete steps without causing undue pressure fluctuations or cavitation in the circuit. It was demonstrated that the test rig could emulate the velocity and position of a Wavestar

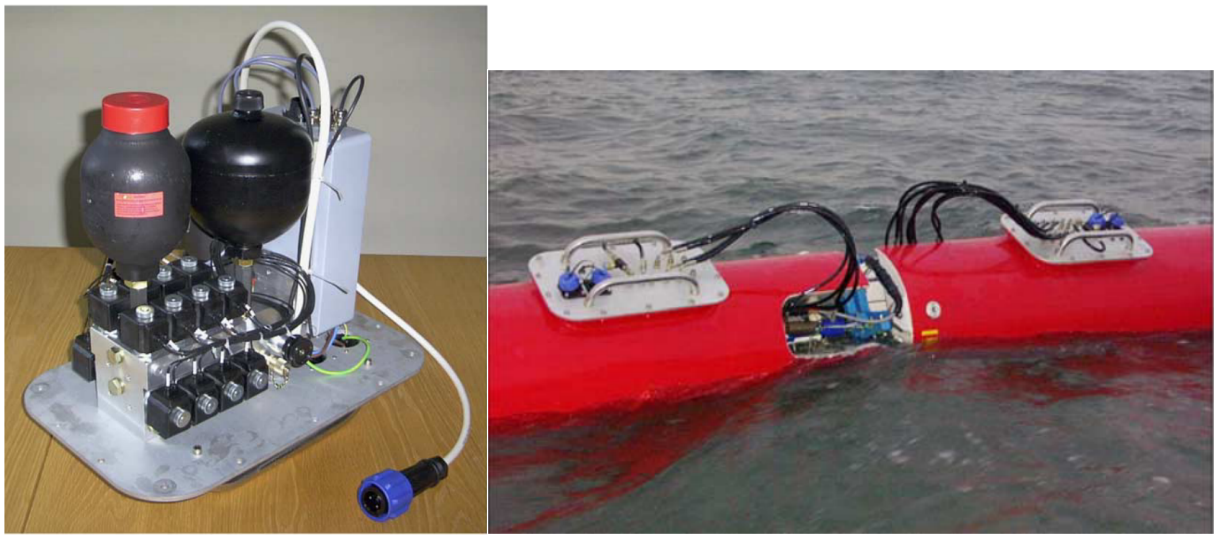

(a) (b)

(c) (d)

Figure 2.13 *(a) shows the 1/7th scale PTO, (c) shows the initial test rig for the 1/7th scale PTO, (b) shows the PTO in the 1/7th scale model during sea trials and (d) shows the full-scale Pelamis joint rig. Taken from [1]*

absorber float settling in calm water. This test rig was used to validate a Simulink model of the designed PTO. Testing was also carried out simulated irregular waves, where the average absorbed power was approximately 10 kW. It appears that there was also an effort made to actuate the cylinder in a way which was representative of the Wavestar float motion in irregular seas, but the details of this are not explained and it does not appear from Figure 2.15 that the test rig for the DDC involved any inertia [11]. A primary transmission efficiency result of 91.5% is reported for one bench-tested case of irregular waves but this single result is not a full picture of the performance of this PTO, since it does not represent the conversion of absorbed hydraulic power to electrical power and is only for one wave case. It should be noted that this bench-testing only seems to have encompassed linear damping of the PTO and no reactive control. More detail goes into the model validation and PTO design than the design of the test rig in this paper.

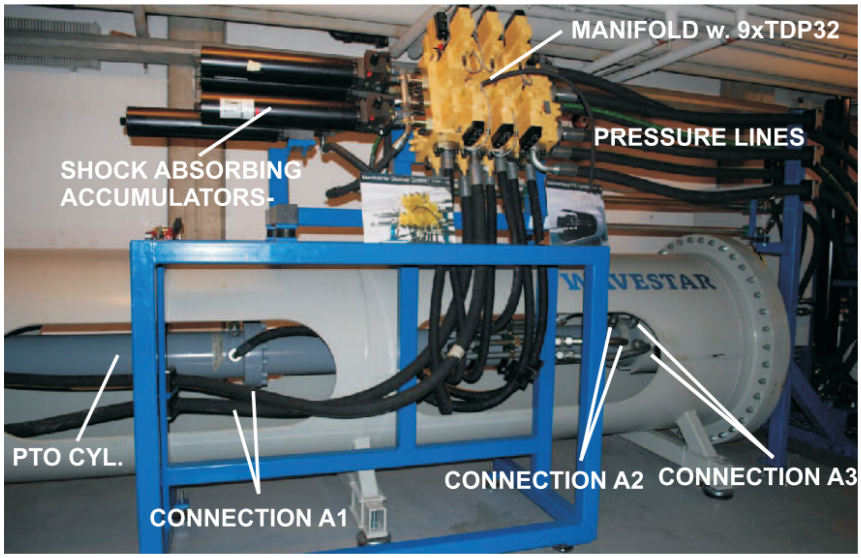

Figure 2.14 *Photograph of bench-tested prototype DDC from [11].*

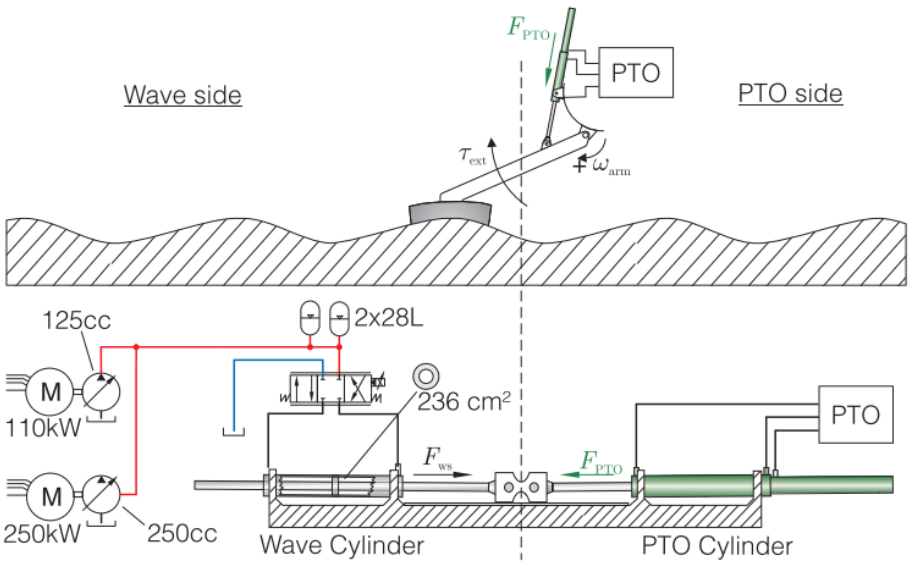

Figure 2.15 *Schematic of bench test setup for Wavestar prototype DDC [11].*

2.5.3 Wave Pioneer

[15] describes a test rig with an electrical PTO, built to emulate the full dynamics of a WEC system, including inertia. A WEC is modelled; a heaving buoy (with heave being the only degree of freedom) mounted on a winch attached to a rotary PTO. The 'WEC emulator' is rated to 30 kW and so Froude scaling was used to bring the modelled WEC dynamics down to a regime achievable for the emulator. The writers use a HIL system to control the rig so that the measured PTO torque applied by the lab PTO is used in the calculation of the hydrodynamic force from the WEC model.

The use of open-loop torque control and real inertias is a good approach to ensure that the dynamics of the sea-going system are represented. There were slight errors between the speeds achieved on the rig and what was expected from the model, particularly in the low-power sea states. This may be partly explained by imperfect matching of the inertia in the model to that entrained in the driveline.

The authors describe carrying out Froude scaling using the ratio of length between the full-scale WEC and the model-scale WEC, to bring the system represented within the capabilities of the lab system. However, a consequence of this scaling is that the rotational speeds involved increase. However the authors then say that after having carried out this scaling, they add inertia to the rig to reduce the rotational speeds to preserve the torque to speed ratio of the full-scale system, to assess thermal behaviour and keep the mechanical speed within the system's safe operating limits.

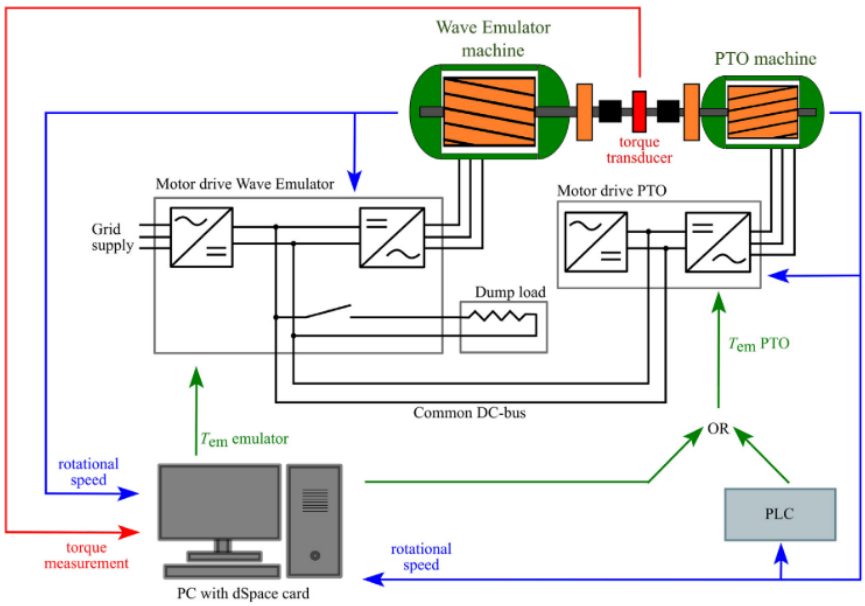

Figure 2.16 *Schematic of Wave Pioneer wave emulator and PTO from [15].*

2.5.4 WavePOD

[73] describes a test rig constructed to test the WavePOD, which was designed to be a standardised hydraulic wave energy PTO made with simple, lower-cost components. An 8% scaled power test rig was built at RWTH Aachen University in 2014. The maximum output power was 80 kW and the maximum input power was 1 MW. A scaled WEC model was employed in a HIL fashion, where the position of the model WEC was fed to the drive cylinder representing the WEC. The measured PTO force from the rig was fed back into this WEC model so that the calculated WEC response included the PTO force.

The work is continued in [74], where simulation and validation of results using data from the test rig described. Physical properties of the test rig were validated in the simulation, including pressure/flow characteristics of valves, valve response times, thermal effects in the accumulator and friction in the PTO cylinder. The authors acknowledge that further work is required to improve the accuracy of their model for control system development.

2.5.5 Linear Test Rig for Electrical Power Take-Off

[75] describes the construction of a test rig specifically for direct-drive linear electrical PTOs. This was rated to approximately 30 kW with maximum output force of 26 kN. This consisted of linear reciprocating prime mover which could drive a linear PTO. Little of the performance of the test rig is described as the paper focuses more on the build of the PTO which was tested.

2.5.6 Dry and Wet Test Rigs for Reciprocating Ball Screw Generator

As part of the WES Stage 2 PTO programme, Umbra Cuscinetti of Italy developed a ball screw which can convert linear motion to rotary motion [16]. The rotating nut acts as the rotor of an electrical generator.

A dry test bench was constructed, shown in Figure 2.17a, where the ball screw generator was axially connected to an electromechanical actuator (EMA). The EMA was controlled so that the ball screw was subject to a specific axial position profile. The electrical load here was purely resistive (i.e. damping). These tests were carried out to assess the generator performance for a range of axial screw speeds and electrical loads. The maximum speed tested was 0.95 m/s and the maximum force tested was 35 kN. The intention is to scale this prototype up to 60 kW but the report does not mention the force

or speed rating of the next iteration.

Wet tests were also carried out, in which the generator was attached to a point-pivoted buoy in a wave tank and subjected to both regular and irregular waves. Very little detail is given about how this test rig relates to an expected WEC system, for example in terms of representative speeds and forces. The ball screw generator was connected to a resistive electrical load again, so it seems that no tests have been carried out on the reactive power capabilities of this PTO. The efficiency was between 70 and 80% for most of the tests but there is no information about what operating conditions were the best or worst for its performance.

(a) *Dry test rig for ball screw generator.*

(b) *Wet test rig for ball screw generator with a point-pivoted buoy. The generator is attached to the blue frame on the left.*

Figure 2.17 *Photographs of ball screw generator test rigs [16].*

2.5.7 Corpower Dry PTO Test Rig

Whilst limited information is available in the literature about the Corpower test rig, some information was obtained from correspondence with the company. This is a HIL test rig (shown in Figure 2.18) with a peak power rating of 500 kW, capable of simulating a full range of sea states. This rig can simulate hydrodynamic loading in both heave and surge. The entire Corpower buoy was mounted horizontally on it and driven with a linear actuator. The main aim of this test rig seems to have been to test the machinery in the range of load conditions it would experience in Scapa Flow, to establish the reliability of components, rather than to represent the dynamics and inertias to test the PTO.

Figure 2.18 *Photo of Corpower HIL test rig (image supplied by contact).*

2.6 Summary

Wave energy extraction is a technically challenging area of engineering, as evidenced by the many approaches which have been attempted over the years, still without reaching commercial viability. The use of hydraulics in WEC PTOs has been suggested since the early days of wave energy design and many different PTO topologies have been proposed, although only a few have been tested at sea. OWCs systems using air turbines have been demonstrated but are necessarily location and sea-state specific. This means they are not broadly applicable, especially as they cannot effectively work reactively. Electrical direct drive systems have some advantages such as fewer conversion stages, but require complex power electronics to produce grid-compliant electricity and cannot easily store energy. Whilst developing any type of wave energy PTO is complex, the natural advantages of hydraulic systems for this application make them a compelling choice.

Hydraulics are intrinsically well-suited to wave applications due to the very high power density, even at low speeds, as indicated by the success of Pelamis. Pelamis demonstrated efficiencies of over 70% in real seas using a novel quantising approach to hydraulics. However, conventional hydraulic machines do not have the efficiency performance required for WEC systems. Conventional machines tend to have very poor efficiency at part load, which is an inevitable operating condition in a WEC. The impact of poor efficiency becomes especially marked when reactive control is used, as the power effectively flows both backwards and forwards through the PTO, experiencing the losses twice. Hydraulic machines such as DDPMs, as manufactured by AIP, have the controllability and efficiency necessary to handle the varying flows and torques inevitable in wave energy applications.

Many different control strategies for WECs have been proposed in the literature, with

a great number of different ways to maximise the power capture or other variables such as the LCOE. Of these, some, such as latching, would be mechanically very difficult to implement and subject the WEC structure to very high forces, making them somewhat impractical. The most profitable strategies in terms of power output rely on reactive power capabilities of the PTO and the ability to produce smooth torque following a demand signal. Very few control methods mentioned above actually have the PTO hardware available to either verify the control approach or reap the purported benefits of these systems. New control strategies are not especially useful until the existing ideas can be tested and more fully developed in practice. Whilst Pelamis did have reactive control, the quantised torque affected the hydrodynamic response and made these strategies relying on a smooth PTO torque unachievable. Developing a PTO with the capabilities required to utilise these control strategies would be a major step forward. The results of this research did indicate that the Quantor should demonstrate improved power capture on the test rig when using reactive control, instead of pure damping.

Many different test rigs have been constructed for wave PTOs of different topologies with different test purposes in mind. Some test rigs have been constructed for control system development, some for testing component reliability and some for testing the dynamics of the PTO in simulated irregular sea conditions with real inertia. Whilst the first two types are undoubtedly useful within their scope, they do not give full insight into the operation of the PTO in the sea. The latter type allows realistic hardware and software development, as well as being useful for troubleshooting and commissioning. Without a representative rig involving inertia, a control loop which works fine in the lab may be impossible to close in the sea. However, it seems that the majority of WEC developers have not invested in a step like this, perhaps feeling that it was too time-consuming or expensive. There are very few examples of dynamically representative test rigs and none that the author has encountered on a scale greater than 30 kW. Many problems of WEC PTO design emerge at scale, so care must be taken when interpreting the results from very low-power test rigs. This is a conceptually challenging type of rig to design, so the process of developing a representative rig at higher power scales is a useful contribution to the sector.

In the Quantor PTO itself, the use of quantised actuators is not novel, having been used in Pelamis and bench-tested for Wavestar. However, the combination of this with DDPM machines to smooth the PTO torque is novel. The learning from Pelamis is especially relevant to the Quantor, as there are various hydraulic engineering techniques (such as using a two-stage valve opening to the quantised chambers) which will greatly benefit the design and control of the quantised service.

The approach to the Quantor test rig is most similar to that of the Wave Pioneer, compared to the other rigs surveyed. The other rigs were designed with different objectives in mind and most make more compromises in how they represent the behaviour of the WEC in waves. In both the Wave Pioneer and Quantor rigs the aim is to use a real inertia to accurately represent model dynamics. The key difference between the two is that, rather than trying to preserve the full-scale torque-speed ratio, the speed of the PTO motors is perfectly preserved with that of the model WEC. Also, rather than applying Froude-scaling to a full-scale WEC, the Quantor hydrodynamic model is based on a half-scale WEC device, which is resonant in seas of energy period 3 to 5 s. The scale of the Quantor test rig is also an order of magnitude greater than that of the Wave Pioneer test rig, but the HIL approach and model WEC chosen are similar.

To conclude, the Quantor PTO project, with its novel combination of quantised control and Digital Displacement machines, is a new approach to hydraulic WEC PTO systems. It should represent a further advance on successful quantised hydraulic WEC PTOs by permitting smooth control torque. Many control strategies which have so far only existed in the literature should become practically feasible with the Quantor PTO. The design and construction of a test rig, capable of testing the Quantor with realistic inertias and dynamics at a power scale of approximately 300 kW, is also believed to be novel based on reviewing this literature. Therefore this project is building on previous literature by; expanding on the design of other PTOs; demonstrating practical feasibility of researched control strategies; and developing a WEC PTO test rig of greater scope, scale and complexity than existing examples.

Chapter 3

Quantor Stage 2 Project

Before embarking on the WES PTO Stage 3 Project, Quoceant and AIP completed a Stage 2 project to verify the technical feasibility of various aspects of the Quantor PTO. The aspects of this project which are most relevant to the thesis are discussed in this chapter, as this is prior work which gives context for both the Stage 3 project and the thesis.

3.1 WES PTO Stage 2 Aims

As described in Section 1.2.2, a key aim of the Stage 2 project was to demonstrate the control and machine functionality to successfully integrate AIP DDPM technology with a Pelamis-like PTO [2]. This essentially meant that the transforming function of the DDPMs had to be experimentally demonstrated, where DDPM B controls the pressure in one chamber and DDPM A smooths the shaft torque and exports power from the accumulator (see Figure 1.3a). There were other work packages as well, including simulation of various WECs with the Quantor PTO, control system development of the combined continuous and quantised functions, and techno-economic assessments (which are not discussed here).

3.2 Specification of Quantor for Stage 2 Project

3.2.1 Reference WEC

For the Stage 2 project the 'reference WEC' agreed on was a Pelamis single-axis system under the control of 8 or 12 chambers, with a moment arm of 4 to 5.5 m long. This

meant the PTO had a nominal load range of ±8 MN m with an individual discrete load step size of approximately 2 MN m. The target maximum instantaneous transmitted power was 3 MW in extreme conditions with 1 MW being a regular occurrence. The target average generated power while maintaining continuous control was 50 kW, with the quantised system being able to efficiently operate in average powers of up to 200 kW [42]. The desired damping coefficients are 100×10^6 to 250×10^6 MN m s/rad at response amplitudes corresponding to relevant 'power-generating' wave regimes. This reference WEC was chosen as a realistic example for the simulation and experimental work carried out on the Quantor.

3.2.2 Sizing of the DDPM

The sizing of DDPM B (which does continuous control) for the Quantor system was based on its flow limits and required responsiveness as it controls the pressure in one chamber. This affects the achievable PTO control gain and consequently the potential system performance. The PTO control gain is the relationship between the PTO motion and the forces it applies, which can also be described as the mechanical impedance of the PTO. It is often complex, with both resistive and reactive terms, so the relative phasing of loads and flows can affect the sizing of components. The expected limiting factors on the PTO control gain for the Quantor were the flow range and latency of DDPM B and its relationship with the hydraulic chamber size and speed, as well as the corresponding latency of the quantised system, signal measurements and control loops, and any stiffness or backlash in the system [42].

Flow Requirements

There are two contributions to the flow requirement for the DDPM; the geometric flow and the gain flow. The geometric flow Q_{geo} is due to the extension or compression of hydraulic cylinders at constant pressure and is given by Equation (3.1)

$$Q_{geo} = A\dot{h} \tag{3.1}$$

where A is the cylinder area and $\dot{h}$ is the speed of the stroke. The gain flow Q_{gain} is required to change the pressure of the chamber, given by Equation (3.2)

$$Q_{gain} = \frac{V}{B}\dot{p} \tag{3.2}$$

where V is the volume of fluid in the chamber to be pressurised (which is a function of stroke h), B is the oil bulk modulus and $\dot{p}$ is the rate of change of pressure. These equations give the total flow requirement Q_{total} of the DDPM (see Equation (3.3)).

$$Q_{total} = Q_{geo} + Q_{gain} = A\dot{h} + \frac{V}{B}\dot{p} \tag{3.3}$$

The geometric flow is in phase with the WEC motion and the gain flow is in phase with the load, which means that the total flow requirement is also dependent on the mechanical impedance required by the controller. If the controller is using a pure damping function to derive the required mechanical impedance, the geometric and gain flows will be out of phase, reducing the total flow demand on the machine [42]. There are additional complexities in the flow requirement due to the compressibility of hydraulic oil, as this changes non-linearly with response amplitude and frequency (which corresponds to the wave conditions) [42].

A damping term is required for net power absorption. Assuming a pure damping PTO system on the above reference WEC estimates a 500 l/min maximum flow is required to achieve the desired damping coefficients. With dominant damping terms in the load control, the geometric flow and gain flow are out of phase, which means that the maximum flow requirements for each helpfully do not coincide. In the case of this reference WEC, the geometric and gain flow requirements saturate in similar wave conditions, which simplifies the task of sizing the DDPM. This may be different in other WECs with different mechanical impedances or phasing [42].

The performance of the hybrid quantised-continuous (Quantor) system may degrade towards that of the pure quantised system in increasing waves where the WEC response is larger. The impact of this may be reduced by limiting the rate of change of the demanded moment to match the maximum DDPM flow, maintaining continuous control throughout.

The DDPM must be able to change flow rapidly to change the pressure in the continuously controlled chamber to counter the activity of the discrete system [42]. This may require a slowing of the discrete system pressure transitions to allow DDPM B to keep up, without reducing the overall rate of chamber pressurisation.

Pressure Control Requirements

The most significant control challenge for the Quantor system is matching the pressure changes in the continuously controlled chamber to the quantised pressure transitions. Figure 3.1 illustrates how the quantised transitions lead to rapid variations in pressure

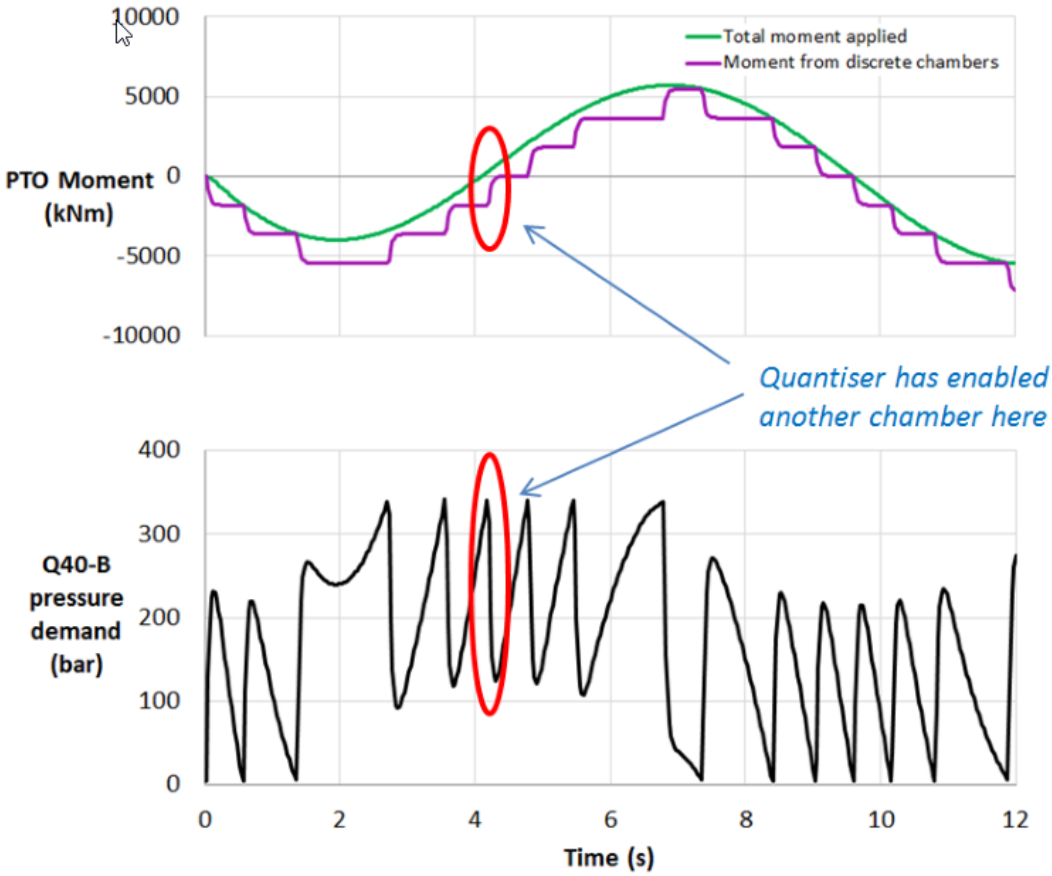

Figure 3.1 *Graphs showing the difference between the quantised moment and moment demand which must be supplied by DDPM B following the pressure demand in the lower graph [17].*

demand in the stiff service. This requires that the latency of the DDPM flow control is less than that of the quantised chambers, so that the DDPM can act simultaneously with the discrete system, and that peak rate of change of chamber pressures can be matched by the continuously controlled chamber, allowing the DDPM to cancel the step change on the total load. The quantised chamber switching valves in Pelamis consisted of digital valves with very high flow capacities, which can transition chamber pressure faster than the DDPM. However, such rapid changes will make the control problem described very challenging and may also cause pressure shocks affecting the whole PTO system. Using the adjustable mechanism of two staggered digital valves for pressurising and depressurising chambers were demonstrated in Pelamis to remove pressure shocks. A similar system may be applied in the Quantor PTO to tune the rate of chamber pressurisation and depressurisation so that it is compatible with the DDPM response [42].

The control of the pressure in the continuously controlled chamber, which compensates

for the error between ideal PTO demand and quantised system load, is achieved through the flow control of DDPM B. The main flow demand was produced from open-loop feedforward terms (for example from calculations estimating the required geometric flow), supplemented by a closed pressure control loop which acts to minimise any error between the desired chamber pressure and the measured chamber pressure [42].

To maintain continuously variable pressure across any residual gaps in the underlying quantisation process, DDPM B may provide a slightly higher pressure than the energy storage accumulators. Assuming a nominal rating of 300 to 350 bar for the main system, a 400 bar pressure limit for the DDPM B service was chosen.

The high part-load efficiency (see Figure 1.4) of the DDPM is of major benefit to this project. Whilst these losses will still be greater than those of the quantised chambers, the overall controllability and improved absorption of the Quantor system should outweigh the additional losses in a single chamber [42].

DDPM Stage 2 Project Specification Summary

- Two DDPMs on a common shaft providing transforming between two services
- Maximum 500 l/min flow rate for each of the two DDPM services
- Maximum pressure of 400 bar
- Rapid response, low-latency flow control of DDPM
- Control of DDPM pressure transitions able to match the quantised system transitions

3.3 WES PTO Stage 2 Test Rig

In Stage 2, a test rig was constructed with AIP hydraulic machines representing the flow and pressure from different components of a WEC so that the pressure control of a DDPM could be demonstrated with real hardware. Figure 1.3a shows the WEC system represented by this test rig illustrated in Figure 3.2b. The hardware tested was DDPMs A and B, which were two DDPM machines mounted on the same shaft connected to an electric generator. These machines were tested to demonstrate three key functions they would need to fulfil for Quantor to perform as desired;

- **Pressure control**: DDPM B must be able to rapidly vary the pressure in

the continuously controlled chamber to counteract the force steps caused by the activation or deactivation of quantised chambers.

- **Pressure transforming**: This is defined as the control of two different pressures on separate services of the same machine without any net energy transfer. DDPMs A and B can be considered as a single machine with two different A and B services, which operate at different pressures. For the power exported by the generator to be smooth, usable electricity, DDPM A must counteract the rapidly varying torque of DDPM B caused by the aggressive changes in pressure in the stiff service.
- **Power export**: Simultaneously with the above two functions, DDPM A must motor at a constant rate using the energy stored in the accumulator to export smooth and continuous power to the generator.

AIP had an available test rig known as Wind Rig 1 (WR1), which was originally used to develop DD PTO transmission for a 7 MW hydraulic offshore wind turbine. Figure 3.2b shows the laboratory schematic for this project, which was supposed to replicate the system shown in Figure 1.3a. The R110 DDP is a 340 l/ rev pump which provided a variable flow representing the output from the quantised system. The C40 DDPM (a 480 cm^3/ rev machine) represented the continuously controlled chamber. This test rig featured two 800 kW, 960 cm^3/ rev Q40 DDPM machines. One of these was modified to provide a two-service pump motor, which can be thought of as two distinct 480 cm^3/ rev machines on a shared shaft (see Figure 3.3. Q40 B was used to control the pressure in the continuously controlled chamber to demonstrate the capability of DDPMs to respond to rapidly varying pressure demand. Q40 A counteracted the variable torque produced by Q40 B and extracted power from the accumulator on the compliant service, to result in smooth output power from the generator which ran at a constant speed. This required the Q40 to first behave as a transforming machine which can convert energy at one pressure in one service to energy at a different pressure in a different service without consuming energy from external sources. Once transformation was demonstrated, exporting power to the generator followed by having Q40 A steadily motor in addition to its role in transforming. The Q40 ran at a constant speed of 1500 rpm which allowed the induction motor/generator to operate at synchronous speed, removing the need for power electronics when feeding electricity into the grid [42].

A HIL control system was used which had a real-time WEC model running parallel to the physical testing. The pressure setpoint for the continuously controlled chamber, flow demand for the C40 and input power demand for the R110 were calculated in the controller, and the measured pressure in the continuously controlled chamber and

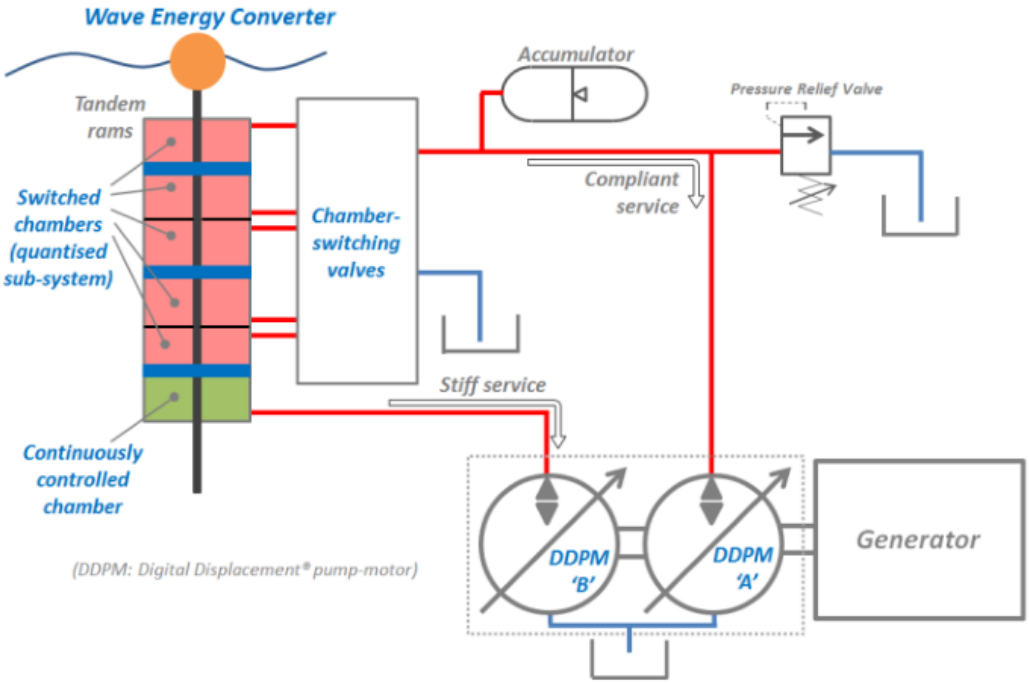

(a) *Schematic of Quantor with single-degree-of-freedom WEC (repeat of Figure 1.3a.) [2].*

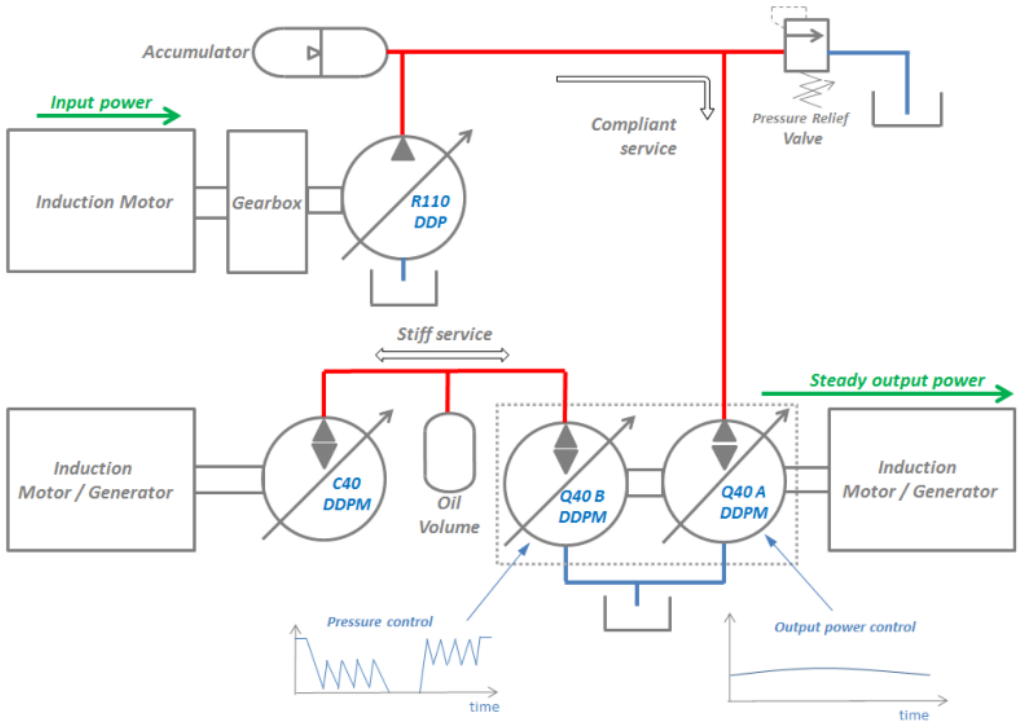

(b) *Schematic of Stage 2 test rig, analogous to the WEC and Quantor shown in Figure 1.3a. The development of the transforming DDPM (Q40) was the key outcome of the Stage 2 project [2].*

Figure 3.2 *Schematics of Quantor in WEC and of AIP experimental setup for Stage 2 project [2] shown together for comparison.*

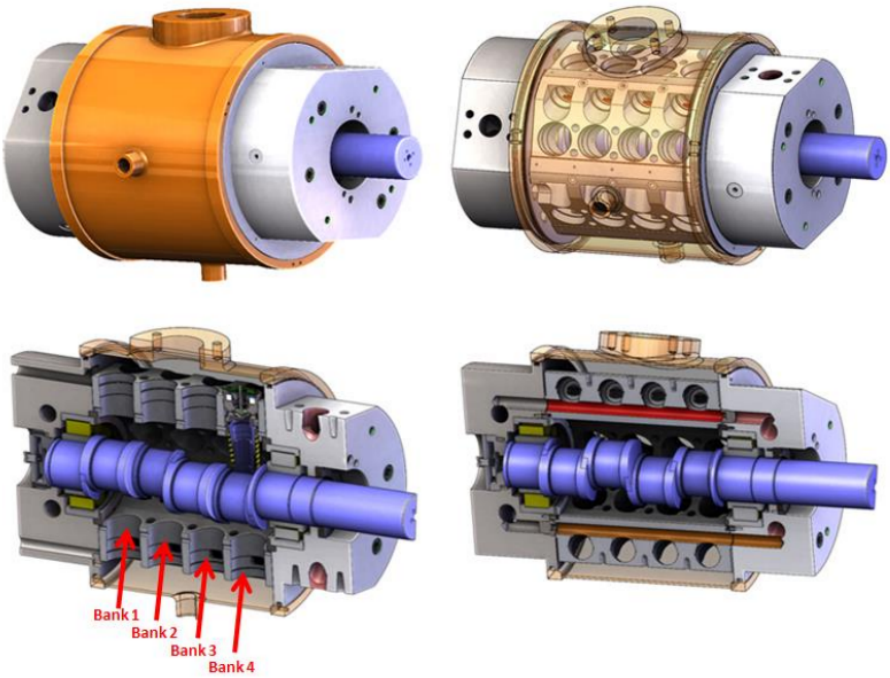

Figure 3.3 *The internal arrangement of the Q40 DDPM, showing valve positions in the crankcase, the arrangement of four banks along the crankshaft and the two different high pressure services (red and orange galleries) [18].*

quantised service were fed back into the real-time WEC model to calculate the speed and position of the simulated PTO cylinders, dynamically updating the system pressure setpoints to demonstrate continuous control of the generated power [42].

The continuously controlled chamber was represented by the fixed oil volume connected to the C40 DDPM machine. In a real WEC the chamber volume would vary due to the motion of the cylinder (Q_{geo} requirement) but this, and the changing pressure demand (Q_{gain} requirement), can be represented by changing the pressure with the C40. The compliance of this chamber was a key parameter to be matched between the rig and the reference WEC as this dictates the required rate of change of pressure and hence the possible control loop gain which can be used for stable operation [42]. To realistically represent the oil compliance, a large hose was added between the C40 and Q40 B high pressure services to increase the fluid volume, making it more representative of a hydraulic cylinder.

Figure 3.4 shows the hydraulic machines and their arrangement on the test rig in the Artemis laboratory.

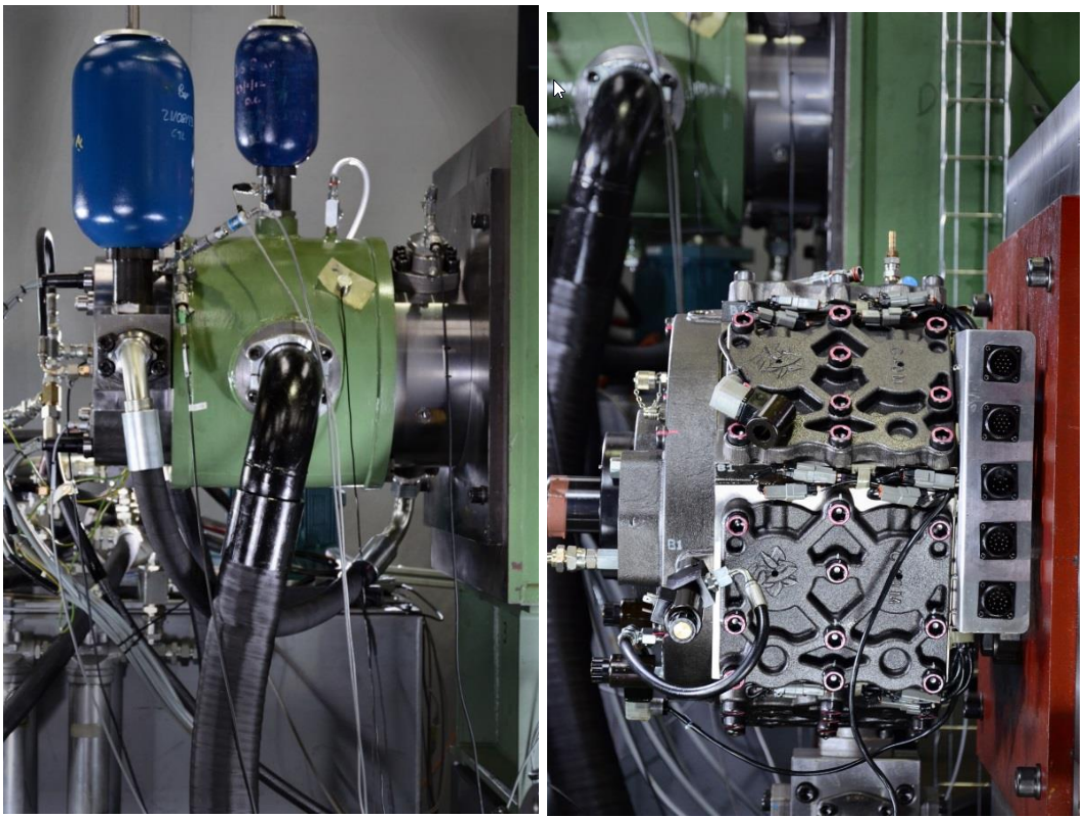

(a) **(b)**

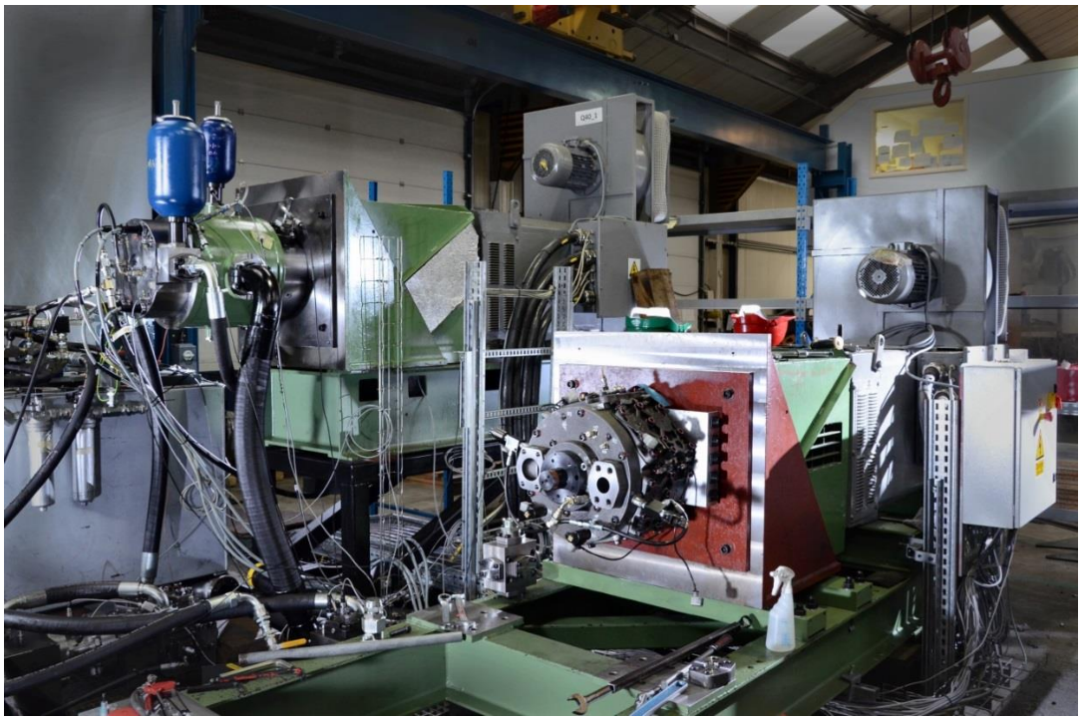

(c)

Figure 3.4 *(a) shows the Q40 transforming machine, (b) shows the C40 supplying the continuously controlled chamber and (c) shows these hydraulic machines set up in the test rig with their connections to accumulators, electric motors and hoses.*

3.4 Experimental Work

A number of preparatory tests had to be carried out to tune various parts of the test rig and ensure that control strategies were working as expected. These included Q40 efficiency tests, Q40 step-response tests, 'slug' response tests, pressure control setup and pressure transforming tests.

Figure 3.5 shows spot measurements of the pumping efficiency of the combined a and B services of the Q40 machine. Pumping efficiency η_p is defined according to Equation (3.4)

$$\eta_p = \frac{P_{fluid}}{P_{mech}} = \frac{Q\Delta p}{\tau\omega} \tag{3.4}$$

where P_{fluid} is fluid power, P_{mech} is mechanical power, Q is flow, Δp is differential pressure, τ is shaft torque and ω is shaft rotational speed.

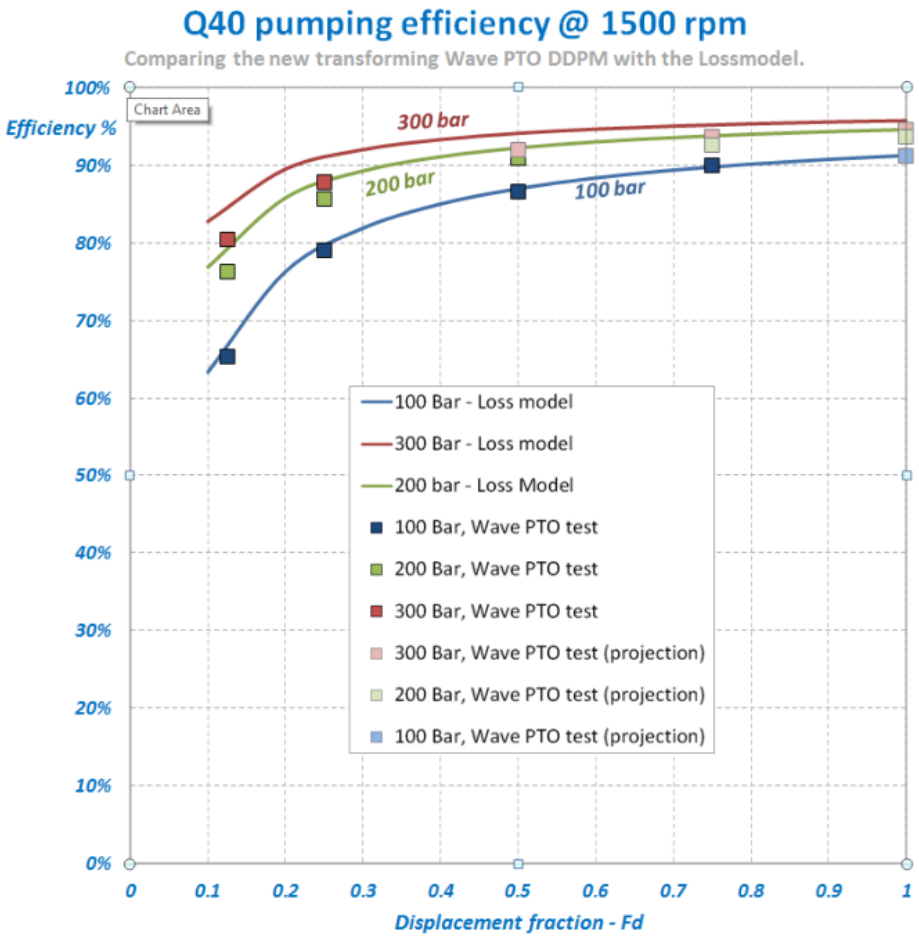

Figure 3.5 *Comparison of measured pumping efficiency of Q40 with loss model based on previous experimental data gathered by Artemis [17].*

The Q40 was operated at a constant speed of 1500 rpm and a pressure relief valve was

used to set the pressures at 100, 200 and 300 bar. Shaft torque and output flow were measured. The results show that there is good agreement with the loss model at 100 bar but that the results are several per cent lower at the higher pressures. This may be due to many factors such as machine age (the Q40 had previously been used to test the wind system), the two service modifications or different bearing design [17].

The Q40's step response capability was also tested, as the Quantor PTO requires very fast actuation of the Q40 B service in response to moment step-changes in the quantised chambers. There are two main sources of delay in step response; the command response delay between to control signal and the energising of the valve solenoid, and the valve response delay between the solenoid being energised and the valve being open [17]. The command response delay was measured by measuring the time between the displacement step command given in the controller and the increase in valve current which had a mean of 8.5 ms [17]. The valve response delay was measured by measuring the time between the rise in valve current and the production of the full demanded torque. The valve response delay was measured to be 32 ms at 1500 rpm [17].

The most challenging feature of the DDPM demand signal is the 'slug' response, which is the pre-emptive flow delivered to the continuously controlled chamber to counteract the rapid moment changes due to quantised transitions. Figure 3.1 shows how the pressure in the continuously controlled chamber should respond to the enabling or disabling of quantised chambers. The sharp pressure spikes corresponding to the required slug flow. Since the pressurisation of the quantised chambers is very repeatable, it was decided to pre-program Q40B to provide a counteracting flow profile timed according to advance knowledge of the quantiser transitions. The flow for a given rate of change of pressure is given by Equation (3.5) where V is the volume of fluid undergoing strain (i.e. the volume of the continuously controlled chamber), B is the fluid bulk modulus and $\dot{p}$ is the rate of change of pressure.

$$Q_{slug}(t) = \frac{V}{B}\dot{p}(t) \tag{3.5}$$

It was experimentally confirmed that the DDPM B service was capable of following the flow profile calculated for a change of quantised state based on the above equation, both for pumping and motoring, i.e. for both an increasing and decreasing quantised state [17].

After confirmation of the correct operation of all the feedforward terms, it remained to tune the pressure control loop for Q40 B, which was tuned to be as responsive as possible without causing instability [17]. The C40 was set to provide a range of different fixed flow rates in both pumping and motoring directions and it was confirmed that in all cases Q40 B could produce the sawtooth pressure profile demanded by the controller [20].

Figure 3.6, shows Q40 power in the three different modes of operation necessary for the Quantor project to succeed. First, Q40 B must control the pressure precisely in the chamber so that an overall smooth response torque will be experienced by the WEC. At this point Q40 A is idle. This process requires power from the electrical machine, which behaves as a motor. The spikes in the Q40 power reflect the rapidly varying torque on the shaft in this operational mode (as the electrical machine is running at constant speed). This kind of fluctuation is not acceptable for the generation of grid quality electricity. Second, transforming control is added to the pressure control, in which the A-side counteracts the B-side pressure control to smooth the torque seen by the generator. This neither consumes nor produces power and demonstrates simultaneous pressure control and transforming. Finally, power is exported via the A-side in addition to the transforming function. This shows that the required accuracy of pressure control could be achieved along with instantaneous power exchanges resulting in smooth average shaft power at the generator. The results shown in Figure 3.6 demonstrates a successful outcome of the Stage 2 project, in that the Q40 DD machine was indeed capable of performing its technically demanding role in a fully integrated Quantor system. During the exporting phase of the results shown in Figure 3.6, 112 kW is supplied by the R110 to Q40A (minus losses). 18 kW is absorbed by the C40 from Q40B, leaving a net of 94 kW of which 54 kW is exported to the generator shaft [20].

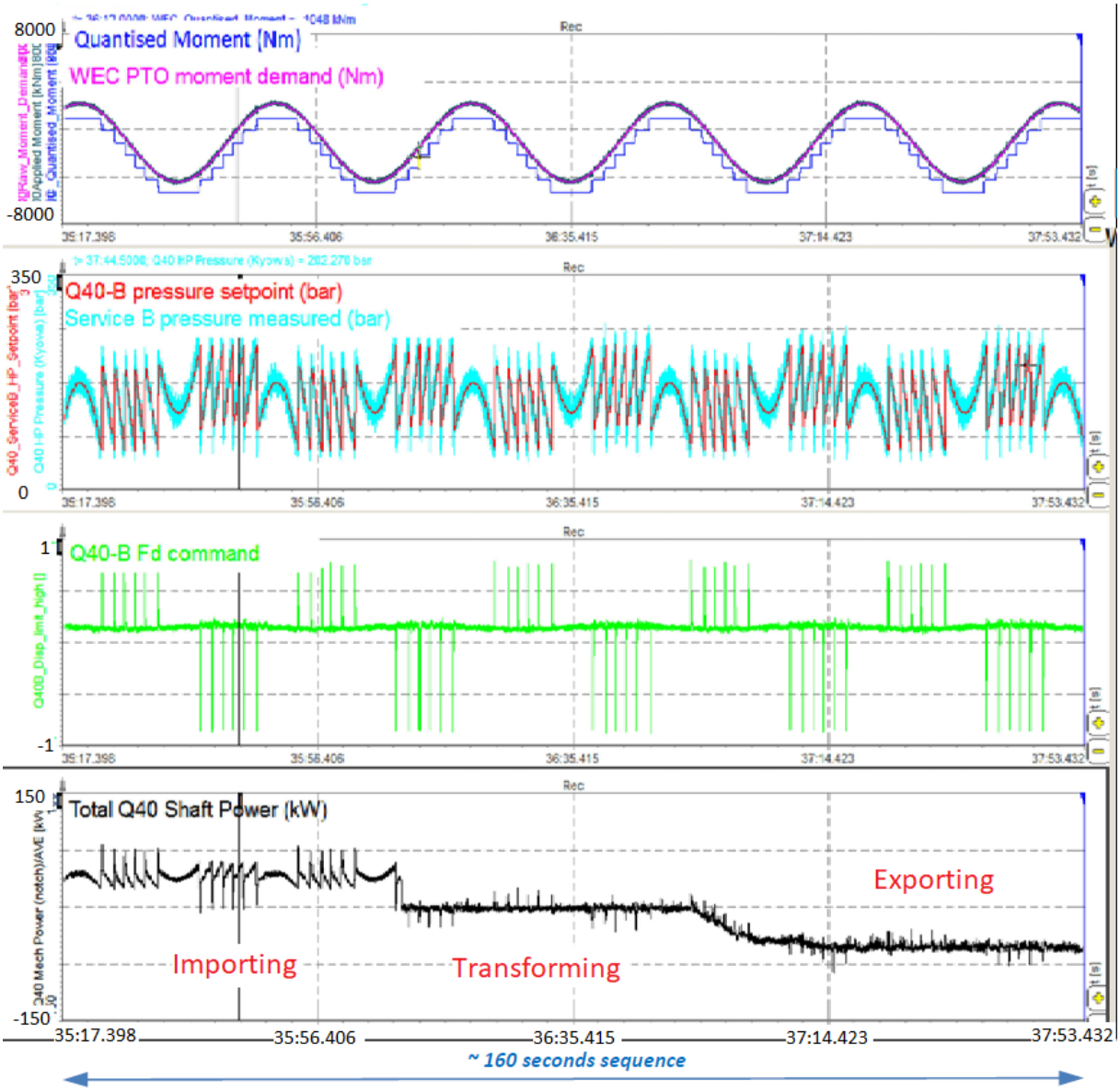

Figure 3.6 *Key experimental result of torque demand, service B pressure demand, service B Fd demand and DDPM shaft power against time, showing pressure control, transforming and exporting operation of two-service DDPM machine [2].*

3.5 Simulation of Quantor PTO

Simulation work was also a major component of the Stage 2 project. The potential performance of the Quantor was evaluated against the validated simulations of the Pelamis WEC to assess the benefit of continuous control over quantised control [2]. Simulations to compare between quantised and continuous control for a simple single-degree-of-freedom WEC (heaving buoy) to understand where the benefits of continuous control are most evident.

3.5.1 Simulation of Reference WEC (Pelamis)

The 'PELs' simulation suite was used by Pelamis Wave Power to explore the impact of different PTO systems on the performance of Pelamis [19]. Two distinct methods of control were applied to the Pelamis; multiple-input-multiple-output (MIMO) and diagonal control. In diagonal control, each joint of the Pelamis is controlled independently. In MIMO the force required at each of the eight joint axes is calculated with respect to the forces on all the others, giving an eight-by-eight control matrix [17]. The selection of appropriate hysteresis values is key for the performance of the quantised PTO. This should enable the quantiser to change state in a stable way which doesn't involve limit-cycling between two states. Figure 3.7 compares simulated results of smooth control and quantised control with differing hysteresis values. The limit-cycling behaviour of the green trace with lower hysteresis is shown, which is avoided by having a larger hysteresis value. However, it can also be seen that the larger hysteresis causes a more significant phase shift, which generally leads to lower power absorption. As was done for Pelamis, the minimum hysteresis value which prevented stuttering was applied [19].

Power table results were generated for this WEC for a range of representative ocean sea states. The probability of occurrence of each sea state of a particular significant wave height H_s and energy period T_e was calculated from a set of wave buoy measurements carried out by the EMEC. The sea states were assumed to follow the Pierson Moskowitz spectrum [19]. Power tables were calculated for different combinations of the parameters shown in Table 3.1. Note that the number of quantised steps $N = 2$ means that the states available are $-2, -1, 0, +1$ and $+2$. This was to establish the potential benefit to the reference WEC of the hybrid control in different conditions. The number of quantised steps available to the system is tied to the physical implementation of the PTO, in terms of how many ram chambers or fixed displacement motors are available. The more discrete states available, the better the system can track the ideal PTO demand with only quantised control. The phase shift introduced by the hysteresis may reduce the

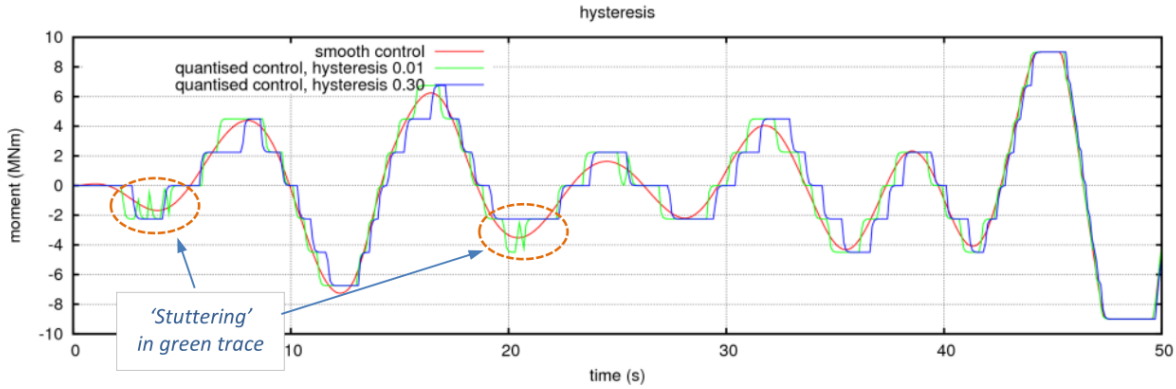

Figure 3.7 *Comparison of joint moment from continuous control and quantised control for two different hysteresis values of 0.01 and 0.3 [19].*

Table 3.1 *Parameters compared in power table analysis to understand the potential impact of Quantor PTO on power generation.*

Parameter	Options
Pelamis Control	Diagonal, MIMO
PTO Control	Quantised, Quantor
Number of quantised steps	2, 3, 4
Hysteresis	0.3, 0.6, 0.9
Sea States	H_s=0.75 to 6.75 m, T_e= 5.5 to 11.5 s

power capture, and comparing the results for different values of hysteresis will show how the different PTO control methods can compensate for this.

Conclusions

[17] provides fully detailed results from 30-minute time-domain simulations after the optimisation of control parameters for each case. Overall the main findings from the PELs simulations were that;

- Continuous control has a greater benefit in small and moderate seas.
- The diagonal control scenario benefits far more from the continuous PTO than the MIMO scenario.
- Larger increases in power capture with continuous control are available for systems with lower numbers of quantised steps, systems with limited reactive capability and those with low inertia which require greater hysteresis [17].

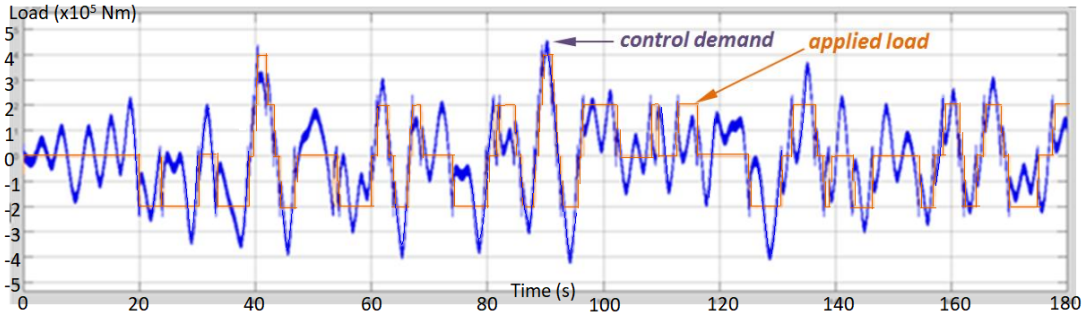

Figure 3.8 *Control demand and applied load of buoy in irregular waves with quantised control [17].*

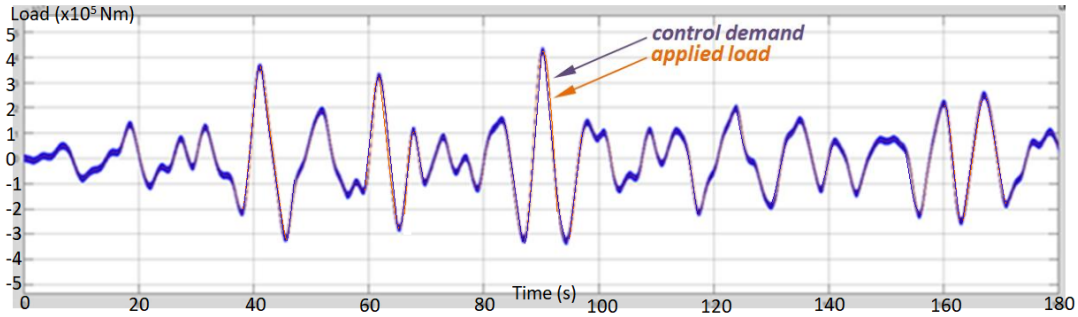

Figure 3.9 *Control demand and applied load of buoy in irregular waves with smooth control [17].*

3.5.2 Simulation of Heaving Buoy

In addition to the PELs simulation work on the Pelamis reference WEC, a Simulink model of a heaving buoy was built to explore the effect of Quantor relative to a purely quantised PTO on a single-degree-of-freedom WEC. This was conceptualised as a spherical buoy with a diameter of 5 m, anchored to the seabed, with the PTO extracting power from the heave motion referenced to the seabed. This had an annual average power of 20 kW. The PTO control coefficients were set to maximise power absorption by bringing the buoy into resonance and limiting the PTO excursion to less than or equal to the buoy diameter. The number of PTO steps $N = 2$, which means the quantisation is relatively coarse. Figure 3.8 and Figure 3.9 show the output from this model for both quantised and smooth control in an irregular sea of 2.25 m H_s and 8.5 s T_e, which is a relatively high occurrence sea state in the EMEC data. The hybrid control can perfectly match the demand load, whereas there are significant differences between the applied quantised load and the load demanded. The smooth control gave an improvement of 15% in power conversion over the quantised control. This confirms that the Quantor approach is likely to yield a significant performance improvement over simple quantised systems [17].

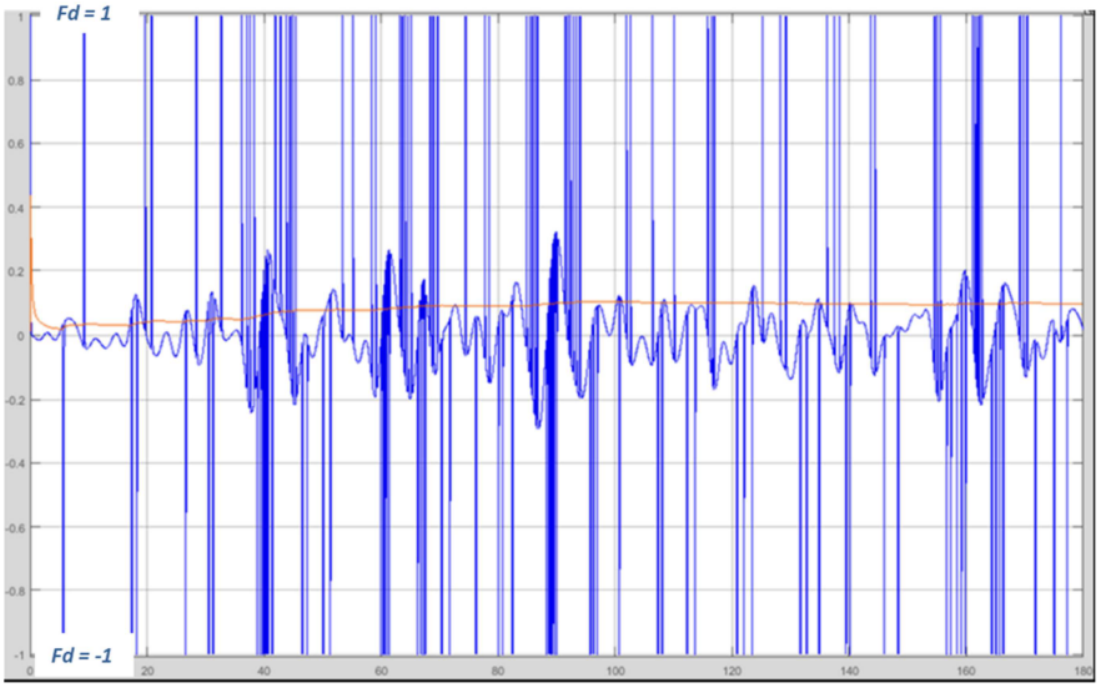

Figure 3.10 *Displacement fraction (blue) and cumulatively averaged absolute displacement fraction (red) of DDPM B in irregular wave simulation with H_s of* 2.25 m *and a T_e of* 8.5 s *[20].*

This Simulink model was also used to estimate powers and efficiencies for the Quantor in a heaving buoy in different wave cases [20]. The losses of the DDPM A and B services were of particular interest, as a fraction of the total system power. In a regular wave case, using ± 4 quantised states the average total power transferred was 100 kW. DDPM B provided on average 35% of the total joint energy transmission. The total energy loss of the DDPM was about 35% of its energy throughput, meaning that the DDPM loss as a percentage of the whole Quantor system power was about 13% (35×35). In an irregular case with an H_s of 2.25 m and a T_e of 8.5 s, which had an average power absorption of 30 kW, the DDPM is responsible for over 50% of the Quantor energy transfer because for much of the run time the forces are too low for the quantised system to engage in much of the power transfer. Since this DDPM operating point is a low speed, low displacement, high loss regime, the total power lost in the DDPM is 35% of the total Quantor power [20]. Figure 3.10 shows the displacement fraction of DDPM B throughout of the simulation. The large transient spikes correspond to the slug flow, but apart from these, the displacement fraction is very low, averaging out to about 0.1. This is an operating regime of high loss for the DDPMs.

In a more energetic irregular sea with an H_s of 3.375 m and a T_e of 8.5 s the total power transmitted increased to 75 kW. The DDPM had an average loss of 48% whilst handling

35% of the total power transferred, giving a net loss of 17%, which is only slightly higher than that of the regular case. It is suggested that increasing the average F_d to 0.25 would bring the average efficiency up to over 80%.

Conclusions

This study showed that for the Quantor to perform at an acceptable efficiency, the sizing of the system is critical. It is necessary that both the average displacement of the DDPM should be as high as possible without saturation, and that a good proportion of the energy should pass through the quantised system [20]. The large size of the DDPM is necessary to provide the large transient flows, yet the displacement is relatively low between the quantised transitions. If it were possible to match the DDPM size to the geometric and gain flow requirements, disregarding the slug flow, a smaller machine could be used which would result in a proportionally higher displacement and therefore higher efficiency. A way to do this was suggested: using a flexible number of continuously controlled chambers, where the DDPM can control more chambers in small seas, maintaining an acceptable displacement fraction [20].

It was concluded based on simulation that the Quantor could provide a net improvement in annual net power absorption over a single degree of freedom state-of-the-art (SOTA) system of between 5 and 24%, depending on the size of DDPM B.

3.6 Summary

The key aims of the Stage 2 project were to de-risk various technical challenges of the Quantor PTO concept. The most critical of these was to confirm that AIP DD machines were capable of responsive pressure control which could counteract the load steps in a quantised system, transform energy between two services and export smooth power to a synchronous generator. These aims have all been met through the experimental work carried out on WR1 at AIP premises. This meant that a functional control system was developed for the transforming DDPM which can then be extended to include more Quantor functions in the Stage 3 project.

Simulation work explored the potential benefit of Quantor to various types of WEC in different conditions and helped identify potential improvements to the Quantor system. It was shown that the Quantor offered limited benefit to a multiple degree-of-freedom, high inertia system with MIMO control such as the Pelamis, because the control already implemented in this system approximated continuous control. However, it offered much

greater benefit to the same system with diagonal control and simple systems with limited degrees of freedom and low inertia. Systems of this type are far more common, as they are cheaper to develop. Very few companies at this time are developing WECs of the inertia and scale of Pelamis, and the majority of active developers' machines fall into the latter category [45, 76].

The key area of improvement identified was the sizing of the DDPM, which operates more efficiently when it uses >0.25 of its displacement range. However, the need for large transient (slug) flows resulted in the DDPM being oversized for the majority of its runtime. The strategy of using a variable number of continuously controlled chambers were identified to reduce the necessary size of the DDPM and implemented in the Stage 3 project.

This work meant that the Stage 3 project could go ahead with confidence that the fundamental DDPM pressure control, transforming and exporting functions had been demonstrated, and with the beginnings of a full Quantor control strategy that could be adapted to the needs of the Stage 3 test rig.

Chapter 4

Quantor Efficiency Modelling

4.1 Introduction

A significant aspect of this project and the WES Stage 3 project was modelling the Quantor PTO. This was necessary both for control strategy development and performance modelling. One of the desired project outputs was a Simulink model of Quantor which had been fully validated using data from the Quantor test rig at AIP. This model can then be used in conjunction with developers' WEC models to explore how a Quantor PTO would work in their system.

The control of the Quantor is complex, as two DDPMs must be controlled in addition to a large number of switching valves. This must happen in response to the measured speed and position of the WEC PTO shaft, i.e. there is no overarching predictive control. This must be able to handle the highly variable input loads of irregular seas with good instantaneous power absorption and smoothing of the power output. Developing valve-switching algorithms and the DDPM control in a model-based environment was very beneficial for the project.

It was also important to understand in advance of using the test rig how the various parts of the Quantor would interact. Whilst Pelamis had extensively tested the quantising PTO functions with linear actuators, and AIP have experience of using DDPMs in a broad range of applications, combining these systems had a lot of potentially unknown consequences. Whilst the WES Stage 2 project had de-risked some of the technical aspects of the Quantor (for example, the rapid-response pressure control and tandem DDPM transforming functions), it used supply pumps to emulate the behaviour of the quantised and continuous service inputs from the PTO actuators. This means that using

the hardware for the actuators and valve switching is a major novel technical step and requires careful consideration. This is especially true as it involves the use of very complex components with behaviours which may not be easy to predict, such as the manifold block for switching the chambers.

Estimating the performance of the Quantor in advance of testing with the WEC emulator was considered an important aim, as this would give some sense of what performance to expect to see on the rig. Therefore if the real Quantor performance was falling short of the modelled Quantor performance, it could be explained by either an inaccuracy in the model (which could be improved with test rig data) or by a problem with the hardware or software on the rig which needed to be resolved. Setting this performance benchmark in a range of wave conditions was, therefore, a highly valuable exercise. An iterative two-way process was then followed, consisting of adjusting the model to be more realistic with measured data, and improving the hardware behaviour to more closely match the ideal model response. The performance benchmarking was initially carried out by modelling the Quantor installed on a hypothetical simple WEC, in four different wave conditions, two of which were regular and two irregular. Details of the model and results are discussed below in Section 4.2.

4.2 Description of Technology

The Quantor PTO is based on the Pelamis PTO, with an additional continuous service to smooth the output PTO torque. The Pelamis PTO used a novel digital approach to provide a discrete set of net loads from pressurising or not pressurising individual piston areas. This 'quantised' system could approximate continuous control by choosing the number of discrete load steps which were enabled (pressurised) at any one time [42]. This system meant that absorbed power was transferred directly to (and from) the energy storage accumulators, so that instantaneous power absorption could be very high with minimal losses (only a few per cent flow losses through the valves and pipework) and absorbed power was decoupled from average exported power. This PTO demonstrated an average wave-to-wire efficiency of over 70% in real seas [1].

However, a disadvantage of this discretised system was that the PTO could only provide a quantised approximation to a continuously variable load, which limited the power absorption [42] and made the system inapplicable to low inertia WEC types where the quantised resolution would have been too coarse. A compromise is required between the WEC mass, the quantised step size, and the resulting distortion in control. Control strategies which could yield power or reliability performance improvements rely on

continuously variable PTO force to achieve optimal power capture.

Adding a continuously controlled load of the same range as one or more of the quantised load steps would make it possible to achieve continuous control across the full load and power range. For this to work, the control of the continuously variable load must be fast enough to compensate for the step changes in the underlying quantised load [42]. Figure 1.2 shows the idealised Quantor concept combining a quantised system with a continuously controlled load, producing a smooth PTO load which can follow the ideal demand from the controller.

Figure 1.3a shows a simple schematic of the Quantor PTO with a single-degree-of-freedom WEC with linear hydraulic actuators (cylinders). These cylinders have multiple chambers, like those used in Pelamis. As the WEC moves in heave, the Quantor PTO system must provide the required PTO load for extracting power, consisting of both resistive and reactive components. The quantised chambers are connected via the digitally controlled chamber switching valves (housed in manifold blocks) to either the accumulator or to tank. This means they provide steps of force or torque as shown by the red line in Figure 1.2. Hydraulic energy collected by these quantised chambers from the WEC is buffered by the accumulator which functions as a compliant energy store. Meanwhile, the continuously controlled chamber is connected to a DDPM machine (DDPM B), which provides the smoothing contribution (green line in Figure 1.2) by controlling the chamber pressure at high bandwidth. This rapidly varying pressure signal from DDPM B results in a similarly irregular torque on the common fixed-speed shaft, which is connected to the generator and an opposing DDPM machine (DDPM A). The role of DDPM A is both to counteract this irregular torque, smoothing the output to the generator shaft; and to extract energy from the accumulator to provide a net power export.

Whilst it is anticipated that the Quantor will generally have one PTO actuator bidirectionally controlled by the stiff service, the system is flexible enough to use other options. Similarly to the Quantor Stage 2 project a single actuator could be operated unidirectionally by the stiff service. Or multiple PTO actuators could be bidirectionally operated by the stiff service, which may improve the efficiency in low energy sea states.

Whilst the Quantor PTO could function with either linear (multi-chambered cylinders as in Pelamis) or rotary (fixed displacement pump-motors) actuators, rotary actuators were chosen for the Quantor test rig, as they were more applicable to the current WEC market and more appropriate for the space available. Whilst Figure 1.3a shows a WEC with a linear system as an example, the model used rotary PTO actuators as a rotary system will be constructed for validation on the test rig.

4.2.1 Valve Manifold Block

The manifold block is a key component and has many functions within the Quantor, but the main purpose is that it connects the appropriate motor ports to either the HP gallery, DDPM gallery or LP gallery according to the control algorithm acting in real-time. Each fixed displacement motor (or linear actuator) has a corresponding manifold block to control its port connections. Each manifold block contains approximately forty valves, twelve of which are solenoid-operated and seven of which have manually tunable settings, such as adjustable pressure relief valves or needle valves. Figure 4.1 shows the hydraulic schematic of the manifold block.

Quantising Control Function

Figure 4.2 shows the manifold block schematic with the relevant components to the quantising function highlighted. The quantiser discretises a smooth PTO torque demand by connecting actuator ports to either high or low pressure almost instantaneously, resulting in a step-change in the torque. The torque can be stepped up or down according to the demand by pressurising or depressurising actuator chambers in the relevant direction. Pressurising an actuator chamber means connecting it to the HP gallery, and depressurising means connecting it to the LP gallery, both of which are marked.

The motors chosen for the PTO actuators can be pressurised on either port but not both simultaneously. (If simultaneous pressurisation of both ports was possible more options would be available for the control algorithm.) A convention was chosen so that motor port A being pressurised generated torque in the positive direction and port B being pressurised generated torque in the negative direction (see Figure 5.6 for a diagram of the rig torque convention). To allow for either motor port to be pressurised and depressurised, four sets of valves are required, as shown in Table 4.1. However, rapid pressurisation and depressurisation of the chambers would cause significant transients which would make stable control of the system challenging, as well as increasing the shock loads on the system which reduces the lifetime of components. Therefore the pressurisation and depressurisation processes are split into two steps, the first of which is opening the desired transient flow valves to change the chamber pressure to that of the relevant gallery, and the second of which is opening the accompanying main flow valve to which allows the majority of the flow into or out of the chamber to happen. This method for reducing transient behaviour was demonstrated in Pelamis [49]. Figure 4.2 shows eight different sets of quantising valves, with the transient flow valves indicated in

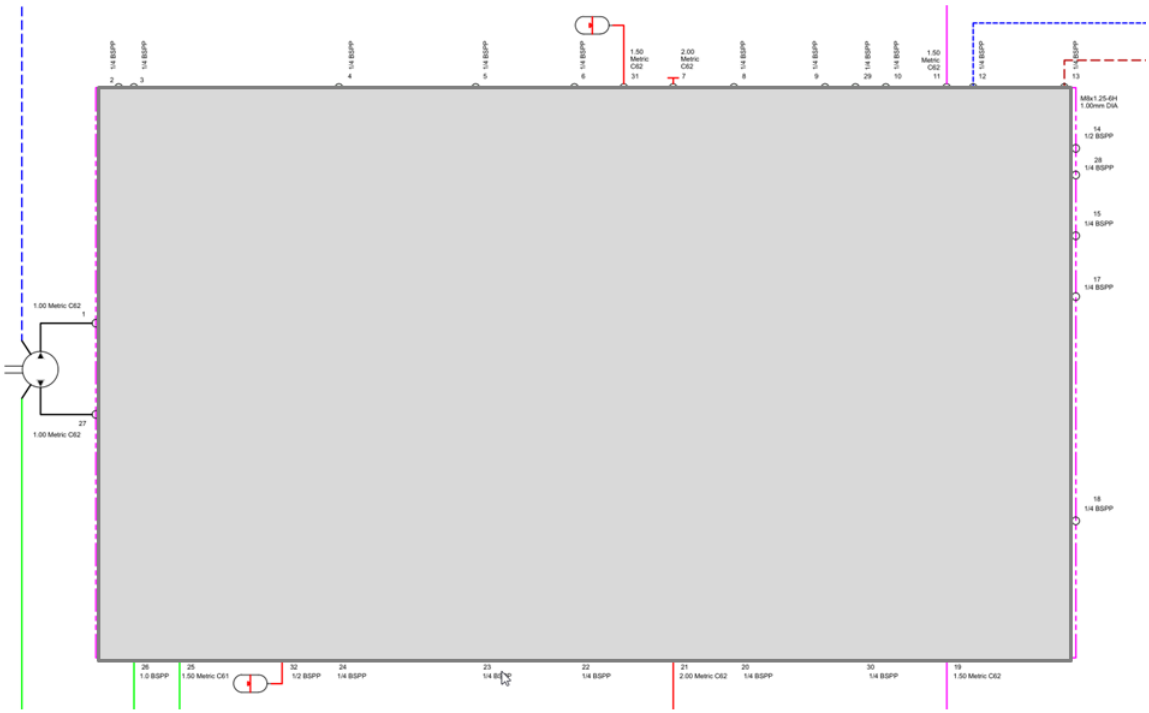

Figure 4.1 *Manifold block schematic (redacted)*

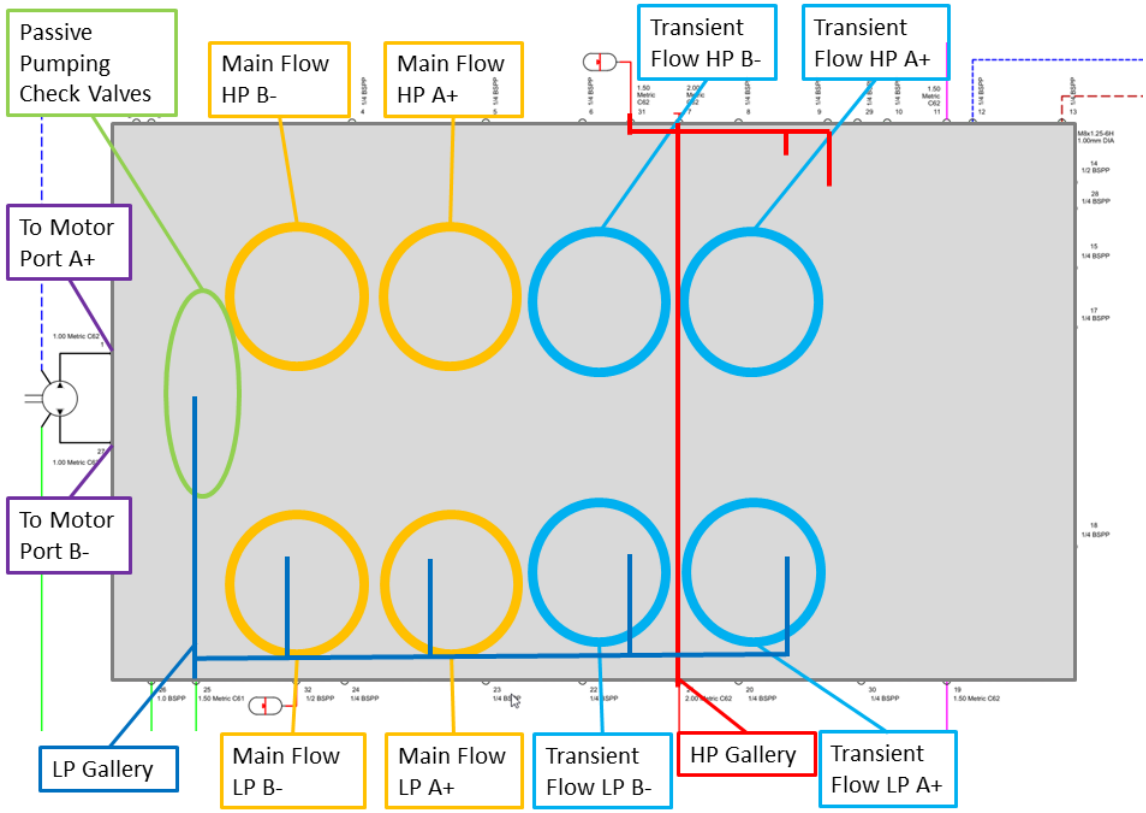

Figure 4.2 *Schematic of manifold block indicating the valves used for the quantising function (redacted).*

Table 4.1 *Matrix of quantising valve names and functions*

Process	Port A+	Port B-
Pressurisation	HP A+	HP B-
Depressurisation	LP A+	LP B-

bright blue and the main flow valves in yellow. In reality, two valves are circled in each case: this is because the solenoid valve which is operated by the controller opens the pilot pressure to the pilot-operated flow valve (main or transient). This means there are, in total, 16 active valves associated with the quantising process per block. The adjustable needle valves on the outlets of the transient flow valves can be used to tune the rate of chamber pressurisation.

There are also passive pumping check valves, which allow the PTO motors to passively pump in either direction into the HP accumulator even when the quantising control or continuous control are not active on the block. This protects the motor from dead-heading.

Continuous Control Function

The role of the continuous control is to provide smoothing torque to correct the error between the quantised torque and the ideal PTO torque demand. This torque must operate both positively and negatively, but the pressure is always positive. There are therefore directional switching valves which change the motor port where pressure from the stiff service is applied, depending on whether the torque demand is negative or positive. The opposing port is then opened to low pressure using the quantising valves described above.

Since the passive pumping check valves can allow flow from the stiff service into the HP accumulator, a way to separate the motor from the compliant service when under continuous control was required. The DDPM engaged isolation valves close the connection between the HP accumulator and the gallery where the passive pumping check valves are, meaning that the compliant and stiff services can generally operate independently. This is important as for the stiff service to be able to fully correct the quantised torque steps, it must have some pressure bandwidth above that of the compliant service for smoothing. However to prevent the pressure in the stiff service from getting too high, a tunable overdrive relief valve is included. This can be set to a chosen pressure value, meaning that if the pressure of the stiff service is greater than the pressure of the compliant service by more than this chosen value, the excess pressure is relieved into the HP accumulator

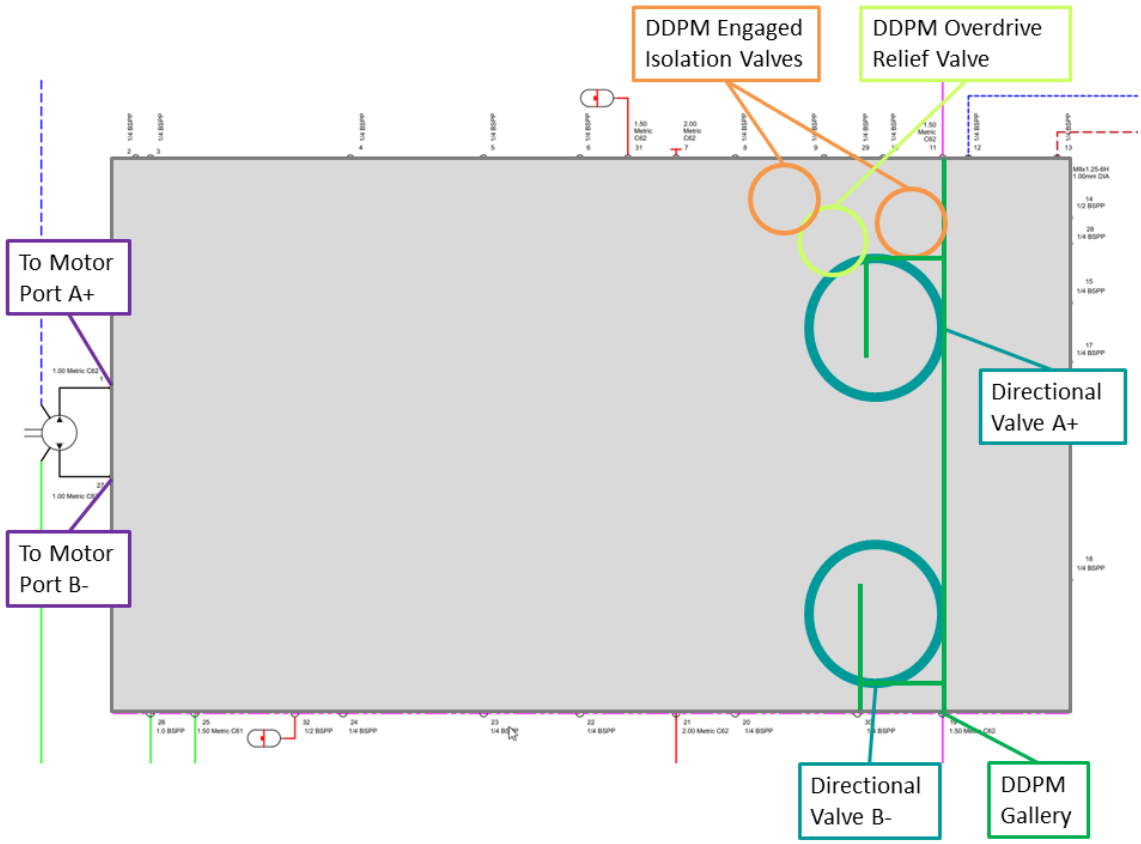

Figure 4.3 *Schematic of manifold block indicating the valves used for the continuous control function (redacted).*

and not to tank. This means that not all the energy extracted from the WEC into the stiff service is lost in the event of a pressure spike, as the pressure drop is some tens of bar rather than around 400 bar.

There is also a further function of the continuous control which actually relies on the use of the quantising valves. When a quantised step of torque is applied to the PTO, the stiff service must respond by counteracting this step of torque precisely and instantaneously to keep the total PTO load smooth. This involves a rapid increase or decrease of pressure in the stiff service, which would require a large instantaneous flow from DDPM B. In the Stage 2 project, it was found that sizing DDPM B to be able to produce this large instantaneous flow meant that it was generally operating at a very low proportion of its displacement (at all times apart from these large transients) and therefore was not working as efficiently as it could [20]. These transients were provided for using the 'slug flow' (see Section 3.2.2), and the number of chambers connected to the stiff service was made variable for Stage 3, so that more chambers could be connected to the continuous service in cases where the displacement of DDPM B was very low.

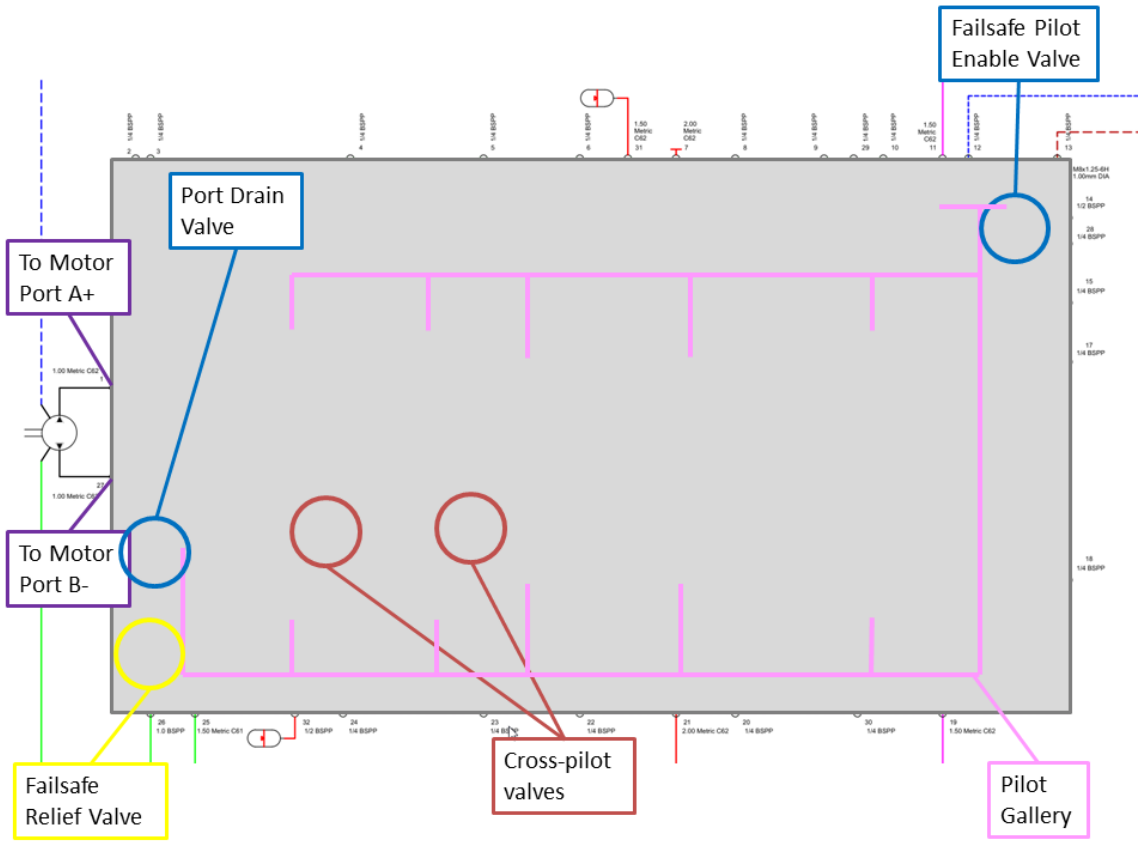

Figure 4.4 *Schematic of manifold block indicating the auxiliary valves (redacted).*

Auxiliary Functions

Figure 4.4 shows the auxiliary valves in the block which are not directly involved in either the quantising function or the continuous control function. The failsafe pilot enable valve connects pilot pressure from the pilot supply manifold (outside the block) to the block's internal pilot gallery (highlighted). None of the other controlled valves in the block can operate without pilot pressure, so the failsafe valve must be enabled before the block can perform any other function. This is an important safety feature for the test rig and also for a possible WEC deployment, as it provides a way of hydraulically shutting down each manifold block in the Quantor.

As well as supplying pilot pressure to the pilot gallery, engaging the failsafe pilot enable valve also closes the port drain valve. This means that any pumping by the PTO motor is diverted into either the HP gallery or DDPM gallery, rather than out to tank via the failsafe relief valve. The setting on the failsafe relief valve should be a pressure of at least a few tens of bar, as in an emergency shutdown situation the pumping of the motors against this relief valve will provide some hydraulic braking against the motion of the

PTO shaft.

The cross-pilot valves prevent simultaneous pressurisation of both ports on the motor by relieving into the LP gallery if both ports are pressurised to over a set pressure determined by a manual setting on the valve.

4.3 Description of Model

4.3.1 Model Overview

Figure 4.5 is a schematic of the system which was modelled. A time-series of regular or irregular waves was fed into a simple WEC model (acting only in heave), which was then used to calculate the PTO shaft speed. This was fed into the modelled splitter gear which divided the applied torque between four fixed displacement PTO motors. These are connected via hoses (which are all of equal length) to the ports on the manifold blocks. The active valves within each manifold block were modelled so that the model had the functionality of the ideal real block but did not include auxiliary functions like the pilot gallery. Each block had an HP and LP shock accumulator, and had the compliant and stiff service steel galleries running through them. The compliant gallery was connected to the HP accumulator model and back-up bottles via a hose. It was also connected to the DDPM A model via a hose. The DDPM B model was connected to the stiff service gallery with steel pipe, and both DDPMs were mounted on the same modelled generator shaft. The LP gallery was connected to the inlet of both DDPM models with a hose and the LP accumulator via a hose. There was also an LP reservoir used, which was a way to provide the static boost pressure within the model. This boost was achieved differently in practice on the test rig, using a pump and the volume of the LP accumulator to maintain the boost pressure.

Figure 4.6 shows an overview of the energy flow through the system, characterised by key components, energy stores and measured losses in the model. The input to the system is the mechanical power on the PTO input shaft, which is mechanically driven by the relevant WEC system (in this case, by a winch and ring gear). Losses in the specific WEC systems before the PTO are not included in this model. This input PTO shaft connects to the multiple (in this example, four) PTO motors which, as they convert mechanical energy to fluid energy, will give rise to the first major losses of the system, due to leakage and friction as explained in Section 4.3.6. Rotating machines introduce substantial additional losses over hydraulic cylinders but offer flexibility for different WEC designs (e.g. winches and hinge designs without end stops). The chamber refers to the volume of fluid via which

the motors connect to the manifold blocks, the pressure of which dictates the applied load of the actuator. For rotating motors this volume is dominated by connecting pipework; in the equivalent linear system, this would be dominated by the volume of the chamber inside the cylinder. Volumetric losses can result from energy used to pressurise the oil in the chambers then being vented to tank as part of the control process. Energy is then transferred to the manifold blocks, where it can be lost internally via valve pressure drops and valve leakages. Due to the shock accumulators mounted on the blocks' HP galleries and the internal fluid volumes of the block (such as those encompassed by the galleries), some energy may be stored in the blocks or even extracted from the energy stores in the blocks, for example, if the state of charge of the shock accumulators changes is lower at the end of the simulation than at the start. Depending on the control of the valves in the manifold blocks, the oil may then flow into the DDPM gallery or the accumulator. Again, in both of these galleries, energy may be stored or lost to compressibility. The system to be tested on the rig has a precharge pressure of 150 bar with an oil volume of up to 74 l and gas back-up bottles of a further 75 l. This is scalable to much larger storage volumes in line with the PTO as a whole. The two DDPMs then convert the stored hydraulic energy back into mechanical energy applied to the generator shaft, on which they are both mounted. This conversion incurs energy losses to the system as well, which are defined by the loss model described in Section 4.3.5. In converting the received mechanical energy to electrical energy the generator is not perfectly efficient, but this is assumed to be a constant 94.3% as explained in Section 4.3.7. Block internal losses include a range of processes such as any valve transition which causes high pressure to be relieved to tank, pressure drops across valves, flow losses within the block and leakage.

The losses are divided into primary and secondary losses according to the method proposed in [1], where the main system accumulator divides the system. This means that the primary losses are those incurred in delivering energy from the PTO input to the accumulator and that the secondary losses are those incurred in delivering energy from the accumulator to the generator. However since there are two services, only one of which has an accumulator, this definition is less obvious than in the Pelamis system. Particularly this is because DDPM A is carrying the transforming function of counteracting the irregular torque output of DDPM B by exchanging energy with the accumulator, whilst simultaneously extracting energy from the accumulator to drive the generator. The transforming function can be considered a primary conversion process, whilst exporting to the generator is a secondary conversion process. It is not possible to distinguish the primary and secondary DDPM A losses using the existing simulation, so an equal split is assumed. Therefore the PTO motor losses, valve block losses, hydraulic hose losses, DDPM B losses and half of the DDPM A losses make up the primary losses,

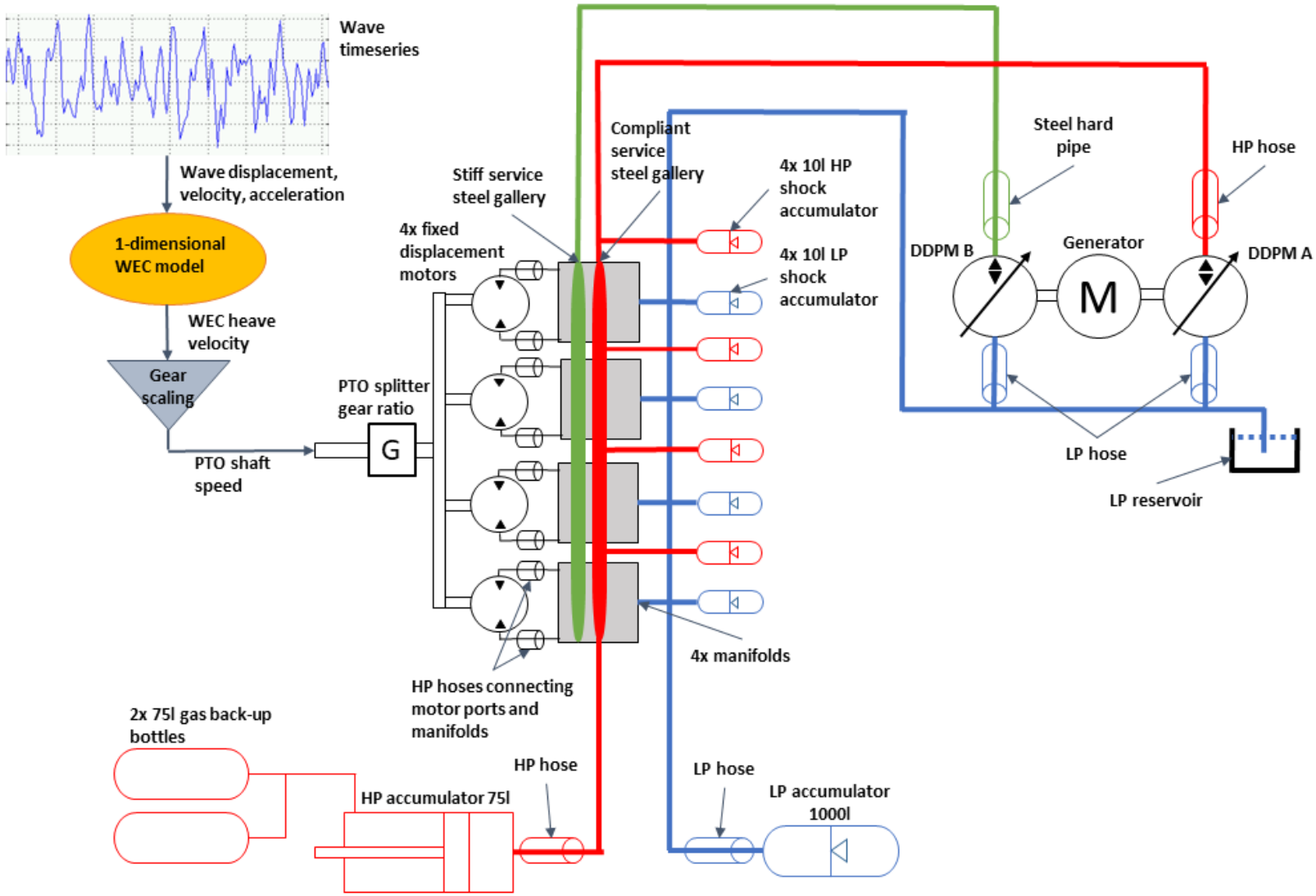

Figure 4.5 *Schematic of Quantor model showing the derivation of PTO shaft speed from WEC model, components included in model and connections between them.*

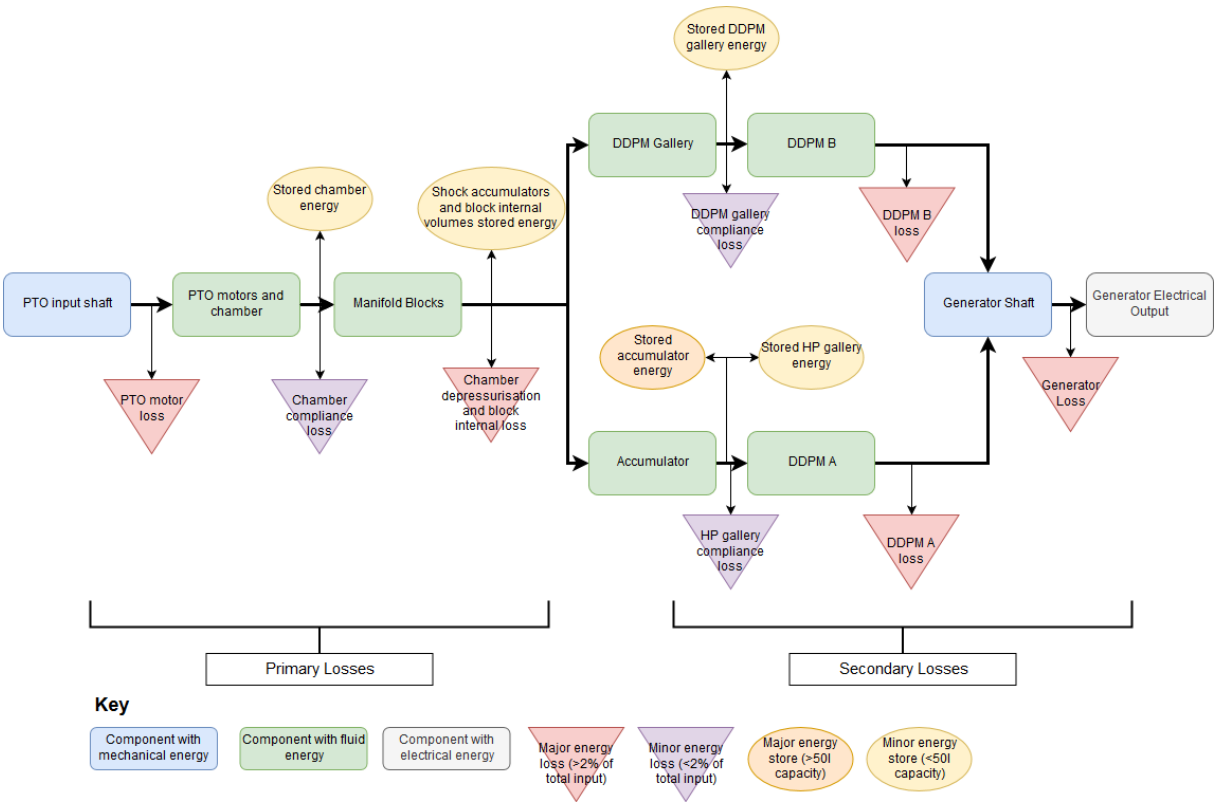

Figure 4.6 *Schematic of Quantor model structure, showing the flow of energy through key components, as well as the positions of energy stores and the energy losses measured at each stage in the model. The 'minor energy stores' are included in this figure because they are included in the model, but the energy stored in them is proportionally very small (0.4% or less) so it is assumed that any stored energy from these components is distributed pro rata to the remaining nodes.*

and the remaining half of the DDPM A losses, along with the generator losses make up the secondary losses.

It should also be noted that energy does not necessarily constantly flow in the directions shown; all the hydraulic machines involved can transfer power in either direction. However the arrows in Figure 4.6 represent the primary direction of energy flow for electricity generation.

Total PTO efficiency is defined as the ratio of the electrical energy generated to total mechanical energy available to the PTO from the wave induced WEC motion. This PTO efficiency is 'WEC-agnostic' and does not include hydrodynamic or other losses in the WECs primary absorption mechanism.

The hydraulic system is simulated using 'Simscape', which is a bidirectional physical modelling package incorporated within the wider Matlab/Simulink environment. Simscape

provides a large library of user-configurable hydraulic component models representing valves, hoses, accumulators, oil properties and hydraulic machines. The AIP DDPM loss models are built in Simulink.

4.3.2 Wave and WEC Model

The model was used to simulate a WEC with a Quantor PTO in both regular and irregular waves, of two different scales each. The WES guidelines for model testing were used to give indicative examples of how to choose sea states [77]. For the regular waves, the simulation was 300 s long and for irregular seas, the simulation was 512 s long. The difference was because it was simply necessary to allow the regular simulation to reach a steady state, whereas, for the irregular sea, 512 s is a reasonable minimum length of time required for the WEC to experience a representative range of the chosen sea spectrum [77]. The irregular waves were modelled using a Pierson-Moskowitz spectrum. The irregular wave time-series were produced using the WAFO Matlab toolbox [78]. The details of each set of input waves are given in Table 4.2. The power per unit crest length (or wave energy flux per unit crest length in the case of irregular waves) is given by Equation (4.1) for regular waves (in deep water) [37] and by Equation (4.2) for irregular waves (in deep water) [79]. These were chosen such that there was both a low and high energy example of regular and irregular waves. R1 and I2 were very similar in terms of the wave energy density, and the four different wave sets together provide a broad spread of input power per unit crest length, from 20 to 100 kW/m.

$$P = \frac{\rho g^2}{32\pi} H^2 T \tag{4.1}$$

$$P = \frac{\rho g^2}{64\pi} H_s^2 T_e \tag{4.2}$$

The WEC was modelled using a one-dimensional linear hydrodynamic equation of motion. The WEC modelled was a simple heaving sphere of 4.5 m diameter. The modelled architecture was a winch PTO system, attached to a ring gear, on the circumference of which the fixed displacement motors of the Quantor PTO are mounted. This enables the fixed-displacement motors on the test rig to run at the same speed as they would on the simulated WEC, thereby grounding the hardware-in-the-loop system in the reality of a sea-based deployment.

Table 4.2 *Characteristics of different input waves used for simulation*

Input Waves	T	T_p(s)	T_e (s)	H or H_s (m)	Wave power per unit crest length (kW/m)
Regular 1 (R1)	7.5			2.5	45.9
Regular 2 (R2)	8.5			3.5	102.1
Irregular 1 (I1)		7.7	6.6	2.5	20.2
Irregular 2 (I2)		9.1	7.8	3.5	46.9

4.3.3 Valve Manifold Block Model

A redacted version of the manifold block model is shown in Figure 4.7. The transient flow valves, main flow valves, directional valves, passive pumping check valves, cross-pilot valves, DDPM engaged isolation valves and overdrive relief valve are all included. However, for simplicity, the failsafe pilot enable valve, port drain valve and the pilot gallery are all omitted. The coloured hexagons show the hydraulic ports (Simscape hydraulic connections) to the motor ports (purple), the HP gallery (red), stiff service gallery (green) and LP gallery (blue). The other black oval connections are for the valve control signals, which connect to Simscape valve actuators with tunable delays and time constants. It was judged that the actuators would model the time for pilot pressurisation adequately. There are many constant volume hydraulic chambers scattered throughout the valve block; these are negligible volumes of $10\,\text{cm}^3$ each, which are provided to give the simulation solver a way to resolve pressure and flow between the other hydraulic components. As there really is some volume in the block galleries this is not unrealistic. Part of model validation may include adjusting these volumes so that the total compliance of the block is representative.

Each modelled manifold block is connected to the two ports of a fixed displacement motor model, and the HP, LP and DDPM galleries. The valves are controlled in such a way as to alternately connect each motor port to the desired HP, LP or DDPM service, for the quantising and continuous functions described in Section 4.2.1. The passive check valves, cross-pilot valves, DDPM engaged isolation valve and DDPM overdrive relief valve were all included so that a range of operating conditions could be tested in simulation. This also meant that the process of switching a block between functions, e.g. from passive operation to quantised operation could be tested. The HP shock accumulator was included in the model of each block to check how this volume interacted with the motors in different

operating conditions. For information about control of the Quantor valves see Section 6.1 in Chapter 6.

Rather than modelling both the solenoid-operated valve and the pilot-operated flow valve for each control stage (as the circuit is truly designed), a simplification was used. The control valves were modelled as Simscape two-way directional valves controlled by two-position valve actuators, characterised by maximum area and opening. This assumes that the valve passage area is linearly dependent on control member displacement [80]. The valve models in Simscape include important loss characteristics (pressure drop) and have a user-specified 'transit time' to simulate their dynamic behaviour. Dynamic behaviour due to spring loading and spool characteristics are omitted to keep complexity and simulation time manageable, given the large number of valves in this system.

Experiments have been carried out on each valve type to characterise its performance in terms of opening time and pressurisation curves for the chambers connected to that valve. These experiments were used to tune the model parameters and match the model to test data. These experiments were done with a small trial manifold using different pairs of solenoid operated pilot valves and pilot-operated flow valves. The final validation of the model will be carried out with data from the full Quantor hardware on the test rig.

Additional components were placed in the manifold block model for the measurement of power flows. The flow into the block and pressure at every inlet or outlet is measured, so that the total power and energy into the block during a simulation is known. Then the hydraulic power is calculated for each component within the block with internal volume, such as the shock accumulator, the constant volume chambers and the pipes for the DDPM and HP galleries. This means that any changes in internal hydraulic energy in these volumes can be measured. The difference between the total energy flow into the block over a simulation run and the changes in the stored energy is attributed to various losses within the block. These losses include pressure drops across valves, the loss incurred when a pressurised quantised chamber is depressurised (venting loss), and losses incurred during transitions in directional valves on the stiff service. During a change in direction on the stiff service, both directional valves and their corresponding low pressure valves are open, meaning that DDPM B is briefly pumping to tank. Theoretically, these transitions are short-lived and DDPM B should be at very low pressure anyway, as these transitions occur when the stiff service demand torque passes through zero.

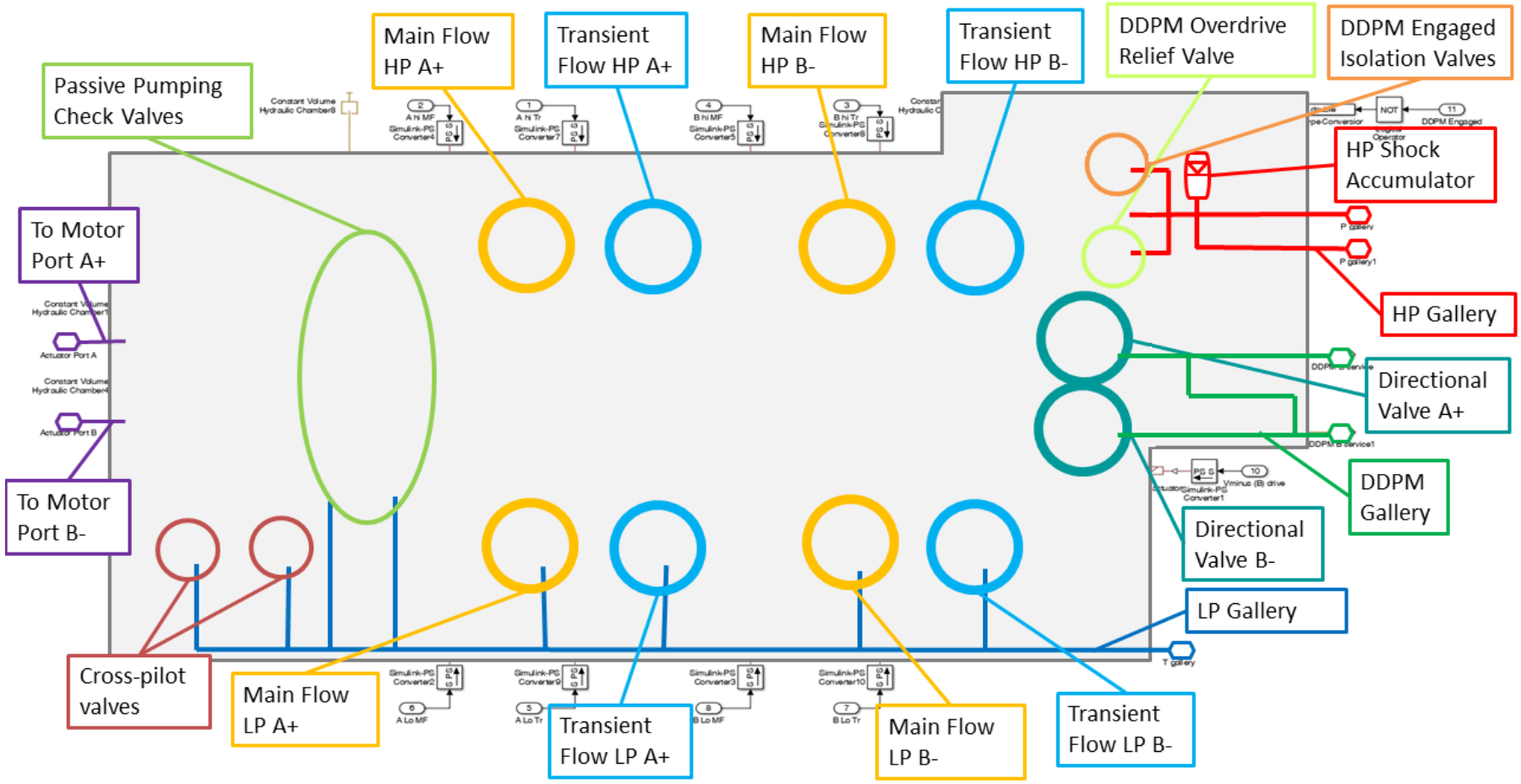

Figure 4.7 *Screenshot of manifold block model showing the position of control valves and actuators (redacted).*

4.3.4 Auxiliary Systems

The simulation of the hydraulic circuit includes all of the major hoses and piping connections between the hydraulic machines, manifold blocks and accumulators, as shown in Figure 4.8. The oil volumes within the HP and DDPM galleries of the manifold blocks are also included, based on approximations derived from the manifold block design. The simulated hydraulic connections account for the bulk modulus of the oil volume in those connections (compliance), pressure drop due to the length and diameter of the connections, and in the case of hydraulic hoses, the additional compliance due to the expansion under pressure of the hose itself. Fluid inertia is omitted from this model since the purpose of this model is to study the performance and efficiency of the Quantor PTO, and the addition of fluid inertia to the hydraulic connections significantly increases the higher frequency dynamics of the system, and hence greatly slows down the simulation solution time without changing the overall system efficiency or performance. These higher-order effects will, of course, be present on the test rig, and if they are significant then will need to be addressed using the model. Since the hydraulic connections are fairly short it is not expected that inertial effects will present significant issues in practice.

Hydraulic accumulators are simulated using the standard polytropic gas model. Losses due to temperature changes of the gas are omitted in this simulation since the accumulators are not rapidly charged or discharged during normal operation, so the effect of thermal losses is assumed to be small.

The low pressure supply was modelled as a Simscape Reservoir of volume $2\,\mathrm{m}^3$ with a constant pressure of 7 bar. On the test rig, the low pressure may vary more due to changing volumes of oil but the low pressure accumulator is so large (75 l accumulator with 975 l of gas back-up bottles) that this effect should be minor.

The modelling of the auxiliary systems meant the processes of the Quantor could be realistically represented. The shafts of the four fixed-displacement motors rotate according to the shaft speed of the model WEC. This builds pressure on their ports and produces simulated flow, which reaches the manifold blocks via hoses. The valve control signals set which service each motor port is connected to. The motors may be pumping into (or motoring from) the quantised service or the continuous service. They are always connected to the LP service on at least one port. On the quantised service there is a modelled accumulator and the modelled flow from DDPM A, which together control the pressure in this service and absorb power from the WEC. The continuous service has the modelled flow from DDPM B, which controls the pressure in the relevant fixed-displacement motors.

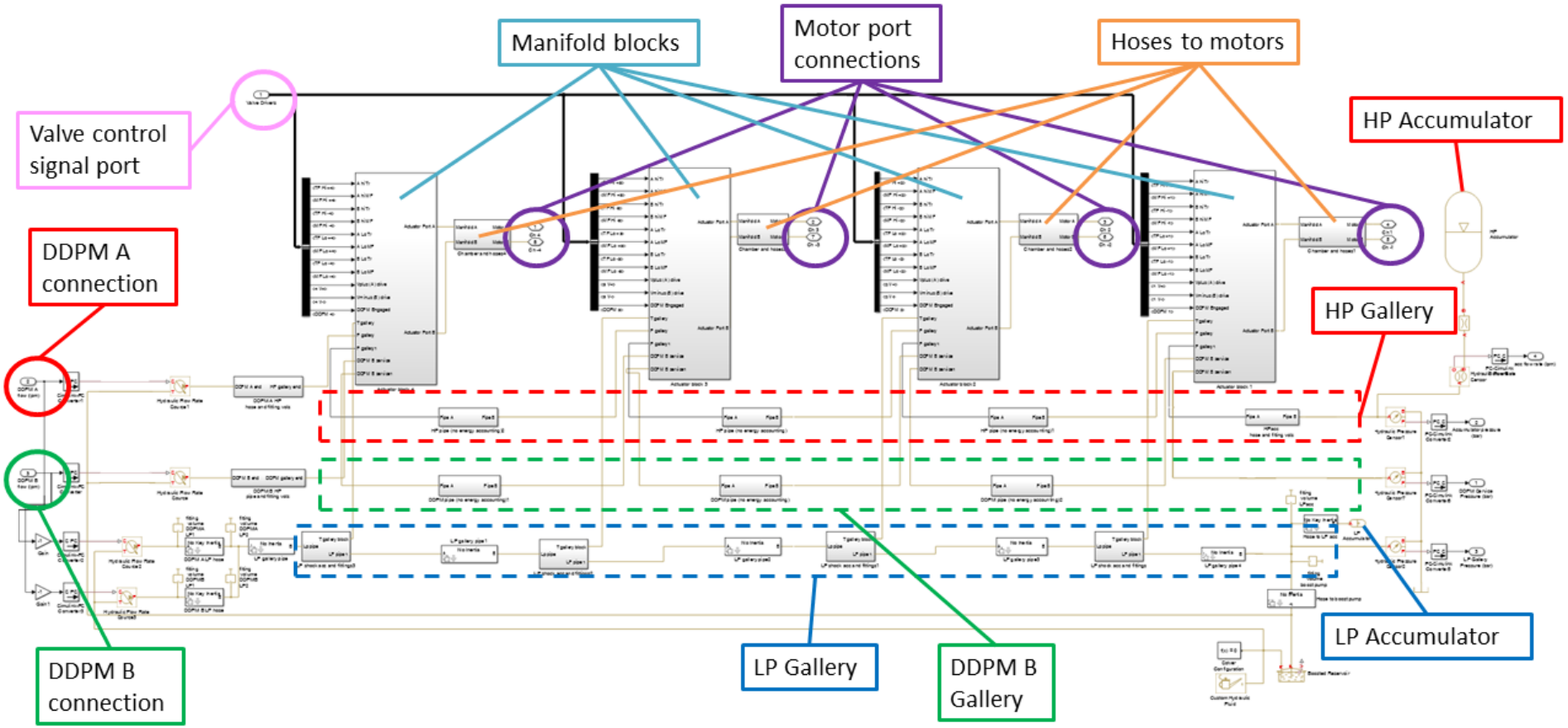

Figure 4.8 *Screenshot of Quantor hardware model including four manifold blocks, HP accumulator, LP accumulator, connections to PTO motors, connections to DDPMs, tank and connecting pipes and hoses. Key model components are annotated.*

4.3.5 DDPM Model

The DDPMs were modelled using existing Artemis Simulink models of the machines, which are based on the loss model proposed by [13]. These are semi-empirical models based on test data collected from real machines at AIP. The loss models are based on data collected from machines operating as pumps, and it is assumed that the same losses apply for a machine acting as a motor. This is because all of the physical mechanisms of loss in the machine (leakage and friction) remain the same in motoring as in pumping and the duration of pressurisation of each cylinder in the machine is roughly the same in both cases. The model does account for the difference in machine effective displacement in the different operating modes since this is significantly different during motoring compared with pumping and does have an impact on the overall ability to transmit power.

4.3.6 PTO Motor Model

The fixed displacement pump-motor selected for use on the test rig was a Poclain MS02 of $255\,\mathrm{cm}^3/\,\mathrm{rev}$, with a maximum speed of 480 rpm. The manufacturer provided performance data which was used to model the friction torque and leakage, as shown in Figure 4.9. It should be noted that any fixed displacement motor could be used in a rotary system or indeed cylinders with multiple chambers could be used for a linear system. The system can be scaled up with the use of much larger motors with very similar efficiency characteristics. This particular model was chosen for its low leakage, suitability to the rig-scale torques, speeds and flows, and for a real WEC of a different scale and entirely different pump-motor may be more suitable.

The Simscape variable-displacement hydraulic machine block was chosen as this operates in both directions as a pump and a motor, unlike the other available Simscape blocks. However, it was decided not to use its inbuilt 'external efficiencies' feature as efficiency curves often have very steep gradients at the corners of the map, leading to problems with extrapolation and interpolation. Given we had measured data for output torque and leakage, it was a more direct approach to apply these to the shaft and the ports respectively. Hence the volumetric and mechanical efficiency of the motor were set to one, along with the displacement, as this is a fixed-displacement machine. For the leakage, a linear hydraulic resistance was used corresponding to a rate of 1/0.0006 bar/lpm. From the calculated friction torque, a lookup table was generated which was applied to the output shaft so that it reduced the output torque in both directions. The motor's internal inertia was also represented.

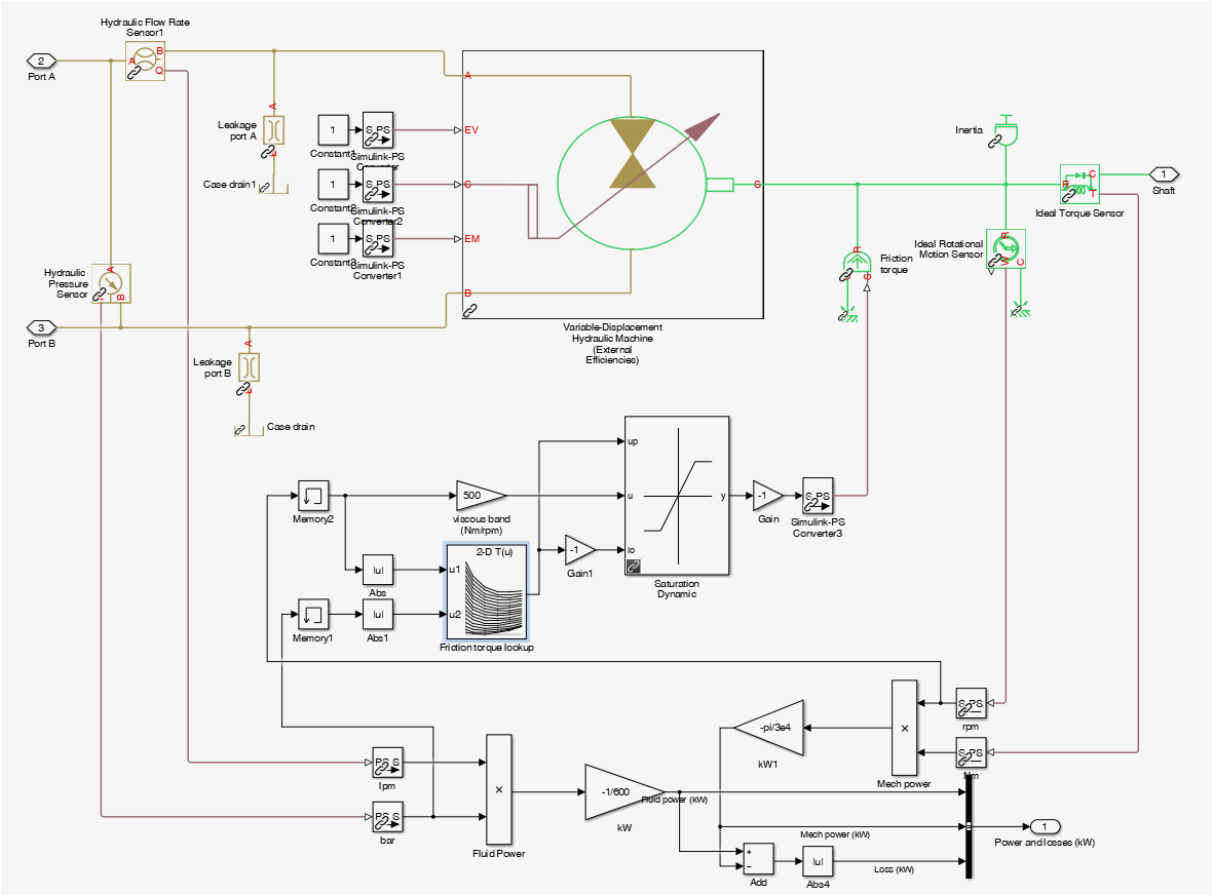

Figure 4.9 *Simulink and Simscape model of Poclain pump-motor, showing the inclusion of leakage, friction torque and inertia.*

4.3.7 Generator

The electric generator on which the DDPMs are through-shafted was modelled very simply in Simulink, according to Equation (4.3), where η_{EM} is the provided motor manufacturer's estimated efficiency of 94.3%, ω is a constant generator speed of 1500 rpm and τ is the total shaft torque, which is calculated by summing the torques of both DDPMs.

$$P_{EM} = \eta_{EM} \tau \omega \tag{4.3}$$

Assuming a constant generator efficiency is not necessarily realistic as it depends on the speed and load of the generator [81]. Whilst the speed of the generator in the Quantor should be maintained at 1500 rpm with only a small error, the load will be variable. However, in the absence of an efficiency vs load curve from the manufacturer (the only supplied value is 94.3%), a simplifying assumption was made that its efficiency is constant. The reason this was simplified is that on the test rig to be used to validate the model, the measurement of output power will be the speed and torque on the generator shaft;

not the electrical power generated. This is because the generator chosen for the test rig is not appropriately sized to the power regime of the Quantor but to give sufficient shaft diameter for the two DDPMs operating 'back-to-back' as a pump-motor test rig, making its electrical output unrepresentative of the intended system using a single generator shaft with the DDPMs connected directly to each other, or sharing the same case. Besides, an induction motor has been used here so that testing can be carried out at different speeds if required, whereas a real WEC deployment would more likely use a synchronous generator. There is little doubt over the established efficiency of standard electrical generators operating at a fixed speed, so this does not undermine the model validation. Indeed, measurements taken throughout the Quantor system will allow a breakdown of losses to be established through the transmission for comparison with the simulation model described here. An avenue for future work would be to then integrate the validated Quantor model with an efficiency model of an appropriately sized generator.

4.3.8 Control

For a description of the control of the modelled Quantor please refer ahead to Section 6.1 in Chapter 6.

4.4 Model Results

The modelled Quantor showed the ability to perform in all four quadrants of force and speed, and smooth overall output torque could be achieved with careful tuning of the control parameters. Figure 4.10 shows a Sankey (energy flow) diagram of the results from modelling sea state I2. The results are shown in percentages of the total input energy on the PTO shaft. The nodes correspond to those shown in Figure 4.6, but those where the percentage of the total energy reaching them is less than 0.1% are omitted for clarity. The accumulator starts and finishes the model run at the same pressure, so there is no net change in its stored energy. Any residual energy in the minor energy stores is assumed to be used 'pro-rata' by the following nodes.

The model result for total electrical energy output is 70.8% of the input energy, with 22.6% going to primary losses and 6.6% going to secondary losses.

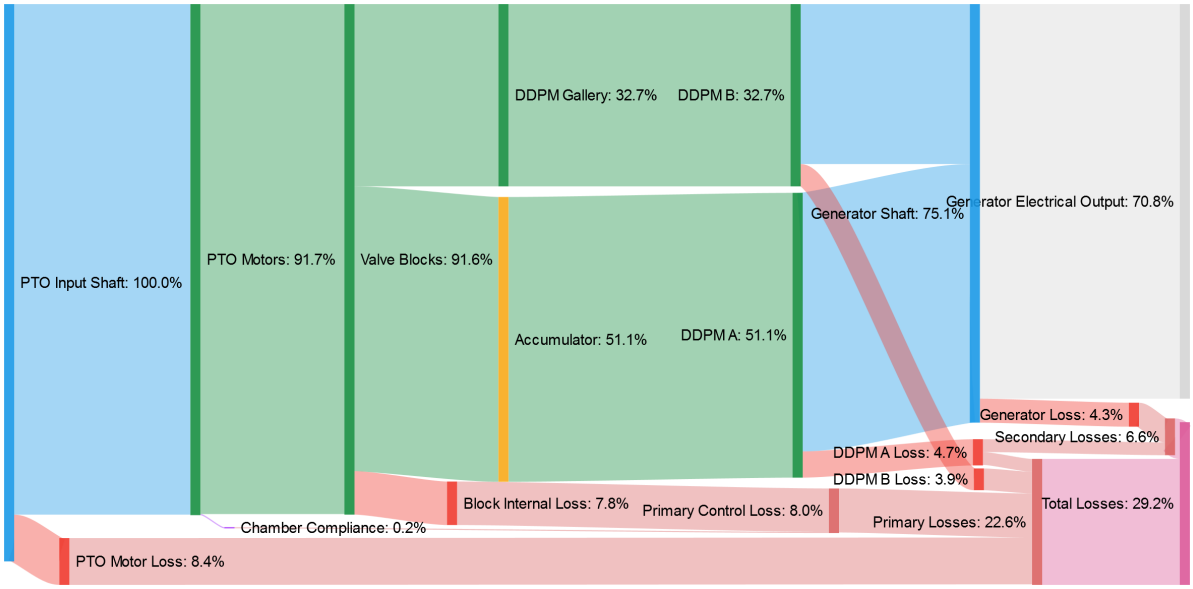

Figure 4.10 *Sankey diagram of model results of sea state I2, with energy flowing from left to right.*

Table 4.3 *Results of modelling for different input waves, including pro-rata allocation of stored energy in efficiency calculation.*

Input Waves	Simulation Length (s)	Total Model Energy Input (kJ)	Total Generated Energy (kJ)	Total Stored Energy (kJ)	Total Lost Energy (kJ)	Quantor Efficiency (%)
R1	300	12 079	8 951	-185	3 313	72.8
R2	300	16 051	11 943	-184	4 293	73.4
I1	512	13 278	8 888	-46	4 436	66.6
I2	512	19 221	13 537	102	5 582	70.8

From Figure 4.10 it is clear that the greatest energy loss in the system is the PTO motors at 8.4%, followed closely by the block internal losses at 7.8%. These elements are exposed to the greatest power variation and therefore are expected to induce a substantial proportion of the losses. As previously mentioned, the PTO motors were chosen for the test rig and may not be the best choice for any given WEC, so this loss could change and could be reduced by selecting more efficient PTO motors of appropriate specification for the application. Larger motors for higher power applications also generally offer higher efficiency. The option of using linear actuators instead of motors would also greatly improve the efficiency of this step. The primary control losses comprise the loss caused by depressurising chambers and venting to tank, chamber compliance and losses within the

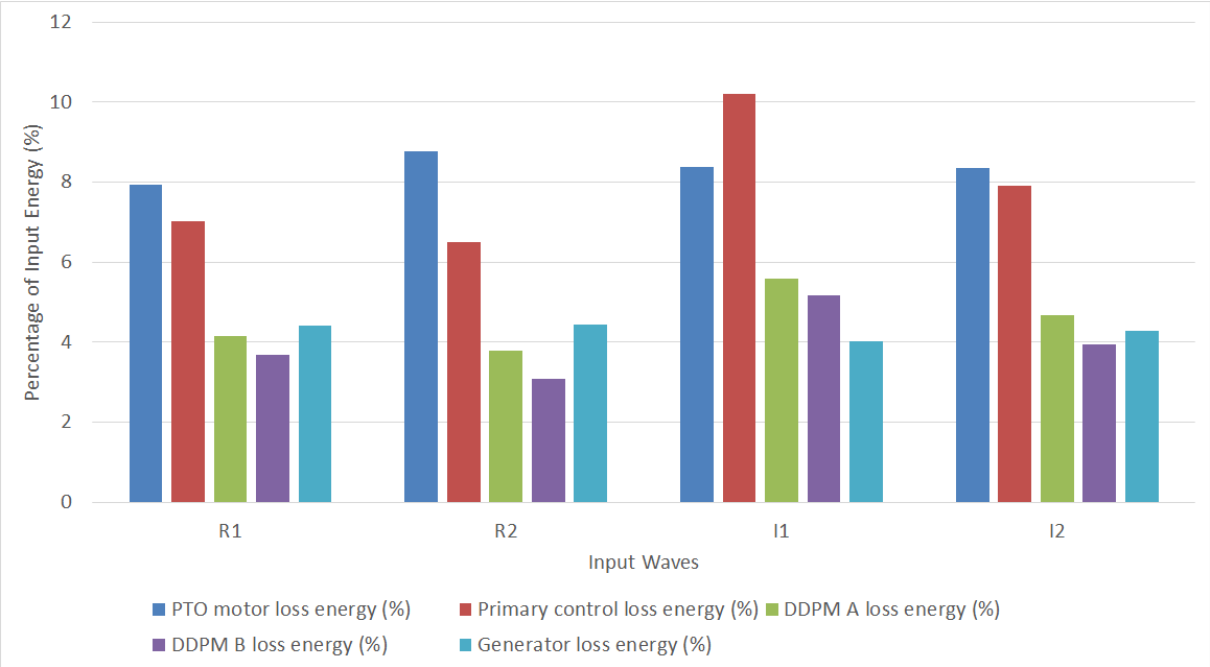

Figure 4.11 *Bar chart showing the breakdown of energy lost for each wave input as a percentage of the total input shaft energy*

valve block. Figure 4.12 breaks down the primary control losses into their constituents, as far as was measured within the model. By far the most significant loss in all cases was the combined venting losses and valve pressure drops, of which the venting loss is believed to be the larger. Unfortunately, this venting loss is a necessary evil in a quantising PTO system so cannot be avoided. It is noticeable that the wave conditions which resulted in more energy passing through the quantised service (see Figure 4.13b) had more venting and pressure drop losses, and the wave conditions which delivered more energy through the continuous service suffered more from supplementation losses. The HP supplementation loss is relatively much lower than the LP supplementation loss as the pressure difference between the HP gallery and the DDPM gallery is much smaller than that between the DDPM gallery and LP gallery. The directional change losses would also be expected to be higher in a lower energy wave condition where the demand torque passes through zero more frequently. The valve losses due to pressure drops could be reduced by choosing different valves with lower pressure drops and by redesigning some of the internal galleries. Data from the test rig (e.g. pressure measurements along the flow paths) will allow refinement of the flow loss coefficients for the valves and their immediate flow paths within this complex component.

The DDPM losses are the next most significant losses at 4.7% of the total on machine A and 3.9% on machine B. These are significantly impacted by the operating point of each machine in the chosen input waves. Depending on the operating point, DDPMs have

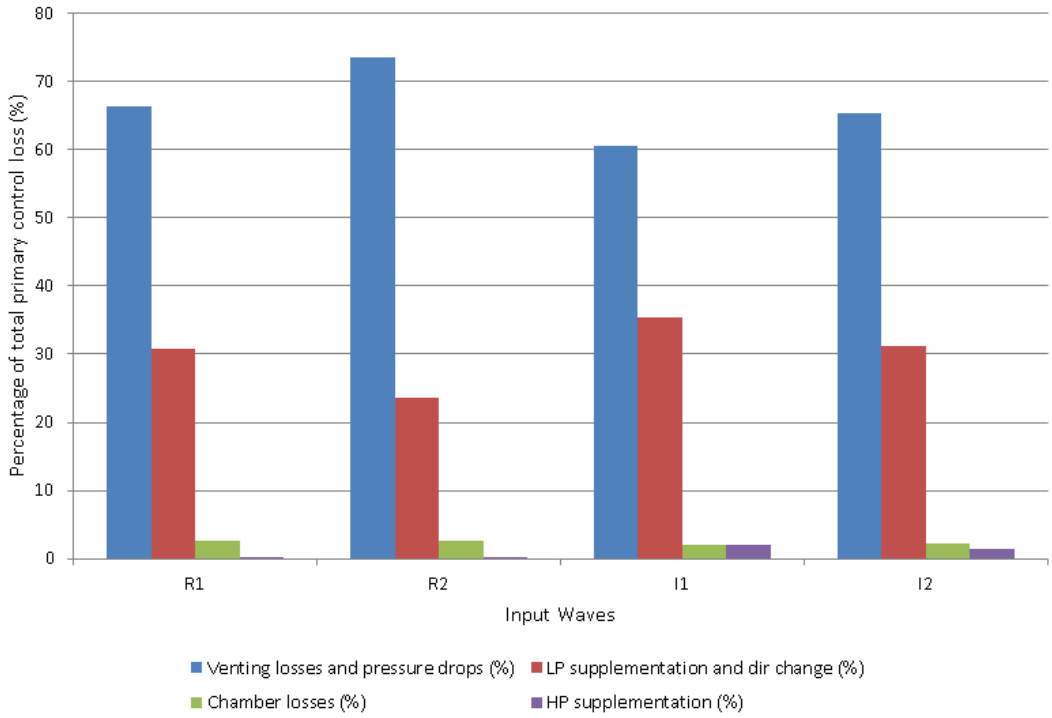

Figure 4.12 *Bar chart showing the breakdown of causes of primary control losses*

shown efficiencies at 1500 rpm (the chosen speed for the DDPMs on the test rig) ranging between 91% and 97% [13]. Generally the higher the displacement, the more efficiently the machine can operate. The average efficiency over this simulation run for DDPM A was 90.9% and for DDPM B was 87.9%. This is because the machines are operating at lower average power than the optimum, particularly DDPM B. This is because DDPM B has to operate at very low pressures and displacements due to the need for torque exerted by the stiff service to regularly pass through zero, which means the corresponding pressure must also go as close to the LP system pressure as possible within the control limitations of the system.

Table 4.3 shows the key model results for all four wave sets in terms of absolute energy input, stored, generated and lost, as well as the percentage efficiency. This percentage energy assumes that the stored energy displayed in the table would be extracted through the generator 'pro-rata', were it to be used. Despite the large variation in the power density of the input waves (between 20 and 100 kW/m, the Quantor efficiency remains around 70%, with 66.6% being the minimum and 73.4% being the maximum.

The results for R1 and R2 are very similar in terms of efficiency and loss breakdown (see Figure 4.11). This is because both wave sets are using the full range of the Quantor system, and in R2, which is the higher energy wave set, the PTO load is fully saturated

at the peak where the PTO motors cannot exert any more torque. It is encouraging to note that once the full load range of the Quantor is exercised, saturation did not lead to excessive additional losses, which suggests that the Quantor could operate in high energy saturation conditions in the sea and the specified load range may be set to saturate at an optimal level for the overall economics and survivability. The PTO motor losses are higher in R2 than R1, due to flow losses and also due to partially bypassing of the DDPM while saturated and hence shedding a proportion of the bypassed energy as the pressure drops from the DDPM 'overdrive' pressure to the accumulator pressure. However, the block losses and DDPM losses are slightly lower proportionally in this case. For the DDPMs this is because they can reach a more efficient operating point as they work with higher displacement.

I1 and I2 results show more variation, despite being closer in power density than R1 and R2. The efficiency of the Quantor in I2 is approximately 4.2% higher than I1. From Figure 4.11 it is clear that the block internal losses are the major contributor to this difference, as they are proportionally much higher for I1. This is because a lower energy sea state involves more zero-crossings in the applied PTO torque, relative to the power extracted. In the case of the Quantor, this means that more valve transitions are involved as the direction of the applied PTO torque changes. In the quantised service a loss occurs every time a chamber is vented from high pressure to low pressure, which is every time the applied quantised moment is stepped down in magnitude. A similar loss occurs in the continuous service because during load reversals the continuously controlled chambers must vent any residual pressure between the minimum DDPM pressure and the tank pressure. During this modelling exercise, the DDPM was assumed to be able to reliably control pressure to a minimum of approximately 30 bar, which may be pessimistic. Establishing this minimum continuously controlled pressure is an early target of upcoming lab tests. Again, the DDPM losses reduce in I2 as they deliver higher flows on average.

An interesting comparison is between R1 and I2, which both have similar wave power densities (45.9 and 46.9 kW/m of crest length respectively). The Quantor is only 2.1% less efficient in I2 than in R1, which demonstrates that it can cope well with the varying loads without 'prior knowledge' of the incoming waves. Again, this difference is likely caused by the requirement for more zero-crossings and valve transitions in the irregular sea state.

The primary and secondary conversion efficiencies of the Quantor in each set of input waves are shown in PTO Figure 4.13a. In all cases the secondary conversion efficiency is higher than the primary conversion efficiency, and varies very little between sea states, remaining between 93.2% and 93.7%. The primary conversion efficiencies for the regular

waves are both over 79%, whereas they are 73.4% and 77.4% for I1 and I2 respectively. As discussed above, a different choice of PTO motor and testing the minimum pressure on the stiff service may help improve the primary conversion efficiency. The peak value of primary conversion efficiency of 79.8% is lower than that of 91.5% reported in [11] in irregular waves for a DDC system which was both simulated and validated experimentally. The efficiency impact of rotary actuators compared to linear actuators may explain this difference. Quantor is designed such that it could use either linear or rotary primary actuators, but so far the only modelling done has been for rotary systems. [11] does not mention the secondary conversion efficiency so it is not possible to do a full comparison.

[1] reports primary conversion efficiencies of over 80% which is higher than the results for the Quantor. The total wave-to-wire efficiency for Pelamis was over 70% [9], with a secondary conversion efficiency of approximately 90% for the P2 Pelamis. The primary conversion efficiency of the Quantor PTO cannot feasibly be as high as that of the Pelamis because the continuously controlled service inherently has higher losses than the quantised service. However, the continuous control should benefit the instantaneous power absorption and WEC control over the pure quantised control.

Figure 4.13b shows the percentage of input energy which is delivered through the quantised (A) and continuous (B) services. The more energy that passes through the quantised service and the less through the continuous service, the higher the primary conversion efficiency. This is because DDPM B is generally at a less efficient operating point than DDPM A, as it must go to lower displacements to continuously control the pressure. The accumulator also acts as an energy store for the quantised service, but DDPM B must either instantaneously absorb the power available from the continuous service or lose it, as this service is very stiff. This result suggests that the quantised service should handle as much of the load as possible, with the continuous service providing only smoothing of the response.

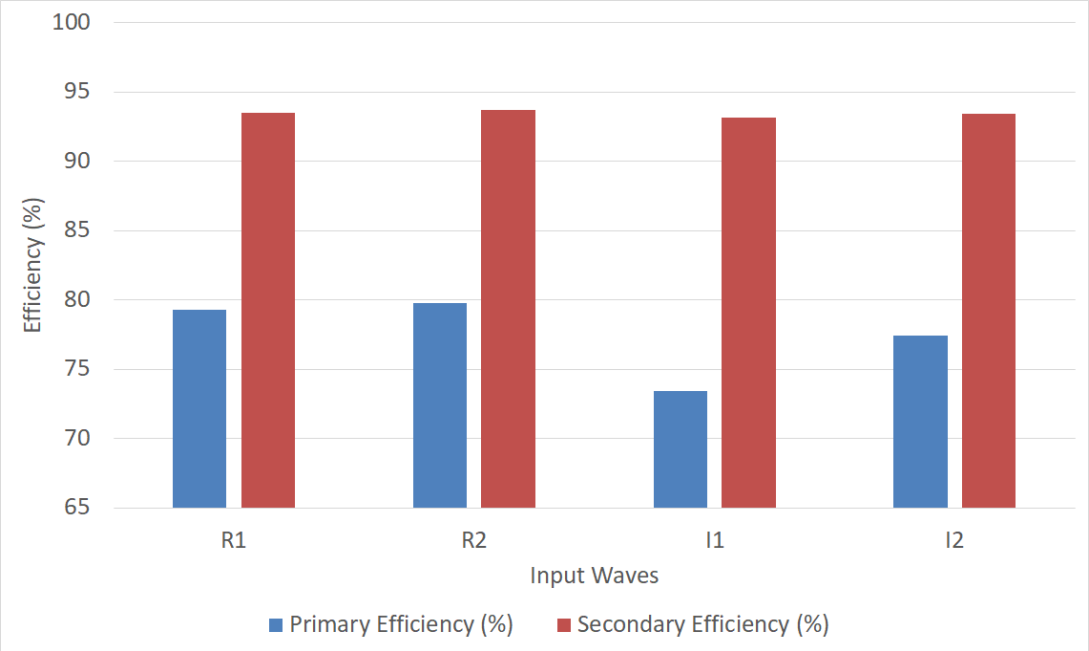

(a) *Bar chart showing the efficiency of primary and secondary conversion for each set of input waves.*

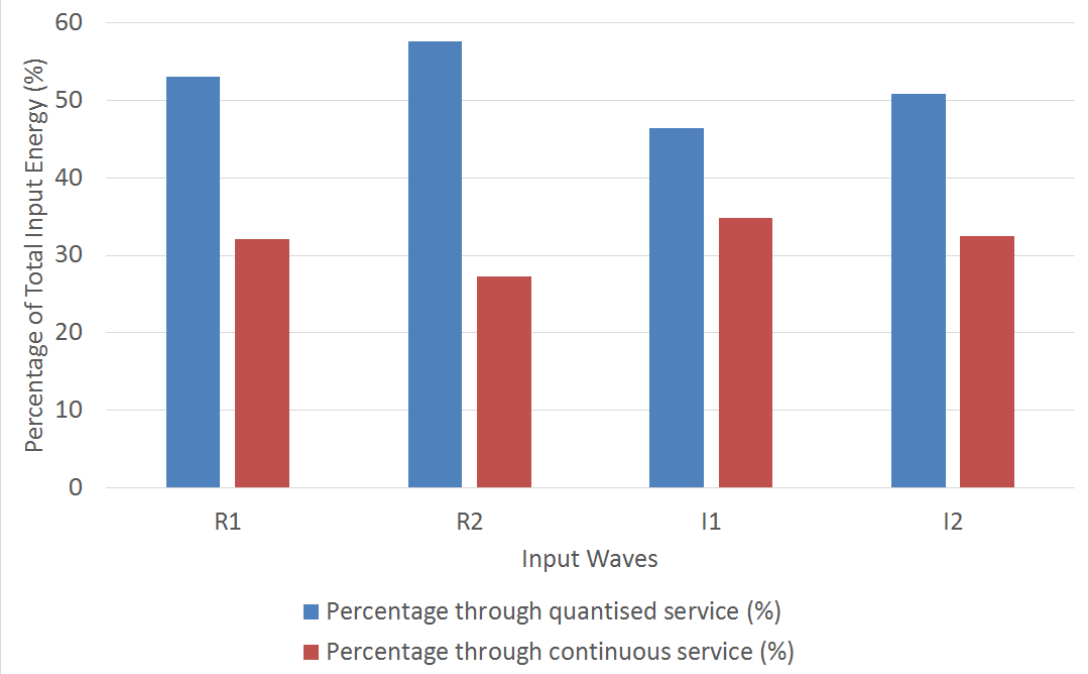

(b) *Bar chart showing the proportion of total input energy delivered through A (quantised) service and B (continuous) service.*

Figure 4.13 *Breakdown of results for different sets of input waves showing primary and secondary conversion efficiency and energy delivery through each service.*

4.5 Model Evaluation

Quantised valve opening times and pressurisation curves have already been validated with experimental data from a prototype manifold block (see Appendix B for more information about these tests). The PTO motor model is based on measured data from the manufacturers. The DDPM loss models are well-validated for pumping, and it is assumed that the motoring losses are the same since the loss mechanisms in this mode are the same. Flow losses through valves and pipes are estimated from physical dimensions using Simscape, which may need further refinement. The auxiliary systems are difficult to model realistically, although every effort was made to accurately represent the physical dimensions and compliance of hydraulic connections. Fluid inertia was ignored as it would have been very computationally expensive to include, so this means that some transient effects may be missing. The accumulator model did not include any thermal losses, which would probably be around 5% in the case of a foam-filled accumulator [82]. This was a limitation of the Simscape accumulator model which did not allow the inclusion of thermal losses [83].

The key processes for Quantor model validation from test rig data are:

- Representative pressurisation and depressurisation of chambers under quantised control
- Representative compliance of chambers, stiff service and auxiliary connections
- Validation of fixed displacement PTO motor losses
- Validation of the DDPM model for motoring performance as well as pumping operation
- Validation of accumulator pressure variation
- Validation of DDPM transforming function for smoothing of output torque

Whilst reasonable effort has been made to accurately model the hydraulic detail of the Quantor PTO, the true test of the model accuracy will be experimental validation on the test rig. The model may then be confidently extrapolated to larger rated powers and loads, and different architectures. It is also anticipated that a validated simplified model of the PTO will allow rapid integration into third-party WEC models for the development of detailed WEC design and control strategies.

4.6 Summary

A Simulink and Simscape model of the Quantor PTO was constructed, which combines the quantising principle of the Pelamis PTO with AIP's DDPM machines. This combination should allow fully reactive WEC control, with the applied PTO torque smoothly matching the demand, while power is transmitted and converted with an efficiency similar to that of the quantised system. Reactive control and smooth PTO torque were shown in the detailed model, although obtaining smooth PTO torque required careful tuning of the control parameters. The detailed modelling of the hydraulics and mechanical systems allowed the various losses to be quantified at each stage of the power transmission.

The Quantor PTO was simulated in a range of input waves, both regular and irregular, covering a wide range of power densities (20 to 100 kW/m of crest length). The overall efficiency of the Quantor varies between 66.6% and 73.4%, which is very stable considering the variety in the input wave conditions. The Quantor performs well in irregular waves, with efficiency decreasing by only 2% between a regular and irregular wave set of similar power density. The largest sources of loss are the primary motors (actuators) and the manifold blocks controlling flow to and from these motors, with the DDPM machines next. The easiest of these to improve is the primary motors where flow losses may be reduced by using alternatives. A system using linear actuators would have substantially lower primary losses, but this introduces end-stops and greater pressure shocks due to the larger chamber volume.

As expected, the Quantor performs more efficiently if a greater proportion of the energy is transferred through the quantised service and a smaller proportion is transferred through the continuous service. The Quantor system modelled here, and subsequently to be physically tested, uses only 4 motors altogether, whereas an applied WEC system could use a larger number of motors with a commensurately larger proportion of energy being transmitted by the quantised service, which would offer increased efficiency. The primary conversion efficiency is slightly lower than that measured in previous studies of linear actuators (because rotary actuators intrinsically have more losses), whilst the secondary conversion efficiency seems comparable to that of Pelamis. As described in Section 4.5, there are many uncertainties in the modelling of the hydraulic components, although effort has been made to represent these as realistically as possible. Validation is therefore essential to provide confidence in the model at both component and system level.

An experimental study of a Quantor prototype which will allow model refinement and validation is the most important piece of further work. A test rig is currently being

commissioned on AIP's premises to enable this. A flywheel of significant inertia will be driven by an electric motor to emulates the hydrodynamic excitation and dynamic response of a WEC in both regular and irregular waves. A Quantor PTO, matching that modelled, will then be tested on this rig, extracting power from the emulated WEC and demonstrating the combination of quantised and continuous control. The data gathered on the rig will be invaluable for confirming the viability and efficiency of the Quantor PTO, and therefore its potential usefulness for WEC applications.

Once a validated Quantor model has been produced, there is also the possibility of simulating different fixed-displacement PTO motors, as well as simulating linear primary actuators. Different power ratings and architectures may also be extrapolated using the validated model elements.

Chapter 5

Hardware-in-the-Loop Test Rig with WEC Emulator and Laboratory-Scale Quantor PTO

This chapter describes the test rig developed at AIP in two parts; the WEC emulator and the laboratory-scale Quantor system, as well as the transducers used for performance measurements. This test rig enabled a realistic representation of the operating conditions of the Quantor so that its performance could be understood, quantified and fed back into models which could then be extended to other systems at a larger scale. A significant commissioning and testing campaign was undertaken on this test rig, which meant valuable experimental data about Quantor performance in many different wave environments and different control modes could be gathered.

5.1 Design of WEC Emulator

The aim of constructing the test rig was to provide a suitable test bench for the Quantor PTO which could emulate a range of WECs in representative sea states. Figure 5.1 indicates the range of different classes of WEC in terms of PTO requirements for present and past WEC designs. The WEC design may impact the PTO in a great number of ways, for example;

- The compromise between WEC force and velocity. Maximum expected forces have a high impact on the cost of a WEC, but trying to reduce these by increasing the velocity by having longer strokes may also increase the cost. This also affects the

control gains needed: typically a WEC moving with low forces at high velocity will require lower control gains to have the optimum damping and spring terms, whilst a WEC moving slowly with very high forces will require higher PTO control gains.

- Mass and added mass 'visible' to the PTO. Mass and inertia impact the control stability of the PTO, in that a WEC with high inertia is easier to operate stably, whilst a WEC with low inertia requires much more accurate force control to close the control loop.

- Structural and drive train compliance. The more compliance a WEC's structure or drivetrain is, the more likely it is to require high-bandwidth, continuous, accurate PTO force control.

- Linear or rotary actuators. Linear actuators will have lower leakage and frictional losses than rotary actuators but higher volumetric losses.

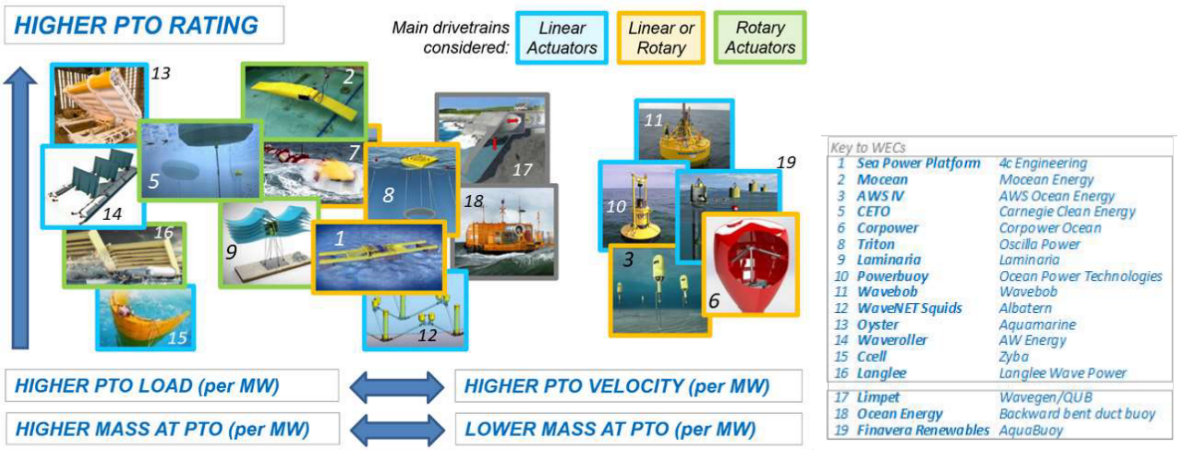

(a) (b)

Figure 5.1 *PTO classification schematic taken from [3], showing different types of WEC design and their relative PTO load, mass, velocity and rating. An indication of what type of actuator (rotary or linear) would be most appropriate is provided.*

5.1.1 Scaling of WEC

A basic challenge of designing a test rig for a WEC PTO at lab scale is that the very low speeds and high torques of WEC motion are challenging to recreate in a safe, controllable and affordable way. The Pelamis full-scale joint test rig used a very large hydraulic power pack to generate the forces (up to 1 MN) required to actuate the tested PTO [1]. As previously mentioned, electric machines generally operate in a very different speed and

torque regime, yet are a straightforward option for lab installation. The fundamental premise of the test rig is that the Quantor PTO motors operate at the same speed as on the WEC being emulated by the test rig. Therefore it was decided to use a gear between an electric motor and a lab PTO system to better match the two regimes. However, even a significant gear ratio of 18, for example, would not fully bridge the gap. To enable the electric motor on the rig to run at achievable speeds, and to preserve the relationship between the WEC PTO and the rig PTO, a further gear scaling is used, which is applied in the HIL model. This provides a ratio between the speed of the WEC and the speed of the WEC emulator on the test rig. Figure 5.2 illustrates this, using the example of a heaving buoy style WEC with a winch drum converting the vertical heave motion of the WEC to rotary motion (shown in Figure 5.2a). The internal integration of the Quantor PTO with the winch drum is illustrated in Figure 5.2b. A splitter gear of ratio G_{WEC} could be used to connect a large number of PTO motors to the winch drum so that the Quantor PTO has relatively fine discretisation over a large load range. The inertia of the WEC is illustrated as being in line with the winch. This is not a physical mechanical connection but is included (with dashed lines) to better portray the relationship between the example WEC system and the test rig. In a WEC the PTO must control the inertia in the system, so the inclusion of the flywheel in the test rig (shown in Figure 5.2c) was important to represent the behaviour properly. Figure 5.2c shows the electric motor, drive gear, flywheel, splitter gear and PTO motors used on the test rig. To remain within the scale and budget of the rig, only four motors were used, as this was judged to provide adequate proof of Quantor performance.

The speed of the PTO motors ($\dot{\theta}_m$) on the WEC is given by Equation (5.1), where r is the radius of the winch drum, $\dot{x}_{WEC}$ is the linear velocity of the WEC in heave and G_{WEC} is the gear ratio in the WEC.

$$\dot{\theta}_m = \frac{\dot{x}_{WEC} G_{WEC}}{r} \tag{5.1}$$

On the test rig, the speed of the PTO motors is given by Equation (5.2), where $\dot{\theta}_{EM}$ is the angular velocity of the electric motor, G_d is the test rig drive gear ratio and G_{PTO} is the PTO splitter gear ratio.

$$\dot{\theta}_m = \dot{\theta}_{EM} G_d G_{PTO} \tag{5.2}$$

Equating these two expressions gives the condition for the PTO motor speed on the WEC

and test rig to be identical:

$$\frac{\dot{x}_{WEC} G_{WEC}}{r} = \dot{\theta}_{EM} G_d G_{PTO} \tag{5.3}$$

$$\dot{\theta}_{EM} = \frac{\dot{x}_{WEC} G_{WEC}}{r G_d G_{PTO}} \tag{5.4}$$

and the relationship of the rig PTO shaft speed $\dot{\theta}_{rig}$ to the WEC velocity is

$$\dot{\theta}_{rig} = \dot{\theta}_{EM} G_d \tag{5.5}$$

$$= \frac{\dot{x}_{WEC} G_{WEC}}{r G_{PTO}} \tag{5.6}$$

$$= \frac{\dot{x}_{WEC}}{G_s} \tag{5.7}$$

Equation (5.4) can be used to derive the speed control signal for the electric motor. The combination of all the terms in Equation (5.7) relating the WEC velocity to the PTO shaft speed is known as the 'gear scaling' (G_s). This is also described in terms of force and torque in Section 6.1. Some parameters are physically fixed by the choice of test rig equipment but those relating to the proposed WEC can be chosen more flexibly (within commonsense engineering guidelines, for example, the diameter of the ring gear cannot exceed the diameter of the WEC). This means that the WEC emulator can represent a range of WECs within its operating envelope. This is an example of how one possible WEC configuration could be represented on the test rig: the gear scaling term could also be used to describe other cases such as a rack and pinion system or a linear PTO. The choice of gear scaling could generally be in the range of 8 to 14, depending on the WEC chosen.

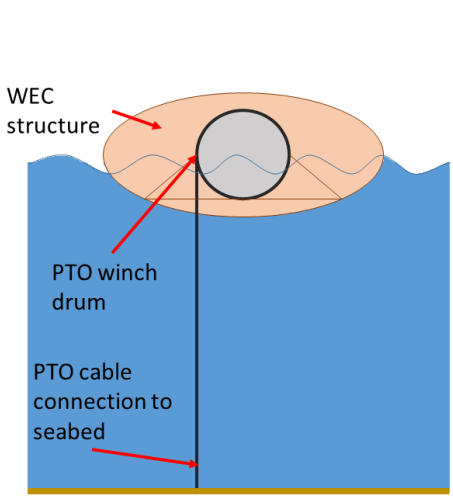

(a) *Diagram of example rotary Quantor WEC application featuring a heaving buoy with a winch drum PTO system, which converts the heave motion of the buoy to rotary motion of the winch drum.*

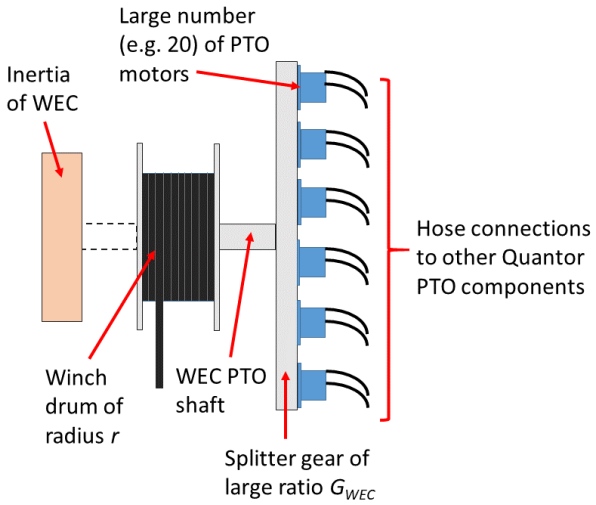

(b) *Diagram of Quantor integration with winch drum PTO, via ring gear in example WEC application shown in Figure 5.2a. The inertia of the WEC is shown in line to highlight its influence on the PTO, although this is not how the winch and WEC would be mechanically connected.*

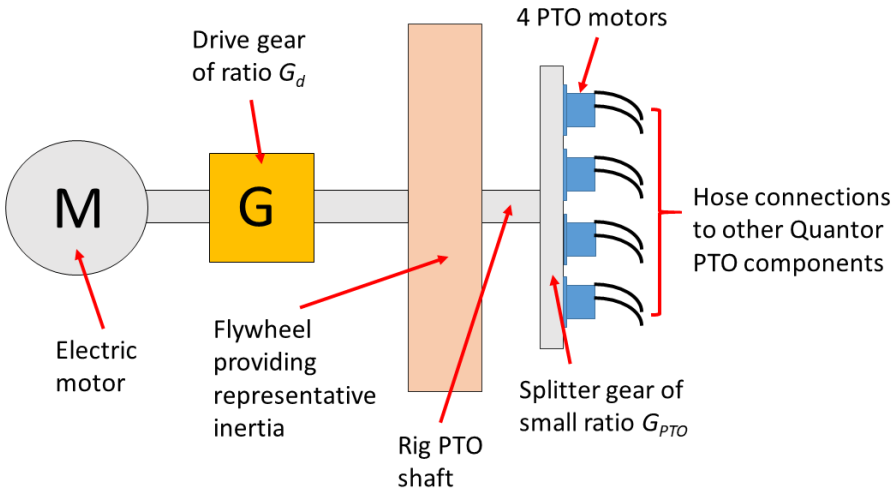

(c) *Diagram of Quantor integration with WEC emulator consisting of the electric motor, drive gear, flywheel, splitter gear and PTO motors on the test rig.*

Figure 5.2 *Set of diagrams showing the relationship of WEC gearing to test rig gearing. Figure 5.2a and Figure 5.2b show how Quantor could be integrated into a WEC. Figure 5.2c shows how Quantor was integrated with the WEC emulator on the test rig.*

5.1.2 WEC Emulator Control

Two possible ways of controlling the WEC emulator were considered: torque control and speed control, which are both illustrated in Figure 5.3. The torque control scenario requires that the total entrained inertia of the WEC emulator is equal to that of the WEC being simulated [15]. However, it can be tricky to obtain precisely the correct driveline inertia in practice. The best approach is to design the driveline so that its total inertia matches that of the simulated WEC as closely as possible, and to then verify the inertia experimentally [15].

The difficulty with this approach on the test rig was the issue of reflected inertia. Resolving the equations which define a gear ratio (G) (Equation (5.8)) (where the subscripts 1 and 2 refer to the shaft before and after the gear respectively), and the relationship between torque (τ), moment of inertia (I) and angular velocity (ω)(Equation (5.9)), gives the result in Equation (5.10) for inertia 'reflected' through a gear. This can be considered as the apparent moment of inertia on one side of the gear due to the physically embodied inertia on the other side of the gear.

$$G = \frac{\omega_2}{\omega_1} = \frac{\tau_1}{\tau_2} \tag{5.8}$$

$$\tau = I\omega \tag{5.9}$$

$$I_1 = G^2 I_2 \tag{5.10}$$

The reason this is significant for the designed test rig is that the total moment of inertia 'visible' to the PTO must be equal to that of the WEC. However, the need for a large drive gear ratio between the electric motor and the flywheel means that the intrinsic inertia of the electric motor is apparent at a much greater value on the PTO end of the driveline. For example, an electric motor with an inertia of $2\,\mathrm{kg\,m^2}$ which is geared down to the flywheel at a ratio of 18 will have an apparent inertia at the PTO of $2 \times 18^2 = 648\ \mathrm{kg\,m^2}$. This is undesirable as this reflected inertia could easily end up exceeding the flywheel inertia, and the presence of a gear in between two significant inertias with different torques being applied to each could lead to serious issues of backlash and reduced controllability of the WEC emulator, making the test unrepresentative of sea conditions. Therefore, having as much of the inertia apparent to the PTO being entrained in the flywheel was considered desirable, therefore a low inertia electric motor was sought. This lead to conflicting aims in the test rig design: a higher gear ratio allows better matching of speed regimes, but will generate more reflected inertia.

Torque Control

- All the mass is real
- Inverter gets a torque demand
- Model input is position of the flywheel
- Each WEC requires the physical mass to be correct to achieve the expected dynamic behaviour.

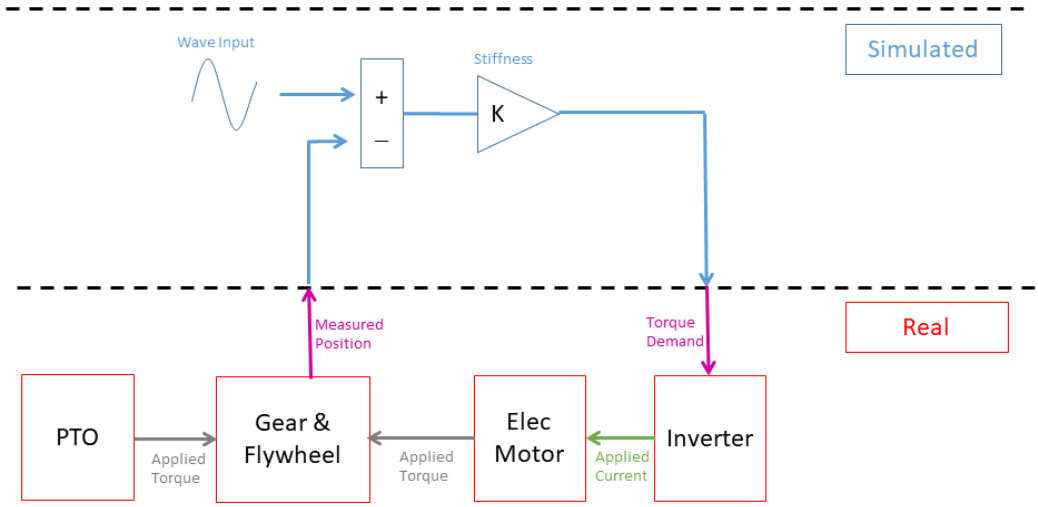

(a) *Rig control diagram for torque control. Blue arrows show the calculations carried out by the controller, purple arrows show control signals governing interaction between controller and hardware, grey arrows represent real mechanical signals and green represent real electrical signals.*

Position Control

- The mass is simulated, however some real mass is required for stability.
- Inverter gets a position (or speed) demand.
- Model input is torque
- A range of WECs can be simulated without changing the physical mass
- Similar concept to a vehicle dyno.

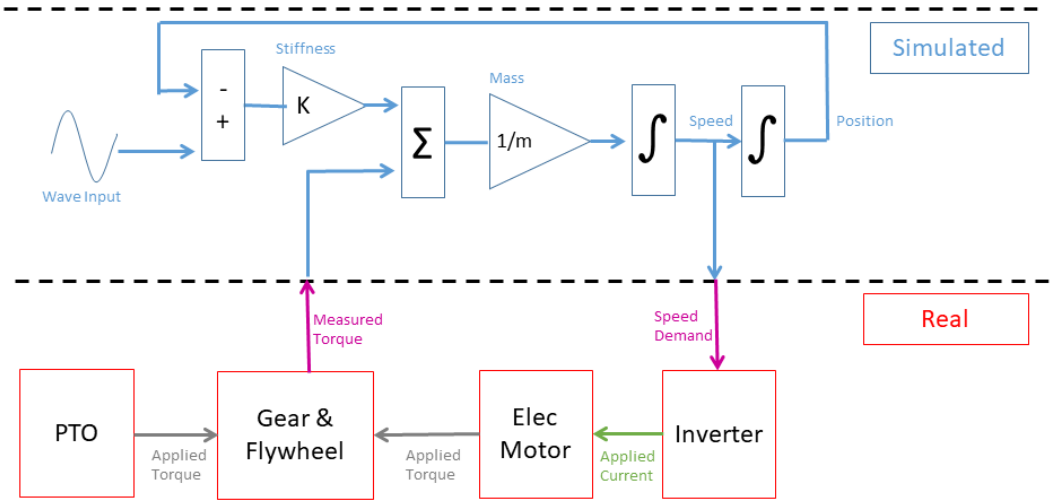

(b) *Rig control diagram for speed control. Arrow colours as for Figure 5.3a.*

Figure 5.3 *Control schematics for two different WEC emulator control options (figure made by Daniil Dumnov).*

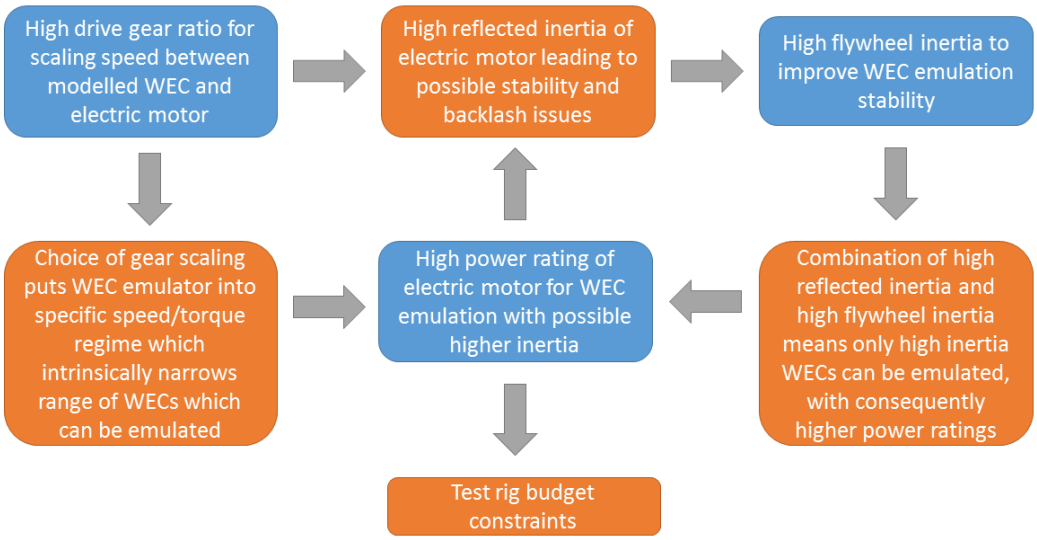

Figure 5.4 *Summary of design requirements (blue) and their consequences (orange) for the design of the WEC emulator in torque control.*

The issue of reflected inertia and the consequent desire to have a large flywheel inertia meant that total inertia of the modelled WEC would have to be fairly substantial. However, this automatically meant that the WEC would be operating in a higher power regime. For example, rather than being a small scale WEC such as a 4 m diameter buoy resonant in a sea state of energy period 3 to 5 s, it would have to have a larger diameter of 6 m (to have greater mass) and be resonant in waves of energy period 5 to 8 s. This then means that the total power rating of the WEC emulator must be increased, without increasing the inertia unduly. Increasing the power rating of the rig will also ultimately mean reaching budget constraints. These conflicting design requirements are illustrated in Figure 5.4.

To increase the range of WECs which could be emulated, a speed control approach was also considered. The advantage of this strategy is that the inertia entrained on the test rig does not need to perfectly match the inertia of the modelled WEC: it simply needs to be within the electric motor's ability to follow the required speed demand with whatever inertia is present on the driveline. The disadvantage is that it is possibly a less representative test, as more of the WEC emulation is resolved in the model and not in the physical hardware. However it would be possible to verify any difference between these two by carrying out the same test for the same WEC in the same sea state, but one case using speed control and one case using torque control. This means that the flywheel inertia is there to provide stability and to demonstrate the Quantor's ability to respond

to inertia. This is also probably an easier case to close a control loop on. This is still a HIL system as the measured PTO torque is fed back into the WEC model running in real-time, so the WEC response is updated with information from the PTO behaviour.

5.1.3 Selection of Components

Components were selected through an iterative process of modelling exercises and research on the hardware available. Simulations were carried out of two different WECs (a floating hemisphere and floating spar) which have different torque/speed regimes, to try to cover some of the variety of WECs shown in Figure 5.1. Different drive gear ratios and different sea states (regular and irregular) were explored, as well as the possibility of Froude scaling the simulated WEC. The issue with Froude scaling is that it has the effect of 'speeding up' time, which means that the hydraulic processes in the Quantor have to happen much more rapidly, with flows increasing, and the viscosity does not scale correctly, making the results unrepresentative. This served to narrow the design envelope so that the compromises between different test rig designs and capabilities of WEC emulation were clear. It also meant peak and mean power requirements for the electric motor and drive could be assessed. The potential for over-driving particular components such as the electric drive and motor for short periods was also investigated, which was relevant to intermittent high power wave groups in irregular seas.

Electric Motor and Drive

A 304 kW asynchronous servomotor was selected (the Vascat MAC QI 250S), with a nominal speed of 1700 rpm and nominal torque of 1750 N m. The maximum speed was 3400 rpm and maximum torque 2800 N m. The intermittent power output of this motor could go as high as 350 kW. A key advantage of this motor was its relatively low inertia of 1.65 kg m^2. More information about this motor is available at [84].

Drive Gear

A drive gear with was a challenge to procure because there were few offerings on the market with both an appropriate gear ratio and the correct torque rating. In the end, a Bonfiglioli gearbox with a ratio of 17.4 was chosen. This was a higher gear ratio than was desired for the decreasing the electric motor speed (ideally 12-14 would have been available) but this was not available with the torque rating required.

PTO Gear

This was chosen as the smallest gear ratio it was possible to design (i.e. as close to 1 as possible) whilst still having four fixed displacement motors mounted on pinions arranged around a central hub. This meant the ratio ended up being 40:26 which is approximately 1.53. This choice does not affect the representation of the WEC as the gear scaling is arbitrary (within an envelope), so this physical gear can be considered to contribute to the gear scaling. This was designed as a floating arrangement so that load cells could be used to measure the torque on the central hub.

Figure 5.5 shows how the PTO splitter gear was assembled and the connection of the floating gearbox to the base frame via the load cells. Figure 5.6 shows how the PTO gear appeared from the control cabin and the chosen conventions for integration with Quantor.

5.1.4 Transducers

The transducers on the WEC emulator section of the lab setup were a Heidenhain ROD 436 incremental encoder on the electric motor, an HBM T40 50 kN m torque transducer on the high speed shaft before the Bonfiglioli gearbox and a PT100 temperature sensor on the Bonfiglioli gearbox. These were not used as control feedback signals (the inverter does the PI control of the speed or torque on the electric motor) but simply to monitor the state of the flywheel and to ensure that we were not overloading the Bonfiglioli gearbox which had a more restricted specification than the other components.

5.1.5 Control

The WEC emulator was controlled via a CANOpen link from the system controller (Speedgoat) to the inverter. This could be controlled to move at a set constant speed, at a prescribed sinusoidal speed or to follow the speed demand generated by a WEC model in either regular or irregular waves, using feedback from the real PTO torque measurement as part of a HIL system. This could also be done in torque control as well, with the measured speed of the flywheel shaft being the feedback variable.

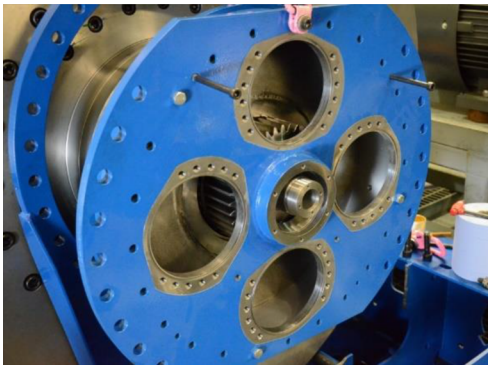

(a) *Photograph of floating PTO splitter gearbox with the central gear installed.*

(b) *Photograph of PTO splitter gearbox with PTO motors installed on their pinions*

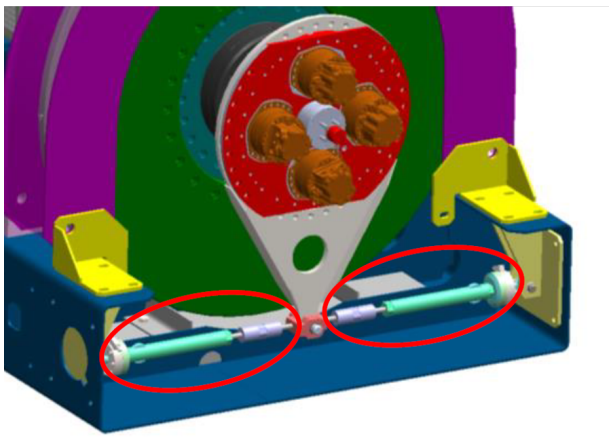

(c) *CAD drawing of floating PTO gear assembly connected to the base frame with load cells (circled in red)*

Figure 5.5 *Details of PTO splitter gearbox and load cells for torque measurement (from [17])*

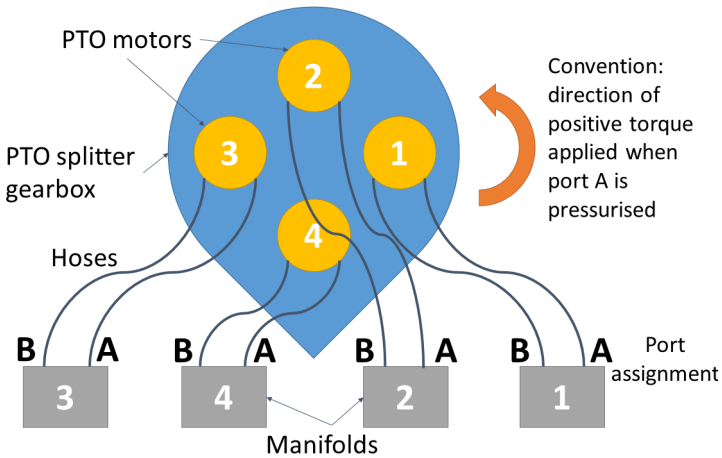

Figure 5.6 *Diagram of the front view of PTO splitter gear, Poclain motors and manifolds, indicating motor and manifold numbering convention, port assignment convention and torque direction convention.*

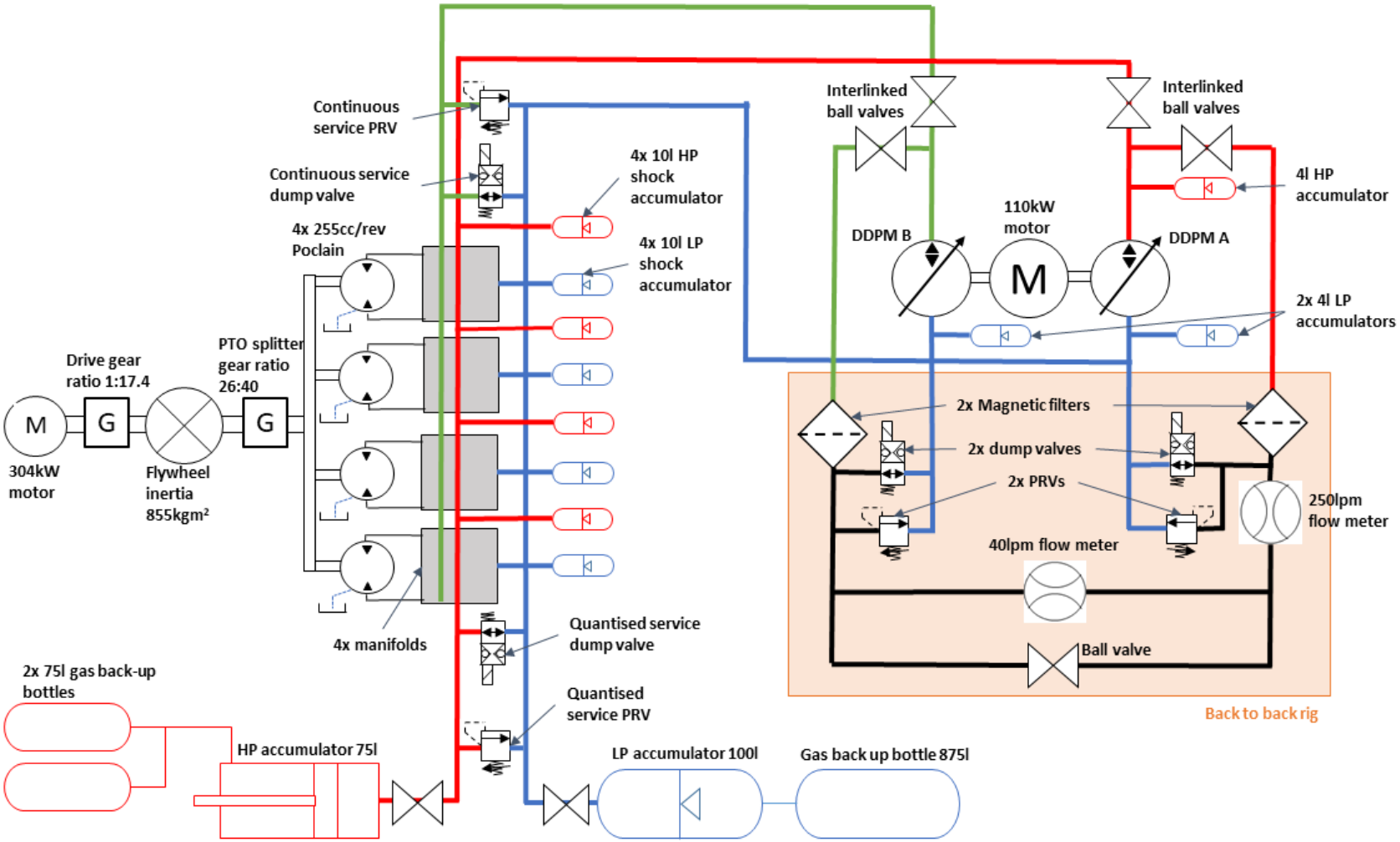

Figure 5.7 *Schematic of WEC emulator, Quantor and back-to-back test rig. The manifold internal structure, and auxiliary systems including boost pumps and pilot system are omitted for clarity.*

5.2 Laboratory Implementation of Quantor System

Figure 5.7 shows the full hydraulic schematic of the test rig, including the back-to-back rig and the auxiliary systems. Figure 5.8 shows the completed test rig and Quantor with annotations of the key pieces of equipment and Figure 5.9 shows the side view of the apparatus. For interest, Appendix B describes the commissioning process in more detail.

5.2.1 Quantor Components

Fixed Displacement Motors

The four fixed displacement motors used were Poclain MS02 pump motors with a displacement of 255 cm^3/ rev. They have a maximum working speed of 480 rpm and maximum working pressure of 450 bar. A low leakage variant (option H for reinforced piston sealing for higher volumetric efficiency) [85] was selected. They are connected to the ports on the manifold blocks by 25 mm diameter high pressure hoses. Originally during the rig design, a PTO gear ratio of 1:1 was anticipated and the displacement of the motors selected so that an average power rating of 30 kW could be anticipated from the Quantor. However, when the gear ratio of 1.53 was chosen the displacement of the motors was scaled down by the same ratio so that the flows seen by the rest of the Quantor system would not change.

Manifold Blocks

The four manifold blocks (one to control each motor) were installed on rails in front of the flywheel and PTO motors. The manifolds had been redesigned from the prototype block as described in Appendix B. The manifolds are designed so that the hard-piped HP and DDPM galleries run straight through them all. So that the pressure in the hard-piped galleries does not drive the manifolds apart, reaction struts are in place to hold the blocks in place, as shown in Figure 5.11.

Accumulators

The HP accumulation consisted of a 74 l piston accumulator with measuring rod, backed up by a further 150 l of gas. The LP accumulator had a volume of 100 l with 875 l of gas back-up to keep the boost pressure variation minimal. Flexible hoses connected the ends of the hard-piped HP and boost galleries to the respective accumulators. Each manifold

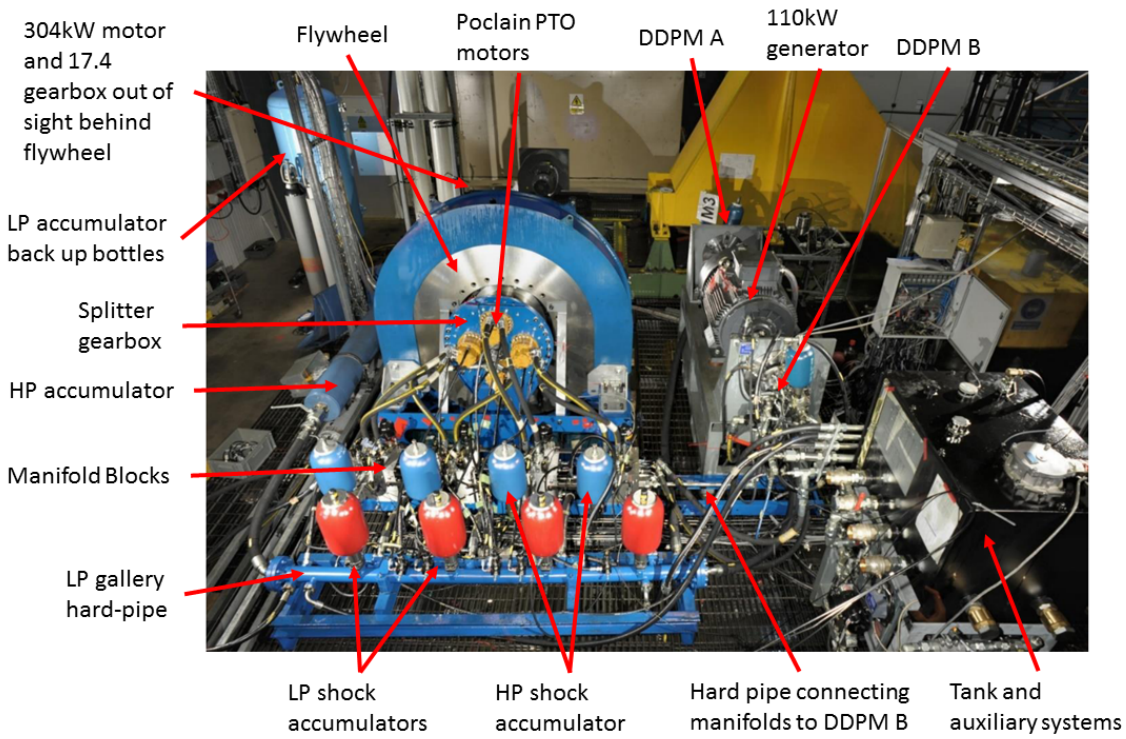

Figure 5.8 *Annotated photograph of the completed test rig. [21]*

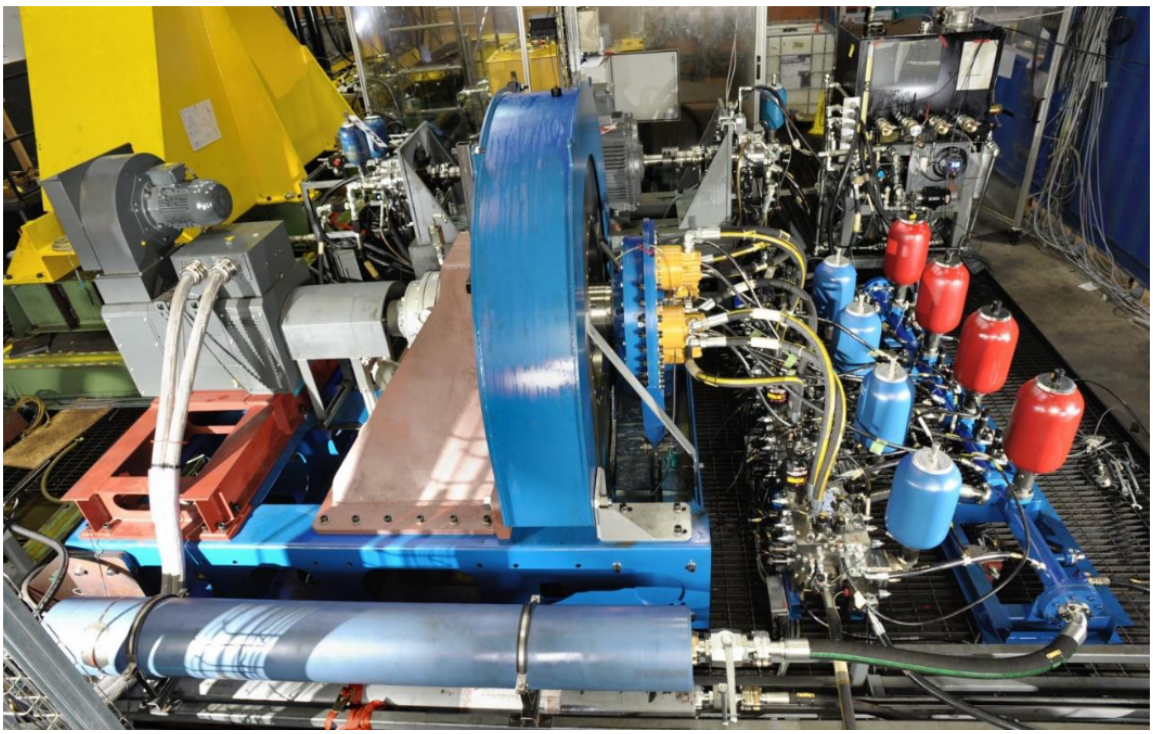

Figure 5.9 *Side view photograph of completed WEC emulator and Quantor. [21]*

Figure 5.10 *Photograph of Poclain MS02 motor used in Quantor lab system as PTO actuators [22].*

had an HP shock accumulator of volume 10 l attached, and an LP shock accumulator (also of volume 10 l) at the connection from the manifold to the boost gallery. There was also a small HP bladder of 4 l on the outlet of DDPM B to reduce the pressure ripple in this very stiff system. The precharge pressure of the HP system for most tests was 150 bar and for the LP system was 5 bar.

DDPMs

The DDPMs are two M96 pump motors of displacement 96 cm^3/ rev each. They are mounted on either end of a through-shafted generator. Each machine has 12 solenoid-

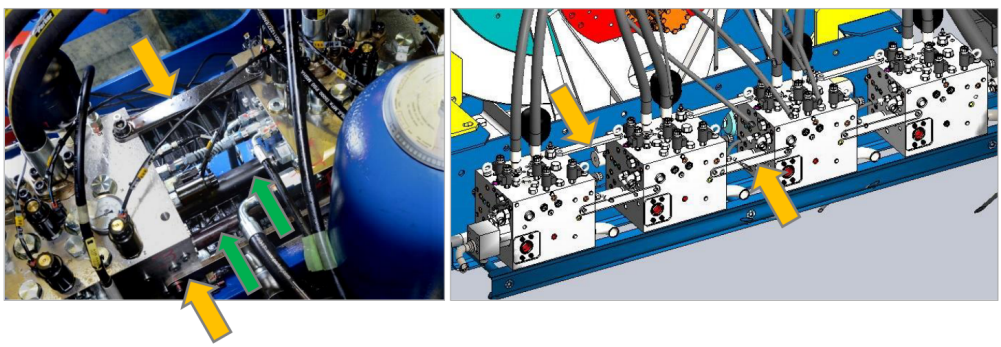

Figure 5.11 *Showing the floating hard-pipe connections, arrowed in green on the left, and the reaction struts, arrowed in yellow in both images. The image on the right also shows one of the two (blue) 'C' section rails to which the blocks are bolted [23].*

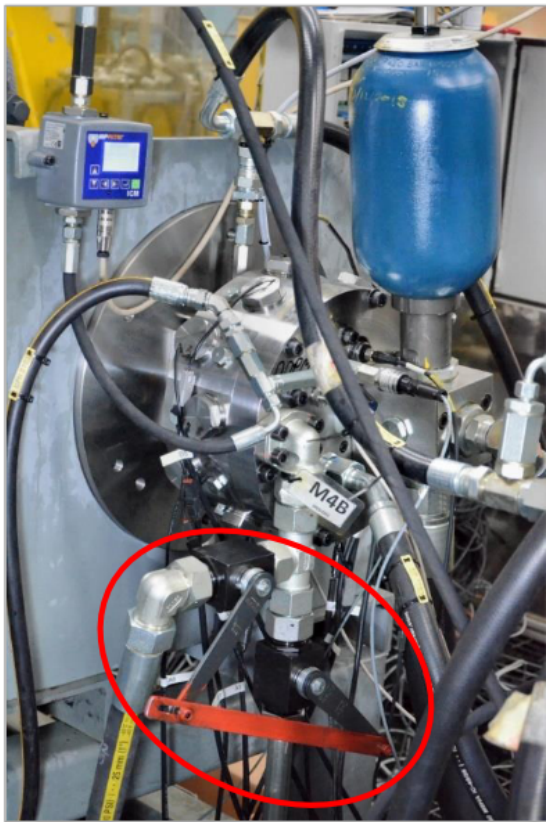

Figure 5.12 *Photograph of DDPM B showing* 4 l *accumulator, 2×two-way ball valves for connection to back-to-back rig (circled), hard-pipe connection to Quantor rig and other connections [21]*

actuated valves, arranged in two banks of six. The maximum pressure is 400 bar and for the Quantor they run at a constant synchronous speed of 1500 rpm. Each machine has a dedicated controller; the AIP-designed Artemis Modular Controller (AMC2), which runs the algorithm which fires each valve as required.

DDPM B, as it is on the stiff service, has a steel hard-pipe connection to the gallery running through the manifolds blocks. DDPM A has a long hose connection to its gallery.

Both DDPMs also can be disconnected from the Quantor test rig and connected into the back-to-back test rig for specified testing or debugging, as shown in Figure 5.12.

Generator

The generator is a 110 kW, 4-pole, through-shafted induction motor supplied by TEC Electric Motors (reference 110.043TECCB3-IE2). This is fairly oversized for the expected maximum output power of 30 kW but a larger generator was necessary to obtain the required shaft torque rating. This also allows the M96 machines to operate up to full power

in the back-to-back rig configuration. For a real Quantor system in a WEC, the generator would be matched more appropriately to the expected output power (which would also presumably be greater than 30 kW). Incidentally, the real mismatch in the Quantor lab system is between the Poclain motor and the DDPMs; the maximum average output from the combined Poclains would be expected to be approximately 50 kW, compared to the 150 kW capability of the combined DDPMs.

Back to Back Test Rig

There was a separate circuit, known as the 'back-to-back rig' which connects the two DDPMs directly, isolating them from the Quantor rig by the system of two-way ball valves pictured in Figure 5.12. On this rig, either machine can act as a pump or a motor, and there are flowmeters and magnetic filters between the two machines. This means that the model of the DDPM flow can be verified separately to the Quantor tests.

Control

The main system controller was a Speedgoat, which is an xPC target machine with a range of analogue and digital I/O modules, as well as ethernet and CAN connectivity. The control software developed in Simulink could be loaded onto the Speedgoat, which had supervision of the other system controllers, for example, the inverter driving the WEC emulator and the AMC2s controlling the DDPMs. The AMC2s acted as low-level controllers for the DDPMs, following the displacement demand set by the Speedgoat.

Auxiliary Systems

There were also several auxiliary systems required for the running of the test rig, some of which would not exist in an implementation of Quantor in a WEC (which, for example, would have a static boost system). There was an oil tank and boost pump controlled by the Speedgoat to maintain both boost pressure and oil tank volume. There was a flushing circuit for the PTO motor casings, in case they required cooling. There was also filtration and two oil condition monitors. There was the pilot system, which was pressurised from the HP gallery via a check valve, and featured small bladders mounted on each block to ensure each valve always had a ready supply of pilot pressure. These systems are all shown in Figure 5.7.

5.3 Transducers

The location of sensors on the test rig is shown in the schematics Figure 5.13 and Figure 5.14. Table 5.1 provides details of the corresponding sensors. Pressure transducers were fitted to every manifold block's motor ports and pilot gallery. Measuring the pressure on the motor ports meant that an estimation of the applied torque from the applied pressure (in addition to the actual torque measurement) and the hydraulic power could be derived in later loss modelling. On Block 1 there were pressure sensors fitted to the pilot lines of every active valve so that more detailed analysis can be done on the control signals and transient behaviour using this block. There were pressure transducers on the inlet and outlet ports of both DDPM machines, which meant the fluid and mechanical power of the DDPMs could be estimated using models. There were both oil and gas pressure sensors on each accumulator. The high pressure accumulator had a piston with a string potentiometer attached, which means that the volume of oil in the accumulator at any time is known. This meant that an accurate measurement of the accumulator's stored energy and losses was possible.

There are torque transducers on the shaft of each DDPM. The 110 kW motor is a through-shafted, with a DDPM on each end, which allows the output torque of each machine to be measured independently so that the output mechanical power of the Quantor is known. The PTO torque is measured by two load cells mounted to the PTO splitter gearbox. This, combined with the very accurate PTO shaft encoder (65536 edges) means an accurate measurement of the input mechanical power to the Quantor PTO can be obtained. Drive torque is also measured, on the high speed electric motor shaft before the Bonfiglioli gearbox, so that backlash in the WEC emulator system can be assessed.

Each DDPM has an encoder which is required by its AMC2 controller for making valve firing decisions. Although the 110 kW motor is supposed to maintain a constant speed, the torque applied by either DDPM during pumping or (especially) motoring may decelerate or accelerate the shaft.

Current clamps are placed on the DDPM control valves for checking the calibration of the two DDPMs to maintain the efficiency and the stability of the machines and the Quantor valves, for debugging control issues.

There are also other sensors, such as the oil tank level sensor which provides important information about the volume of oil in the system. Given that both the HP and LP accumulators are very large, it would potentially be easy to drain the tank in filling the accumulators, which would eventually cause the boost pressure to collapse, damaging the

machines. This meant that the boost control needed information about the tank level to control the LP side of the Quantor safely. Temperature sensors are in place on some of the relief valves and the Bonfiglioli gearbox, to prevent overheating of the respective components.

There are no flowmeters on the Quantor test rig, which means the hydraulic power (the product of pressure and flow) cannot be directly measured. This means that the flow from the Poclain motors is inferred from the measured speed and the manufacturer's leakage data. The flow from the DDPMs is estimated from the loss model (except when using the back-to-back test rig which has flowmeters).

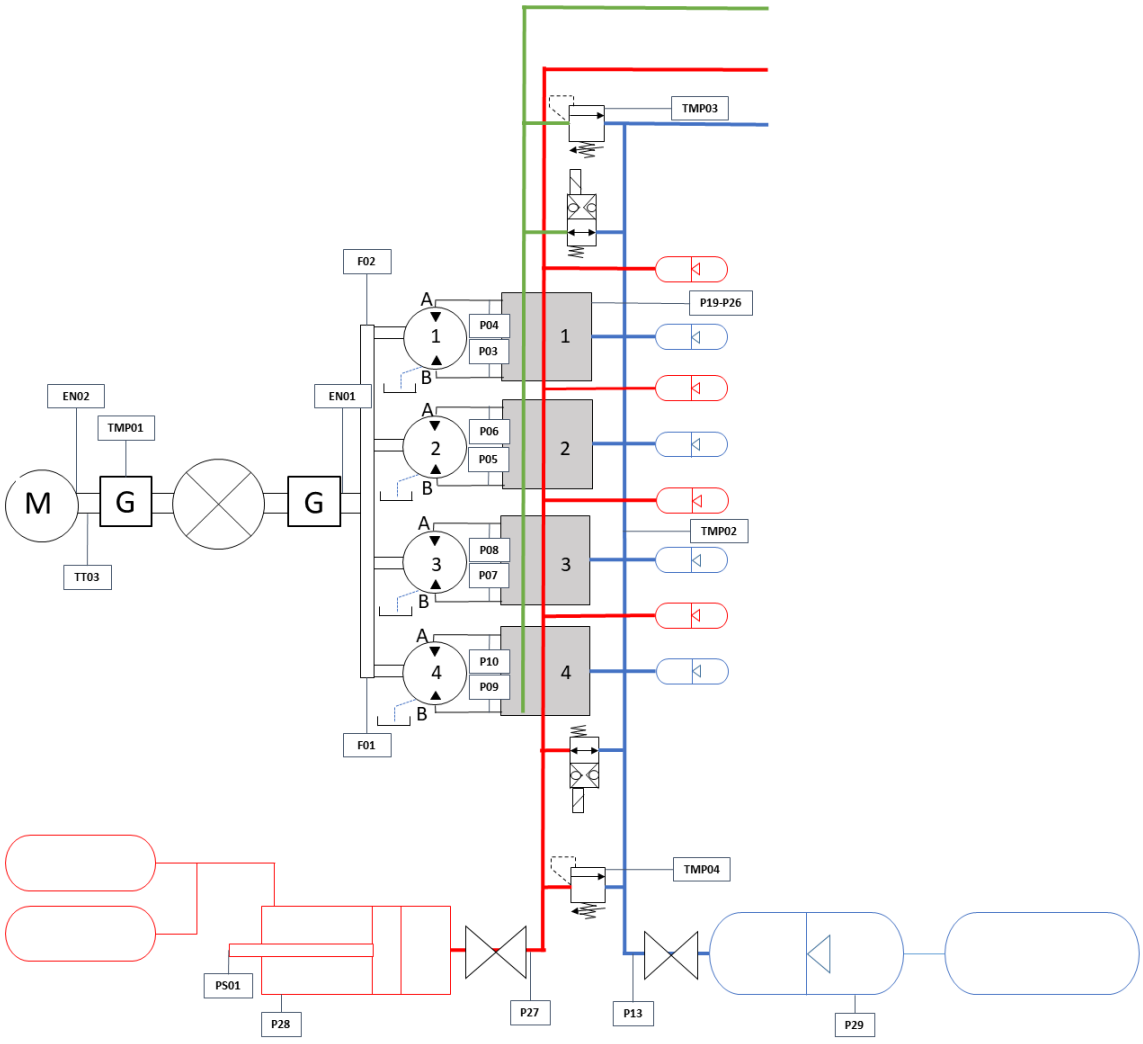

Figure 5.13 *Location of transducers (listed in Table 5.1) on the WEC emulator and Quantor primary actuators (see Figure 5.7 for full test rig schematic).*

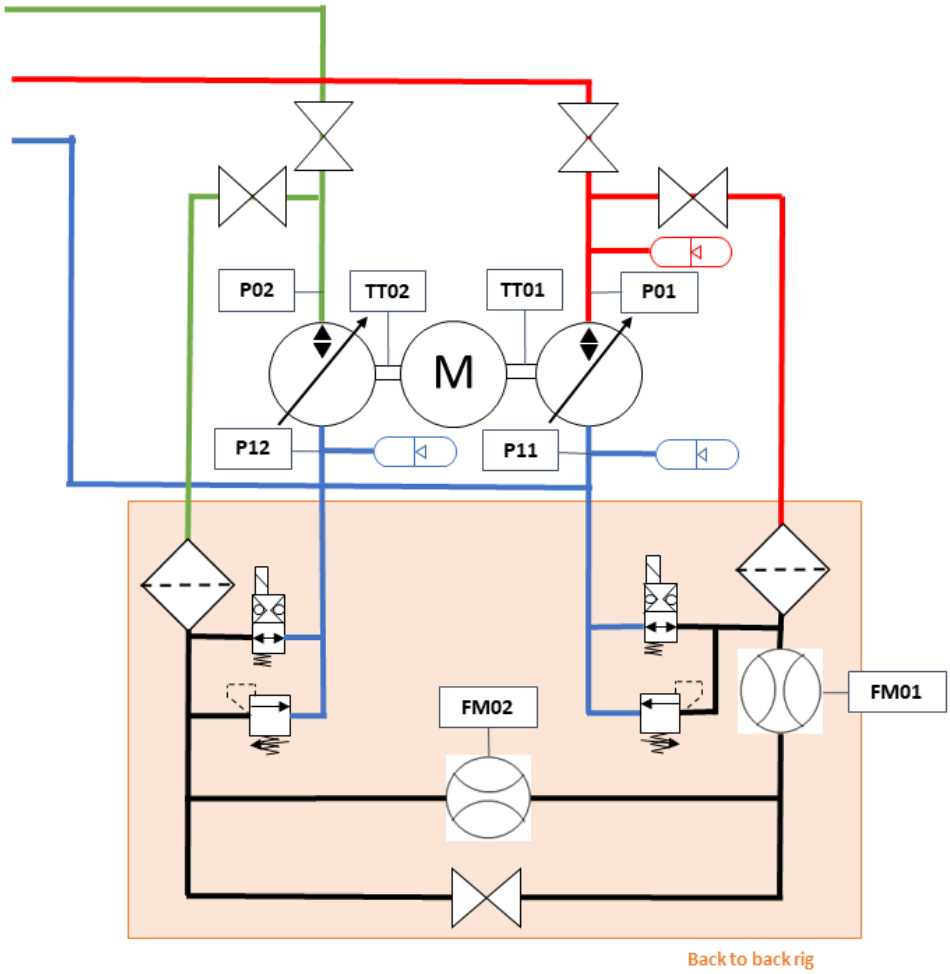

Figure 5.14 *Location of transducers (listed in Table 5.1) on the DDPMs and back-to-back rig (see Figure 5.7 for full test rig schematic).*

Table 5.1 *List of measured quantities and transducers used on the test rig.*

Code	Name	Type	Measurement range	Manufacturer	Part number
		Analogue			
P01	DDPM A Outlet Pressure	Pressure transmitter	0 to 600 bar	Danfoss	MBS1250
P02	DDPM B Outlet Pressure	Pressure transmitter	0 to 600 bar	Danfoss	MBS1250
P03	Poclain Motor 1 Port B	Pressure transmitter	0 to 600 bar	Danfoss	MBS1250
P04	Poclain Motor 1 Port A	Pressure transmitter	0 to 600 bar	Danfoss	MBS1250
P05	Poclain Motor 2 Port B	Pressure transmitter	0 to 600 bar	Danfoss	MBS1250
P06	Poclain Motor 2 Port A	Pressure transmitter	0 to 600 bar	Danfoss	MBS1250
P07	Poclain Motor 3 Port B	Pressure transmitter	0 to 600 bar	Danfoss	MBS1250
P08	Poclain Motor 3 Port A	Pressure transmitter	0 to 600 bar	Danfoss	MBS1250
P09	Poclain Motor 4 Port B	Pressure transmitter	0 to 600 bar	Danfoss	MBS1250
P10	Poclain Motor 4 Port A	Pressure transmitter	0 to 600 bar	Danfoss	MBS1250
P11	DDPM A Tank Pressure	Pressure transmitter	0 to 40 bar	Hydac	HDA-8446-A-0040-000
P12	DDPM B Tank Pressure	Pressure transmitter	0 to 40 bar	Hydac	HDA-8446-A-0040-000
P13	Boost Pressure	Pressure transmitter	0 to 40 bar	Hydac	HDA-8446-A-0040-000
P14	Pilot Supply Pressure	Pressure transmitter	0 to 400 bar	Hydac	HDA-8446-A-0400-000
P15	Pilot Pressure Manifold 1	Pressure transmitter	0 to 600 bar	Danfoss	MBS1250
P16	Pilot Pressure Manifold 2	Pressure transmitter	0 to 600 bar	Danfoss	MBS1250
P17	Pilot Pressure Manifold 3	Pressure transmitter	0 to 600 bar	Danfoss	MBS1250
P18	Pilot Pressure Manifold 4	Pressure transmitter	0 to 600 bar	Danfoss	MBS1250
P19	Trans Flow Hi + (mfd1 port 8)	Pressure transmitter	0 to 600 bar	Danfoss	MBS1250
P20	Trans Flow Hi - (mfd 1 port 6)	Pressure transmitter	0 to 600 bar	Danfoss	MBS1250

P21	Trans Flow Lo + (mfd 1 port 20)	Pressure transmitter	0 to 600 bar	Danfoss	MBS1250
P22	Trans Flow Lo - (mfd 1 port 22)	Pressure transmitter	0 to 600 bar	Danfoss	MBS1250
P23	Main Flow Hi + (mfd 1 port 5)	Pressure transmitter	0 to 600 bar	Danfoss	MBS1250
P24	Main Flow Hi - (mfd 1 port 4)	Pressure transmitter	0 to 600 bar	Danfoss	MBS1250
P25	Main Flow Lo + (mfd 1 port 23)	Pressure transmitter	0 to 600 bar	Danfoss	MBS1250
P26	Main Flow Lo - (mfd 1 port 24)	Pressure transmitter	0 to 600 bar	Danfoss	MBS1250
P27	HP Accumulator Pressure	Pressure transmitter	0 to 600 bar	Danfoss	MBS1250
P28	HP Accumulator Gas Pressure	Pressure transmitter	0 to 600 bar	Danfoss	MBS1250
P29	LP Accumulator Gas Pressure	Pressure transmitter	0 to 40 bar	Hydac	HDA-8446-A-0040-000
PS01	HP Accumulator Piston Position	String Potentiometer	0 to 3 m	Celesco	SR1A-125
CC01	DDPM A Valve Current	Current Clamp	0 to 20 A	Pico	TA018
CC02	DDPM B Valve Current	Current Clamp	0 to 20 A	Pico	TA018
CC03	Quantor Valve Current	Current Clamp	0 to 600 A	Pico	TA019
TT01	DDPM A Torque	Torque Transducer	0 to 5 kN m	HBM	T40
TT02	DDPM B Torque	Torque Transducer	0 to 5 kN m	HBM	T40
TT03	Drive Torque	Torque Transducer	0 to 5 kN m	HBM	T40
LS01	Oil Level Sensor	Level Sensor	0-Full tank	Omni	DUT-E A10
F01	Orbital Gearbox Force 1 (left)	Load Cell	0 to 50 kN	PCM	BD-TC4
F02	Orbital Gearbox Force 2 (right)	Load Cell	0 to 50 kN	PCM	BD-TC4
TMP01	Bonfig Gearbox Temperature	PT100	−40 to 120 °C	NOVUS	TX-RAIL
TMP02	LP Manifold Temperature	PT100	−50 to 150 °C	E-DAM	9015
TMP03	Stiff PRV Temperature	PT100	−50 to 150 °C	E-DAM	9015
TMP04	Compliant PRV Temperature	PT100	−50 to 150 °C	E-DAM	9015

		Quadrature			
TT01	DDPM A Shaft Speed	Torque Transducer		HBM	T40
EN01	Flywheel Speed	Incremental Encoder	Pulse Train	SICK	DFS60A-S4CC65536
EN02	Drive Electric Motor Speed	Incremental Encoder	Pulse Train	Heidenhain	ROD 436
FM01	Back to Back Flow 1	Flowmeter	0 to 250 l/min	VSE	Vci 4/10
FM02	Back to Back Flow 2	Flowmeter	1 to 40 l/min	KRACHT	

5.4 Summary

A complex test rig, comprising of a WEC emulator and a laboratory-scale Quantor PTO was constructed at AIP premises. This test rig was carefully instrumented, so that functioning of the control system could be well understood and so that all the information required for detailed loss model validation was available. Commissioning of this test rig was a complex and in-depth process which took many months and several iterations of small-scale experimental rigs. This process is partially described in Appendix B, for the reader's interest. The designed test rig, despite its technical detail, was successfully built and instrumented to the required specification to a point where Quantor testing could proceed.

Chapter 6

Quantor Testing

The following chapter describes the testing of the Quantor carried out in the laboratory, on the test rig described in Chapter 5. The commissioning of Quantor on this test rig was a highly involved process which will not be explored in detail here. Similarly, the control strategy and refinement is only described briefly. This chapter aims to give context to the data gathered for loss breakdown analysis and model validation which is discussed in Chapters 7 to 8.

A broad range of control modes was tested. This is because, depending on the WEC design, mooring system, wave conditions, any faults in the Quantor, and the demanded torque, it may be necessary or more efficient to operate in a particular way. For example, in small seas, it may be more efficient to only use continuous control and not introduce any quantised states until the average input power reaches a certain threshold. This also allowed us to investigate the impact of different components and control modes on the loss breakdown in a progressive way. It was also important to understand what may be the most efficient mode of operation at different power levels, so that an improved controller with the ability to switch between control modes as conditions require could be developed for the future.

6.1 Control

The Quantor PTO force demand (F_{PTO}) is calculated based on the WEC position (x_{WEC}) and velocity ($\dot{x}_{WEC}$) according to Equation (6.1), where c_{PTO} and k_{PTO} are the PTO damping and spring coefficients respectively.

$$F_{PTO} = c_{PTO}\dot{x}_{WEC} + k_{PTO}x_{WEC} \tag{6.1}$$

x_{WEC} is in units of metres and $\dot{x_{WEC}}$ has units of metres per second, as they refer to the heave motion of the modelled WEC. The linear quantities in this equation must then be related to the rotary motions of the test rig via the gear scaling G_s, as shown in Equation (6.2) and Equation (6.3), where τ_{PTO} is the PTO torque applied on the test rig, θ_{rig} is the measured angular position of the PTO shaft position on the test rig and $\dot{\theta}_{rig}$ is the measured angular velocity of the test rig PTO shaft. The gear ratio is the ratio between the test rig PTO shaft speed and the WEC PTO shaft speed. Depending on how the envisaged WEC is structured, this could relate to different physical components such as a large ring gear with the PTO motors mounted on its circumference.

$$G_s = \frac{F_{PTO}}{\tau_{PTO}} \tag{6.2}$$

$$\frac{x_{WEC}}{\theta_{rig}} = \frac{\dot{x}_{WEC}}{\dot{\theta}_{rig}} = G_s \tag{6.3}$$

This calculation of the rig PTO torque demand is the first key step in the control of Quantor and impacts all subsequent control processes.

Friction Compensation

Once the model of the PTO motor friction had been validated (as described in Section 7.4.1), the rig PTO torque demand was modified accordingly. Without this modification, the friction torque was effectively added to the applied Quantor torque, which meant that the PTO torque applied exceeded the demanded PTO torque by the value of the friction torque. By subtracting the modelled friction torque from the PTO torque demand calculated from Equation (6.1), the applied Quantor torque matched the demand much more closely. An example of this is shown in Figure 6.4.

6.1.1 Chamber Port Settings and Control Words

An important aspect of the Quantor control software is the control words which feed into the algorithm. These words tell the algorithm what each chamber of the Quantor is available to do. The available options and their significance is detailed in Table 6.1.

These quantiser port settings are then converted into control words by some Simulink logic, which are then fed on to the relevant parts of the control system, such as the quantiser algorithm.

Table 6.1 *Descriptions of quantiser algorithm input port settings*

Quantiser Setting	Description
0	Active: Available for the quantiser algorithm to use
1	LP override: Chamber low pressure valves are held open so that chamber remains at low pressure
2	HP override: Chamber high pressure valves are held open so that chamber remains at HP accumulator pressure
3	Passive: No quantiser or directional valves are open, but the failsafe is engaged so that the PTO motor can passively pump through the passive check valves into the accumulator
4	DDPM B enabled: The chamber is available to the DDPM B-controlled stiff service and isolated from the HP gallery

6.1.2 Quantised Service Control

The role of the quantised service is to connect and disconnect PTO motor ports to the HP accumulator in a way which produces a quantised approximation of the demand torque. Each motor port is connected to four valves; one high pressure transient valve, one high pressure main flow valve, and the equivalent for low pressure. Each of these valves is controlled by a separate solenoid control signal.

Before the quantiser algorithm, the torque demand input to the quantiser must be offset, to account for the fact that some of the chambers may be under the control of DDPM B and therefore the quantiser may not be required to meet the full Quantor torque demand. This is labelled as the 'modified demand' in Figure 6.1.

At the heart of the control of the quantised service is the quantiser algorithm. This takes the quantiser demand torque and converts it into a vector of quantiser states, according to whether the states are available, whether the demanded torque is sufficient to warrant a change in state and optional refinements such as a weighting to minimise shear load on the PTO shaft. The quantiser state vector consists of ones and zeros; ones for active states and zeros for inactive states.

After the quantiser algorithm valve engine splits the quantised state vector into commands

to the transient high and low pressure valves. A state change from zero to one activates the transient high pressure valves and a change from one to zero activates the low pressure valves.

The main flow valve control signals are based directly on the transient valve signals described above, with a delay applied to allow each chamber to pressurise before supplying it with a large volume of flow. This prevents hydraulic shocks.

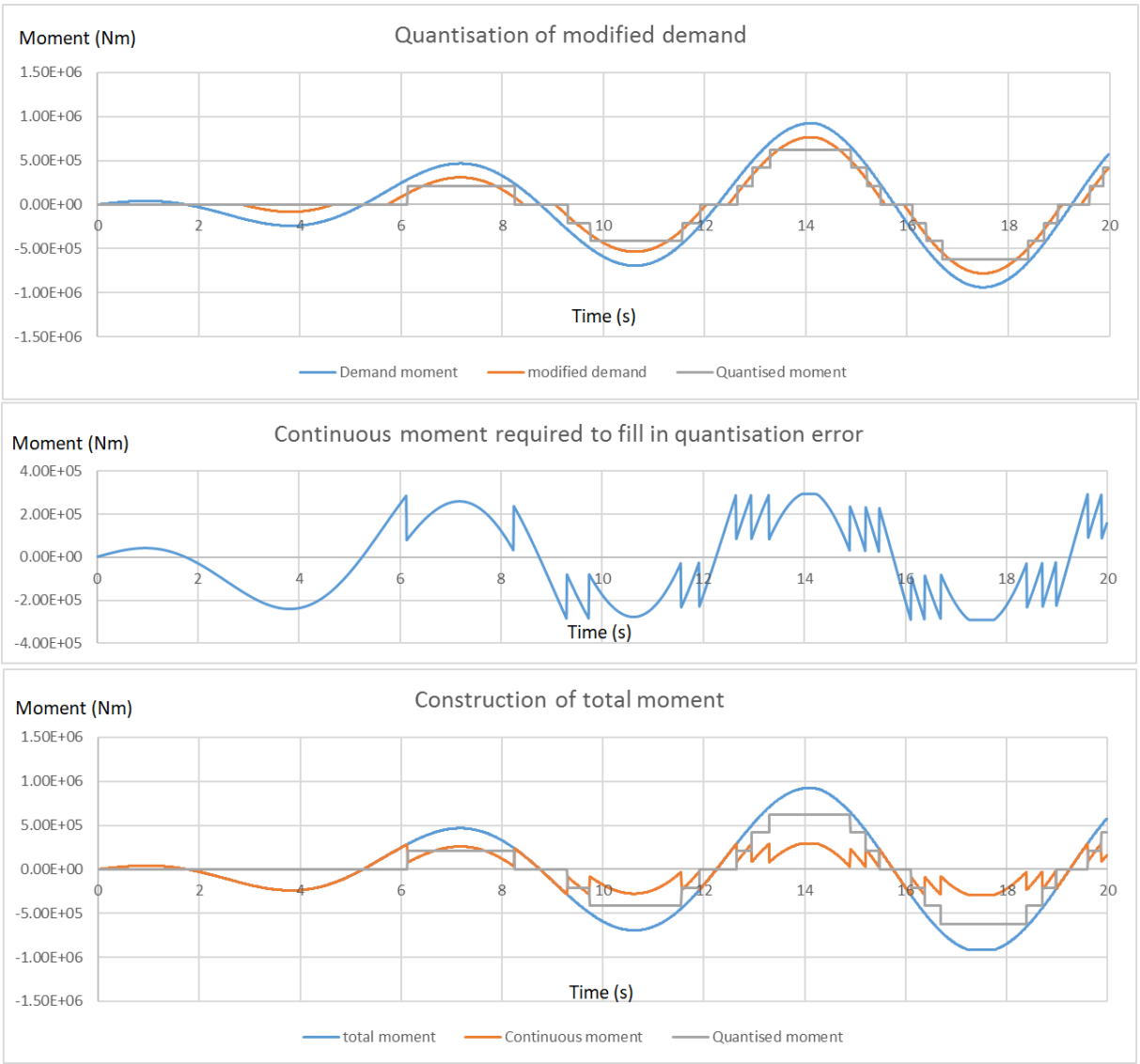

Figure 6.1 *Top: conversion of demand moment to quantised moment via the modified demand, Middle: resulting continuous moment error, Bottom: Combination of the quantised moment and continuous moment to meet the demand moment [3].*

6.1.3 DDPM A Control

DDPM A has two feedforward control terms and a third pressure control term. There is a power extraction term, which is effectively a low pass filter applied to the measured PTO shaft power. This is multiplied by a gain (which sets how rapidly the power captured by the PTO is then extracted by DDPM A) and then converted to an fractional displacement (Fd) demand, which dictates how much power DDPM A motors from the accumulator. There is the cancellation torque feedforward term, which is to allow DDPM A to smooth the rapidly varying torque produced by DDPM B. This estimates the torque applied by DDPM B from pressure and displacement, then converts this to a displacement demand for DDPM A. There is also an accumulator pressure control term, consisting of a PI loop with an anti-windup. In the irregular sea cases, the control of this is fairly relaxed, allowing the accumulator pressure to vary over its full range whilst protecting the end limits. However, for many of the prescribed motion cases, the gains were increased so that the accumulator pressure remained near-constant. In a WEC scenario, the accumulator pressure setpoint would vary depending on the average input mechanical power of the PTO.

6.1.4 Stiff Service Control

The continuous (stiff) torque demand is generated by subtracting the measured quantised moment (derived from pressure in quantised chambers multiplied by the displacement of the actuators) from the total torque demand. This is the portion of the demand torque which the continuous service must fill in (see the middle plot in Figure 6.1). This continuous torque demand is converted into a pressure demand for DDPM B by dividing by the displacement of the number of chambers under the stiff service control.

The directional valves in the manifold blocks are then controlled according to whether the continuous torque demand is positive or negative. If it is positive the 'positive' directional valve is open to the PTO motor, so that torque is applied in the positive direction and vice versa. They also have some hysteresis applied to prevent limit-cycling. When the torque direction changes so that one directional valve must be closed and its opponent opened, the valves are overlapped so that there is a brief time (of the order of a few milliseconds) where both the directional valves are open, so that the DDPM is not dead-headed at any point.

6.1.5 DDPM B Control

There are four components to the DDPM B pressure control: three feedforward terms and one closed-loop pressure control term. The first feedforward term accounts for the geometric flow of the Poclain motors under continuous control. The second accounts for the anticipated demanded pressure change in the stiff service, which is based on the rate of change of the stiff service torque demand signal. The third is known as the 'slug' and is a short burst of flow to smooth the net output torque around the quantised transitions, when DDPM B pressure needs to rise or fall very rapidly to counteract the torque a quantised chamber being switched on or off. The pressure control loop is to correct for any residual error apart from what the feedforward terms can account for. This is a simple PI loop with anti-wind-up.

6.1.6 Control Terminology

'Quantised' refers to cases where only quantising chambers are used to meet the torque demand and there is no contribution from the continuous service.

'Quantor' generically refers to cases where both the quantised and continuous service are active.

'Mode n' for n>0 refers to the number of PTO motors n under bidirectional control of the continuous service, e.g. Quantor mode 2 refers to a case where two PTO motors (4 chambers) are on the continuous service. 'Bidirectional' means that the stiff service can apply torque in both directions using the directional valves. Quantor mode 4 is a special case where all 8 chambers are under the control of the continuous service. Whilst this means that no quantising is occurring, the quantised service is still used because energy is exchanged between the accumulator and both DDPMs in the process of transforming.

'Mode 0' refers to the unidirectional case with one chamber under control of the continuous service. The directional valves are not switched over so DDPM B can only apply torque in one direction. This means that the modified demand of the quantised service (see Section 6.1.2) must be offset in one direction across the whole range of positive and negative PTO torque demand.

'Slug only' refers to cases where the smoothing of the torque caused by the quantising steps is carried out using only the slug feedforward term in the DDPM B control. The capacity of DDPM B is relatively high compared to the PTO motors on the test rig, so it can supply enough intermittent flow to rapidly change the chamber pressures for

smoothing quantised transitions.

'Slug and X' refers to cases where both the slug feedforward and another control feature (X) are used to smooth the torque of the quantising steps.

'Damping and spring' refers to the coefficients used to generate the PTO torque demand according to Equation (6.1). These are respectively c_{PTO} and k_{PTO} at WEC scale, and are presented in brackets in the figure legends in Section 6.3 as (c_{PTO} [kN s/m], k_{PTO} [kN/m]).

'Friction compensation' refers to the control feature where the PTO motor friction is estimated from a model and subtracted from the Quantor torque demand so that the final torque seen on the shaft matched the demand more closely.

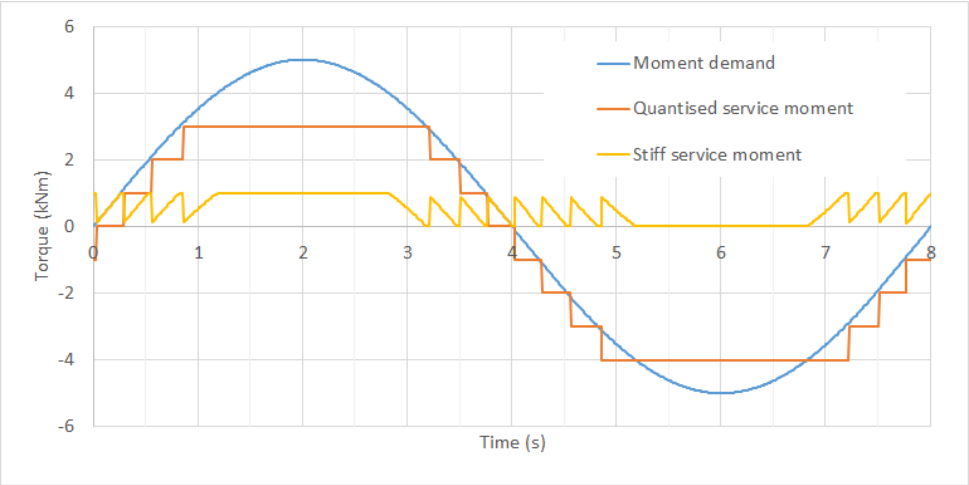

(a) *Torque demand, quantised service applied torque and stiff service applied torque for Quantor mode 0 (one actuator, unidirectional).*

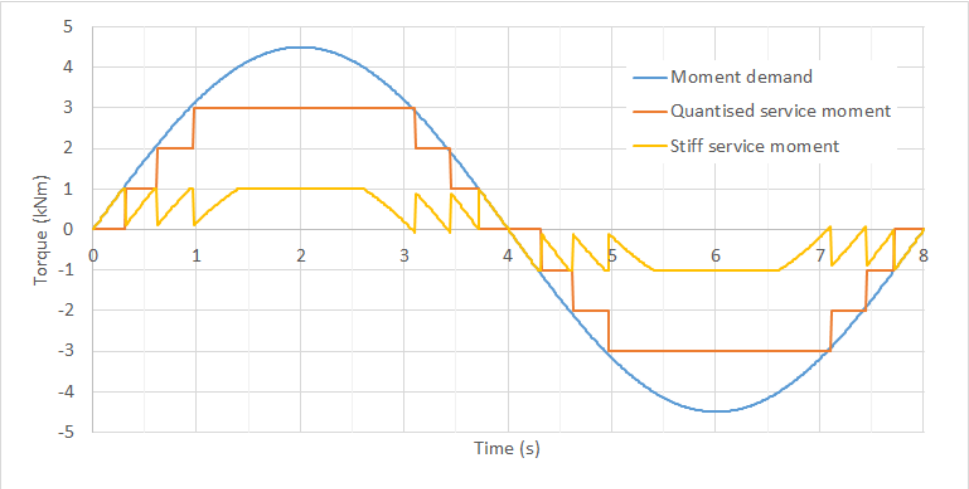

(b) *Torque demand, quantised service applied torque and stiff service applied torque for Quantor mode 1 (one actuator, bidirectional).*

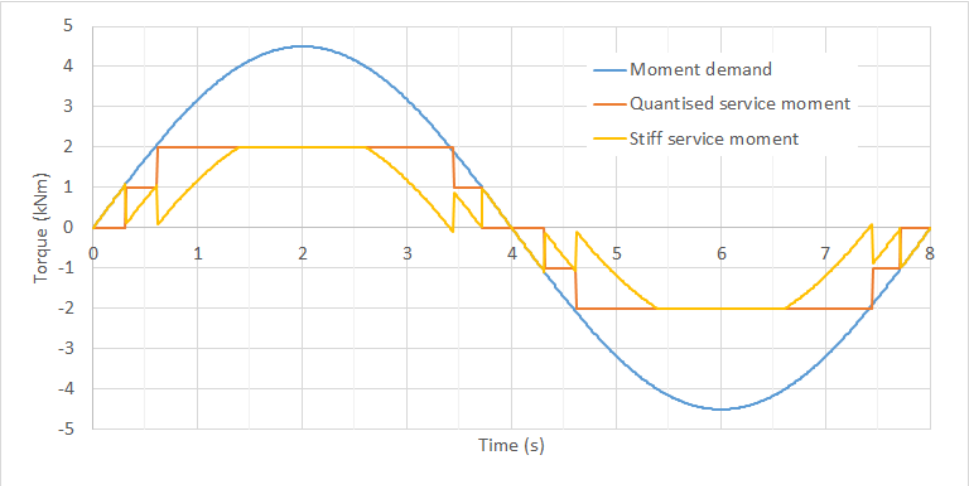

(c) *Torque demand, quantised service applied torque and stiff service applied torque for Quantor mode 2 (two actuators, bidirectional).*

Figure 6.2 *Comparison of Quantor control modes 0, 1 and 2. Modes 3 and 4 can be understood by extending the concept shown in these graphs.*

6.2 Test Methods

6.2.1 Pre-Test Procedure

A procedure was followed before every efficiency test carried out, to ensure consistency between tests and to check that transducers had not drifted since the previous experiment.
PTO torque offset check

- Open all LP valves on the motor ports.
- Run 5 cycles of sinusoidal speed on the electric motor (500 rpm amplitude, 5 s period)
- Check that the measured friction range is centred on zero over these cycles. Adjust offset accordingly if not.

Pressure transducer calibration and leakage test

- Before running the test rig, check that the pressure transducers have not shifted relative to each other.
- Run the boost pump and set all ports to 'LP override' to check that all the transducers read the same boost pressure.
- Spin flywheel to charge up HP accumulator to approx 200 bar.
- Set flywheel speed to 0 rpm.
- Set chambers +1, -2, +3, -4 to HP override and check they all read the same as the HP accumulator pressure sensor.
- Change the above chambers to passive and check that pressure is held.
- Repeat for chambers -1, +2, -3, +4.

Oil Temperature

- Heat oil to approximately 40 °C by running the electric motor at 300 rpm and motoring at an Fd of -0.1 on DDPM A.

Transient Valve Checks

- Set all ports to quantised mode with the main flow valves off.

- Generate a sinusoidal PTO torque demand of 10 s period and increasing amplitude up to 5800 N m and drive the electric motor accordingly.

- Check that pressurisation and depressurisation curves are all reasonably similar and that they haven't changed from the test where the needle valves were tuned (indicating that the needle valves have not changed their setting).

6.2.2 Steady Speed Tests

These were simple tests carried out in the initial commissioning stage, which involve relatively few components and therefore are useful for the first stages of loss breakdown analysis. They also mean that quantities such as PTO motor friction can be characterised over a range of test speeds and pressures. The flywheel was driven at constant unidirectional speed so that the PTO motors pumped through the passive check valves into the accumulator. DDPM A controlled the pressure in the accumulator to the relevant setpoint by motoring.

6.2.3 Prescribed Motion

The majority of Quantor testing was carried out using prescribed motion control. In these tests, no WEC or wave model was used. The flywheel was driven through a sinusoidal motion and the Quantor responded to the torque demand generated from the measured speed of the PTO shaft. For most cases a power curve (of efficiency vs input power) was generated by gradually increasing the amplitude of the sine wave, allowing the Quantor to settle to the new operating point and repeating the process. This meant many power curves could be generated for a range of control modes. Unless otherwise stated, the period of the sinusoidal motion was 10 s.

Passive Pumping

In these tests, no quantising or Quantor control was used. All ports were set to 'Passive' mode, so that they pump through the passive check valves into the accumulator, with DDPM A controlling the pressure. There is one passive check valve on each port of the PTO motors, so that the check valve used reverses with each reversal of speed of the flywheel.

Quantised

In these tests, all chambers were set to 'quantised' mode, so that only a quantised torque can be produced. For this to work correctly, the hysteresis in the transition between quantised states had to be set high enough to avoid limit cycling between states, which introduced a slight phase shift.

Quantor Mode 4

In these tests, DDPM B controlled all four motors. This was anticipated to be the most efficient control mode at low input powers.

Quantor Modes 2 and 3

These were carried out to examine the best point to change the number of motors on the continuous service.

Quantor Mode 1

Since this is the mode most similar to how Quantor is expected to run in a real WEC (with high numbers of PTO actuators and only one under continuous control), many tests were carried out in this mode and included varying the control between 'slug only' and 'slug and X', changing the damping and spring terms and changing the wave period.

6.2.4 Regular Wave Tests

This was a step up in complexity from prescribed motion, in that this used a WEC hydrodynamic model moving in regular waves as part of the HIL system, so that the measured PTO torque on the test rig was then fed back into the WEC model. For most cases mentioned below a model of the AWS WEC was used, which is a submerged buoy which vertically compresses and extends according to the increase in pressure due to the waves passing over it. This is a device which is likely to benefit from the continuous control of the Quantor PTO because it has a low inertia and therefore is unsuitable for a pure quantised approach. [86] provides more detail about this device. Since Quoceant had worked with AWS on a previous project, the hydrodynamic coefficients for this WEC were available. The rig controller could simulate other types of WEC but due to time constraints on testing, this was not possible.

6.2.5 Irregular Wave Tests

Regular wave motions are useful for PTO characterisation and development, but the statistics of real sea states are quite different, with average powers being lower and instantaneous peak values higher. In typical irregular seas, overall average efficiency is impacted by the amount of time spent at lower powers, where fixed losses are particularly penalising.

It is important to demonstrate Quantor's ability to deal with real wave conditions whilst providing smooth output power. It is also desirable to demonstrate PTO control strategies in irregular waves, where the effects of nonlinearities play out.

The WEC emulator drive was sized so that it could only represent a limited range of sea states and reduced WEC scales. However, this has been enough to prove Quantor's functionality and to quantify performance and validate simulation models.

Compression Applied to Wave Profiles

The very high ratio of instantaneous to average power in irregular waves is more challenging to the WEC emulator drive system than to the Quantor PTO. This limits the seas that can be represented but only due to the biggest wave peaks, accounting for only a tiny percentage of average power and response statistics.

A practical method to increase the effective incident wave power range of the drive was developed. A 'compression' process smoothly reduces only the largest wave peaks in the spectra, leaving the rest unaffected along with the overall power and load regime. This allows the significant wave height to be increased substantially, and the PTO to be tested in more powerful wave regimes than the rig drive would be capable of representing. While here this process only applies to the water surface elevation, more sophisticated WEC hydrodynamics models might require the process to apply to other input signals. The control logic used for this is shown in Figure 6.3a. When the wave position amplitude reaches above a certain threshold, the logic multiplies the difference by a variable factor (which increases smoothly as the amplitude above the threshold increases) and subtracts this value from the wave amplitude to obtain the smoothly limited output.

Figure 6.3b shows the effect of the compressor on the irregular wave profile in both the time domain and the frequency domain. In the frequency domain, the amplitudes of some frequencies are reduced by the compression process but overall the frequency behaviour remains very similar. The peaks in the spectrum have not moved to different

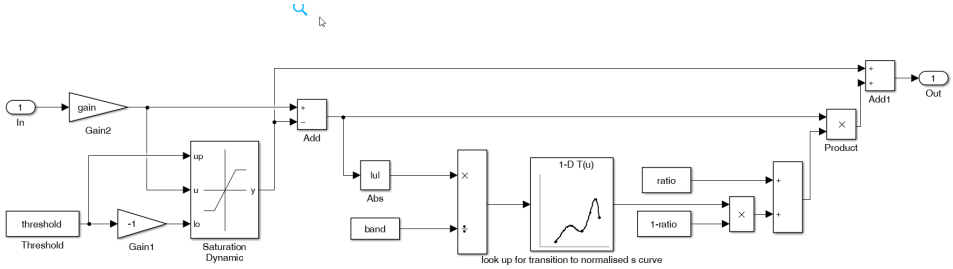

(a) *Compressor control logic in Simulink.*

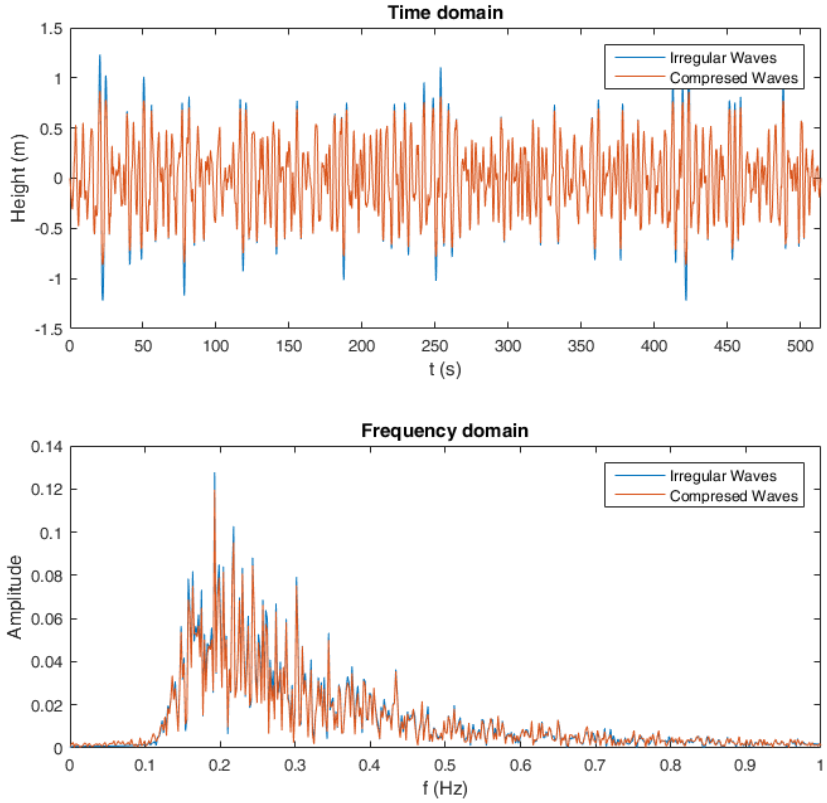

(b) *Example showing the effect of the compressor in the time and frequency domains on an irregular sea time-series.*

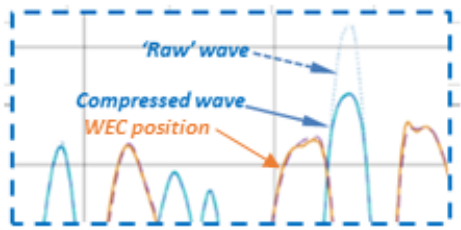

(c) *Zoomed-in image of the effect of the compressor on the peaks of the amplitude of motion.*

Figure 6.3 *Design and behaviour of the compressor used to reduce the peak amplitudes of irregular wave time-series.*

frequencies, which suggests the compression process will not drastically change the Quantor performance results. Figure 6.3c gives a zoomed-in example of the compressor behaviour at the peak's of the motion, showing how the wave amplitude is smoothly reduced for a single high-power wave event.

The impact on the PTO results is minimal they are dominated by the rest of the spectra and the load is typically saturated in the largest waves anyway. This is only true because the key PTO results (e.g. average losses) are not sensitive to the reduction in instant peak powers. This may not be the case for alternative PTO systems. Similarly, this approach is not valid for testing the PTO with respect to the dynamic conditions being compressed, which must be assessed outside the limitations of the WEC emulator.

6.3 Results

The key results of Quantor testing and the cases most relevant for loss breakdown analysis and model validation are presented. It must be remembered that the efficiencies presented here describe the transmission from the input shaft to the generator shaft and do not include the losses of the electrical generator, as the sizing of the generator on the test rig was not representative of a sea-going system.

6.3.1 Prescribed Motion

Figure 6.4 shows some example results of torque control improving as new control features are added. In the quantised only scenario (A) the final PTO torque is a quantised approximation to the demand, as it would be in the Pelamis system. Adding the continuous service (B) makes the applied torque sinusoidal, but the residuals around the quantised transitions are very obviously disrupting the smoothness of the PTO torque. Adding the final feature smooths the torque (C), but there is still a small error between the demand and the applied torque. This is removed by the friction compensation control term (D). Figure 6.5 shows how the chamber pressures change for each of these torque results.

Figure 6.6a shows a comparison of the efficiency of the quantised and Quantor mode 1 control modes at different pressures. For the quantised cases, the DDPM correction refers to the fact that the idle losses of DDPM B have been removed from the efficiency calculation. This is because in a system which was always operating in quantised mode, there would be no need for the continuous service and therefore no need for DDPM B. This means that including the idle losses of DDPM B is not representative of the quantised

system performance and therefore they are removed from the calculation. This means a more realistic comparison between a quantised system and a Quantor system can be carried out, showing the effect on the efficiency of the introduction of another machine (necessary for the continuous service) with its incorporated losses.

The graph shows that the Quantor mode 1 case is about 10% less efficient than the pure quantised case in the low power range (<15 kW) but that as absorbed power increases the gap narrows to around 5%. For both quantised and Quantor modes the efficiency decreases as the pressure increases, presumably because of the effect of pressure-dependent losses. This may have implications for sea deployments, as it suggests that operating at a lower pressure is generally better for efficient power generation. However, this must be balanced against the higher PTO torque available with high accumulator pressure, which may be necessary in more powerful sea states. In these more powerful sea states, the mechanical input power to the PTO should be higher anyway, so even at a lower average efficiency, the Quantor may be able to deliver more power to the grid by operating at a higher pressure. Further study would be required to establish how to optimise the operating pressure across the power spectrum. However, once the absorbed power reached 30 kW, all cases have an efficiency of 70% or over. Chapter 8 explores the reasons for the variation in efficiency across these cases in more detail.

Figure 6.6b shows the efficiency against absorbed power for a range of Quantor control modes (see Section 6.1.6 for an explanation of how each mode works). The possible implications of these results for control of a deployed Quantor are significant. Firstly, it is interesting to note that Quantor mode 4 is equally or more efficient than the quantised case (which is theoretically the most efficient operating mode due to only having one DDPM) until the absorbed power reaches 20 kW. This suggests that the minimum 'cut-in' power for quantised control is higher than that of Quantor mode 4, so that in small seas Quantor mode 4 is the optimum operating mode. In Quantor modes 1-3 there are slight dips in the efficiency at particular points (most clearly visible in Quantor mode 3 at around 8 kW when this curve separates from the Quantor mode 4 curve). These occur when the torque demand crosses the threshold for a new quantised state is reached and the full losses of both the quantised and continuous service are applied. Quantor mode 0 is the least efficient operating mode but converges with mode 1 at approximately 16 kW. This is probably because at the very low absorbed power levels Quantor mode 0 must still have a quantised state operational in one direction and the continuous service correcting in the other direction. For example, if the single continuous chamber applies torque in the positive direction, to meet a negative torque demand a negative quantised chamber must be enabled and the continuous chamber must still correct the quantised torque in the

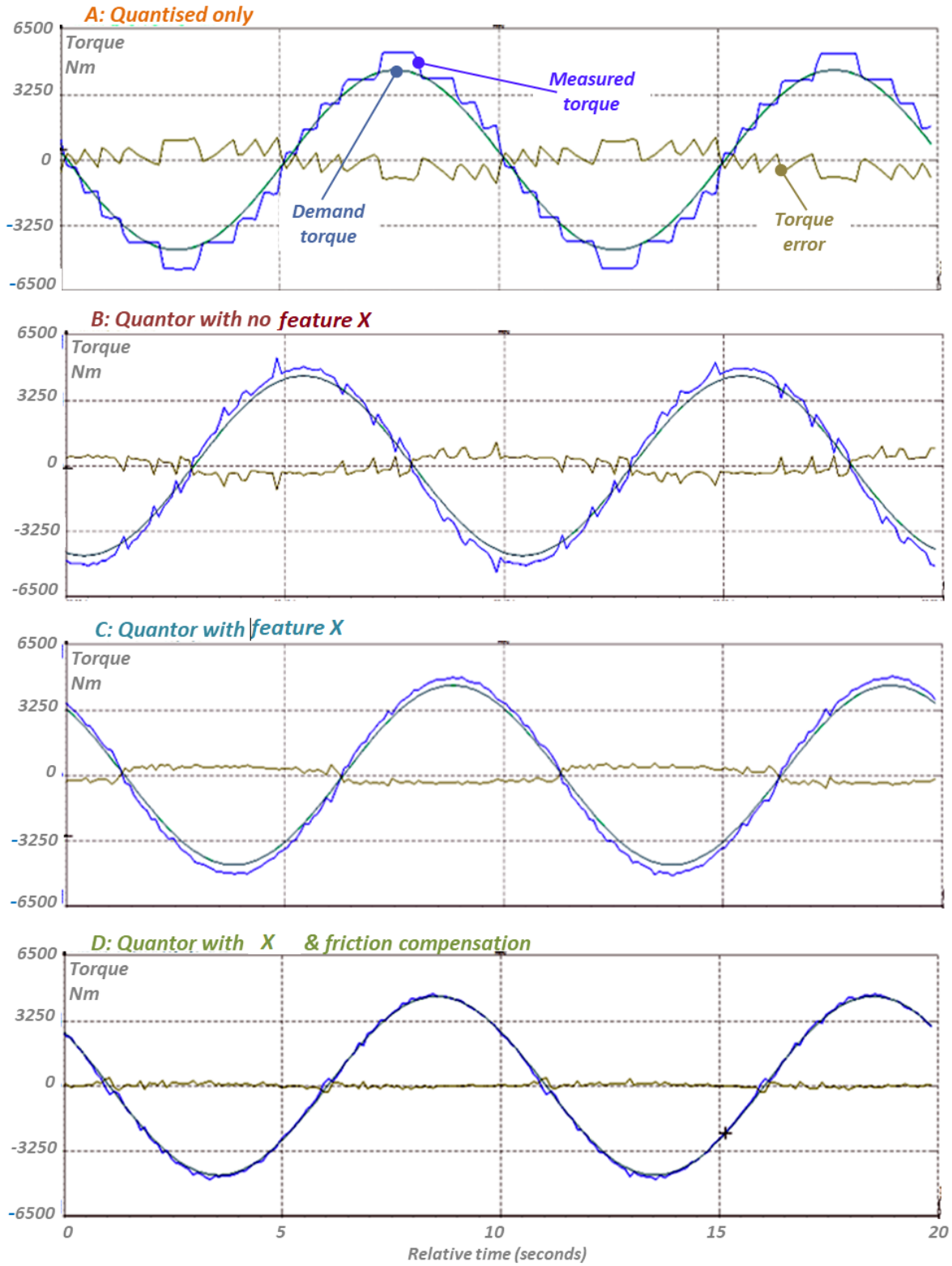

Figure 6.4 *Improvement in output torque as new control features are added.*

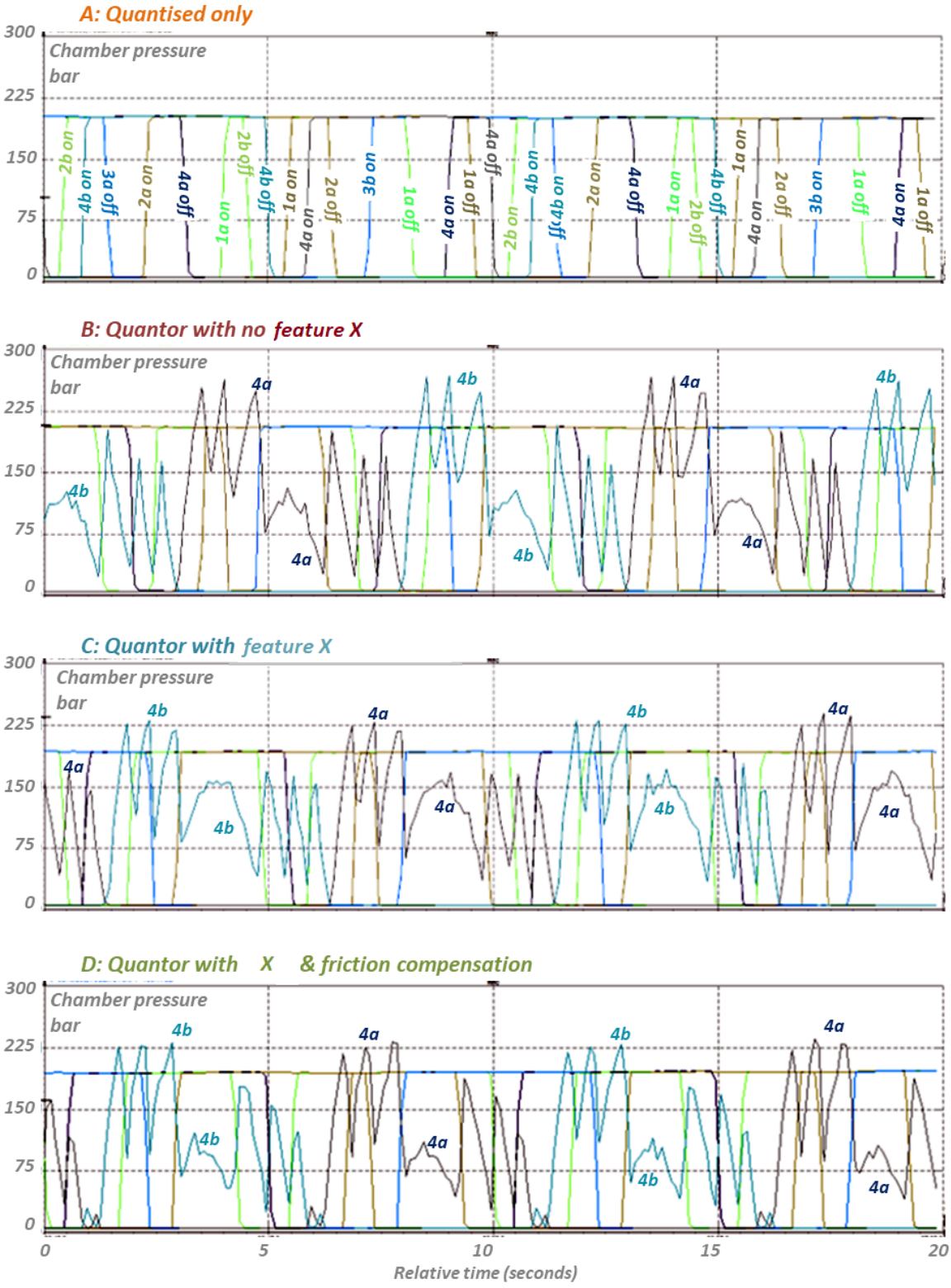

Figure 6.5 *Quantor chamber pressures under various control features corresponding to torque shown in Figure 6.4. The port label convention ('A' and 'B') is shown in the diagram Figure 5.6.*

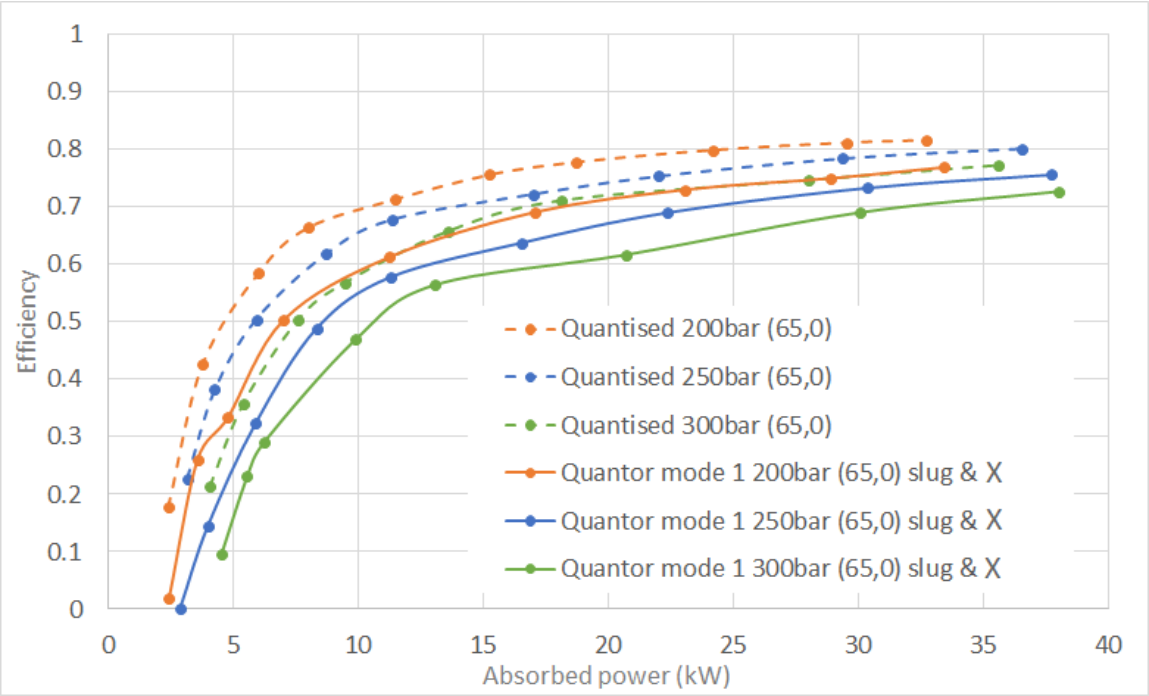

(a) *Efficiency against absorbed power comparison at three pressures. Quantised and Quantor mode 1 PTO operation in prescribed motion control with* 10 s *period.*

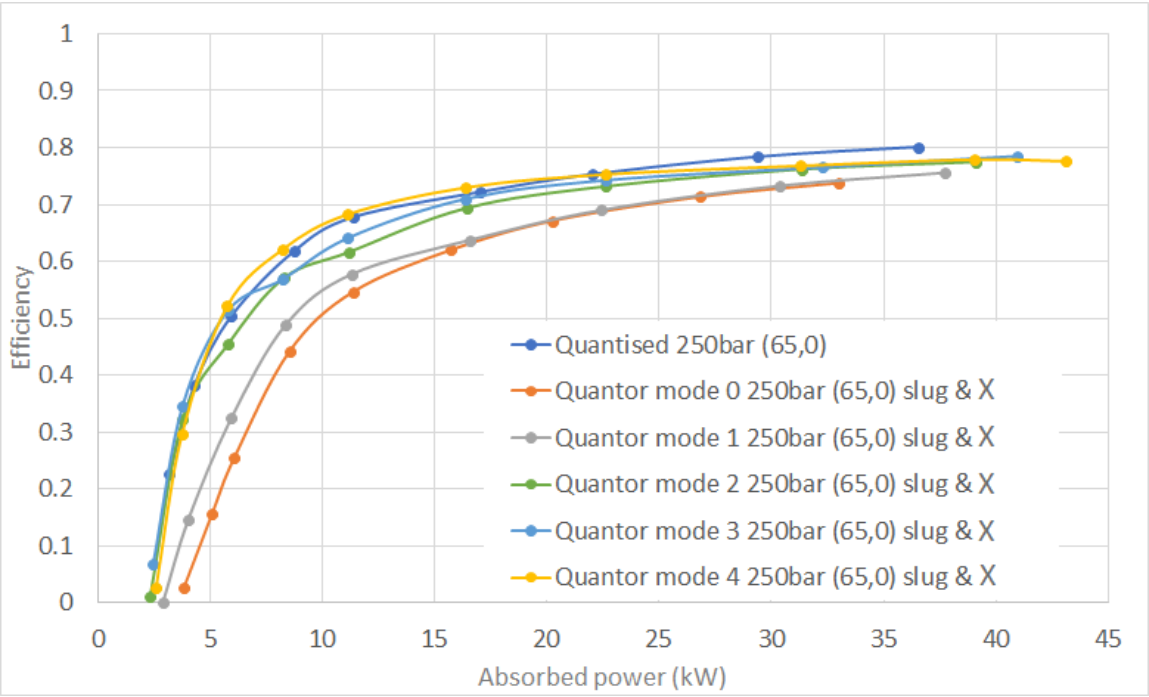

(b) *Variation in efficiency with absorbed power in different Quantor operating modes (unidirectional control of one continuous chamber in mode zero, then 1, 2, 3 and 4 motors directionally controlled in the other modes)*

Figure 6.6 *Measured efficiency results for a variety of control modes and pressures. The quantised cases have had the idle losses of DDPM B removed. The numbers in the brackets refer to the damping and spring coefficients respectively at WEC scale, with the units being* kN s/m *for the damping coefficient and* kN/m *for the spring coefficient.*

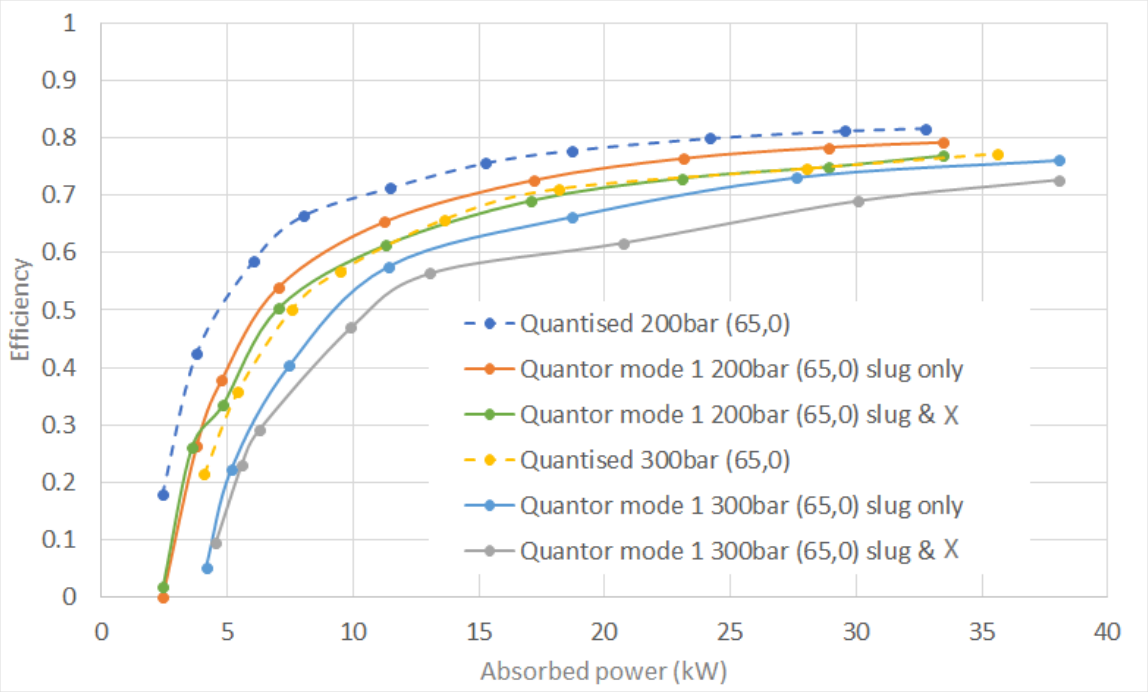

(a) *Effect of slug control and slug and X on the efficiency at* 200 bar *and* 300 bar.

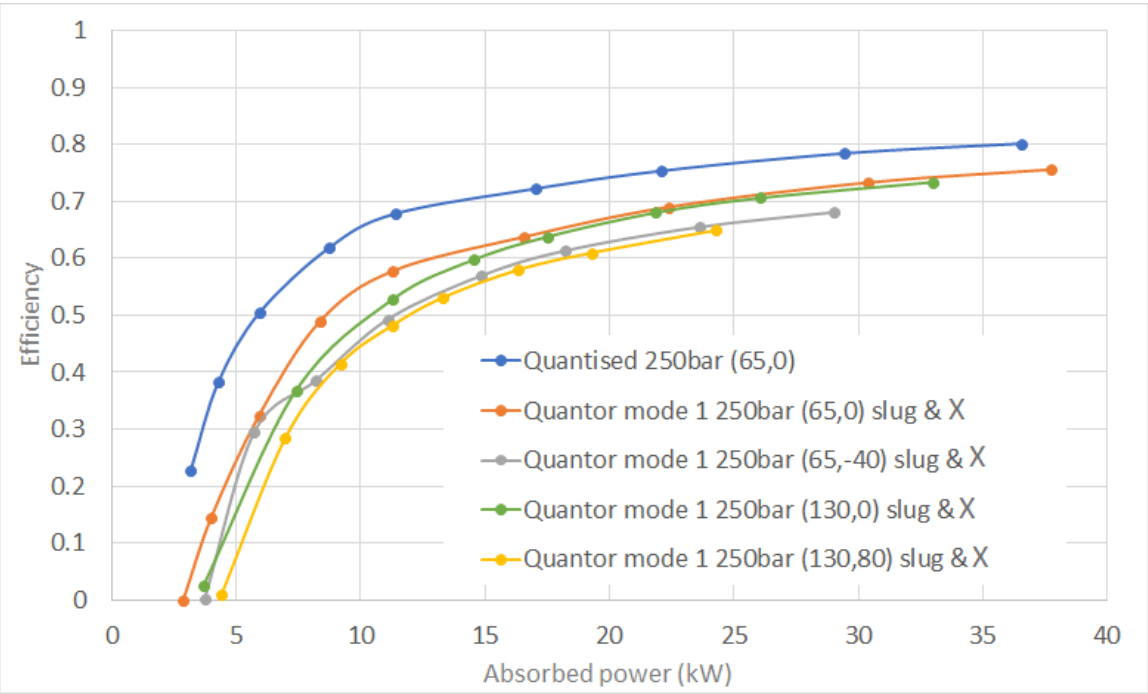

(b) *Effect of various levels of damping and spring terms on the efficiency of Quantor mode 1 at* 250 bar.

Figure 6.7 *Variation in Quantor efficiency due to different control methods for torque smoothing and for changing reactive power. The quantised cases have had the idle losses of DDPM B removed.*

positive direction. This would increase the losses as there are two chambers pressurised simultaneously rather than having two continuous chambers pressurised alternately. As the power level increases the efficiencies of all Quantor cases appear to converge, but the use of a validated model would be required to explore how the different cases perform at higher absorbed powers. It may turn out that at each Quantor mode has an optimum operating range and that switching between them at particular absorbed power thresholds optimises the transmission efficiency over the whole range.

The implication of DDPM B being able to control all four motors is that the Quantor front end (PTO actuators) is underrated in terms of power and flow relative to the back end (DDPMs and generator). This is an artefact of the constraints on the WEC emulator and the availability of DDPMs in particular sizes. The electric motor driving the flywheel (WEC emulator) has a nominal power rating of 304 kW, which can be overdriven to 350 kW. Assuming a 15 to 1 ratio of peak to mean power in irregular seas, the absolute maximum mean power possible to emulate in an irregular sea is approximately 25 kW. The PTO motors were sized so that that this is a reasonable operating point for them (maximum power for each single motor is 18 kW [85], but for the pressures and speeds on the rig they were peaking at around 12 kW each). This means that the total rating of the actuators of approximately 50 kW is only a quarter of the combined rating of the DDPMs of 220 kW. In a real Quantor system for a WEC, the system would be designed such that the rating of the DDPMs was lower than that of the front end and the HP accumulator would be relied on for energy storage and smoothing. Therefore, whilst in a real WEC the DDPM would be able to provide enough flow for several chambers simultaneously, it would not usually be able to supply all the chambers of the Quantor.

The levelling off of the efficiency curves has encouraging implications for system scale-up, as it suggests that with a higher rating of PTO actuator the absorbed power could increase up to the full rating of the DDPMs with efficiency remaining greater than 70%.

Figure 6.7a shows the effect of slug only and slug and X control on the efficiency over the power range. It is clear that adding in the X control feature negatively impacts the transmission efficiency, with the effect more pronounced at higher pressure. The implication of this is that the improved torque smoothness resulting from this feature comes at an efficiency cost, although possibly there are ways to improve its efficiency.

Figure 6.7b shows the effect of various levels of damping and spring on the efficiency of the Quantor. As expected, pure damping cases are more efficient than reactive cases. This is because reactive control requires a reversal of power flow, meaning that losses are incurred in both directions of power flow in the system [40]. However, the extra losses only

reduce the efficiency by about 4%, and being able to force the WEC back into resonance with reactive control may ultimately lead to greater power capture over a broad range of sea states. It is also interesting to note that doubling the damping and spring coefficients results in almost identical efficiency above a certain 'cut-in' power. This suggests that the Quantor can provide demanded torque of high rates of change with only a small change in efficiency.

6.3.2 Regular Wave Tests

Figure 6.8 shows the variation in absorbed power from the half-scale AWS WEC rig emulation taken through a range of incident wave heights, with example changes to control settings. Knees in the curves are due to saturation of torque, and correspond to the loss of PTO control over the response stroke – a feature of most WECs depending on the specified PTO load limits.

The capture width of the AWS WEC depends on the wave period and PTO control settings, but is estimated to be several metres in most of the cases shown. Reductions in power absorption for reasons apart from the Quantor PTO (e.g. compliance in the mooring system) are not considered for the purposes of these tests. These example control cases for a specific WEC are not intended to show absolute performance optimisation of the WEC in question but demonstrate the capability of the test rig and Quantor system to enact different controls and wave regimes.

The different control cases show the effect of negative spring in inducing more resonant response and hence power absorption. A dedicated speed limiting control is shown to greatly increase power absorption in smaller waves; this also maximises the range of seas that can be operated in for a given force limit.

Figure 6.9 shows screenshots of the data acquisition software for three different control modes of the AWS model, which are provided in Table 6.2. Case A is a pure damping case, in which the x-y plot of force and velocity (middle right of each figure) is a straight line, remaining only in two quadrants. Case B used reactive control, and hence the x-y plot becomes a loop as the Quantor moves through all four quadrants. As velocity goes through zero there is a ripple in the applied torque, which may require improvement for a sea trial. Case C demonstrates a velocity-limiting type of control, which could be used to protect end-stops in a WEC with limited range. The Quantor is impressively responsive to the aggressive force demand in this case, which reverses direction rapidly and has very steep gradients. This shows Quantor's suitability for a range of control algorithms.

Figure 6.10 shows comparisons between the measured power curves for prescribed motion cases and the equivalent AWS regular wave cases. Across all three control modes (quantised, Quantor mode 1 slug only and Quantor mode 1 slug and X) the agreement is very good, suggesting that the PTO does not behave markedly differently when responding to prescribed motion and when controlling the WEC HIL. The only major difference is during 'cut-in', where the addition of the torque resulting from quantised transitions has a greater impact on modelled WEC and causes a more significant dip in the efficiency, presumably because the addition of such a discrete torque step causes the model WEC to reduce in velocity. These figures support the assumption that the efficiency curves gathered for prescribed motion cases are representative of the efficiency curves for the equivalent regular wave cases.

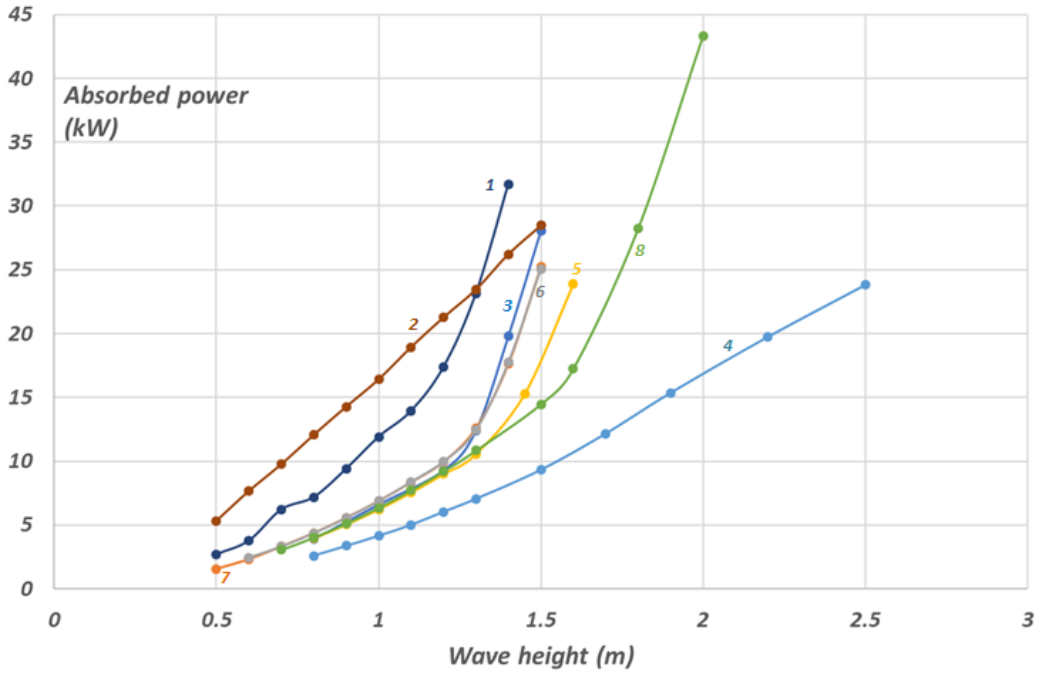

Ref		Mode	Pressure bar	Wave period sec	Damping kNs/m	Spring kN/m	Setting
1		Quantised	250	5	65	-60	
2		Quantised	250	5	20	-60	Speed limit
3		Quantised	250	5	130	-40	
4		Mode 1	250	10	130	0	Slug only
5		Mode 1	250	5	130	0	X & slug
6		Mode 1	250	5	130	-40	Slug only
7		Mode 1	250	5	130	-40	X & slug
8		Mode 4	250	5	130	0	

Figure 6.8 *Absorbed power against wave height, for 0.5 scale, AWS WEC in regular waves, for different control types, each with parameters optimised to maximise absorbed power while remaining within stroke limits.*

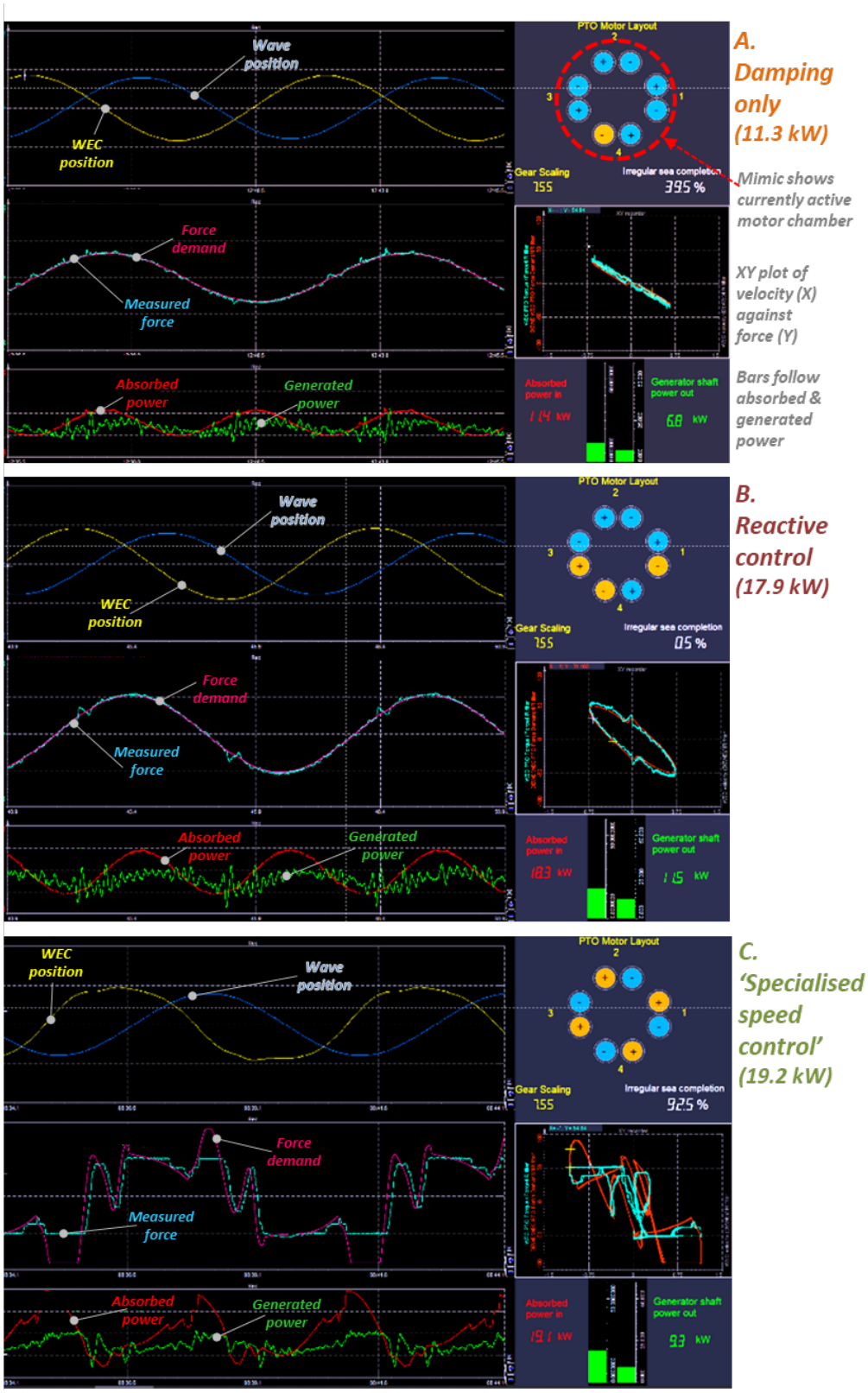

Figure 6.9 *Showing 4-quadrant control. Hardware in the loop testing of the AWS WEC, in a simulated regular wave of H:*1.2 m *and T:* 6 s*, with 3 control strategies. The power values in brackets are averages over the length of the run. A – damping only, B - damping and spring (using reactive power), and C – using speed limiting control on a reactive impedance.*

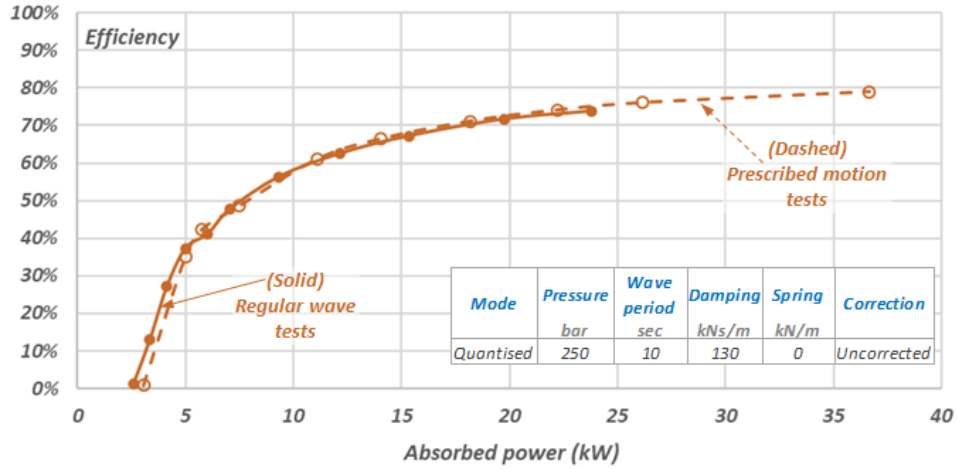

(a) *Quantised comparison between prescribed motion and regular wave tests (*250 bar *and* 130 kN s/m *damping).*

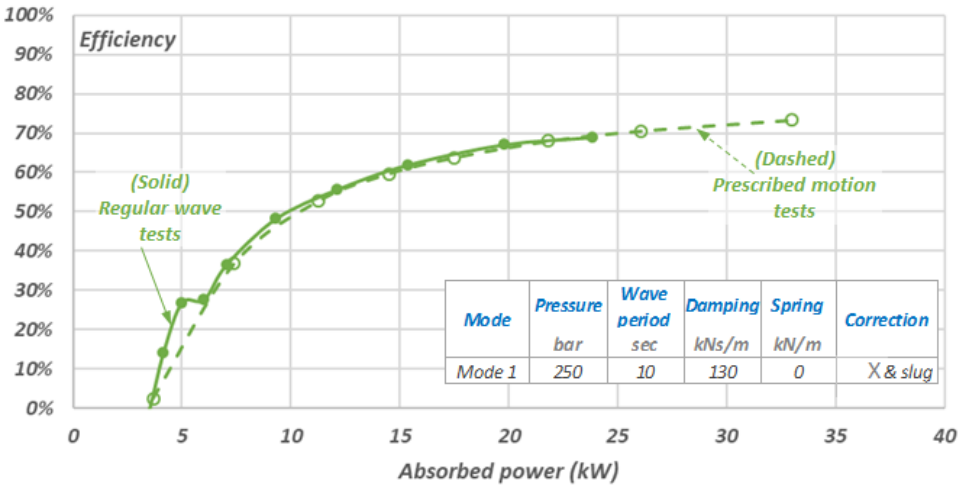

(b) *Quantor mode 1 (slug and X control) comparison between prescribed motion and regular* 10 s *wave tests (*250 bar *and* 130 kN s/m *damping).*

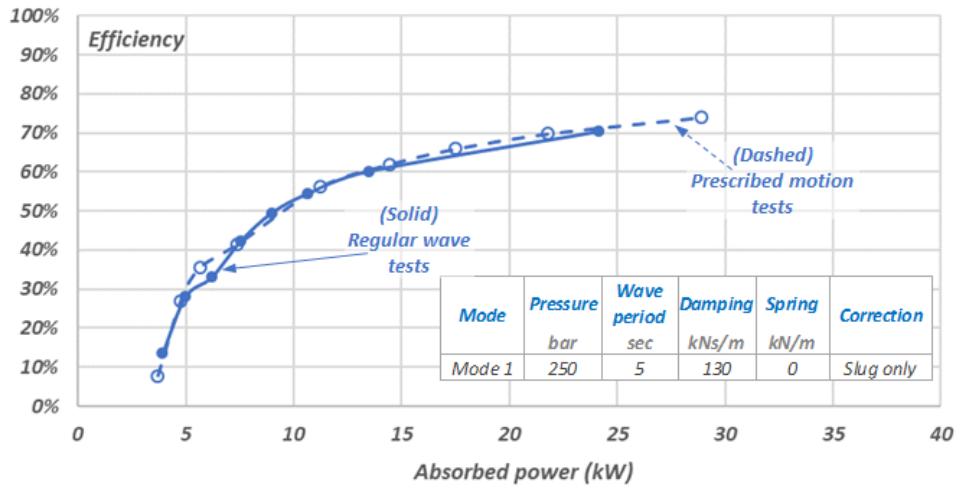

(c) *Quantor mode 1 (slug only control) comparison between prescribed motion and regular* 5 s *wave tests (*250 bar *and* 130 kN s/m *damping).*

Figure 6.10 *Efficiency against absorbed power. Comparison of regular wave tests (solid lines) with prescribed motion tests (dashed lines) for 3 different modes.*

Table 6.2 *Settings and comparative energy capture for the three cases shown in Figure 6.9*

Reference	Damping (kNs/m)	Spring (kN/m)	Velocity limit?	Mean absorbed power (kW)	Relative Improvement (%)
A	50	0	No	11.3	
B	65	-40	No	17.9	58%
C	10	-80	Yes	19.2	70%

6.3.3 Irregular Wave Tests

Table 6.3 shows irregular sea results for the AWS WEC in three different control modes. The wave time-series in all three cases is a Pierson-Moskowitz, with energy period 6.6 s and significant wave height 1.5 m, which was allowed to run for 512 s, except for the quantised case which was unfortunately curtailed at 390 s due to an incorrect control setting which was only discovered after the test. Quantor mode 4 is the most efficient case, which is probably due to it being a more efficient operating mode at low absorbed powers (see Figure 6.6b).

In the irregular wave cases, the average input power is much lower than in the regular cases, because the WEC emulator was not able to supply the required very high peak powers, even with compression of the speed demand. This means that the Quantor efficiencies appear very low in these cases, but the efficiencies are commensurate with those expected for regular waves at a similar power level.

Table 6.3 *Results of three example irregular wave cases for the AWS WEC*

	Quantised	Quantor mode 4	Quantor mode 1 (slug only)
Input Power (kW)	9.55	10.04	9.87
Damping (kNs/m)	80	80	80
Spring (kN/m)	-40	-40	-40
Efficiency (%)	50.95	59.94	47.67

Figures 6.11 to 6.12 show time-series of model wave and WEC position, demand force and applied force, and input and output power for the three different irregular cases, with additional torque and pressure detail supplied for Quantor mode 1. In all cases, the Quantor matches the demanded PTO torque very well despite the irregular profile. The improvement in the smoothness of torque in the Quantor cases relative to the quantised case is visible to the naked eye. The peak force applied is highest for Quantor mode 4. This is because the stiff service has a higher maximum pressure than the quantised service, due to the overdrive feature. Having all four PTO motors able to reach this maximum

pressure results in a higher torque than in the mode 1 case, where three of the motors cannot go higher than the accumulator pressure. In all cases, the requirement for reactive power is clear as the 'generated power' is negative.

Examining Figure 6.12b shows how only the continuous service is used to supply the PTO torque at very low demands, and how the quantised chambers are gradually introduced with increasing demand right up to saturation, where the Quantor can no longer follow the demand torque.

A useful tool in evaluating Quantor's performance across different WEC cases and wave conditions is to map regular wave results to irregular wave inputs. The curves of efficiency versus power can be weighted by an irregular input power time series to give an overall efficiency estimate. The simple process of using regular wave efficiency data to estimate average efficiency in irregular waves is illustrated in Figure 6.13. This is accurate even at low efficiency on the steep part of the curve. The applied power curve should be derived with the same or similar controls, and within the range of wave periods of the spectra. The time constant for smoothing the absorbed power should roughly correspond to that of the generation control process. The robustness of the power curves despite different control settings gives rise to fairly robust estimates using this method, with conservative selection of the efficiency curve corresponding to conservative results.

This suggested that for irregular seas of higher average powers the Quantor could match the performance shown in the equivalent regular waves.

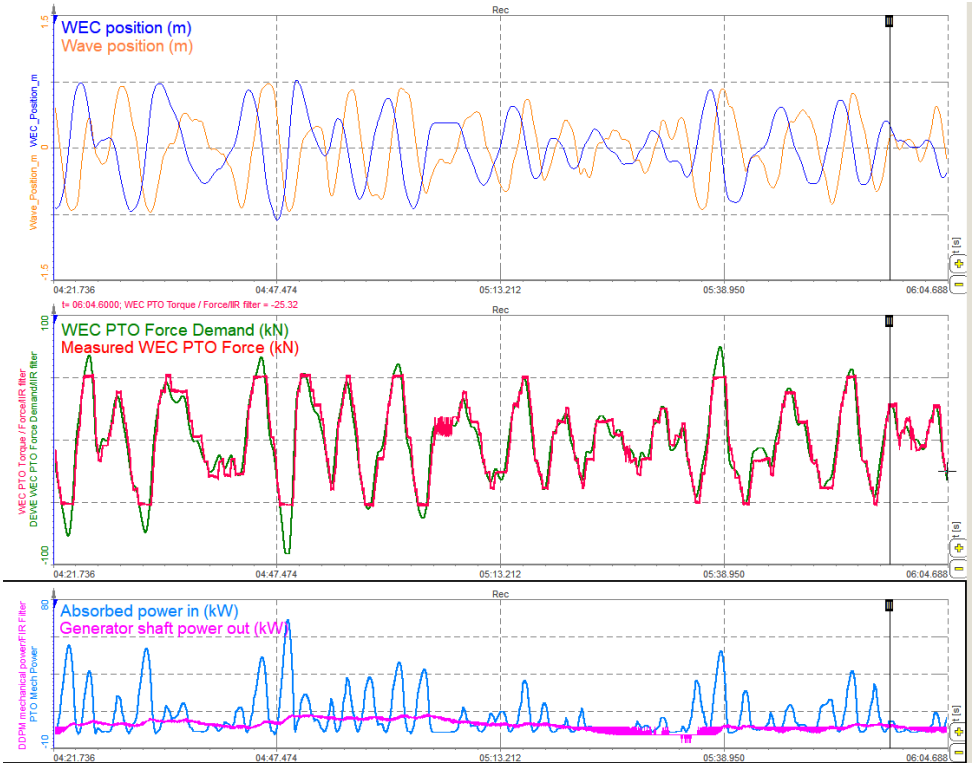

(a) *Top: model wave and WEC position, Middle: WEC PTO force demand and measured PTO force, Bottom: absorbed power and generated power for quantised irregular case*

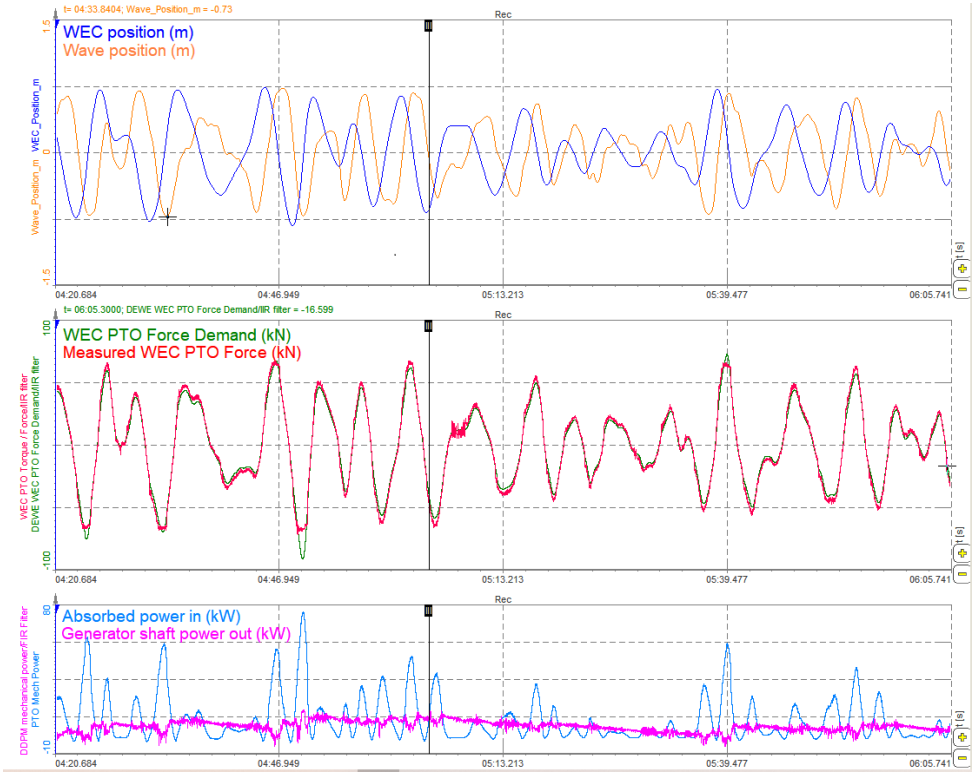

(b) *Equivalent images to Figure 6.11a for Quantor mode 4 operating mode.*

Figure 6.11 *Example data acquisition screenshots from irregular cases*

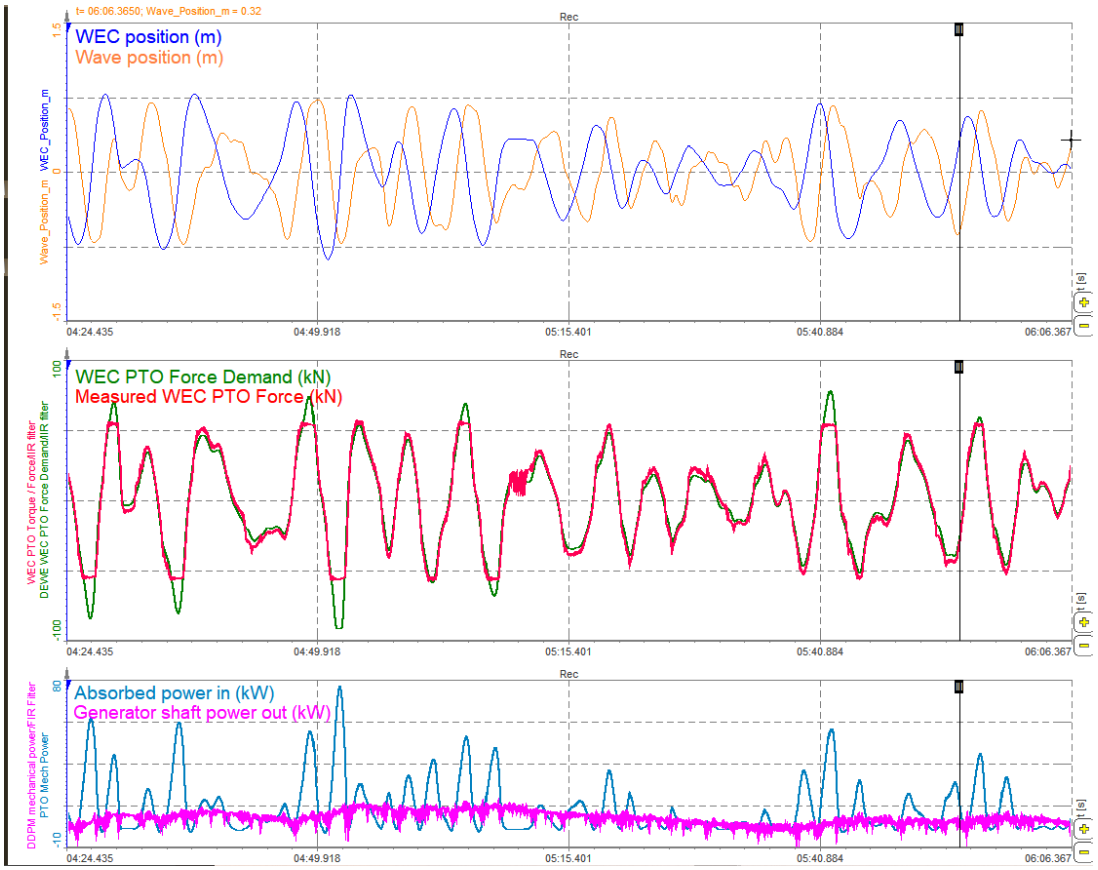

(a) *Equivalent images to Figure 6.11a for Quantor mode 1 operating mode.*

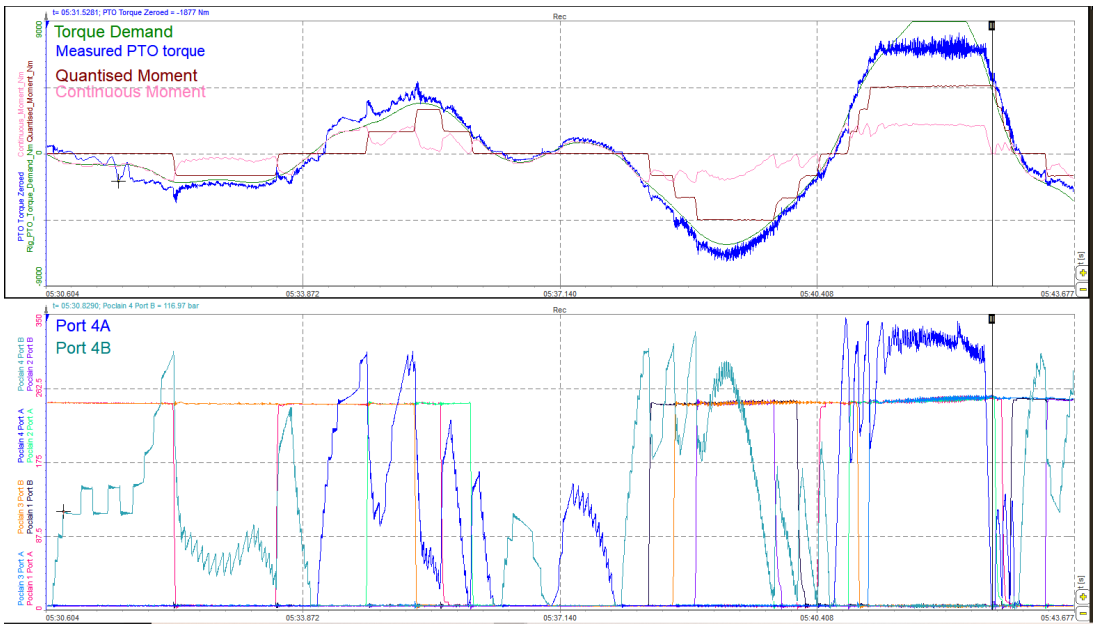

(b) *Zoomed in section of irregular Quantor mode 1 case showing; torque demand, measured PTO torque, quantised moment and continuous moment (all in* N m*) in the top plot; and all chamber pressures in bar on the bottom plot, with the continuous chambers highlighted.*

Figure 6.12 *Data from Quantor mode 1 irregular time-series.*

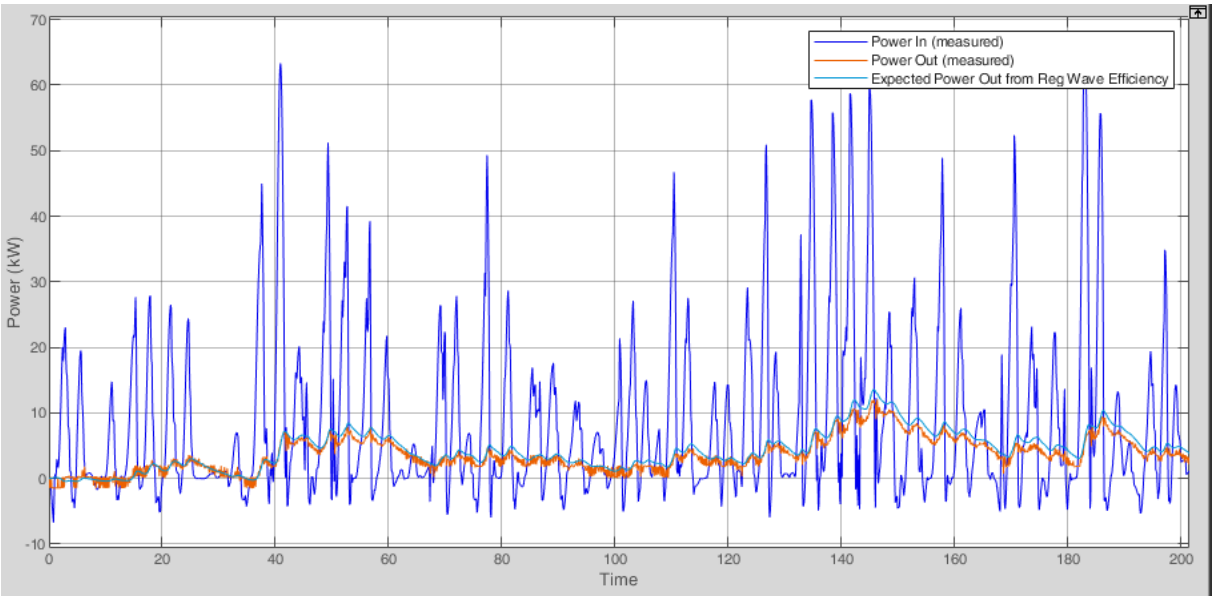

Figure 6.13 *Using the characteristic power curve to estimate average efficiency in irregular waves. Here the measured instantaneous absorbed power (blue) is filtered to provide a look-up signal for the characteristic efficiency curve derived in regular prescribed motion tests. The look-up efficiency is applied to the power which is filtered to the same time constant as the generation control process which provides an estimated output power output (cyan), which closely matches the measured output power (orange) to within a few per cent.*

6.4 Summary

Using the WEC emulator and Quantor lab system designed and built at AIP, the Quantor performance was tested in a range of conditions. The majority of tests were carried out in prescribed motion conditions, which was the most simple way to evaluate the impact of different control terms. The results from tests using a WEC model in regular waves were shown to agree well with the prescribed motion tests, showing that the efficiency curves from prescribed motion tests can be reasonably assumed to resemble those of the regular WEC model cases. A small selection of irregular cases was tested, which all had relatively low efficiencies due to having low average absorbed powers. These efficiencies were shown to be commensurate with the efficiencies for prescribed motion cases of the same control mode at the same average power level. This implies that for irregular cases of higher average powers, the Quantor transmission efficiency could approach the values seen in the prescribed motion results.

The shaft-to-shaft transmission efficiency (not including the generator) for most cases was over 70% above a varying minimum absorbed power, with many cases approaching

80% as absorbed power increased. Efficiency decreased as pressure increased, suggesting that the influence of pressure-dependent losses in the transmission is significant. The most efficient case at low input power was Quantor mode 4, with the pure quantised case being the most efficient at higher powers. The addition of feature X for torque smoothing negatively impacted the efficiency, by around 5% at 30 kW absorbed power. As expected, the introduction of reactive control increased the losses slightly, but the Quantor was able to operate in all four quadrants as long as the demanded torque was within its capabilities. There was also a demonstration of a speed-limiting control, which the Quantor was able to perform even though the torque demand rapidly switched direction and had steep gradients. Over the course of testing, the control was refined and new features were added to improve the matching of the PTO torque to the demand. The Quantor was able to control torque smoothly in irregular waves as well as regular.

Having demonstrated the functional capability of the Quantor, the next step was to analyse the data to produce a loss breakdown and to validate the Simscape model. This is discussed in Chapters 7 to 8.

Chapter 7

Quantor Model Validation: Component-Level Validation

A key deliverable of the project was a Quantor model which had been validated by test data. The ultimate desired output of this was a simple model which could be used to size full-scale Quantor systems with a range of architectures, such as different PTO motors, linear actuators, a greater number of actuators or larger DDPMs. It was also important to validate the Simscape model which was used to examine the details of the system's hydraulic behaviour and to design the control system. This meant that two validated models would exist; one suitable for exploring new Quantor system architectures but with realistic estimates of the efficiency and losses; and one suitable for refining control on the test rig and examining details such as transient pressure spikes. Both these models would be able to represent the real-life behaviour of Quantor at distinct levels of detail, but have similar output efficiencies and loss breakdowns based on real measured data.

7.1 Transient Valves and Needle Valves

One key aspect of the model to be validated was the setting of the needle valves on the transient flow valve paths, for both high and low pressure transient valves. These will affect the model estimation of pressure drops and flow losses through these orifices.

7.1.1 LP Needle Valves

Figure 7.1 shows a screenshot from the model validation tool used to compare the test rig data and the model data. Model data is shown in blue and test rig data is shown

in orange. Each plot is for a single chamber and shows both the model and rig data overlaid. The test shown here involved all transient low pressure valves being held open and the flywheel being spun in a sine wave of period 10 s and amplitude of 86.2 rpm (corresponding to 1500 rpm on the high speed side). The result of this is that the fixed displacement motors pump against the needle valves in either direction, and the pressure drop generated by this allows the orifice diameter of the needle valves to be tuned. It can be seen in Figure 7.1 that the model needle valves are much more 'open' than on the test rig, that is the pressure drop is much lower.

The key part of the data to match is the pressure rise up to the point of inflexion which occurs at between 30 and 40 bar on each curve. This point of inflexion occurs due to flow splitting, possible through either the main flow valves (which are inactive but pressure-compensated so may open slightly) or check valves. This behaviour was not included in the model so the intention is to match the curve before this point and not after. Figure 7.2 shows the results after setting all needle valves to 6.5 mm^2. It was felt that this gave the best compromise using one value across all chambers, although it is clear that some chambers (particularly -2, +3 and -3) are poorly matched in this important region.

It was therefore decided to change the model so that the settings of these LP needle valves could be tuned individually within each block, allowing the closer matching of the physics model with the data recorded on the rig. Figure 7.3 shows the results when individual LP needle valve settings are chosen. Valve settings are shown in Table 7.1.

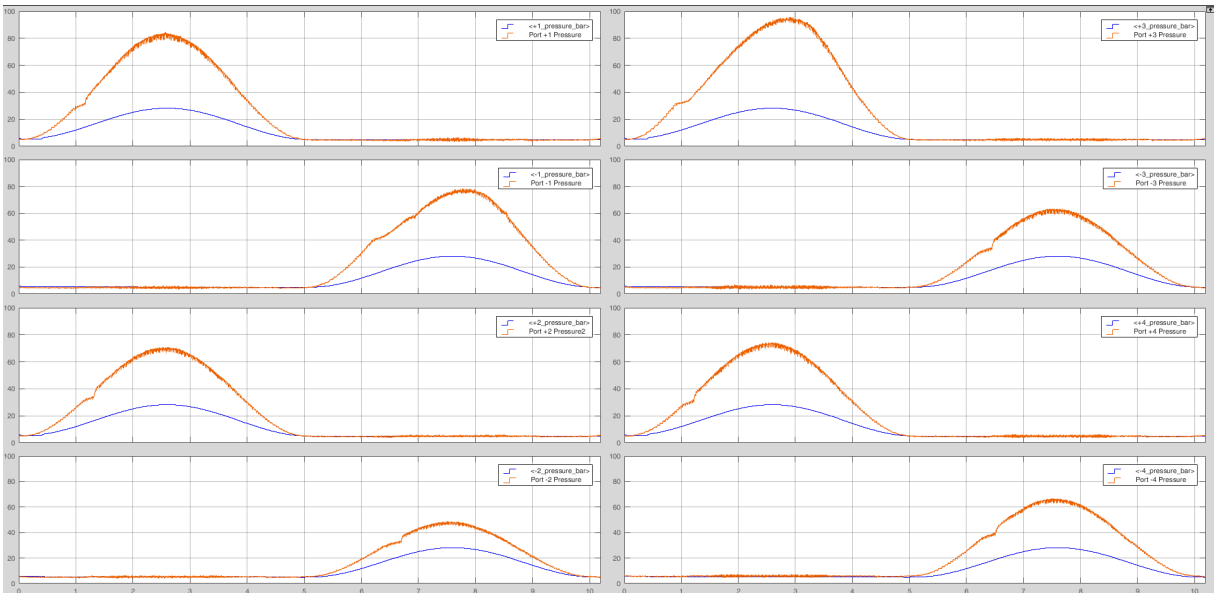

Figure 7.1 *Original comparison of chamber pressures to tune LP needle valve settings in the model with the test rig data, when the model needle valve areas were all set to* 12 mm^2

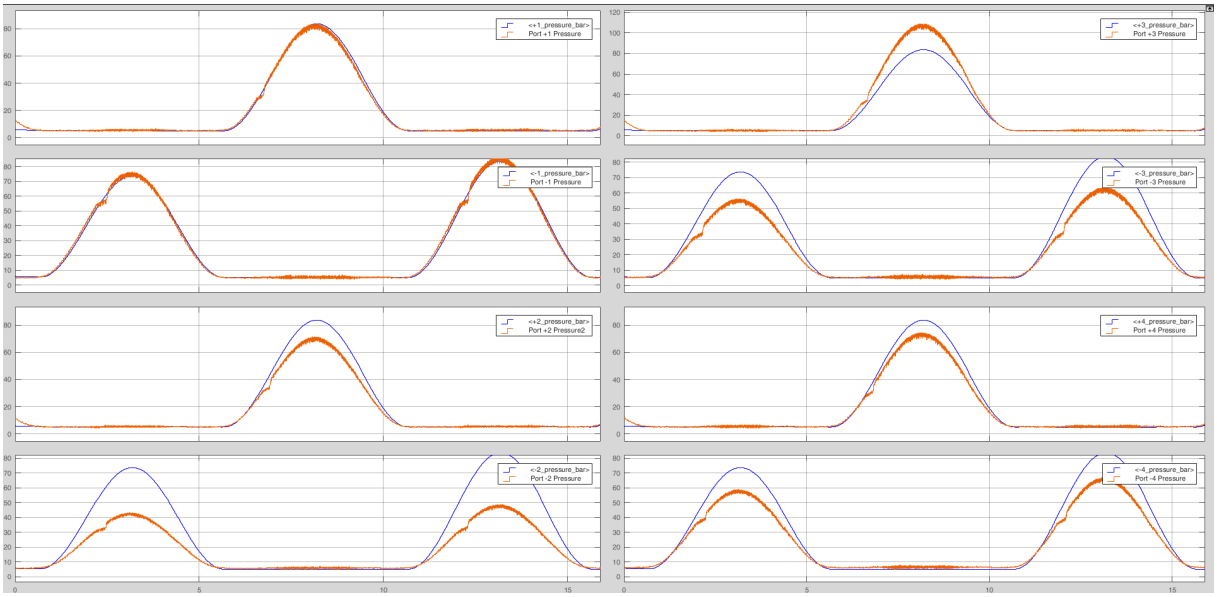

Figure 7.2 *Comparison of chamber pressures with the model; LP needle valve areas all set to* $6.5\,\mathrm{mm}^2$

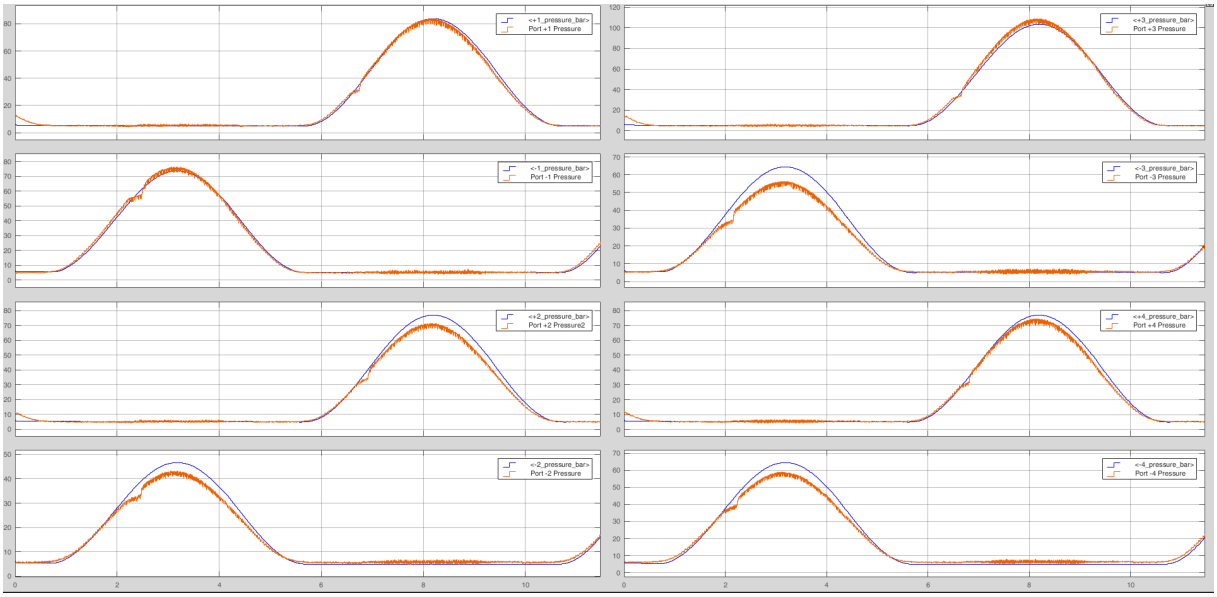

Figure 7.3 *Comparison of chamber pressures with the model; LP needle valve areas all set individually according to Table 7.1*

Table 7.1 *Final settings of LP needle valves*

Port	+1	-1	+2	-2	+3	-3	+4	-4
Setting (mm^2)	6.5	6.5	6.8	8.4	5.8	7.0	6.8	7.0

7.1.2 HP Needle Valves

A similar process was carried out for the HP needle valves so that they were also individually tuned to match data from the test rig. The high pressure transient flow valves were overridden open on opposing ports four at a time such that the net torque was zero, and the main-flow valves overridden shut as in the previous tests. Conducting this test, illustrated in Figure 7.4, allows direct comparison of the associated needle-valve pressure drops with the model.

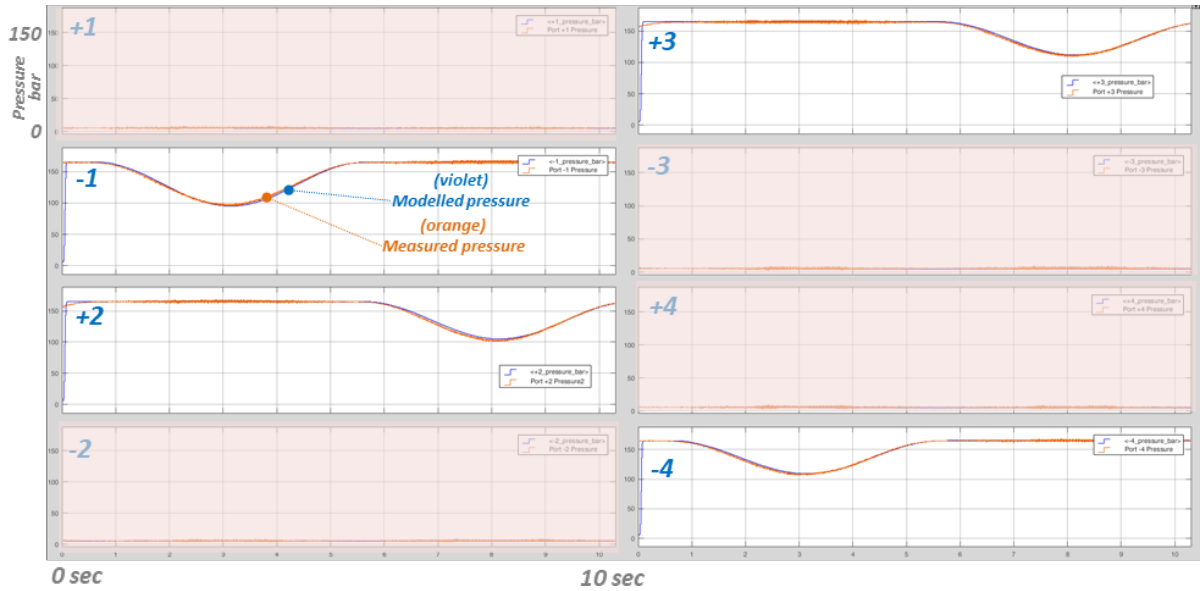

Figure 7.4 *Matching of HP needle valves on four of the eight ports, the other four (pink voids) were matched in a separate test.*

Table 7.2 *Final settings of HP needle valves*

Port	+1	-1	+2	-2	+3	-3	+4	-4
Setting (mm^2)	7.0	7.0	7.6	8.8	8.1	6.5	7.5	7.9

7.1.3 Transient Valve Pressurisation

The transient flow valves were then modelled using the pressure/flow characteristic found on the Sun Hydraulics website for valve DKFS [87]. Once this was complete, validating the pressurisation and depressurisation curves from a quantised test was an appropriate next step. Validating pressurisation and depressurisation curves requires at the very least the matching of the delays between the control signals and the beginning of the pressure change, and the time taken for each pressurisation or depressurisation event to occur. Beyond this, matching the shape of the curves is desirable.

To obtain this test data, the flywheel shaft was held at zero speed by the electric motor. The Quantor was then given a sinusoidal torque demand in a fully quantised mode over several cycles, so that data for multiple quantised transitions for each valve were obtained. In each quantised transition the quantised valve opened to pressurise the chamber from the HP accumulator. The main flow valves were kept closed during this test. Several tests of this type were done to manually adjust the needle valves in each block to all have similar pressurisation and depressurisation times of approximately 40 ms, which was estimated to be a suitable length of transition time to give DDPM B to respond to quantised transitions. Once the rig valves had been suitably set, a fresh set of data was obtained using the same method. This data was then post-processed to produce tables of valve control delays and opening or closing times.

A model was then produced to replicate the chamber pressurisations from the test. The simulated needle-valve and flow path were already set up. These were based on the flow tests described above and known hose and valve properties in the simulation physics model. However, the transient flow during quantised load step changes is much higher and is subject to the valve opening and closing behaviour. Inertial effects may also be important due to rapid fluid accelerations. The mechanical valve delay is set in the model valve block with a 'valve actuator' Simscape block.

The static test data was played back into the model controller so the valve pressurisation and depressurisation curves could be compared. The use of prescribed torque values (recorded via the Controller Area Network (CAN) bus) meant that exact valve timings had to be captured, based on the digital synchronisation signal as previously used for post processing of the test data.

After simulation of the static tests, the same post-processing tools used to characterise the hardware pressure transitions were applied to the modelled data. As shown in Figure 7.6, the pressurisation and depressurisation curves from the model could then

be directly compared with those from the test-rig. Metrics were also extracted to give a more quantitative comparison of the data and the model curves. The pressure in the chamber was compared to the pressure of the high and low pressure galleries, and the difference between them Δp. The delay 'd1' was calculated as the time between the valve control signal and the chamber pressure increasing to 20% of Δp. The 'transit time' was calculated as the time taken between a chamber pressure increase from 20% to 80% of Δp. These were extracted using a Simulink post-processing tool. There was also the overall pressurisation time from LP to HP (or vice versa), which was assessed visually, as noise on the signal and the asymptotic nature of pressurisation and depressurisation curves means that it is challenging to develop a programmatic method for this.

Several model quantities were adjusted to improve the matching between the measured and modelled pressurisations. These included the stroke, delay, switch-on time and switch-off time of each transient valve actuator (see [88] for further detail). The opening of the needle valves had already been tuned from the earlier tests. Several attempts were made to improve the model, with results shown in Figure 7.5. Whilst the delay times were matched fairly well for all ports for both pressurisation and depressurisation (the mean error is 0 ms and the maximum error is 6 ms), the transit times are more tricky due to the different shapes of the curves. For the depressurisations the mean error in transit time is 1 ms but it is 8 ms. However the overall pressurisation times match quite well, and it was found that the model transit time couldn't be matched more closely to the rig transit time without compromising on that, so the error in transit time and shape of pressurisation curves was accepted. To truly replicate the shape of the pressurisation curves, it would be necessary to include valve loading characteristics in the model (including spring force, stiction and friction) which was judged to be excessive detail due to the huge increase in computational time that it would cause.

The influence of fluid inertia on pressure response appears to be negligible, with no discernible overshoot or pressure oscillations.

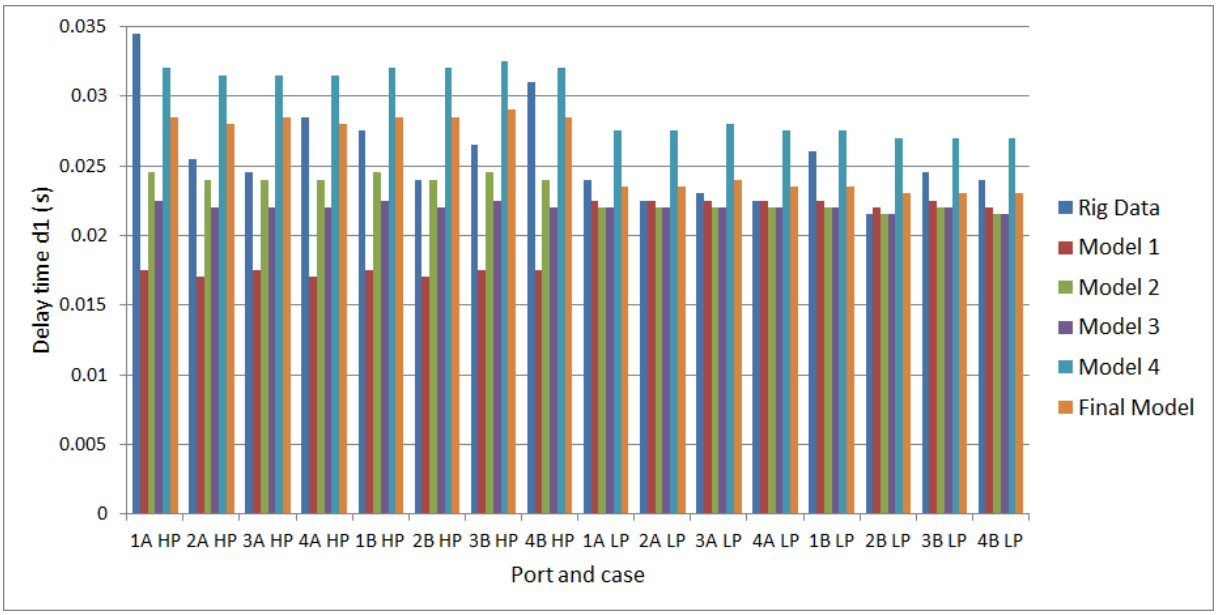

(a) *Comparison of delay time 'd1' resulting from various modelling attempts to rig data.*

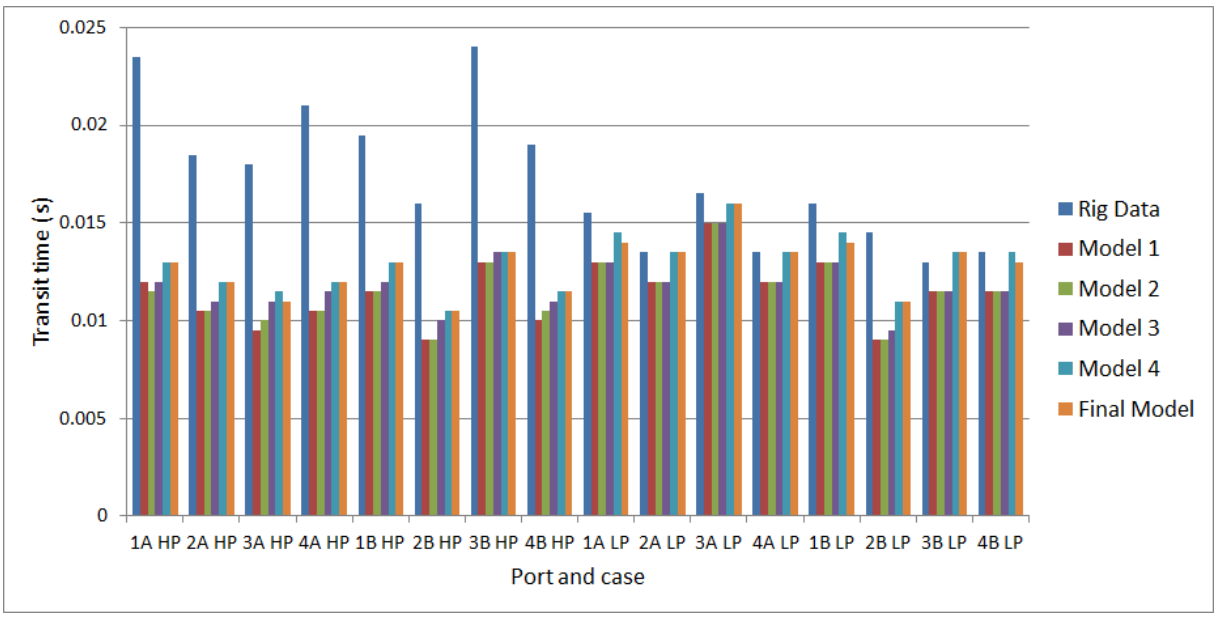

(b) *Comparison of transit time resulting from various modelling attempts to rig data.*

Figure 7.5 *Gradual improvement in the modelling of pressurisations and depressurisations.*

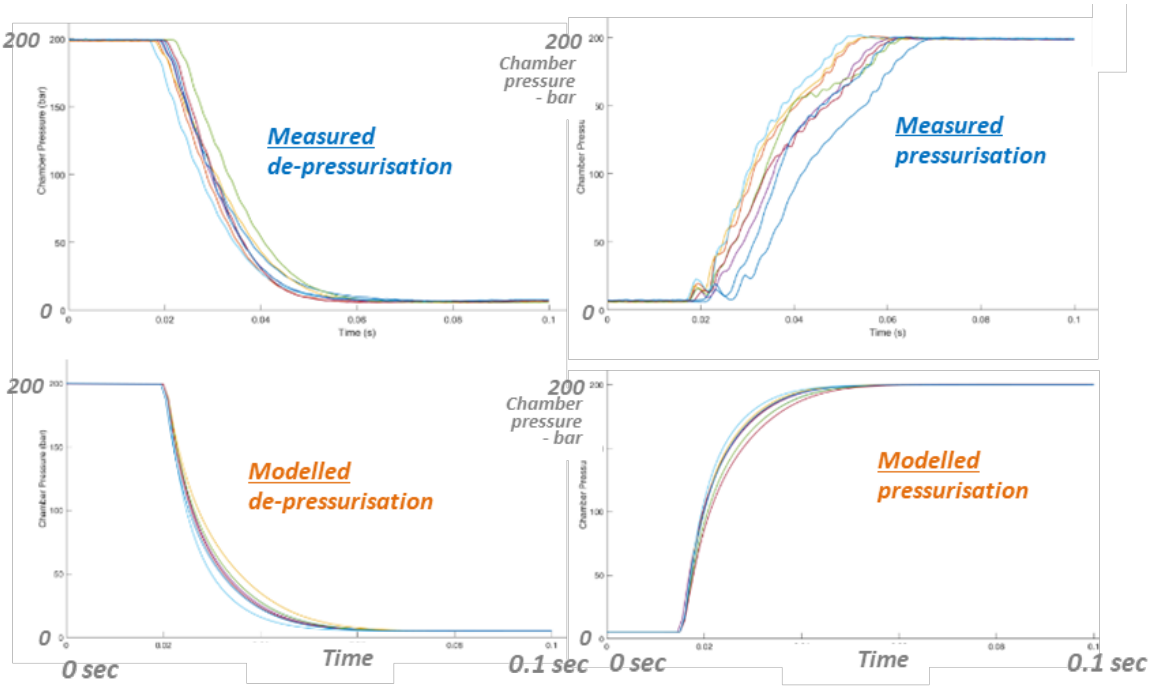

Figure 7.6 *(Top) test-rig measurements for depressurisation and pressurisation profiles of the eight motor ports, and (bottom) the corresponding model results*

7.2 Main Flow Valves

The main flow valve pressure-flow characteristic from [89] was used in the Simscape model blocks for main flow valves. A similar test to that for the transient valves was carried out, where the main LPVs were held open and the flywheel was driven in a sinusoidal motion. Even at high speeds, neither the test data nor the model showed any pressure drop as the valves have a very large flow capacity. Whilst this does not provide experimental validation, it also meant we had no reason to change the model from the data provided by Sun, so the pressure-flow characteristic was assumed to be correct.

7.3 Stiff Service Validation

The pressure response of the stiff service is key to the accuracy of the model. The compliance of this part of the Quantor affects how controllable the pressure is for DDPM B, which directly impacts the overall smoothness of the PTO torque applied by the Quantor. In a real DDPM machine, flow is inherently produced with pulsation, as the radial cylinders are activated through a revolution of the shaft. This can lead to significant pressure ripple in very stiff systems (such as the continuous service of Quantor), which may make a pressure control loop unstable. As the ability of DDPM B to follow a pressure

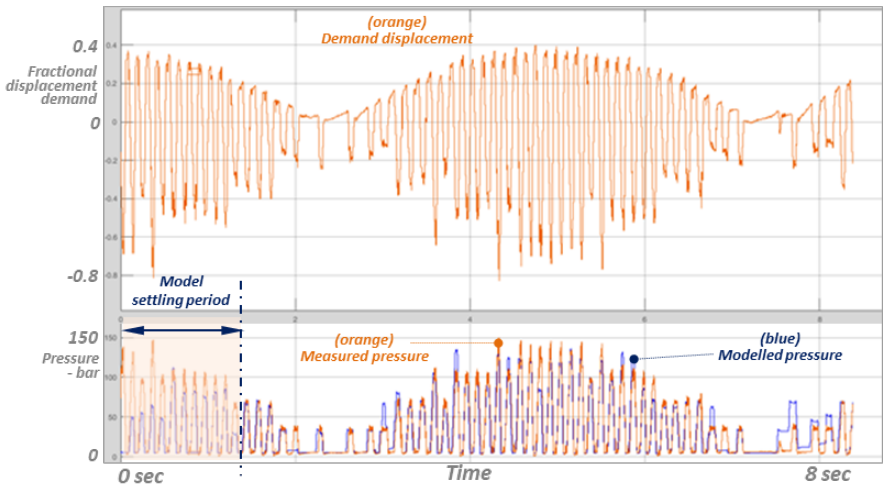

Figure 7.7 *DDPM pressure control. The demand displacement, Fd, of the DDPM recorded on the test-rig and shown in the top plot, was played back into the simulation model (which includes DDPM pulsation behaviour). The modelled pressure is shown by the lower blue trace which can be compared with the recorded test-rig pressure (orange). The differences in some of the peak values result from the uncorrelated low-level timing and selection of DDPM cylinders, between real and modelled DDPMs and small differences in DDPM shaft speeds.*

demand is very important, the compliance in the stiff service was critical to accurate modelling of the Quantor's performance. Also, the lowest possible controllable pressure for DDPM B has a significant potential impact on Quantor efficiency. Whenever the direction of the PTO torque demand changes, the directional valves in the manifold block switch, which means both directional valves momentarily open to the stiff service and low pressure, meaning that any pressure in the stiff service is vented to tank and the energy lost. The lower the minimum controllable pressure in the stiff service, the less energy is lost in this manner, improving the absorption efficiency of Quantor.

The model stiff service was verified in stages by playing back progressively fewer prescribed signals from the test. Firstly, Fd, the 'DDPM displacement' demand signal (resulting from the physical behaviour and feedback from the test) was played back to test the agreement in pressurisation of the controlled volumes. This validates the compliance of the motor hoses and piping. The DDPM model was run with and without realistic pulsation (the explicit discrete bursts of flow from each enabled DDPM piston). The former runs more slowly but, as shown in Figure 7.7, once it has settled to the running conditions it gives a good representation of the measured high frequency behaviour.

If the interest in load control is at the millisecond-scale, we can include the pulsation model to capture high frequency effects. However, since the pulsation model is generally slower

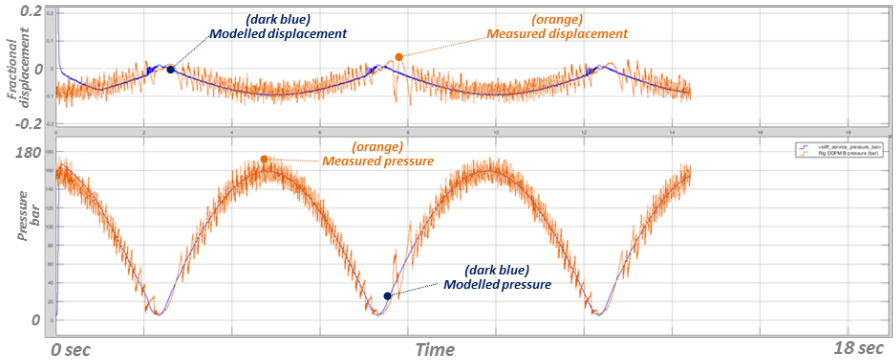

(a) *Comparison of measured (orange) and modelled (blue) DDPM performance with the only input data from the rig being the flywheel shaft speed, without pulsation.*

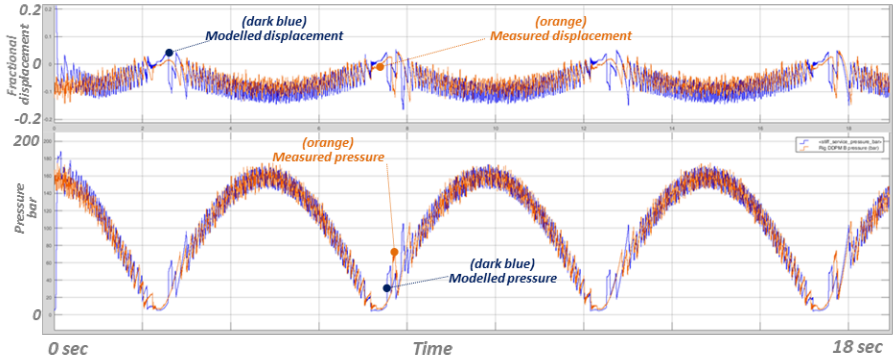

(b) *Comparison of measured (orange) and modelled (blue) DDPM performance with the only input data from the rig being the flywheel shaft speed, with pulsation.*

Figure 7.8 *Comparison of stiff service measured and modelled pressure response.*

(particularly when combined with Simscape physical model elements), it was not typically used as the modelled DDPM efficiency is not affected by the inclusion of pulsation. It was however useful in this instance to increase confidence in the compliance of the stiff service.

Following this validation of the DDPM gallery and chamber pressurisation model against displacement commands, the next stage was to model the same test but with only the recorded flywheel speed supplied to the PTO model and controller, so that the DDPM pressure demand was subject to all the differences between modelled and real systems. This case was expected to produce by far the greatest modelling errors due to the cumulative effect of errors in modelling the quantised chambers. As shown in Figure 7.8a and Figure 7.8b, the agreement was remarkably good. The displacement (upper plots) and pressure (lower plots) compare very well over longer timescales. However, without the pulsation effects included in the DDPM model (Figure 7.8a), its rapid pressure fluctuations

as measured on the test-rig are not present in the model results (blue). With the pulsation model included Figure 7.8b, the model accurately recreates the stochastic fluctuations in pressure and displacement. The individual pulsation events at the fine timescale are not matched directly as this is arbitrary from the uncorrelated DDPM shaft phase and PTO response. However, as can be seen from the signals around the zero-crossings, the signals are stochastically similar over short time scales and under the influence of geometric flow.

Note that individual pulsation events depend on the phases of the DDPMs (spinning at 1500 rpm) and that pressure signal noise will influence the exact timing of their digital commutation. This makes the pulsation effects stochastic with respect to the model validation, and hence the validation we seek is of the pressure range of the pulsation induced effects at similar times and under the influence of geometric flow effects, rather than the tracking of individual pulsation events which are not synchronised.

7.4 Fixed Displacement Motor Validation

7.4.1 Friction

The initial model of the PTO motor friction was based on output torque data supplied by the manufacturer as described in Section 4.3.6. However, it was later discovered that the difference between the ideal torque and the actual output torque should be partially attributed to the internal pressure drop of the motors. This was derived from the curve shown in Figure 7.9. This flow loss was divided by two and implemented in the Simscape model using hydraulic resistances on the motor ports, so that the loss was allocated per motor port. The friction lookup table was then adjusted accordingly so that the output torque still matched the data from the manufacturer.

A series of specific load cases were then tested on the rig to check that the friction model matched the measured friction. These cases included spinning the flywheel sinusoidally with all the chambers open to low pressure (zero-load cases) and alternately loaded cases. In the alternately loaded cases, the ports of the four motors were pressurised so that two applied positive torque to the shaft and two applied negative torque to the shaft, with a sinusoidal shaft speed maintained by the electric drive. This meant that torque induced by the pressure was net zero, but that the friction torque at this higher loading would be more visible. Figure 7.10 shows the results of one such test, and how the measured torque compares to the model torque. The total friction torque at peak speed is well matched to the model without any adjustment. Where the speed crosses through zero and the friction changes direction we see the preliminary model underestimating the friction torque.

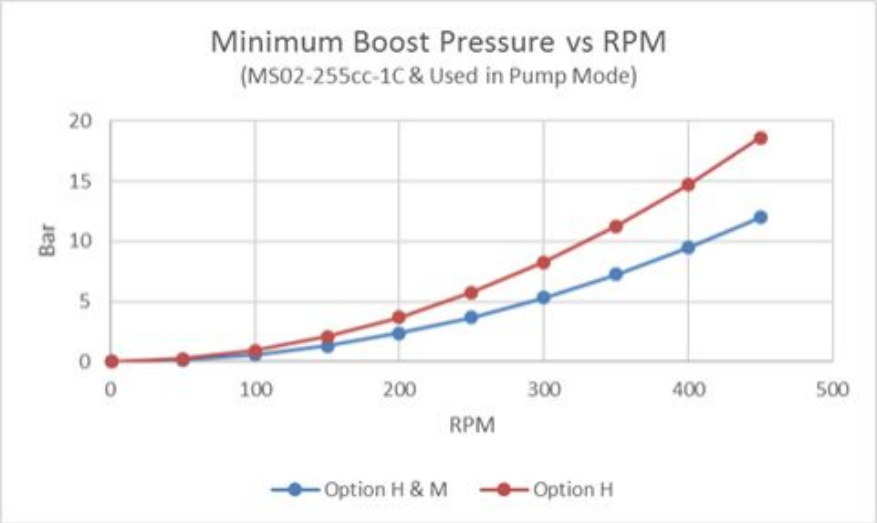

Figure 7.9 *Minimum boost pressure against PTO motor speed as supplied by the manufacturer (H&M is the relevant variant).*

To correct this, a Stribeck term was added for low speeds (below the minimum speed in the data supplied by Poclain, so that the change did not affect their data). The correction is shown in Figure 7.11. Figure 7.12 shows how this improved the match between test rig data and the model. Several other load cases were examined to confirm the Stribeck across a range of data, but one case is shown here for clarity.

On further testing, we found that the wheel-motor friction model with the additional Stribeck term did not perfectly match the measured torque on the test rig, particularly at high speeds. To improve the model, a further 'empirical friction' term was added. Without testing the wheel-motors off the test-rig, we could not verify whether this friction component is due to divergence of the wheel-motors from the manufacturer's data, an artefact of the PTO splitter-gear arrangement or a combination of both.

To compute the empirical term, we ran the existing model of the four wheel-motors and splitter gearbox using test port pressure and shaft speed data. Torque from the model, which includes the Stribeck term, was subtracted from measured torques to find the residual torque error. This was then divided by the number of wheel-motors and added to each motor as a new 'torque correction' lookup function.

Torque corrections were obtained for three pressures, 5, 200 and 300 bar, as shown in Figure 7.13a. In the case of 5 bar (the nominal system 'boost' pressure) the low-pressure valves for each wheel-motor port were held open and the flywheel driven sinusoidally to speeds of 160 rpm, clockwise and anticlockwise, whilst computing the torque errors. Data for the 200 and 300 bar cases were obtained whilst the wheel-motors were held at each

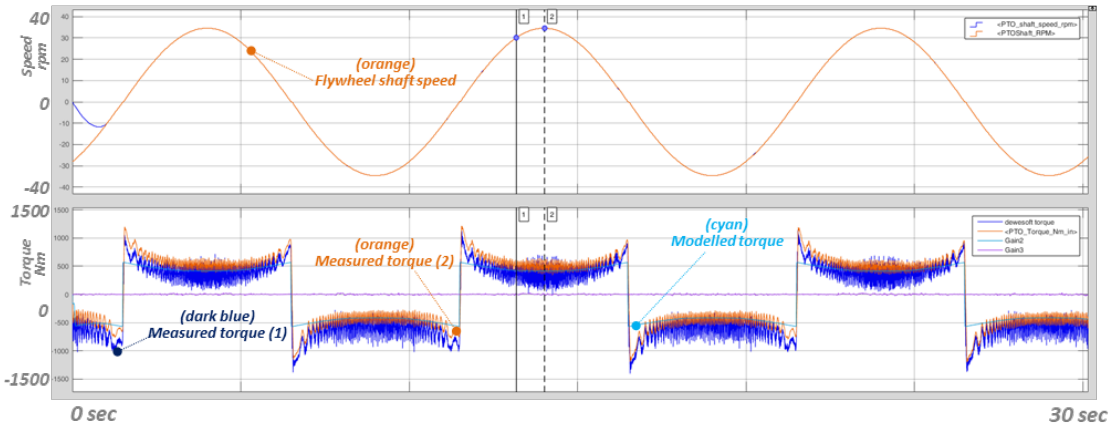

Figure 7.10 *Off-load friction test. Top: Speed of reciprocating drive following* 10 s *period with an amplitude of* ±35 rpm. *Bottom: wheel motor torque - measured (dark blue: unfiltered, orange: filtered) and simulated (cyan). This combines flow losses with the motor friction model.*

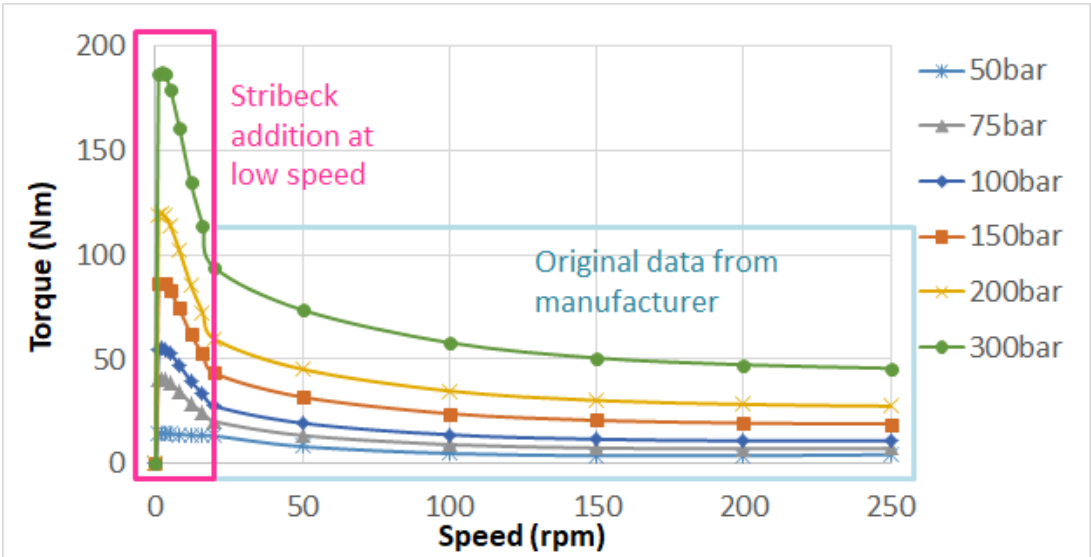

Figure 7.11 *Refined friction torque model for the wheel-motors with added low-speed (<*20 rpm*) values, implemented as an interpolated two-dimensional lookup table against speed (rpm) and pressure (bar).*

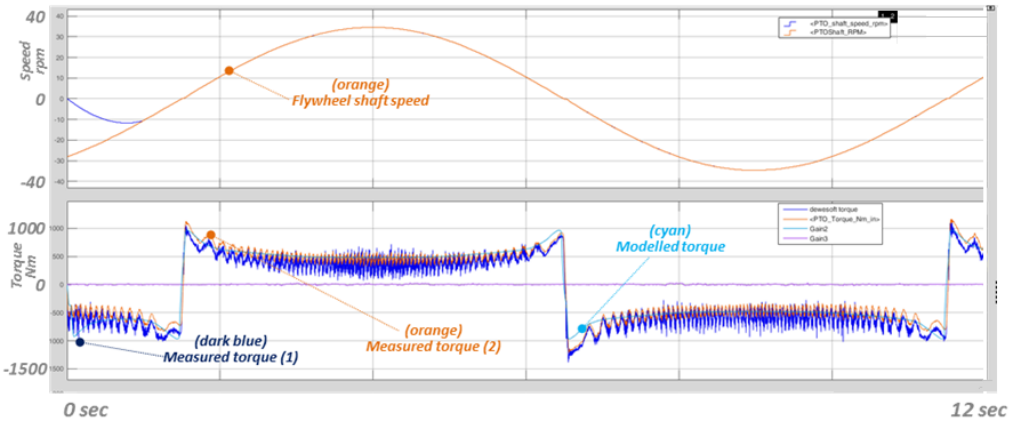

Figure 7.12 *Model screenshot of the same test case as in Figure 7.10. With the refined friction model, the load peaks around zero speed (reversal of direction) are much better captured.*

fixed speed for long enough periods to capture steady error values.

In all three cases, away from the zero-speed axis, the friction torque correction appears to be reasonably linear with speed, and a best-fit straight line was obtained for each case, as shown in Figure 7.13b. The offset in each case was corrected to make the resulting curve symmetrical about zero. This was necessary because the offset of the load cells, although corrected daily before performance testing, tended to drift between measurements. The assumption that the friction correction term should be symmetrical about zero is reasonable given the arrangement and design of the wheel-motors and is consistent with subsequent test experience.

The improved model with friction torque corrections, interpolated from the data shown in Figure 7.13b, was compared to previous load tests as a final validation. Figure 7.14a and Figure 7.14b show the results of this comparison for two different load tests, with the improved model with corrective term showing good agreement with the test-rig data.

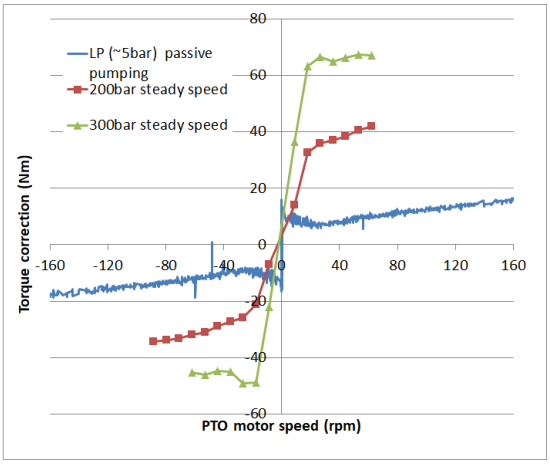

(a) *Raw error between measured PTO torque and modelled PTO motor friction torque.*

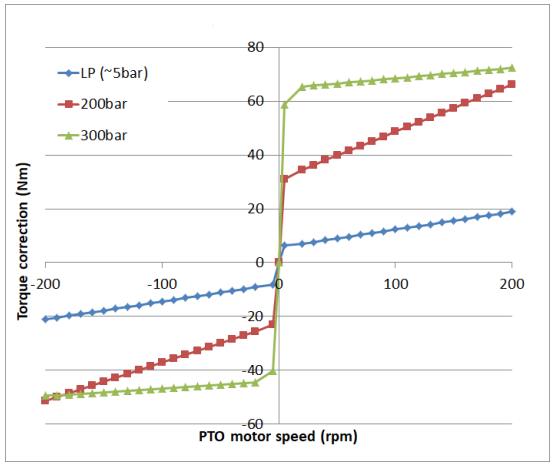

(b) *Empirical correction to PTO friction model based on measured error.*

Figure 7.13 *Empirical torque error as measured and as applied in the model.*

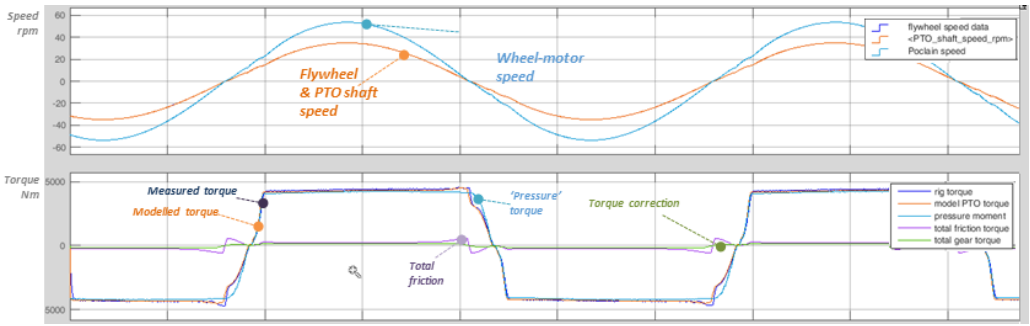

(a) *Wheel-motor torque and friction at a pressure of* 200 bar *whilst passively pumping into the HP accumulator. Top: speed. Bottom: measured and modelled torques (of all four wheel-motors) showing the contribution to the modelled torque from the new correction term as well as the total motor friction torque. The 'pressure' torque line (the product of pressure and displacement) represents the simplest possible torque model.*

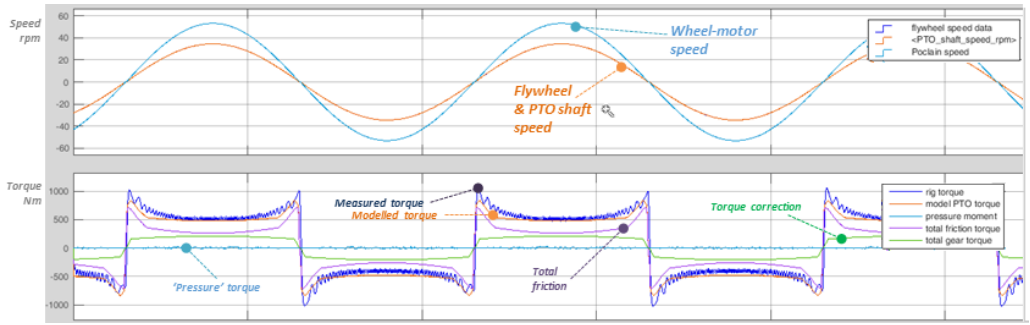

(b) *Motor speeds and torques, as per the descriptions in Figure 7.14a but with their ports connected to the HP accumulator at* 200 bar *with complementary torque polarities such that the net 'useful' torque from the four wheel-motors is zero. In this extreme case, note how closely the modelled torque matches the measured torque and that, since there is no net flow to the wheel-motors, the calculated 'pressure' torque is zero.*

Figure 7.14 *Confirmation of empirical correction by comparison with load cases.*

7.4.2 Leakage

Poclain provided leakage data for the wheel-motors, which we incorporated into the Simscape model in the form of a hydraulic resistance on each motor port, as described in Section 4.3.6. To validate this model we carried out a leakage test as plotted in Figure 7.15. The wheel-motors were actively held stationary by the flywheel drive motor whilst the high-pressure gallery and chamber pressures were raised to a nominal pressure of 250 bar. In turn, the 'B' (negative) wheel-motor ports and then the 'A' (positive) ports were connected to this 250 bar supply and then isolated so that the pressurised chambers could leak to the drain line from the wheel-motor cases. The pressure decay curves as the chambers leaked down was then compared with the Poclain data.

Figure 7.15 shows the measured pressure decay for each motor port. The spreads of individual leakage rates may be due to individual variations between the wheel motors, or the motor piston positions relative to the outlet. If a stationary motor was at a shaft angle so that the pistons overlapped perfectly with the outlet, the leakage rate would be faster than a motor where there was only a partial overlap between the pistons and outlet. Figure 7.16a and Figure 7.16b compare the modelled leakage profile with the measured leakage respectively from the 'A' and 'B' wheel-motor ports. In both cases, the model most closely matches the port with the fastest leakage rate, which is on wheel-motor 4. This meant that the leakage model could be validated conservatively, as it replicates the worst-case leakage seen in experiment.

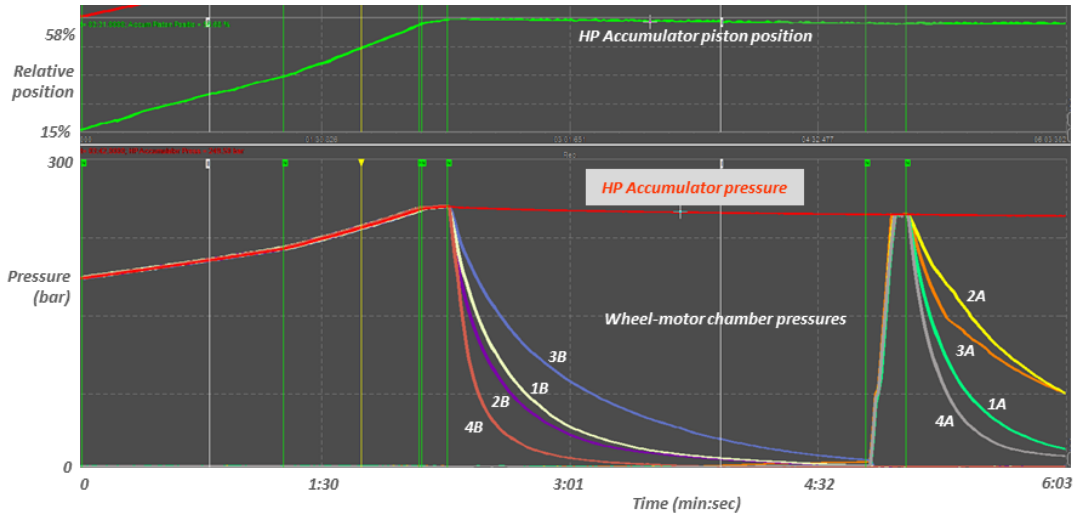

Figure 7.15 *Experimental traces from leakage test showing HP accumulator piston position (top), and HP accumulator pressure and chamber pressures (bottom).*

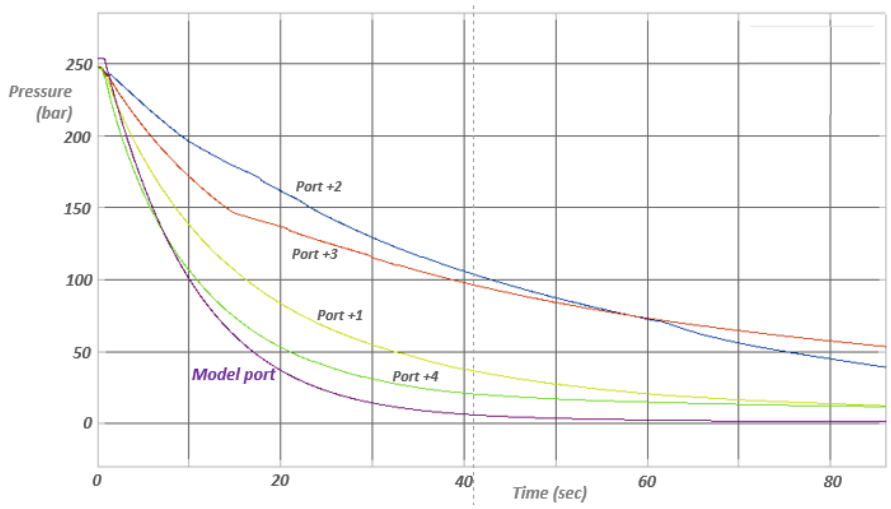

(a) *Comparison of modelled leakage and measured leakage from the 'plus' ports of the four wheel-motors*

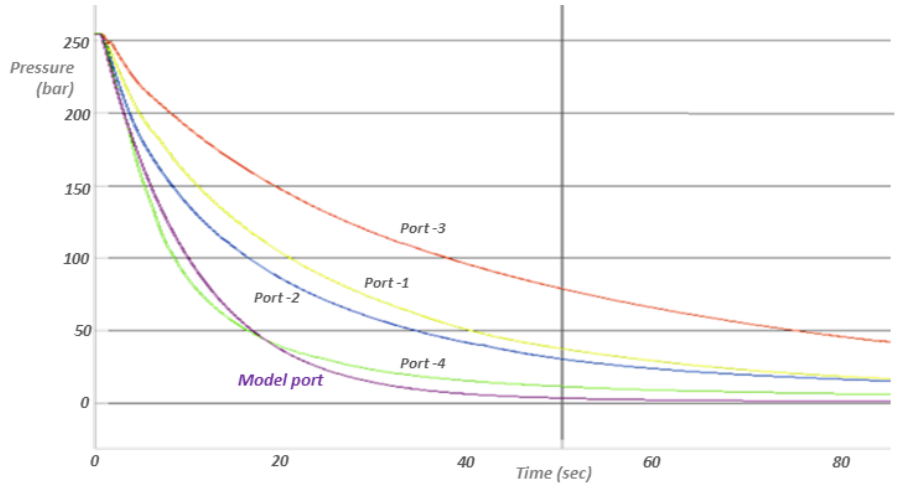

(b) *Comparison of modelled leakage and measured leakage from the 'minus' ports of the four wheel-motors.*

Figure 7.16 *Validation of leakage model for A and B ports with test rig data.*

7.5 Chamber Hose Flow Losses

The chamber hoses connect the motor ports to the manifold blocks. Since the instrumentation to measure these directly was not available a model was used to extract the pressure drop at each flow rate, pictured in Figure 7.17a. This was the Simscape model of the chamber hoses described in Chapter 4, which is based on measured data of the compliance of the appropriate type of hose. Figure 7.17b shows the resulting output. The discontinuity is because the Simscape model includes the change from laminar to turbulent flow. Arguably this is unnecessarily complex but the effect it will have on the loss breakdown is very small.

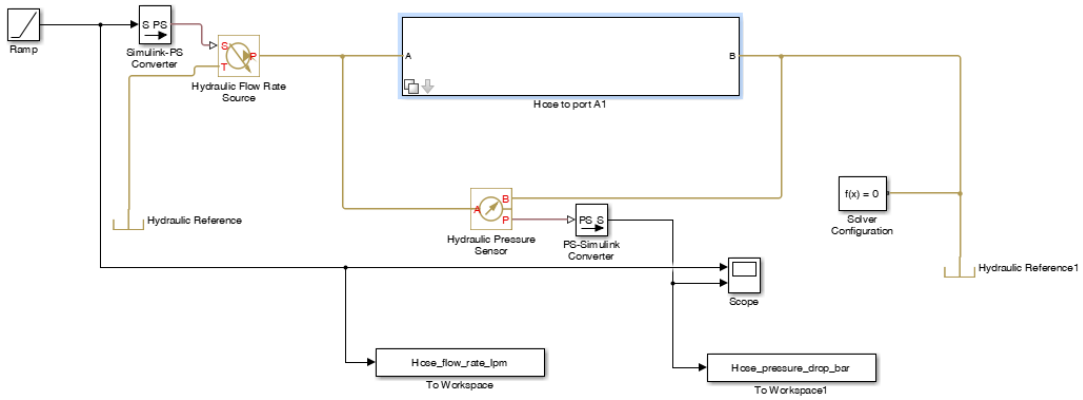

(a) *Simscape model used to estimate the flow losses in chamber hoses*

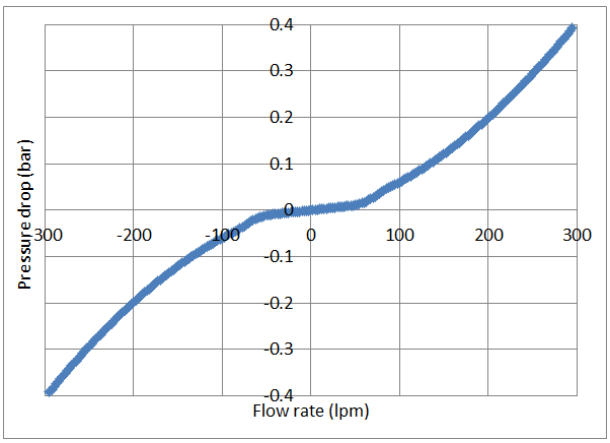

(b) *Resulting pressure drop against flow extracted from the Simscape chamber hose model above*

Figure 7.17 *Simscape model and resulting flow loss model for individual chamber hoses*

7.6 Accumulator Model Validation

The accumulator model was not validated with test rig data in the end, as it was judged to be a low priority task given that this is not novel work [82, 90]. The emphasis was placed on validating the new components and control features of Quantor. To ensure that the losses of the accumulator were still captured when rig test data was played back into the Simscape model, the Fd of DDPM A, DDPM A outlet pressure and HP accumulator pressure were all fed directly into the model. This meant that the modelled PTO motors were not the source of the pressure going into the accumulator, which is a slight abstraction, but the leakage of the Poclains and the DDPM flow model had already been validated, so we had a good estimate of the flow into and out of this gallery.

7.7 DDPM Models

Artemis has a well-established methodology for making semi-empirical simulation models of DDPMs in pumping mode. These are based on loss curves derived from lab measurements. The same loss curves are used for a DDPM in motoring mode, but with an additional capacity factor to account for the shrinkage that occurs. This is because volumetric efficiency is lower in motoring than in pumping due to the pattern of valve operation during motoring [13].

The simulation model assumes that different builds of the same design of DD machines will behave almost identically. The current model for the M96 DDPM was derived from pumping measurements that were carried out on a dedicated test-rig with the M5 machine which has not otherwise been used in this project.

Figure 7.18a shows idle torques measured for the M3 and M4 DDPMs that are used in the Quantor lab system. For comparison, the idling component of the M5 based model is also shown. Clearly, M3 and M4 have slightly higher idling torques than those of the model. To improve the model, the idle torque loss power curve was adjusted accordingly to reflect the average idle torque of the M3 and M4 machines, as shown in Figure 7.18b.

Figure 7.19 shows how closely the M96 simulation model, derived from the M5 tests, agrees with mechanical and fluid power measurements of M3 and M4 in pumping mode made on the back-to-back test rig. On first looking, there may just appear to be four lines in each figure, but close examination shows that each of is, in fact, a pair of coincidental lines corresponding to modelled and measured values. The matches of modelled and measured pumping performances were similarly close for the M4 machine.

7.7.1 DDPM Motoring

Validation of the DDPM motoring model was more challenging because variations in the timing of valve operation can have opposing effects on efficiency and stability.

'Stability' in this context implies that all motoring strokes requested by the controller are implemented and the DDPM is generally tuned to prioritise this. Stability is also affected by pressure, oil viscosity changes with temperature and the ageing of valve components.

The Motoring Annular Valve (MAV) used in these machines is the '10g' version. Continuing improvements through versions to the current '11b' have greatly improved stability and immunity to temperature and age. As the M96 moves toward commercial development, the control of valve timing is expected to be further tightened by the controller being able to sense successful valve actuation, as is now implemented for the E-dyn 96 DD pump.

In the meantime, the calibration of the M3 and M4 valves is a relatively manual process in which the limits of timing stability of each valve are experimentally determined and then buffered against by individually set timing margins within the controller. In comparing results from the simulation model with the subsequent behaviour of M3 and M4 we found that the capacity factor referred to above, which allows for the volumetric shrinkage of a motoring cylinder compared with a pumping cylinder, should also include a pressure dependency. This is likely to be a short-term measure until the timing of the physical valves becomes responsive to the detection of valve actuation information.

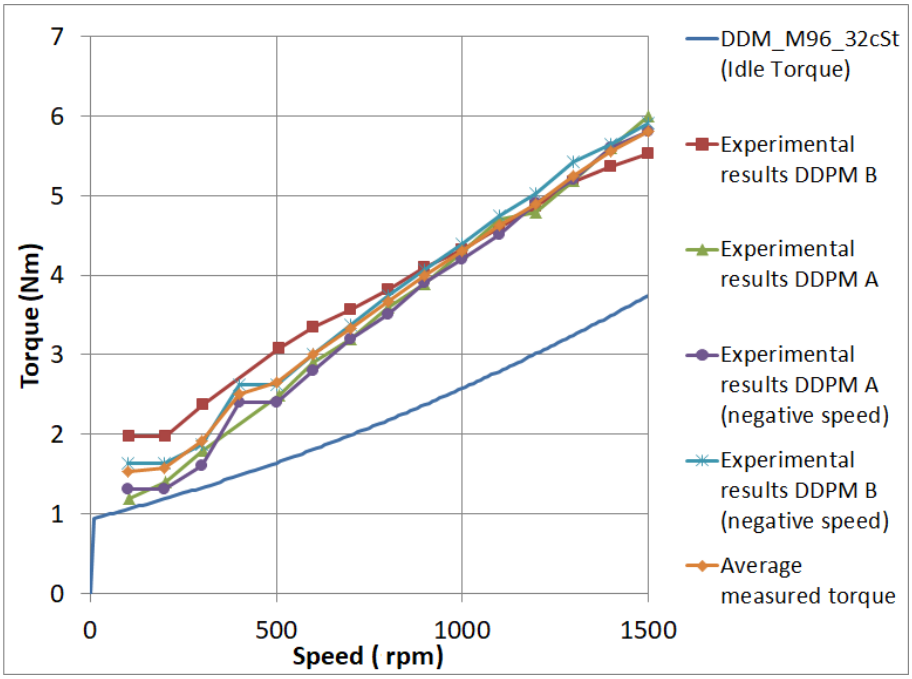

(a) *DDPM idling torque: comparison of measured values for the M3 and M4 machines with the modelled idle torque (labelled as DDM_M96_32cSt).*

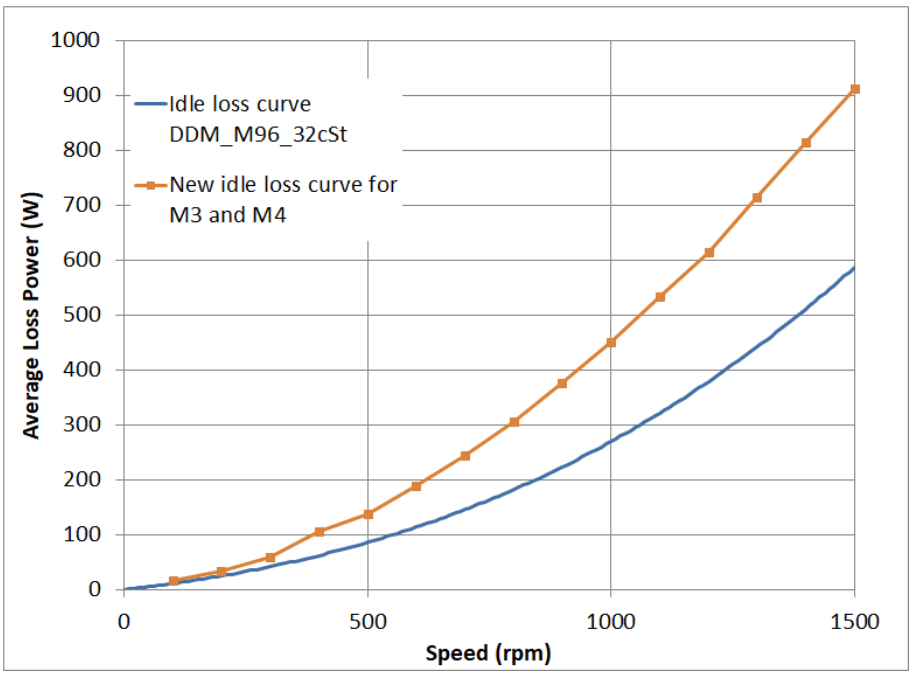

(b) *DDPM idle loss curves: comparison of original model idle loss curve based on M5 measurements (labelled as DDM_M96_32cSt) and new idle loss curve based on M3 and M4 measurements.*

Figure 7.18 *Change of model idle power based on back-to-back test rig measurements.*

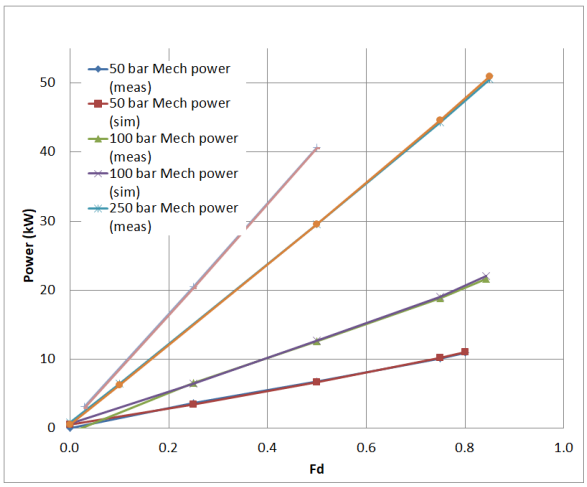

(a) *DDPM A mechanical power comparison*

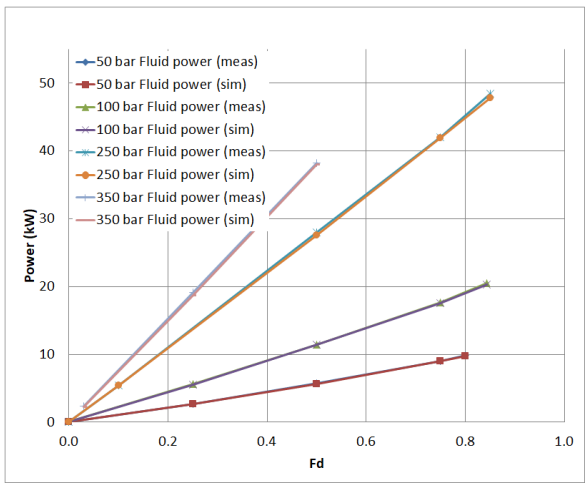

(b) *DDPM A fluid power comparison*

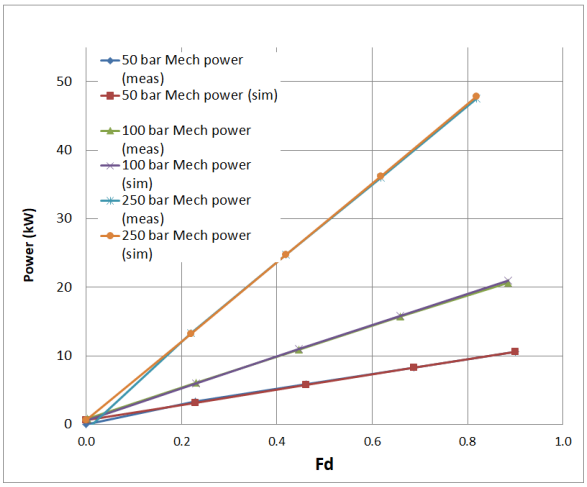

(c) *DDPM B mechanical power comparison*

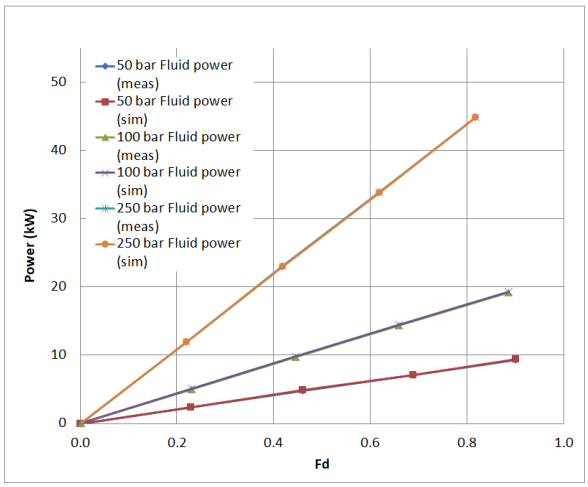

(d) *DDPM B fluid model comparison*

Figure 7.19 *Comparison of model based on M5 data and measured fluid and mechanical power for DDPM A (M3) and DDPM B (M4) in pumping mode at* 1500 rpm.

7.7.2 Motoring Test

Figure 7.20 shows data from a nine-minute motoring run of M3, on the back-to-back test-rig at a pressure of 100 bar, along with a simulation prediction. Fd, the displacement factor was varied from 0 (idling) down to -1 (motoring at full capacity) and the differences between measured and simulated fluid- and mechanical-powers examined.

Whilst the simulated mechanical power matches well at all displacements, the model slightly overestimates the fluid power over most of the range. However, because we have relatively higher confidence in the loss data from pumping, we decided not to adjust it. Instead, we took motoring data for M3 and M4 at pressures of 50, 100, 250 and 350 bar and created a new, pressure-dependent, motoring capacity factor look-up table for each machine. These were verified against the test-rig data using loss breakdown tools which are described later in this section.

This validation process was possible as we had direct measurements of torque, pressure and speed on each DDPM, and the validated leakage model allowed estimation of the flow delivered to the DDPMs by the wheel-motors.

Whilst the M4 motoring simulation model matched the test-rig data with a less than 2.5% error above 8 kW, the M3 model showed a poorer match, with around 5% under-estimation in mechanical power across the power range. We don't yet fully understand this systematic difference, though it is consistent with a possible leak on the M3 side of the back-to-back test-rig between it and the flow sensor.

The final adjustment of the M3 model was therefore carried out using the results of steady speed tests. The flywheel was spun at a constant speed, with the wheel-motors pumping through the passive check valves into the HP gallery, which was pressure-controlled by M3 motoring. Using modelled flow and measured torque, speed and pressure from these tests, the capacity factor of the M3 model was adjusted and the results found to agree within 2.5% with the test-rig data.

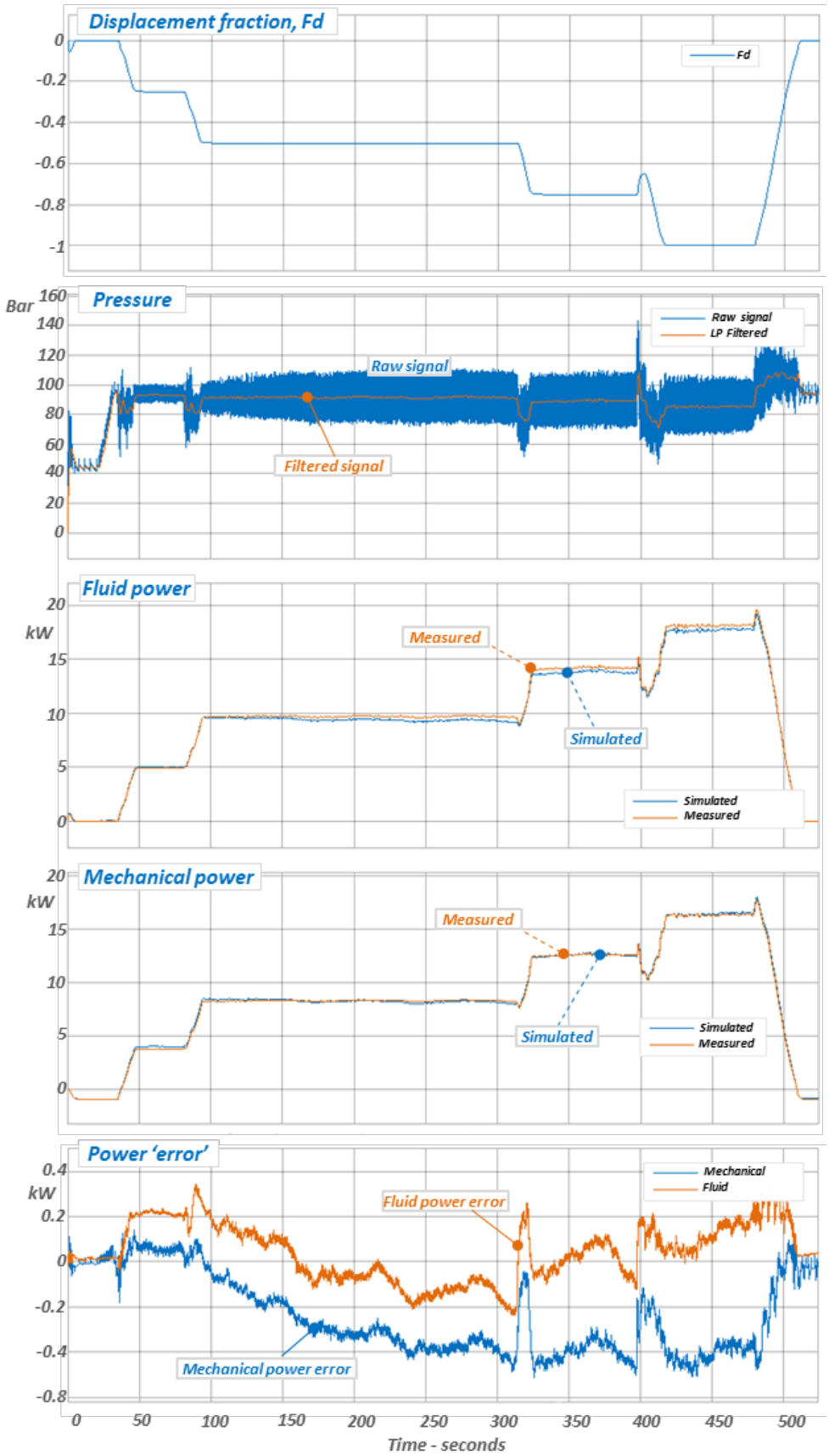

Figure 7.20 *Comparison of M3 (DDPM A) data measured on back-to-back test-rig data and from the simulation model with pressure dependent capacity factor. The nominal pressure is* 100 bar.

7.8 Summary

To validate the component models at an individual level, targeted tests were carried out to isolate the features of interest, such as PTO motor friction or transient valve pressurisation. The model component was then adjusted to better reflect the results obtained on the test rig. In some cases where direct validation in this way was not possible, more detail from the manufacturer's data was implemented in the model, for example in the case of the main flow valves. Direct validation from the test rig was carried out for:

- Transient valve pressurisation and depressurisation
- Stiff service compliance
- PTO motor friction
- PTO motor leakage
- DDPM A and B (separate model for each).

The one major model component which was not validated from the test rig was the HP accumulator, which was judged to be of lower priority as this has been explored in previous research. The Simscape model of the full rig had the measured accumulator pressure played back into it as a way of keeping account of those losses without a validated model.

This component level validation was a useful foundation from which to complete the loss breakdown of the full Quantor system in Chapter 8.

Chapter 8

Quantor Model Validation: Full Quantor Validation

Having validated individual components and produced good empirical results of many parts of Quantor system, bringing the components together into a whole model to analyse the overall Quantor performance and losses was the next step. This process was carried out in two overlapping stages; loss breakdown analysis of rig test data, and Simscape model validation. This was an iterative process repeated over many cycles to gradually reduce the discrepancies in the loss breakdown over many cases.

8.1 Loss Breakdown Analysis Method

The aim of the loss breakdown calculations is that a detailed loss breakdown for each stage in the transmission can be obtained using only the measured signals on the test rig. This involves a combination of direct measurement, validated component models and modelling from theory. It was important and interesting to divide the power in the system into the quantised and continuous services, and to understand how the different control features such as feature X affected the losses. The recorded valve signals from CAN were used to calculate the power allocated to the various galleries and the losses due to various control events. The CAN rate on the rig was relatively low at 100 Hz, compared to the control execution rate of 1 kHz and the analogue sampling rate of 5 kHz, so this approach may have introduced a degree of aliasing. However, we decided to use the CAN data from the tests rather than signals from a model controller because there were occasions where the model controller would exhibit different behaviour (e.g. operating different numbers of quantised states) to the rig controller, despite them having the same software,

same control parameters and the same inputs. Table 8.1 lists the quantities recorded from the rig and used in the loss breakdown analysis, along with their uncertainties. The uncertainties combine the hysteresis, linearity and repeatability provided on manufacturer data sheets (insofar as this was possible). The quantities highlighted as coming from CAN signals are vulnerable to aliasing in addition to the measurement uncertainties shown in the table.

Table 8.1 *Recorded signals and their uncertainties used in loss breakdown calculations. Uncertainties include non-linearity, hysteresis and repeatability. A detailed list of the types of sensors used is available in Table 5.1.*

Type	Location	Uncertainty
Pressure	DDPM A outlet	±0.5% Full scale (FS)
	DDPM B outlet	±0.5% FS
	LP gallery	±0.5% FS
	HP accumulator	±0.5% FS
	Chamber ports (8 total)	±0.5% FS
Force	PTO shaft load cells	±0.15% FS
Torque	DDPM A torque	±0.04% FS
	DDPM B torque	±0.04% FS
Speed	PTO shaft speed	±0.03° in position measurement
	DDPM A speed (CAN)	±1.1° in position measurement
	DDPM B speed (CAN)	at 1500 rpm
Fd	DDPM A Fd (CAN)	±0.01% FS
	DDPM B Fd (CAN)	±0.01% FS
Position	HP accumulator piston position	±0.5% FS
Control	Valve control signals (CAN)	Aliasing due to rate

8.1.1 Sankey Analysis Method

The losses incurred at each stage of the energy flow through the Quantor PTO from the WEC input to the generator output can be quantified for the lab test system and the simulation model. Close agreement between these values, across a range of power levels and dynamic conditions, helps to confirm the accuracy of all elements of the model.

Figure 8.1a is an example screenshot of the Excel tool used for Sankey analysis, and

Figure 8.1b is an example of a Sankey diagram for an irregular Quantor mode 1 case. Sankey diagrams provide an easily grasped way of representing energy flows, but care must be taken to minimise distorting effects from any differences in the stored energy at the beginning and the end of the run.

The energy accounting period used for Sankey diagrams is typically four complete wave cycles for regular waves, and just over 8.5 minutes (512 seconds) for irregular waves (the repeat time of the pseudo-random wave sequence). Energy values and losses are normally expressed as percentages of the input energy over the period, allowing the relative impact of different losses to be seen and the efficiency of each stage to be shown.

At each node of the diagram, the total inflow and outflow of energy throughout the test should ideally balance to zero to give 'node equilibrium'. Measured input and output power measurements from the test system provide the key nodes but, whilst the total loss measurements are made directly, the detailed allocation of specific losses depends on validated models of the PTO components.

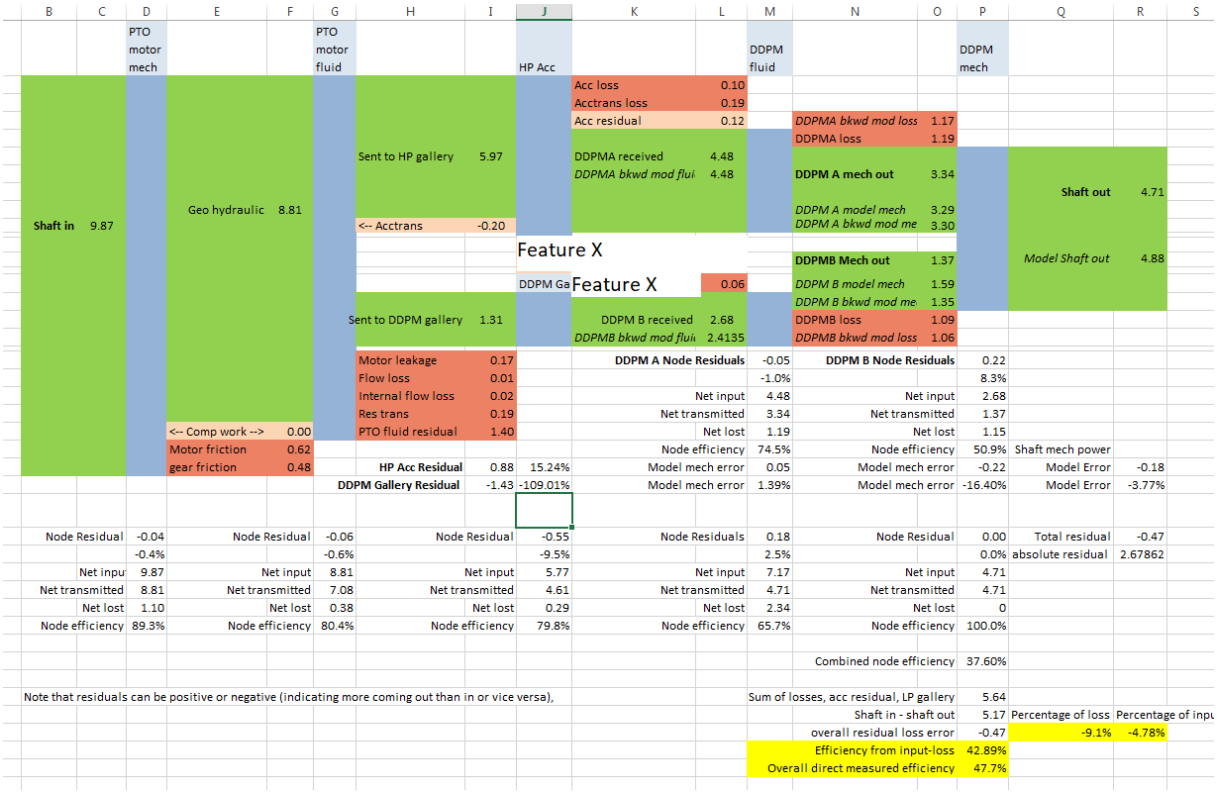

(a) *Example of Excel Sankey analysis tool for an irregular Quantor mode 1 test case.*

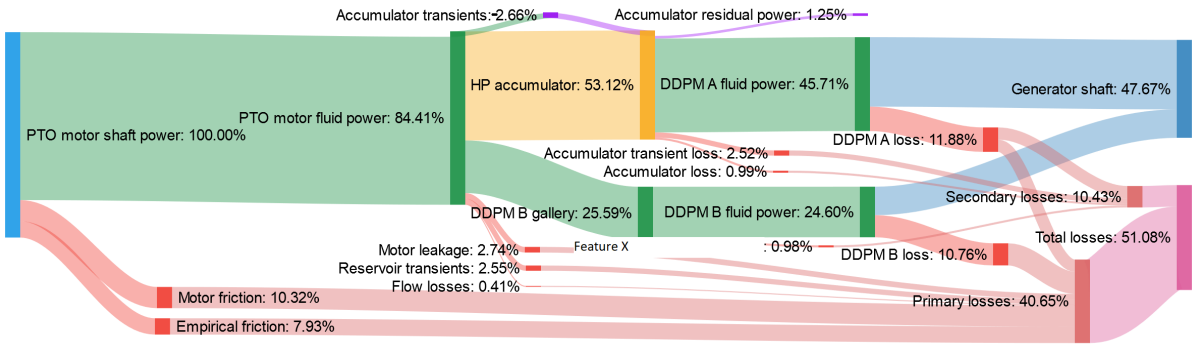

(b) *Example of the output Sankey diagram after normalisation*

Figure 8.1 *Example of the process of Sankey analysis for an irregular case, starting with the un-normalised results from the loss calculation, and ending with final Sankey diagram.*

8.1.2 Loss Models

An independent loss model was developed largely from information, such as wheel-motor friction and valve flow losses, which had already been used to create the Simscape Quantor PTO model. Applying it to measured test-rig data and adjusting it to reduce imbalance at each node helped to refine the Simscape physical model and improve agreement with the test-rig measurements. The model validation process therefore largely consisted of improving the independent loss model to match test-rig measurements and the incorporation of those changes into the Simscape model. The independent loss model was later directly converted into a simplified loss model by making it generically applicable to different numbers and types of PTO actuators. An exception to the hands-on validation of test system component models was the 75l HP piston accumulator which provides Quantor's compliant energy buffer. As validated third-party accumulator models were available, we felt that it was better to use the limited time available on the lab system to acquire new knowledge.

8.1.3 Residuals

The physics-based form of the simulation model means that many sensors on the physical test system can be matched by simulated counterparts. However, in the physical system some important parameters can be inferred only via the model or by deduction from measurements elsewhere. The certainty or uncertainty of the initial energy and loss accounting can be expressed by 'residuals', the differences between the sum of the modelled losses at each node and the measured difference in input shaft and output shaft power. For a given value of residual, some 'normalisation' of individual losses is required if equilibrium is to be achieved at each node and across the system. Figure 8.2a shows, for 14 different cases, the tendency for the net residuals to proportionally reduce as the input power increases. We note though that the individual node residuals may be positive or negative and so there will be some 'cancellation' when they are summed to obtain these net values.

Figure 8.2b shows the higher net residuals values when the absolute values of node residuals are summed. This supports the notion that the model underestimates losses at some nodes and overestimates them at others and supports normalisation on a node-by-node basis. Note that some of the outlying values in Figure 8.2 are due to known control issues which would be resolved in further testing.

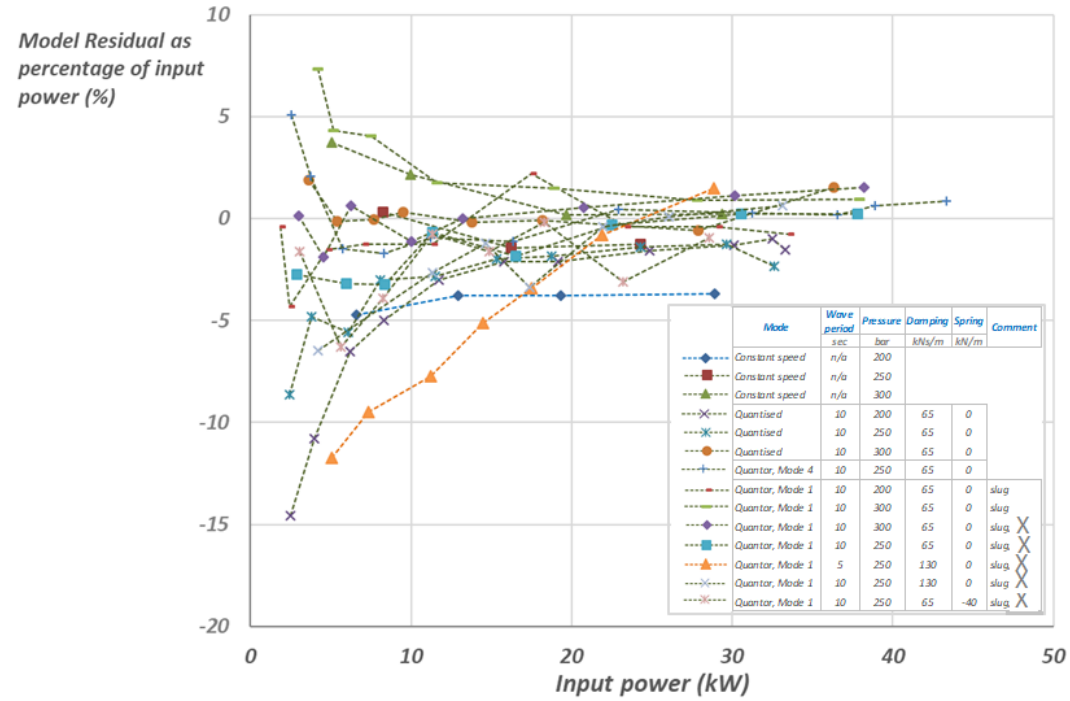

(a) *Loss model residuals (sum of residuals for all nodes) as percentages of measured input shaft power for 14 test cases.*

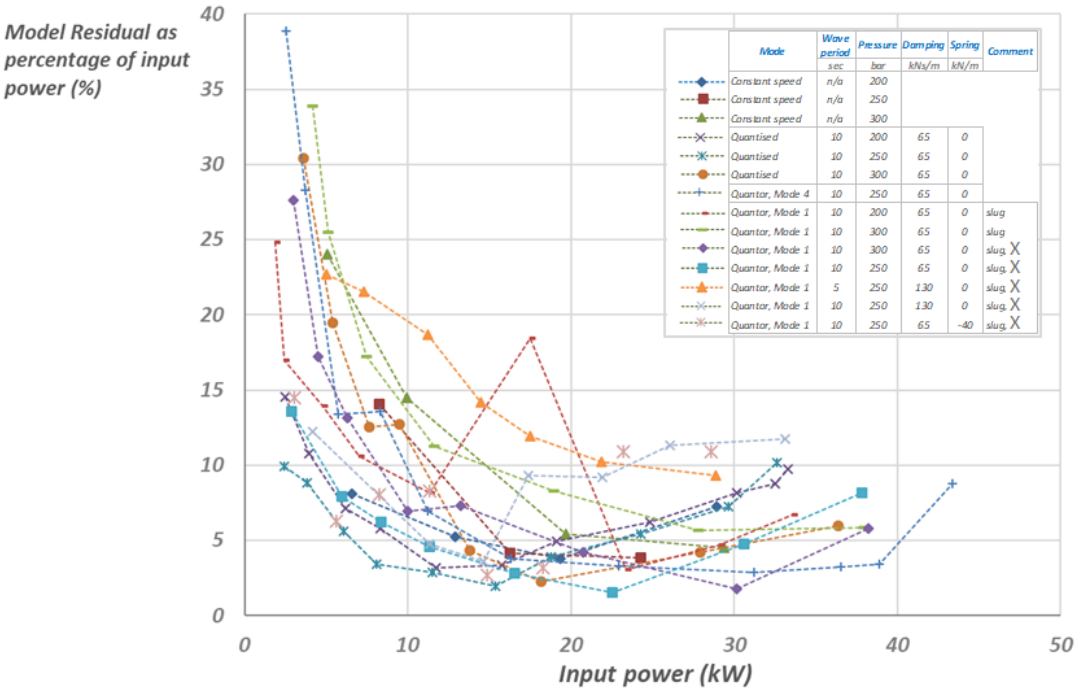

(b) *Loss model absolute residuals (sum of absolute values of node residuals) as percentages of measured input shaft power for 14 test cases.*

Figure 8.2 *Loss model residuals for a variety of test cases*

8.1.4 Normalisation

In the context of energy accounting, 'normalisation' refers to systematic adjustments made to certain loss parameters so as maintain equilibrium across the whole account. Some parameters that could be accurately measured or modelled with confidence based on long experience were left unchanged. The remaining key parameters were then adjusted. Table 8.2 lists the parameters in each of these categories.

Table 8.2 *Treatment of loss model quantities in the normalisation process (see Tables 8.3 and 8.4 and section 8.2 for an explanation of each quantity.*

Trusted measurement	Trusted model	Normalised
Input shaft power	DDPM A loss (backwards)	Friction
Output shaft power	DDPM B loss (backwards)	Leakage
Accumulator loss		Flow Losses
Accumulator residual		Transient Losses

It was important to retain the integrity of the measured input and output shaft powers, so these were not changed. The measured accumulator loss and residual were also unchanged, because we had a direct and accurate measurement of these quantities. The Artemis 'backwards-facing' model of the M96 DDPM losses was trusted as it showed close agreement with the measured mechanical power from the test rig.

The remaining loss parameters were proportionally adjusted so that the measured input energy was equal to the sum of the measured output energy plus total modelled losses. Figure 8.3a and Figure 8.3b show comparisons of quantised and Quantor test results before and after normalisation.

The residual in the un-normalised cases is due in part to losses which were not included in the model, including the following.

- Valve piloting losses.
- Losses in the small shock accumulators.
- Pressure drops in galleries and bends within the manifold blocks, hoses and hard pipes.
- Leakage through closed valves.

- Flow through the oil condition monitoring system.

At low input powers, the loss breakdown is much more sensitive to small errors in the estimation of each loss term. In the quantised case the residual reduces as the input power increases. The relationship is more varied in the Quantor case but the effect of the omitted losses above and the uncertainty in the included losses both reduce as the input power increases, so that the breakdown changes very little after normalisation.

In test runs where the high-pressure accumulator pressure was higher or lower at the end of the run than at the beginning, the corresponding energy differences were redistributed to allow calculation of efficiency and losses as if the accumulator had returned to the same initial state.

8.1.5 Primary and Secondary Losses

The assignment of losses to the primary or secondary side of a purely quantised PTO is uncomplicated. The primary transmission delivers energy from the PTO actuators to the accumulator and the secondary transmission delivers energy from the accumulator to the generator.

This division is less clear in Quantor because of the multiple roles of the DDPM. DDPM A drives the generator and transforms energy between compliant and stiff systems whilst DDPM B provides the stiff, pressure-control, service to the continuously controlled chambers.

The DDPM B losses have been assigned to the primary side as these are generally associated with capturing wave energy from the WEC. Half of the DDPM A losses (from pressure transforming) are also assigned to the primary side and the other half (from delivering accumulator energy to the generator) to the secondary side. This is the rationale in the Sankey diagrams for the A losses being split between primary and secondary sides.

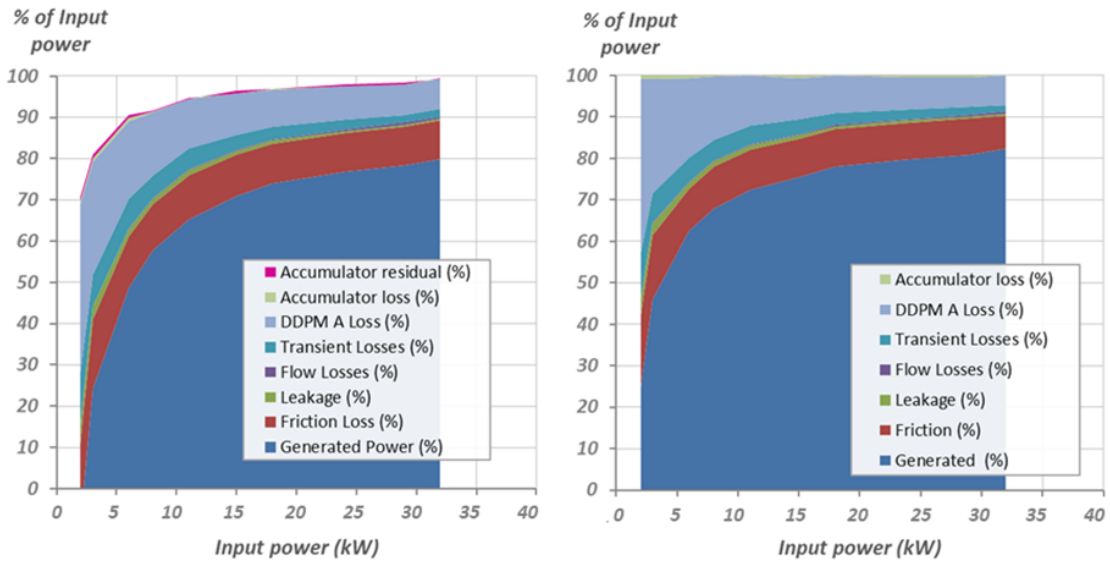

(a) *Comparison of original (left) and normalised (right) measured results for* 200 bar *quantised case.*

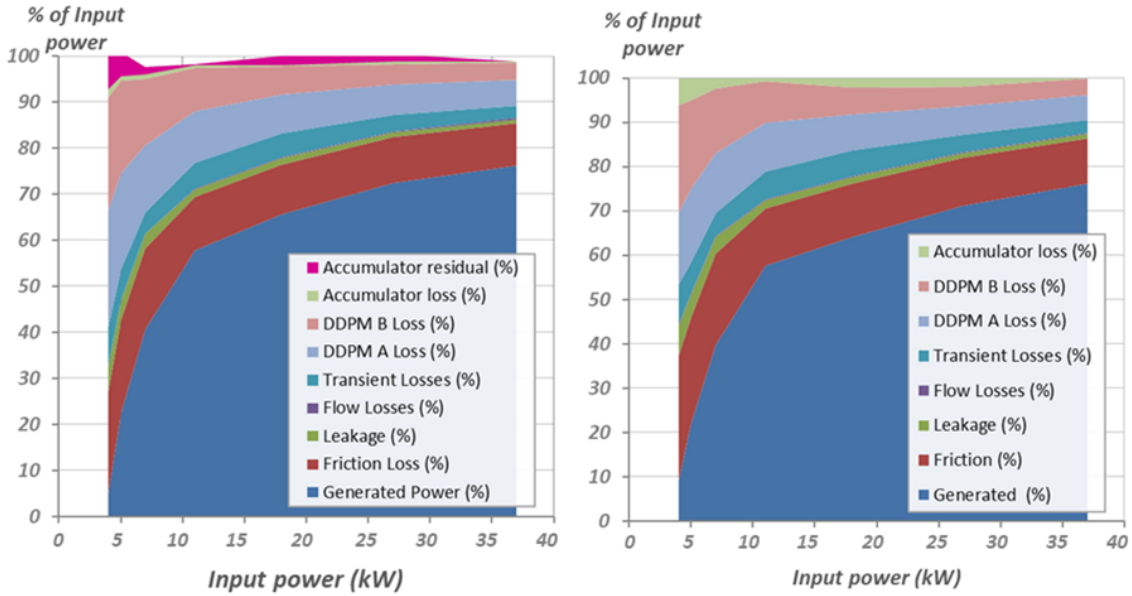

(b) *Comparison of original (left) and normalised (right) measured results for Quantor, mode 1* 300 bar *'slug only' case.*

Figure 8.3 *Effect of normalisation on loss breakdown of two different cases*

8.2 Loss Breakdown Calculations

A Simulink loss breakdown calculation subsystem was constructed, to take in the measured signals listed above in Table 8.1 and to produce a loss breakdown using the following calculations. As far as possible, these calculations were carried out using vectors, with each vector element describing the status of a single chamber port. This was to allow easy transfer from the loss model breakdown to the future simplified model.

Equations (8.1) to (8.4) are some useful fundamental hydraulic equations which were used extensively in these calculations, where Q_{ideal} is ideal flow from a hydraulic machine, ω is rotational speed, D is displacement, τ_{ideal} is ideal torque, Δp is differential pressure, P_{mech} is mechanical power and P_{fluid} is fluid power.

$$Q_{ideal} = \omega D \tag{8.1}$$

$$\tau_{ideal} = \frac{\Delta p D}{2\pi} \tag{8.2}$$

$$P_{mech} = \tau \omega \tag{8.3}$$

$$P_{fluid} = \Delta p Q \tag{8.4}$$

Table 8.3 and Table 8.4 provide information about each quantity in the loss breakdown analysis and give some indication of the confidence in each quantity by indicating its source. Some quantities were obtained by direct measurement and their final combined uncertainty is given according to the propagation method in [91]. In Table 8.3 the values given in the nodes marked as 'transfer' are estimated by addition of other loss model quantities. For example, the average power into the DDPM B gallery node is estimated by subtracting the leakage and flow losses incurred on ports connected to the DDPM gallery from the estimated fluid power delivered to this gallery. From examining these tables and reading the following description of the calculation of individual terms, the reader can see how all terms in the loss breakdown were obtained from the measurements in Table 8.1.

Table 8.3 *Table showing list of other node quantities included in loss breakdown, source of calculated value, quantities used in calculation and combined uncertainty for directly measured values.*

Quantity	Node type	Source			Measured quantities used in calculation	Derived quantities used in calculation	Combined uncertainty (direct measurement)
		Direct measurement	Validated model	Physics model			
PTO motor shaft power	Input	✓			PTO shaft speed, PTO shaft torque		±0.2%
PTO motor fluid power	Transfer			✓	Valve control signals, PTO shaft speed, chamber pressures	PTO motor flow	
Compression work	Transfer			✓	Valve control signals, PTO shaft speed, chamber pressures	PTO motor flow	
Accumulator transients	Transfer			✓	Valve control signals, PTO shaft speed, chamber pressures		
HP Accumulator	Transfer			✓	Valve control signals, PTO shaft speed, chamber pressures	PTO motor fluid power, motor leakage, flow losses, transient losses	

DDPM B Gallery	Transfer	✓	Valve control signals, PTO shaft speed, chamber pressures	PTO motor fluid power, motor leakage, flow losses, transient losses	
DDPM A fluid power	Transfer	✓	DDPM A speed, DDPM A pressure, DDPM A torque, LP gallery pressure		
DDPM B fluid power	Transfer	✓	DDPM B speed, DDPM B pressure, DDPM B torque, LP gallery pressure		
Generator shaft	Output	✓	DDPM A speed, DDPM B speed, DDPM A pressure, DDPM B pressure		±0.3%

Table 8.4 *Table showing list of losses included in loss breakdown, source of calculated value, quantities used in calculation and combined uncertainty for directly measured values.*

Quantity	Grouping	Source			Measured quantities used in calculation	Derived quantities used in calculation	Combined uncertainty (direct measurement)
		Direct measurement	Validated model	Physics model			
Motor Friction	Friction losses		✓		PTO shaft speed, chamber pressures		
Empirical friction			✓		PTO shaft speed, chamber pressures		
Reservoir transients	Transient losses			✓	Valve control signals, chamber pressures, LP gallery pressure		
Accumulator transient loss				✓	Valve control signals, chamber pressures, HP accumulator pressure		
Motor leakage			✓		Chamber pressures		
PTO motor internal flow loss	Flow losses			✓	PTO shaft speed	PTO motor flow	
Manifold block flow loss				✓	Valve control signals, PTO shaft speed	PTO motor flow	

Accumulator loss		✓	HP accumulator pressure, HP accumulator piston position		±0.7%
DDPM A loss		✓	DDPM A speed, DDPM A torque, DDPM A pressure		
DDPM B loss		✓	DDPM B speed, DDPM B torque, DDPM B pressure		

PTO Motor Mechanical Power Node

The measured PTO mechanical power is the product of the directly measured torque and speed on the PTO shaft as in Equation (8.3).

The compression power is calculated as the power exchanged between the PTO shaft and the pressurised chamber volumes when no flow is exiting the chamber because all the valves are closed. This is assumed to only occur in passive pumping mode when the passive check valves are still closed. This assumption is not entirely true as even in the cases with active valves there may still be momentary instances where these conditions are true, but this is small enough in active cases to be ignored. When this condition is met, the compression power is calculated as the product of ideal flow and chamber pressure (Equation (8.4)).

The motor friction calculation (shown in Figure 8.4) is carried out using lookup tables for the friction torque based on the manufacturer's data, which is described earlier. Similar lookup tables are used to obtain the empirical torque correction, described in Section 7.4.1. Multiplying these torques with the shaft speed gives an estimate of the lost power (Equation (8.3)).

8.2.1 Gallery Assignment

We wanted to estimate the flow of power to each of the HP, DDPM and LP galleries and the losses associated with each, to understand the energy flow at each node in the system. The flow losses were also different depending on what gallery the chambers were connected to and therefore which flow path was followed by the oil on leaving the chamber. Figure 8.5 shows a screenshot of the logic used to produce vectors of ones and zeroes indicating which ports were connected to which gallery.

The opening of the directional valves was used as the criterium to assign the port as being connected to DDPM B. HP cases (which weren't passive) were identified as those for which the control settings are either in quantised or HP override mode, and the pressure of the chamber is over 97% of the HP accumulator pressure. Passive HP cases were identified using the same threshold pressure and some logic to confirm that these chambers were under passive control. LP cases were identified similarly, with the threshold being that the chamber pressure must be less than 1.5 times the LP accumulator pressure.

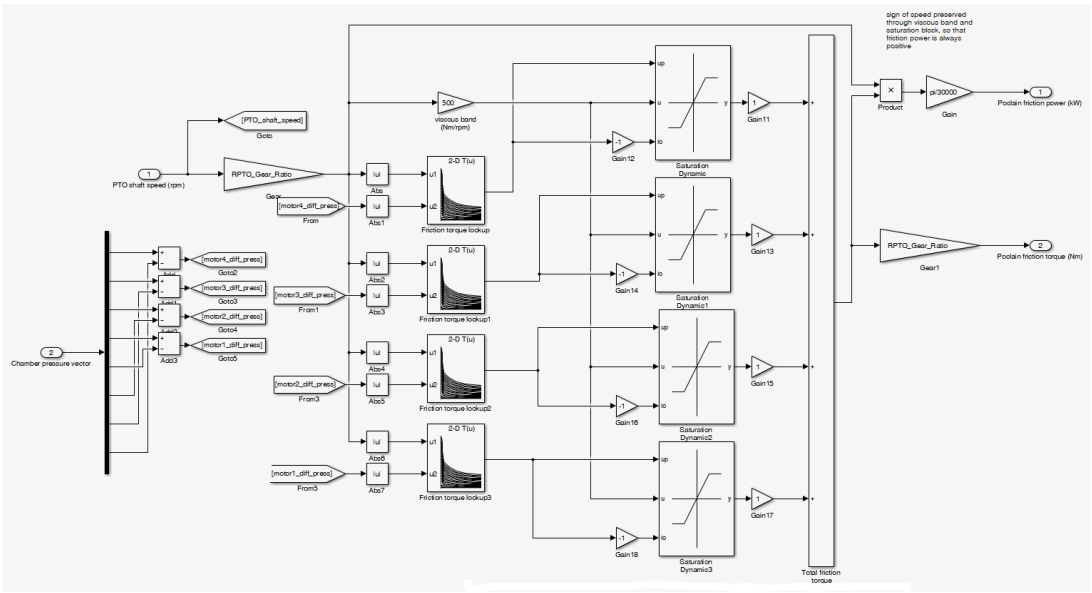

Figure 8.4 *Screenshot of lookup tables to calculate motor friction torque and power lost to friction*

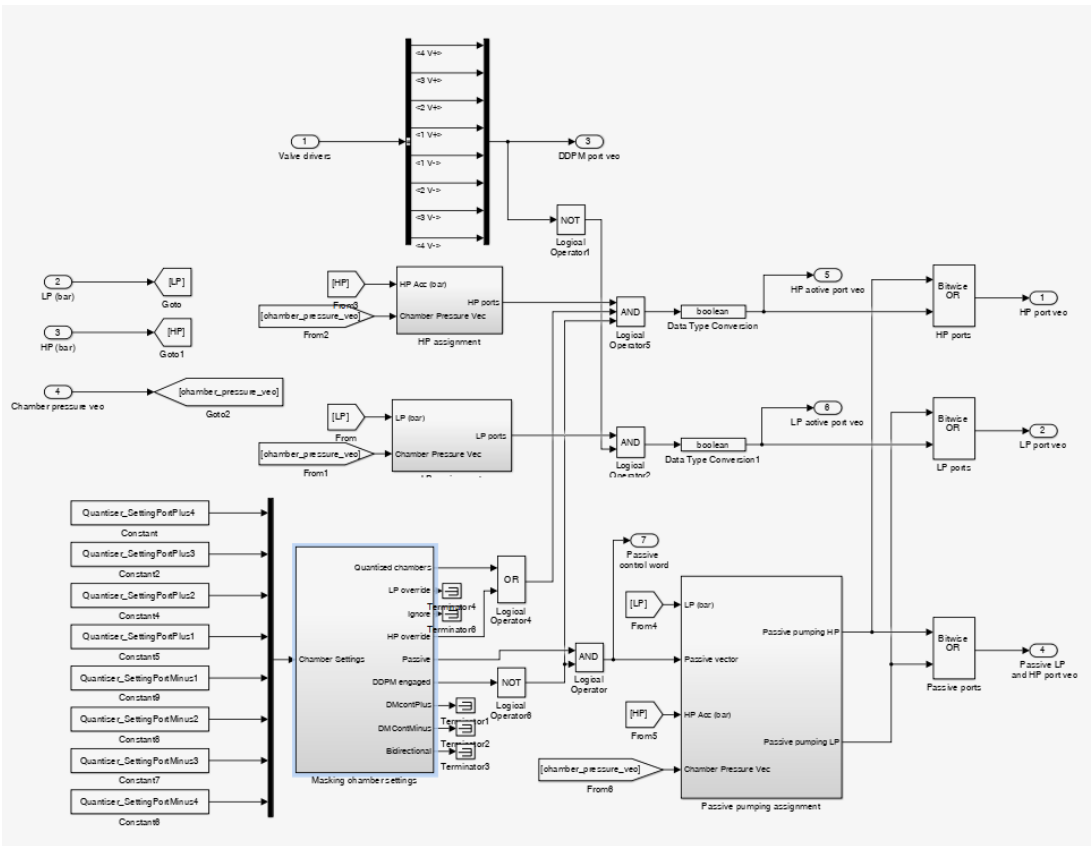

Figure 8.5 *Screenshot of Simulink logic used for gallery assignment in loss breakdown calculations*

8.2.2 PTO Motor Fluid Power Node

The geometric flow of the fixed-displacement PTO motors is defined simply as the product of speed and displacement, as shown in Figure 8.6a. Multiplying the vector of chamber geometric flow by the vector of chamber pressures gives a vector of 'geometric hydraulic power' and taking the sum of the elements of this vector gives a total geometric hydraulic power. The chamber pressure vector refers to the measured chamber pressure at the manifold ports plus the modelled PTO motor and hose pressure drop, obtain a better estimate of the pressure at the PTO motor outlets. Figure 8.6b shows how this was then split out into the different gallery hydraulic powers using the gallery assignment vectors. Lookups for the pressure drops across the passive check valves (based on valve data from Sun hydraulics), directional valves and quantised valves were also used to calculate flow losses within the manifold block according to the flow path taken from a particular chamber. The PTO motor leakage was subtracted from the geometric flow before the pressure drop was extracted from the lookup table, as shown in Figure 8.7.

8.2.3 Transients

The use of the quantising system introduced transient losses: the accumulator transients, the reservoir transients and the accumulator transient losses. These terms are all due to the rapid pressurisation or depressurisation of the fluid in the chambers during the quantised transitions. When a quantised chamber is pressurised or depressurised, the relevant valve is opened to connect the chamber to the HP accumulator or LP system. Work is then done on (or by) the fluid in the chamber to equalise the pressure. The volume (ΔV) taken from the accumulator to achieve this is

$$\Delta V = \frac{V_{cham}}{B}\Delta p \tag{8.5}$$

Where V_{cham} is the chamber volume, B is the bulk modulus of oil and Δp is the change in pressure. Using the following equation for work W

$$W = -\int pdV \tag{8.6}$$

and substituting in the following expression from Equation (8.5)

$$dV = \frac{V_{cham}}{B}dp$$

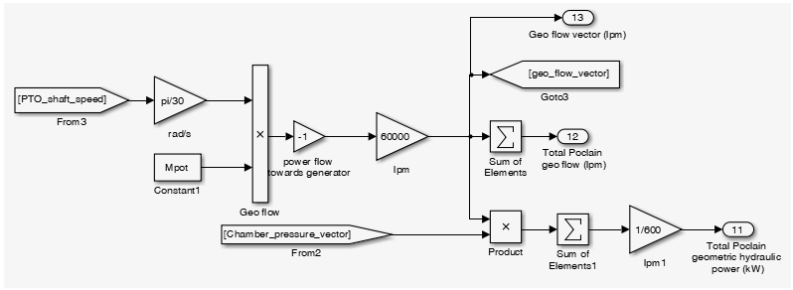

(a) *Calculation of the geometric hydraulic flow and power. 'Mpot' is a vector of the displacements for all eight motor ports multiplied by the PTO gear ratio.*

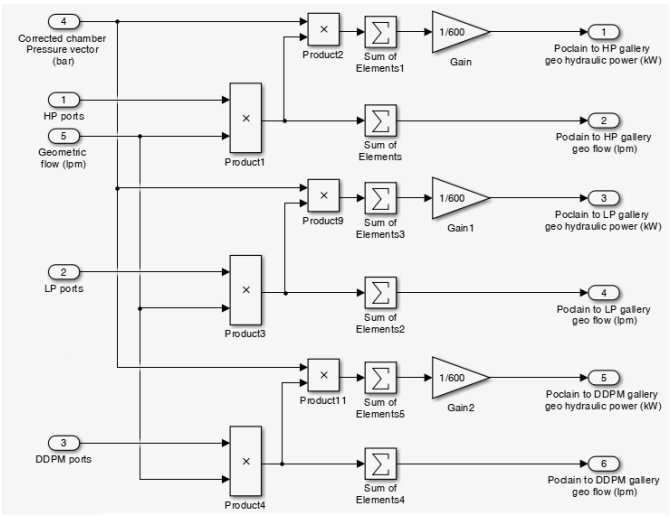

(b) *Calculation of the geometric hydraulic flow and power (total and per gallery)*

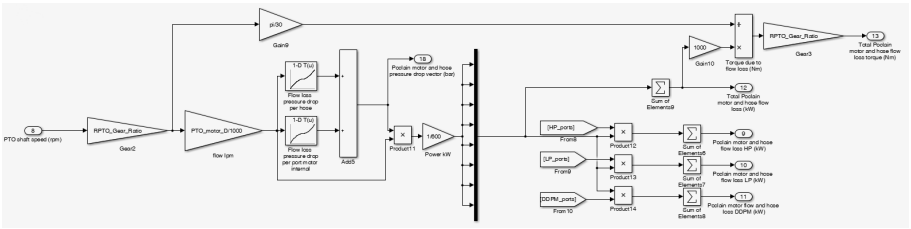

(c) *Calculation of the chamber flow loss (total and per gallery)*

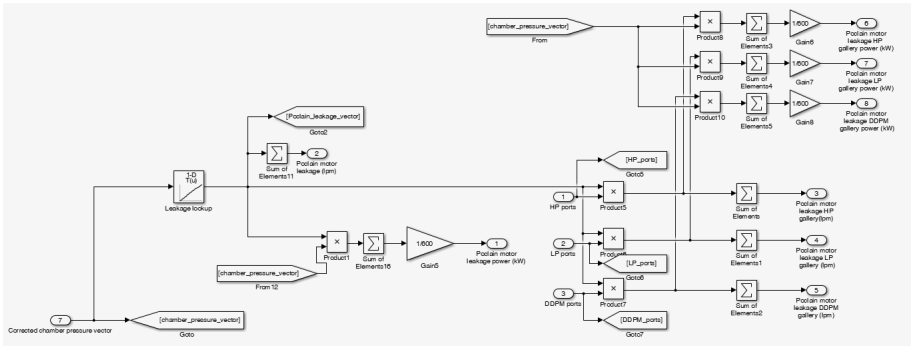

(d) *Calculation of the leakage (total and per gallery)*

Figure 8.6 *Screenshots of various Simulink loss breakdown calculations for PTO motor fluid node*

one obtains the expression given in Equation (8.7) for the energy transferred during accumulator or reservoir transient events (using the simplifying assumption that B is independent of pressure).

$$W = -\frac{1}{2}\left(\frac{V}{B}\right)\Delta p^2 \tag{8.7}$$

This expression is used to calculate the reservoir transients and the accumulator transient terms, using estimated chamber compliance for $(\frac{V}{B})$, which is based on the compliance value from the DDPM B feedforward pressure change control term. This compliance value had been tested on the rig and matched the observed behaviour well. This value was then revised downwards because it comprises the combined volume of a chamber and the DDPM B gallery, whereas for the transient calculations only the chamber volume was required. A value which gave good agreement to the test data was chosen.

Whilst depressurising a quantised chamber to tank is always a loss, there is also a loss associated with the pressurisation of a chamber by the accumulator, as this will not be a perfectly reversible process, due to the dissipation of energy by pressure drops on the path between the accumulator and the chamber. To factor in this dissipation, an efficiency term $\eta_{AccTrans}$ was defined. If the process was perfectly reversible this would be equal to 1, and if the process was completely irreversible it would be equal to 0. Therefore the accumulator transient loss term was given by

$$Loss_{AccTrans} = \frac{1}{2}\left(1 - \eta_{AccTrans}\right)\frac{V_{cham}}{B}\Delta p^2 \tag{8.8}$$

with $\eta_{AccTrans}$ assumed to be 0.05, as we expected the process to be largely dissipative. In the Sankey, diagrams the 'Accumulator transients' term is shown as negative, because we have defined positive power flow as being towards the generator, and this term moves power back towards the chambers.

The number of accumulator or reservoir transient events was counted by looking at the valve control signals and the energy transferred or lost from Equation (8.7) and Equation (8.8) was added up for the total number of events.

8.2.4 High Pressure Accumulator

To calculate the accumulator losses the area between the compression and expansion curves of the accumulator's pressure-volume (PV) diagram must be calculated over all the compression and expansion cycles of the test. This was carried out using Equation (8.6), and partitioning the work done into compression and expansion cycles based on the flow into the accumulator (derived from the piston position). Positive flow into the accumulator

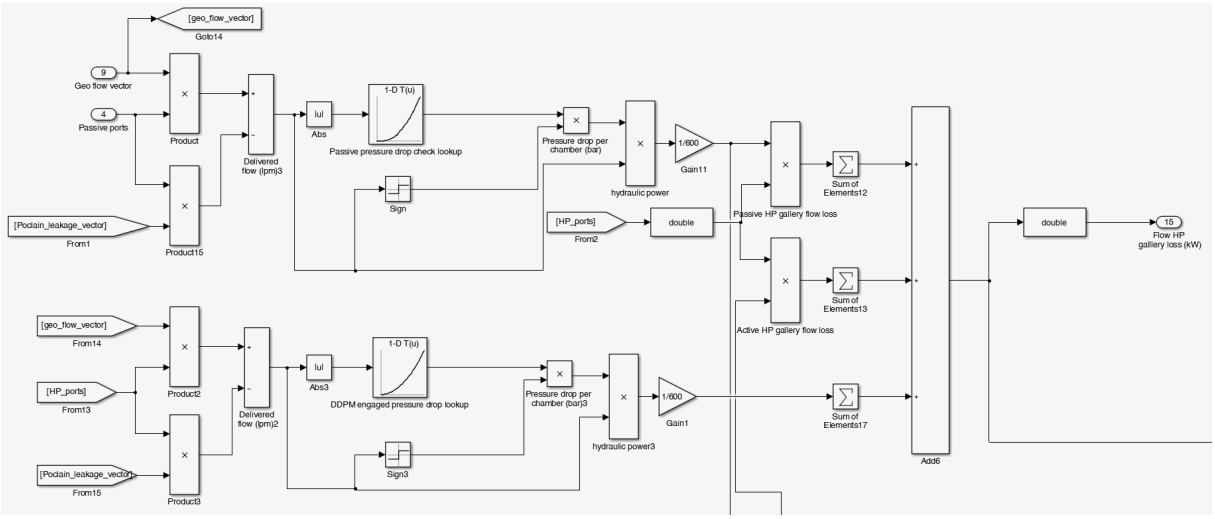

Figure 8.7 *Screenshot of Simulink calculation for passive check and DDPM engaged valve flow losses. A similar approach was taken for the main flow valves and directional valves.*

Figure 8.8 *Screenshot of Simulink calculation for feature X energy exchanges (redacted).*

meant compression was taking place and flow out of the accumulator meant expansion was happening. These difference between the energy into and out of the accumulator was then calculated to obtain the loss.

Equation (8.9) shows the expression for an ideal gas undergoing a polytropic process, where p_0 is initial pressure and V_0 is initial volume [92]. In a process of charging or discharging a vessel $1 < n < 1.4$, which is between the typical values taken for an adiabatic or isothermal process [93]. Substituting this into Equation (8.6) yields the expression Equation (8.10), where V_1 is the final gas volume. This was used to calculate the difference in the energy of the accumulator gas between the start and end of the test (the residual energy) [94]. In most cases, this was very small as an effort was made to ensure that the accumulator started and ended at the same pressure, but in the irregular cases, it became more significant.

$$P = p_0 \left(\frac{V_0}{V}\right)^n \tag{8.9}$$

$$\begin{aligned} W &= -\int p dV \\ &= -\int_{V_0}^{V_1} p_0 \left(\frac{V_0}{V}\right)^n dV \\ &= -p_0 V_0 \int_{V_0}^{V_1} \left(\frac{1}{V}\right)^n dV \\ &= \frac{P_0 V_0^n}{1-n} \left(V_1^{1-n} - V_0^{1-n}\right) \qquad \text{for } n \neq 1 \end{aligned} \tag{8.10}$$

Whilst [94] points out that accumulators are not typically simulated well by using only ideal gas laws, [93] shows that applying Equation (8.9) with an appropriate value of n can replicate the pressurisation and depressurisation curves well given known start and end values of pressure and volume. This is the situation in which we find ourselves with the accumulator test data. n was chosen to be 1.2, to avoid assuming either a purely adiabatic or isothermal process. Also according to [95], the best value of n may differ depending on whether the vessel is charging or discharging. Ideally, specific measurements could be carried out on the accumulator to produce a validated model in accordance with the Benedict-Webb-Rubin equation [94], but this was felt to be a lower priority task than validating other parts of the Quantor model.

8.2.5 DDPM Models

The forwards DDPM models have the inputs of speed, pressure and Fd, and output torque and flow. The backwards DDPM models have inputs of speed, pressure and demand torque, and loop iteratively to obtain an output torque within a user-defined margin of error of the demand torque. They also output the required Fd to achieve this torque and the corresponding flow. Both the forwards and backwards models used the validated parameters described in Section 7.7. This was done to give a cross-check of the estimation of the losses. Generally, it was found that the torque from the backwards model matched the measured torque more closely than the forwards model did (although the forwards model had already been checked to be within 2.5%). Therefore, when doing loss breakdown analysis, the losses predicted by the backwards model were taken as the trusted value for normalisation as described in Table 8.2.

The DDPM models used for loss breakdown include leakage, compressibility, timing effects and friction. These models did not include factors such as pulsation and control delays, as this level of detail was not necessary for loss breakdown analysis.

8.3 Loss Breakdown Examples from Test Data

8.3.1 Steady Speed

The steady speed case is a very simple validation case, where the flywheel shaft is spun at a constant speed in one direction. This results in the PTO motors pumping through the passive check valves into the HP accumulator. DDPM A controls the pressure in the accumulator to a given value, which in this case means it motors from the accumulator delivering power into the generator. As described earlier in the section about normalisation, the idle losses of DDPM B have been subtracted from the output power to represent a purely quantised system.

In this case, the only losses are the friction and leakage of the PTO motors, flow losses through the PTO motors, hoses and manifold blocks, accumulator losses and the DDPM A losses. Note that this Sankey represents mechanical shaft-to-shaft power and not output electrical power from the generator, which was not directly measured on the test rig. There are no transient flows for pressurising or depressurising the quantised chambers and neither are there losses due to feature X, so it is relatively simple to model and a useful check of the simpler loss model components.

Figure 8.9 shows Sankey diagrams for two different steady speed cases, both with an average input shaft power of approximately 29 kW, so they are two comparable examples. Figure 8.9a is for 200 bar and 900 rpm on the electric motor shaft, whilst Figure 8.9b is for 300 bar and 600 rpm on the electric motor shaft. This means that these Sankeys can be used to compare the effect of different pressure and flow regimes on system losses.

For example, the higher pressure case results in higher friction losses and higher motor leakage as the oil is forced out into the case. However the flow losses are higher for the low pressure/high speed case as the flow rate of oil from the hydraulic motors is higher, resulting in greater pressure drops through the valves (which are identical in each case). It is clear that for these cases the friction losses dominate, followed by the DDPM losses.

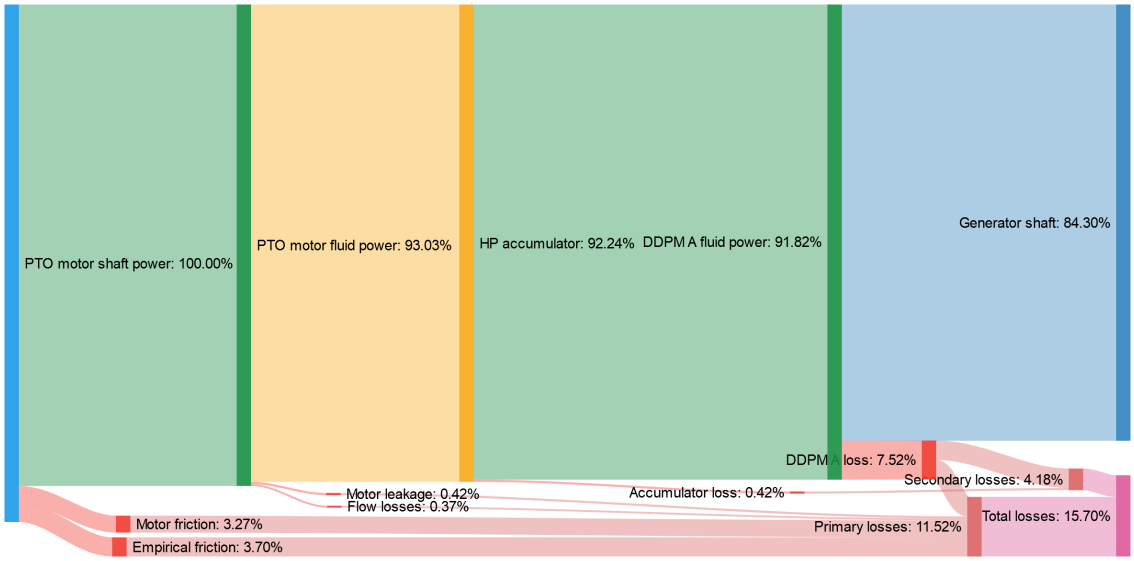

(a) *Efficiencies and losses, from measured data for a flywheel speed of just under* 52 rpm *and an accumulator pressure of* 200 bar*, with losses normalised and accumulator residual distributed 'downstream' with an input shaft power of* 28.9 kW

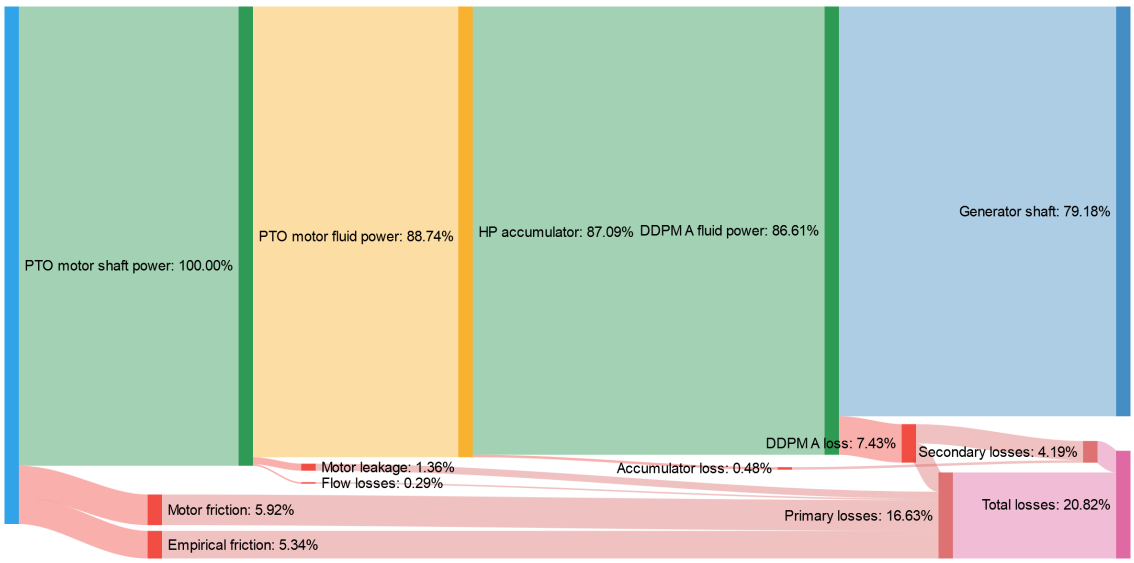

(b) *Sankey diagram showing steady speed case for* 34 rpm *on electric motor shaft and* 300 bar *accumulator pressure, with losses normalised and accumulator residual distributed 'downstream'. (Input shaft power is* 29.4 kW*)*

Figure 8.9 *Comparison of Sankey diagrams for steady speed cases at different speeds and pressures, but similar input shaft powers*

8.3.2 Passive Pumping (Regular Waves)

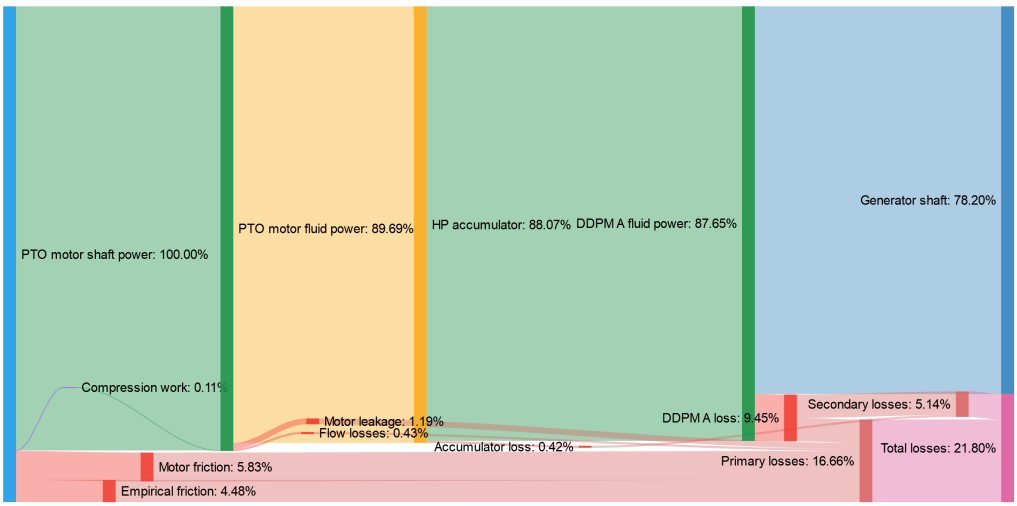

Figure 8.10 *Sankey diagram of a passive pumping case (average input shaft power* 17.3 kW*)*

Unless otherwise stated, the regular wave cases have a wave period of 10 s, with the input power being adjusted by changing the amplitude of the speed sine wave, and are pure damping cases with the damping value at WEC scale being 65 kN s/m.

The passive pumping case is similar to the steady speed case apart from the reversals in speed (and flow) caused by the sinusoidal motion of the flywheel shaft. The flow goes from the PTO motors to the accumulator via the passive check valves, where DDPM A motors to control the pressure. The only new term is the 'compression work term', which is the energy required to compress the fluid in the chamber to the cracking pressure of the passive check valves, which must happen with every change of direction of the shaft in this case. However, this energy is recovered, as it is either a transfer of energy from the shaft to the fluid during compression or vice versa during decompression.

8.3.3 Quantised (Regular Waves)

For these tests, all chambers were in quantised mode, so that there was no continuous control. This means that rather than the passive check valves opening from the chamber to the accumulator, the active quantised valves are being opened and closed to provide a quantised approximation of the demanded PTO torque. This changes the flow losses, as different valves are now being used, and introduces the transient terms to the Sankey.

Figure 8.11 shows Sankey diagrams for pure quantised cases. Figure 8.11a has an accumulator pressure of 200 bar at a low average input power of 8.1 kW. Figure 8.11b is

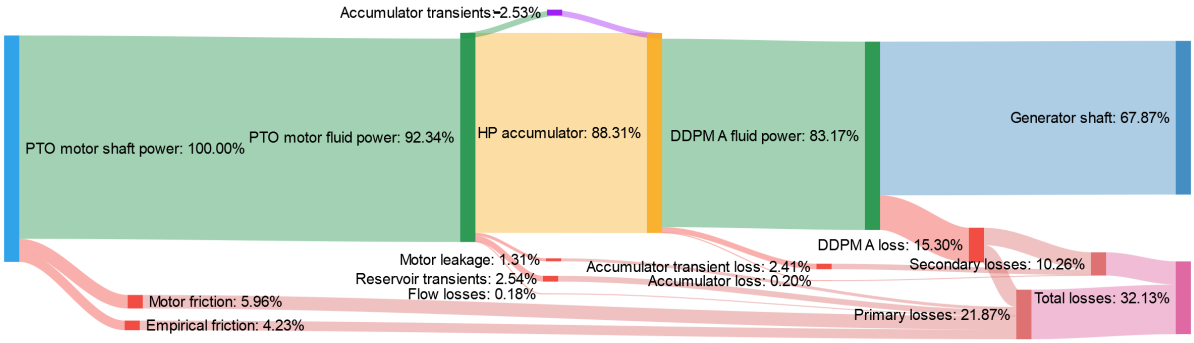

(a) *Sankey for a quantised case at* 200 bar *with an average input power of* 8.1 kW

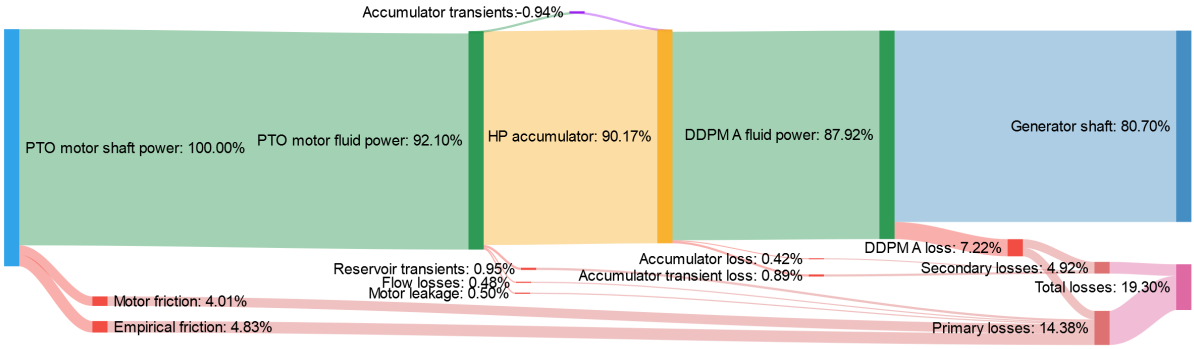

(b) *Measured results of a quantised* 200 bar *case with an average input power of* 29.7 kW

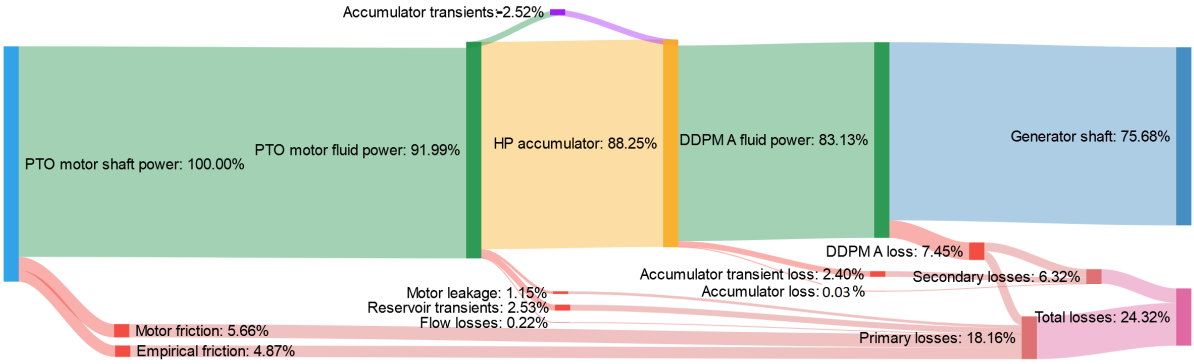

(c) *Quantised* 300 bar *case with an average input shaft power of* 27.9 kW

Figure 8.11 *Comparison of Sankey diagrams for quantised cases at different pressures and input power levels*

for an accumulator pressure of 200 bar and an input shaft power of 29.7 kW. Because the input power was so low for Figure 8.11a, DDPM A is operating at a relatively inefficient point, which means it contributes a much higher proportion of the system losses than in Figure 8.11b. Figure 8.11c is for an accumulator pressure of 300 bar at 27.9 kW. The increase in pressure has a similar effect to the steady speed cases, in that the friction and leakage go up. Since the transient losses are all proportional to ΔP^2, an increase in pressure substantially affects these, as well as the power transferred by the accumulator transients term. Whilst the efficiency is slightly lower at higher pressure (still over 75% shaft to shaft), the possible applied PTO torque is higher. This would prove useful in heavy seas where more force is needed to control the response of the WEC and the more mechanical power is captured from the waves, so the power delivered to the grid would still be relatively high.

8.3.4 Quantor Mode 4 (Regular Waves)

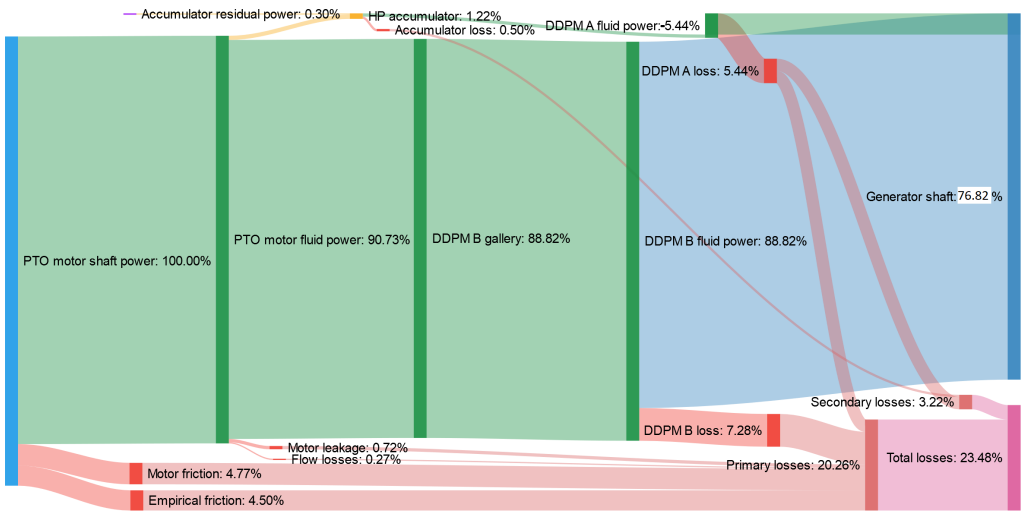

Figure 8.12 *Sankey for test data Quantor mode 4 at accumulator pressure of* 250 bar *with input power of* 31.2 kW*, with losses normalised.)*

Quantor mode 4 refers to the case where DDPM B is exerting continuous control over all 4 chambers (which would be used in low energy sea states to keep the displacement of the DDPM as high as possible so that the efficiency is maintained). The interaction between DDPMs A and B here is interesting as DDPM A must transform between DDPM B and the accumulator to output energy. However this is a very reactive process so whilst all the energy is in some sense passed through DDPM A, it appears very little in the steady state Sankey diagram in Figure 8.12.

8.3.5 Quantor Mode 1 (Regular Waves)

Quantor mode 1 refers to the case where one PTO motor is under the control of the continuous service and the other three are under the control of the quantised service. There are two control options for this scenario: 'slug' or 'slug and X', both of which are for providing the flow to the continuous service required to counteract a quantised transition. 'Slug' control refers to an intermittent spurt of extra flow (either pumping or motoring) from the DDPM supplied to coincide with a quantised transition. The problem is that the DDPM may not be able to supply adequate 'slug' flow in systems with larger PTO motors or chamber volumes (in the laboratory system the PTO motors are relatively undersized compared to the DDPMs).

Figure 8.13a and Figure 8.13b show Quantor mode 1 cases at 200 bar using 'slug only' control. In the quantised case the energy was all delivered to the generator via the accumulator and DDPM A and in the Quantor mode 4 case, all the energy passes from the chambers through DDPM B, where it is exported by DDPM A exchanging energy with the accumulator. However, in the Quantor mode 1 case, energy is delivered from the PTO chambers through both galleries and DDPMs to the generator. DDPM A handles a larger proportion of the power because more chambers are under quantised control than continuous control, but the overdrive (higher chamber pressure) capability of the DDPM B side means that there is not a simple 3:1 power split between DDPM A and DDPM B respectively. The challenging pressure and flow variations on the continuous service mean that DDPM B operates with lower efficiency than DDPM A (82.3% on average compared to 90.2%). This means that there is a compromise between having the control benefit of continuous PTO torque and the efficiency reduction caused by delivering a large proportion of the power through the continuous service. Ideally, even in the cases with continuous control, as large a proportion as possible of the power should be delivered through the quantised service. Comparing Figure 8.13a and Figure 8.13b shows the sensitivity of DDPM efficiency to operating at a very low input power.

Figure 8.13c shows the Sankey diagram for a similar case at 300 bar. As observed before in other cases, many of the primary losses are higher due to the increase in pressure. In this case, DDPM B receives less fluid power as a result, so its efficiency drops to 78.9% (DDPM A is less affected at 89.5%). The implication of this is that the choice of PTO actuators is critical in determining not just the primary efficiency of the Quantor PTO but also the secondary efficiency as it dictates the operating point of the DDPMs. Figure 8.13d shows the Sankey for Quantor mode 1 at 300 bar, with the addition of feature X. This makes the diagram more complex as it introduces another interaction between the galleries and

more loss terms. It is noticeable that the addition of feature X has a significant impact on efficiency, reducing it from 71.23% to 67.04%.

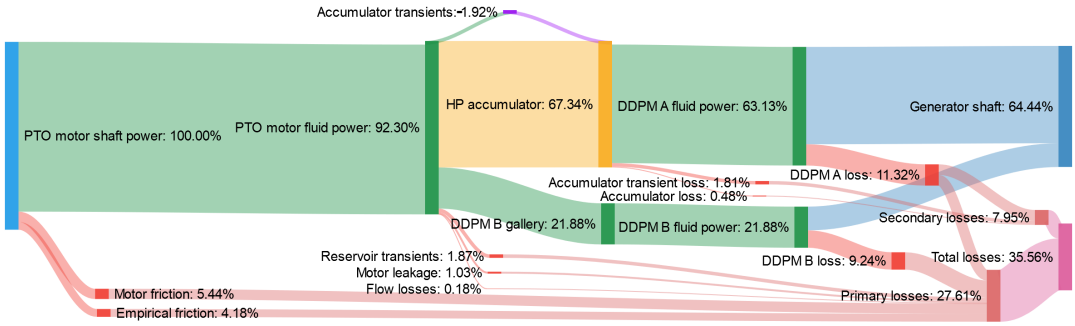

(a) *Sankey for Quantor mode 1 at accumulator pressure of* 200 bar *with 'slug only' control (input shaft power of* 11.3 kW*)*

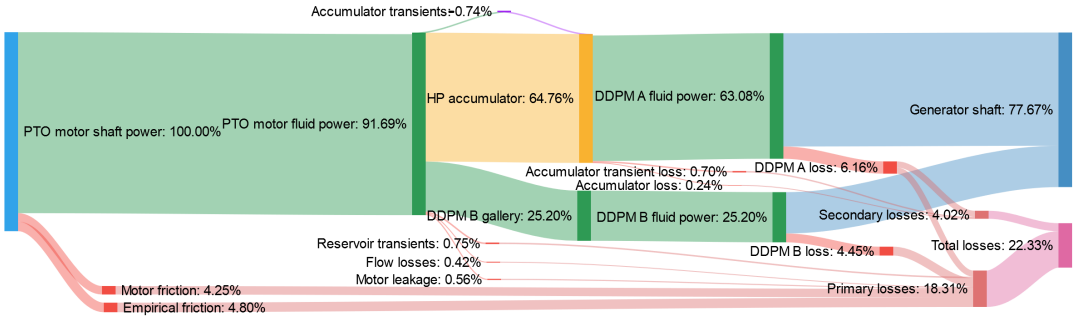

(b) *Sankey for Quantor mode 1 at accumulator pressure of* 200 bar*, with 'slug only' control (input shaft power of* 29 kW*).*

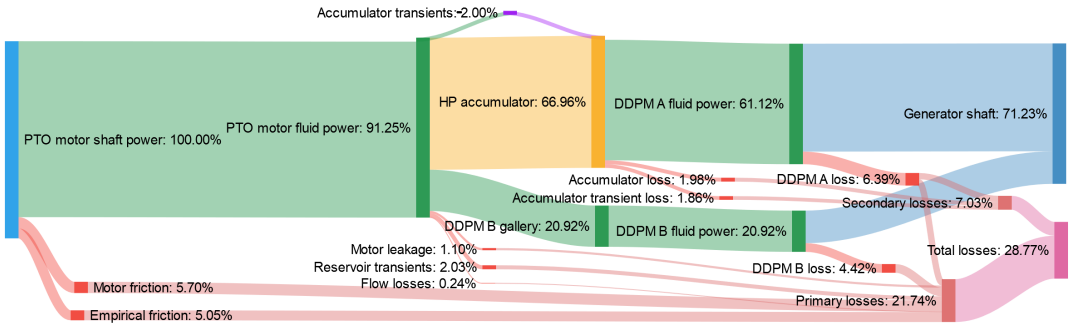

(c) *Sankey for the test case of Quantor mode 1 at* 300 bar*, with 'slug only' control (input shaft power of* 27.8 kW*)*

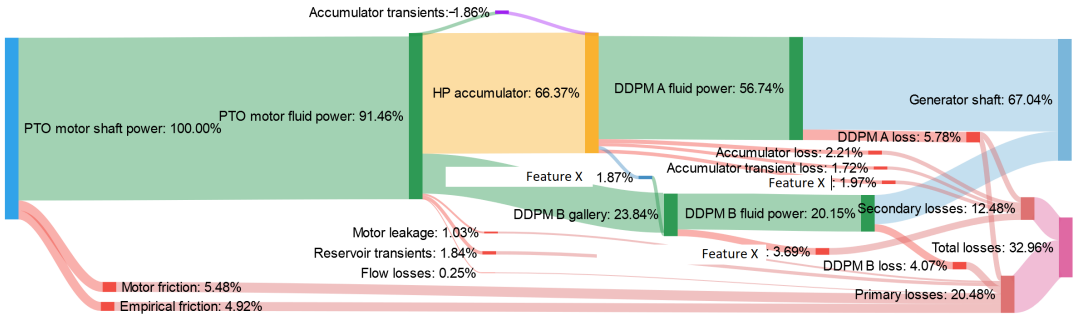

(d) *Sankey for Quantor mode 1 test case at* 300 bar *with 'slug and X' control (input shaft power of* 30.2 kW*)*

Figure 8.13 *Comparison of Sankey diagrams for Quantor mode 1 at different pressures and input power levels, with 'slug only' and 'slug and X' control cases*

8.3.6 Irregular Waves

In the irregular cases, the accumulator residual was not distributed out, as it is more substantial than in other cases and the accumulator's role in smoothing the power output is much more critical in these scenarios. Figure 8.14 shows Sankey diagrams for test cases of irregular seas, in pure quantised control, Quantor mode 4 and Quantor mode 1. In all these cases the friction losses are relatively high, which is likely to be due to the high number of zero-crossings and relatively low average PTO motor speed in the many short waves in these cases. The accumulator losses are also higher, because of the much more variable charging and discharging rate than in the regular cases. Interestingly Quantor mode 4 is the most efficient case in irregular seas at this power level as shown in Figure 8.15. The motor leakage is much lower than in the cases with full or partial quantisation because the motors can be at lower intermediate pressures under the control of DDPM B. In a quantising scenario, they jump between LP and HP accumulator pressures. Since leakage rate is solely dependent on pressure according to the data from Poclain, it is no surprise that the low average power cases involving quantised chambers suffer greatly from leakage losses. This similarly applies to the friction terms, which are also dependent on pressure (although they are affected by other variables as well, unlike the leakage). This means that the primary losses are much lower in the Quantor mode 4 case, resulting in the greatest efficiency in these low power irregular seas.

The Quantor mode 1 case is the least efficient, as all the losses introduced by the more complex control terms are present, such as transient losses and feature X losses, and the losses of both DDPMs must be included (only the DDPM A loss is included in the quantised case). For such low average input powers, this would be a poor operating mode to select.

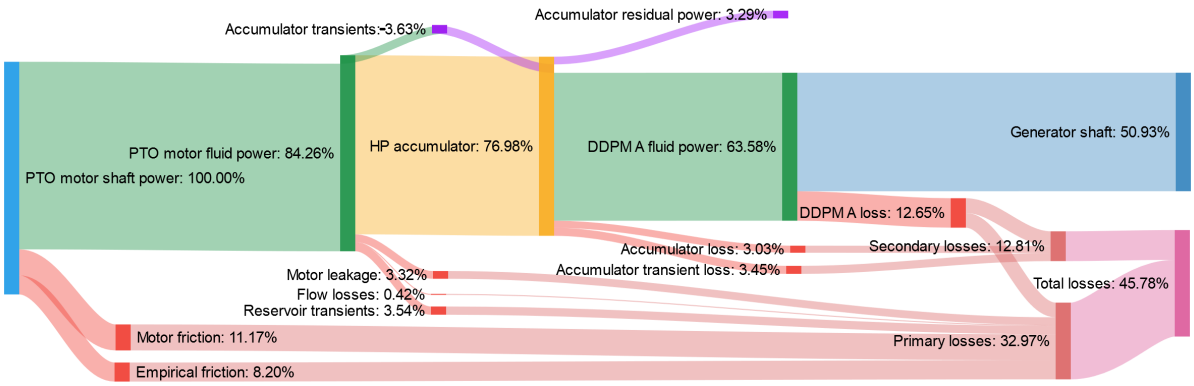

(a) *Sankey diagram for an irregular sea case in quantised control only (average shaft input power* 9.6 kW*)*

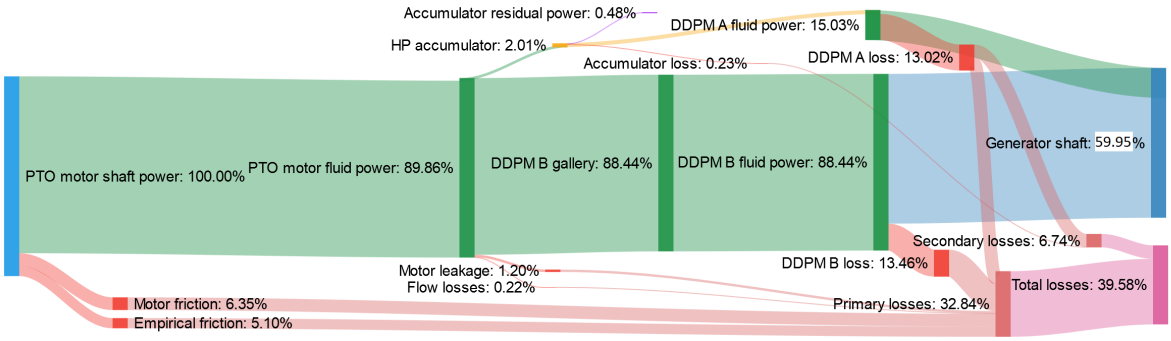

(b) *Sankey diagram for an irregular sea case in Quantor mode 4 (average shaft input power of* 10 kW*).*

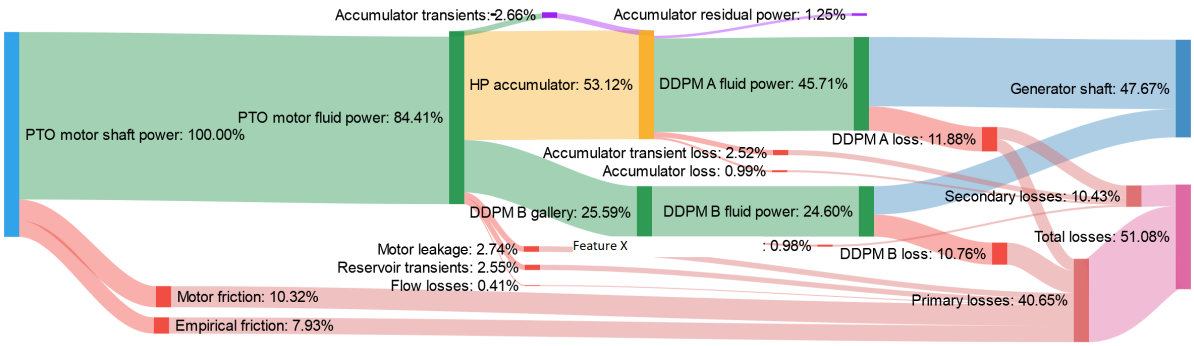

(c) *Sankey of an irregular case in Quantor mode 1 with slug and X (average shaft input power of* 9.9 kW*).*

Figure 8.14 *Sankey diagrams for irregular test cases in different control modes.*

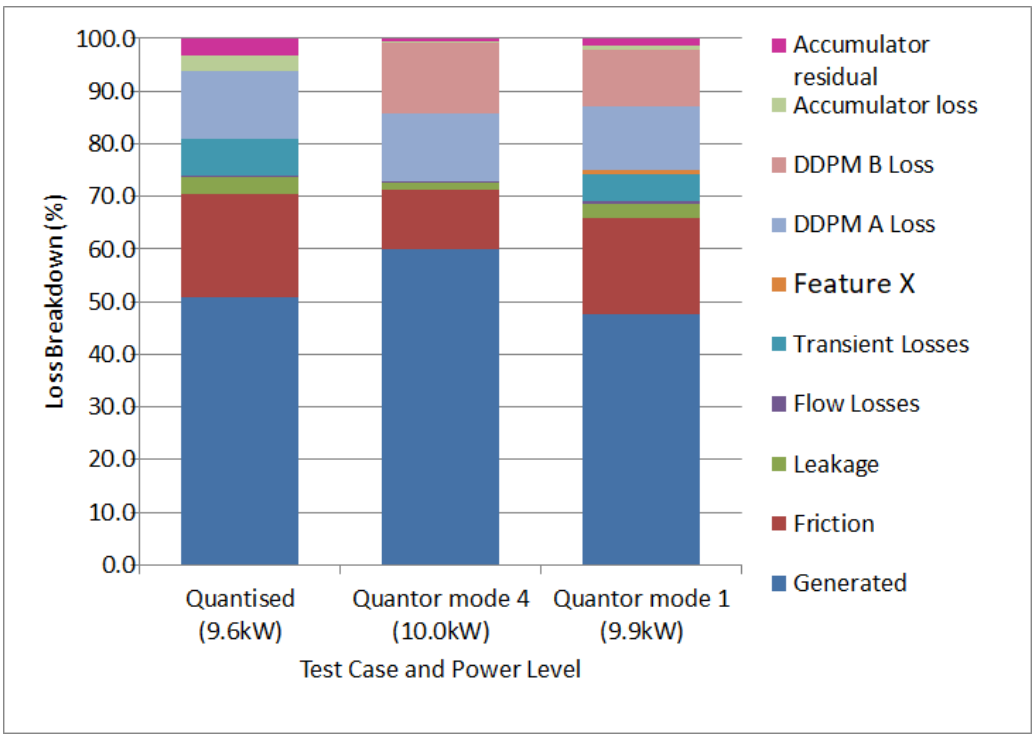

Figure 8.15 *Normalised loss breakdown for irregular waves in three different control modes*

8.3.7 Comparison Between Cases

Figure 8.16 shows the normalised loss breakdown across the tested power range for quantised cases at 200 and 300 bar. The efficiency of the 300 bar case drops at higher powers because the accumulator had supplied some energy into the system. Normalising this out meant that the efficiency then decreased. The biggest change between these two cases is the increase in friction and transient losses at higher pressure.

Figure 8.17a shows the equivalent figure for the very different case of Quantor mode 4. Friction is still a major loss in this case but the leakage is greatly reduced. Also, there are no transient losses, but having the losses of both DDPMs is a significant impact.

Figure 8.17b shows the normalised loss breakdown for Quantor mode 1 with both slug and X control. This introduces the feature X losses, and has the losses of both DDPM machines and the transient losses of the quantising system. Hence over the power range shown this control mode is less efficient. However, as demonstrated for the simple model cases, the test rig is not sized ideally for the Quantor, both in the sense of the WEC emulator is not able to reach the average powers that the existing lab system could potentially absorb, and the four Poclain motors are relatively undersized compared to the DDPMs. So, whilst these results appear relatively poor, the validated simple model

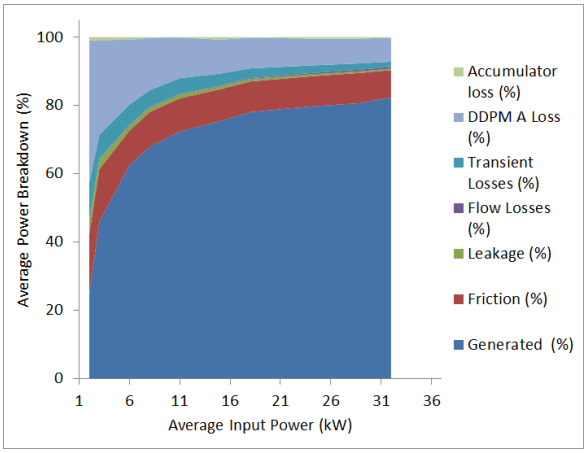

(a) *Normalised loss breakdown across the range of input shaft power for the pure quantised* 200 bar *case, with the accumulator residual redistributed.*

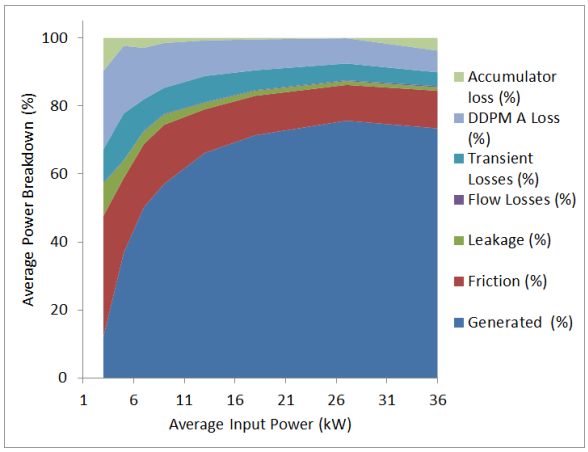

(b) *Normalised loss breakdown across the range of input shaft power for the pure quantised* 300 bar *case, with the accumulator residual redistributed.*

Figure 8.16 *Quantised loss breakdown across the power range.*

shows that with the correct sizing of the components within Quantor and better matching of the power regime, the efficiency in this control mode is much higher.

Figure 8.18a shows the percentage breakdown of generated power and losses, with the accumulator residual energy included. Table 8.5 supplies the details of the 14 test cases. If this is negative it means that the energy in the accumulator has decreased during the test and it has been supplied into the system, hence the total energy is more than 100% of the input shaft power. Figure 8.18b shows the losses in kilowatts to make the details clearer. As one would expect, the more control features added, the higher the losses are as more components and processes are added with their own associated losses. For steady speed, quantised and Quantor mode 1 cases, it can be seen that operating at a higher pressure increases the losses; particularly friction, leakage and transient losses. The introduction of feature X introduces significant extra losses, but has a great benefit for the smoothness of the output torque.

The 5s period case is less efficient, because the shorter period means that quantised transition events occur more frequently, and hence the losses associated with these processes increase. Interestingly the reactive power case (Test 14) at the right-hand side shows almost the same loss breakdown as its non-reactive equivalent (Test 11). The pure damping case has a measured efficiency of 72.9% and the reactive case has an efficiency of 68.8% (without redistributing the accumulator residual). The friction loss is slightly higher and so are the DDPM B losses, but this shows that reversing the flow of power through the system does not change the behaviour of the Quantor; it simply increases the losses as the energy must go through the same components twice.

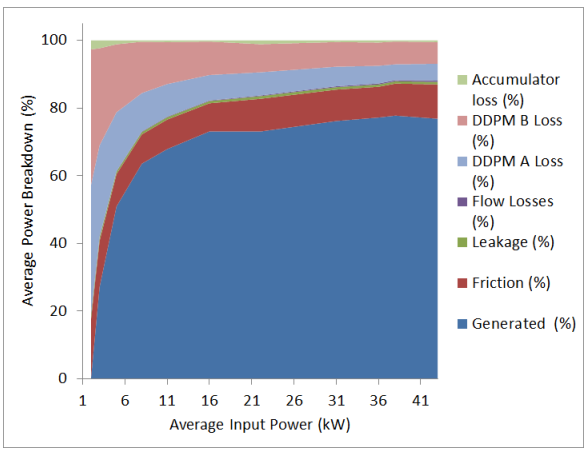

(a) *Normalised loss breakdown across the input shaft power range for Quantor mode 4,* 250 bar *with slug and X control, with the accumulator residual redistributed.*

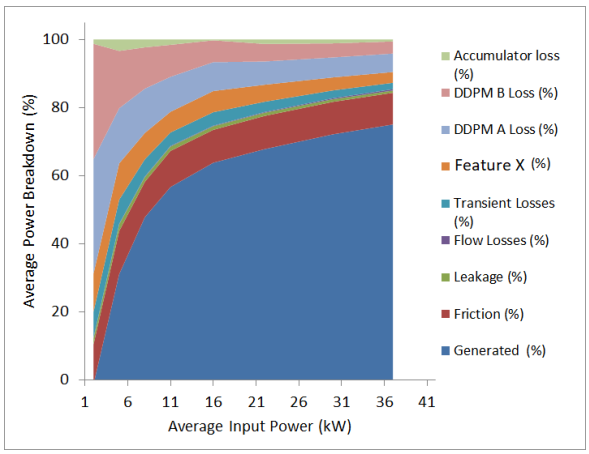

(b) *Normalised loss breakdown across the input shaft power range for Quantor mode 1,* 250 bar *with slug and X control, with the accumulator residual redistributed.*

Figure 8.17 *Quantor mode 4 and mode 1 loss breakdown across the power range.*

Table 8.5 *Description of test cases corresponding to results shown in Figure 8.18*

Test Case	Description	Slug	X	Wave period (s)	Damping kNs/m	Spring kN/m	Average Input Shaft Power (kW)
1	Steady Speed 200 bar			n/a	n/a	n/a	29
2	Steady Speed 250 bar			n/a	n/a	n/a	24
3	Steady Speed 300 bar			n/a	n/a	n/a	29
4	Quantised 200 bar (trans only)			10	65	0	30
5	Quantised 200 bar			10	65	0	30
6	Quantised 300 bar			10	65	0	28
7	Quantor Mode 4 250 bar			10	65	0	32
8	Quantor Mode 1 200 bar	✓		10	65	0	29
9	Quantor Mode 1 300 bar	✓		10	65	0	28
10	Quantor Mode 1 300 bar	✓	✓	10	65	0	30
11	Quantor Mode 1 250 bar	✓	✓	10	65	0	31
12	Quantor Mode 1 250 bar	✓	✓	5	130	0	29
13	Quantor Mode 1 250 bar	✓	✓	10	130	0	33
14	Quantor Mode 1 250 bar	✓	✓	10	65	-40	29

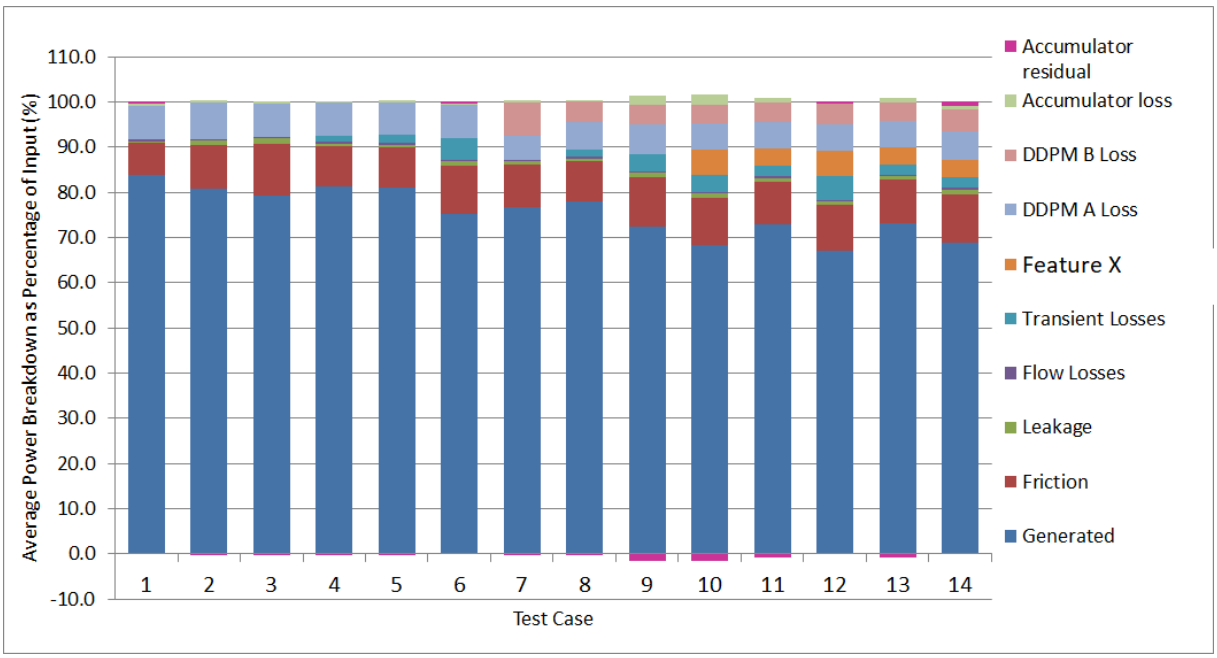

(a) *Normalised loss breakdown with measured accumulator residual included for a range of test cases of similar power levels.*

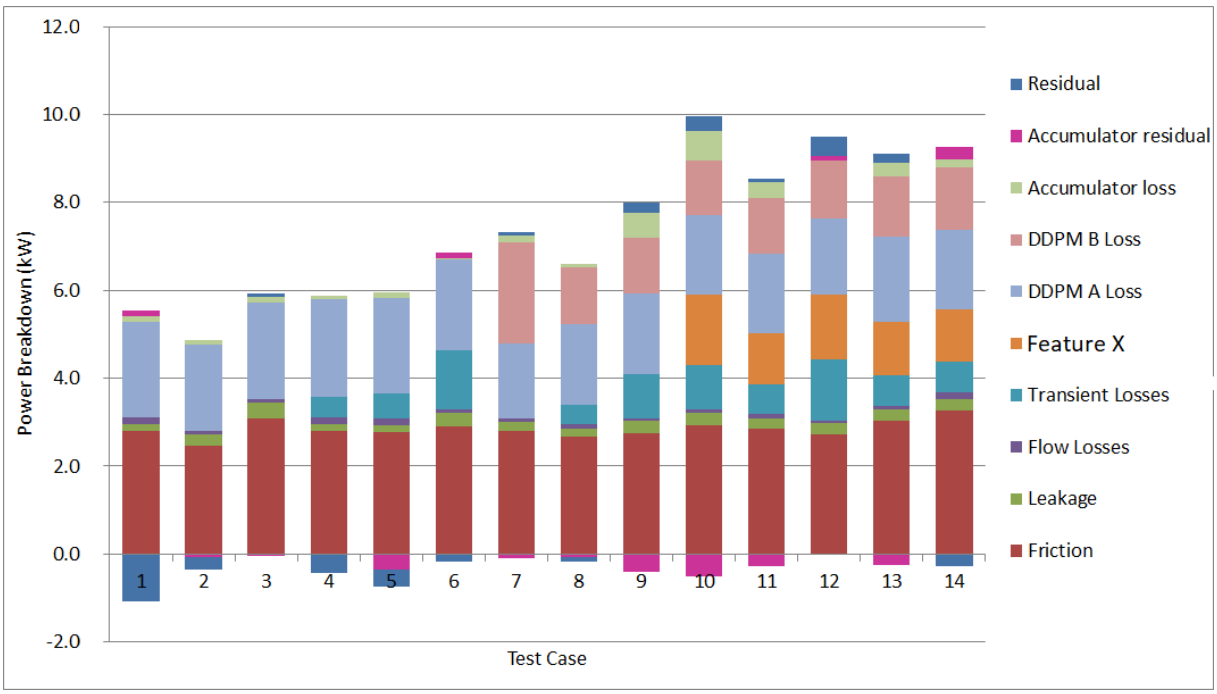

(b) *Loss breakdown in kW with accumulator residual included for a range of cases with approximately the same input power level (30 kW).*

Figure 8.18

8.4 Simscape Model Validation

The original Simscape physical model, which had been used for the design of the control system and hydraulic circuit, was validated against the test rig data. The criteria for validation were that the model could replicate the Quantor output torque given the same flywheel speed and torque demand, and the loss breakdown. The full model is large and slow to execute, and it was planned to use the simpler model for assessment of different Quantor architectures, but it is important to confirm that the Simscape components matched the performance of those tested. The one exception to this was the accumulator. Rather than validating the accumulator model, which is not a new area of research, its pressure was set to follow the measured accumulator pressure and DDPM A was controlled with the same displacement, Fd, as measured on the test-rig. This ensured that the losses of the accumulator and DDPM, and the flows in the gallery were the same in the model and as on the test rig. We will look in some detail at the following cases:

- Steady speed
- Quantised
- Quantor mode 4
- Quantor mode 1

8.4.1 Steady Speed

Figure 8.19 and Figure 8.11b show Sankey diagrams for the steady speed case with the electric motor shaft running at 900 rpm (a flywheel speed of 51.7 rpm) and a 200 bar accumulator pressure. Figure 8.19 is taken from model data and Figure 8.11b is taken from measured data on the test rig. The input shaft powers differ slightly as the modelled output torque is not quite the same as the measured torque, but they are within 3.5% of each other. The generated powers are very close at 24.8 kW for the modelled case and 24.4 kW for the measured case. The distribution of losses is also very similar, with the greatest differences being in the friction terms, which is at least partially related to the slight difference in PTO shaft torque between the two cases.

8.4.2 Quantised

Figure 8.20 shows a screenshot from a model run for a pure quantised model case at 200 bar and an input shaft power of 24 kW, with the measured PTO torque from the rig included

Figure 8.19 *Efficiencies and losses, showing modelled steady speed case for a flywheel speed of just under* 52 rpm *and an accumulator pressure of* 200 bar*, with losses normalised and accumulator residual distributed 'downstream'. The modelled input shaft power was* 29.9 kW*.*

for comparison. Overall the match between the test rig and model is very good. They measured and modelled torques slightly diverge when the flywheel speed is decreasing, which may be related to the accuracy of our modelling of the friction behaviour of the PTO motors at low speed. Figure 8.21 compares the measured and modelled efficiencies across ten different levels of input power. Generally, the model slightly underestimates the efficiency across the range, but the modelled efficiencies are within 3% of the measured for all cases above an input power of 5 kW.

Figure 8.11c shows a Sankey diagram of a quantised test case at 200 bar at an input power of 29.7 kW. Figure 8.22 shows the equivalent Sankey diagram for the model results, which had a slightly higher input shaft power of 30.6 kW. The loss breakdown is very similar again between the two cases, with the efficiencies only different by 0.4%.

8.4.3 Quantor Mode 4

Figure 8.23 shows the model and measured outputs for PTO torque. The torque agrees very well except for a small artefact around zero speed, where the directional valves switch over. This is because the model does not perfectly replicate the behaviour of the directional valves. This could be improved by measuring the control delay of these valves and their pressurisation curves, as was done for the transient valves.

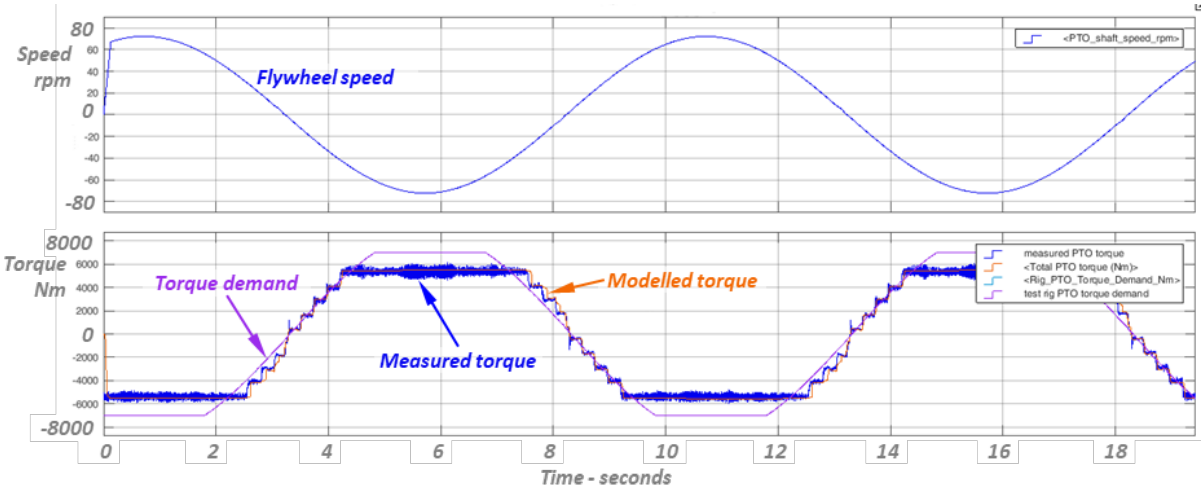

Figure 8.20 *Dewesoft screenshot for the quantised system at an accumulator pressure of* 200 bar *showing good agreement between measured and simulated results.*

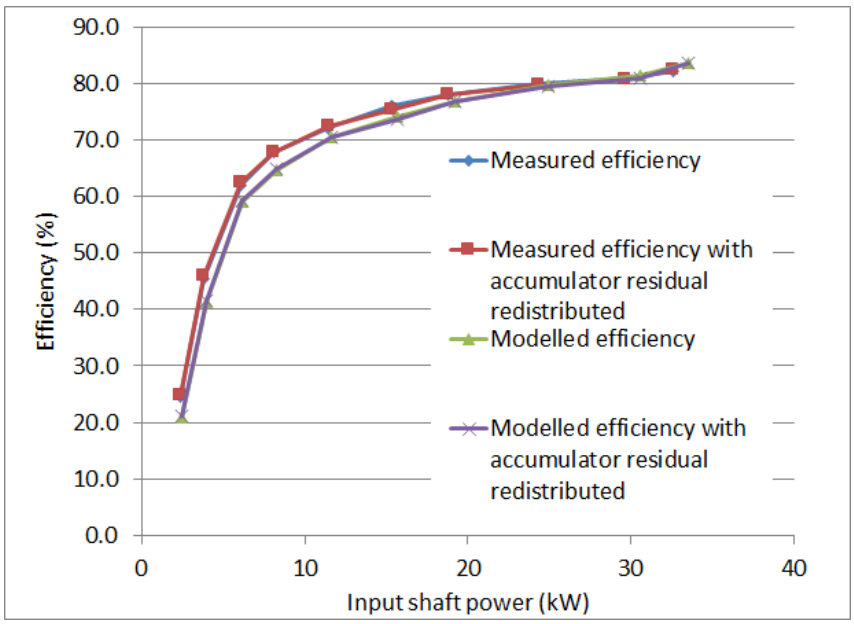

Figure 8.21 *Comparison of measured and modelled efficiency for test case and model for quantised* 200 bar *cases across the power range*

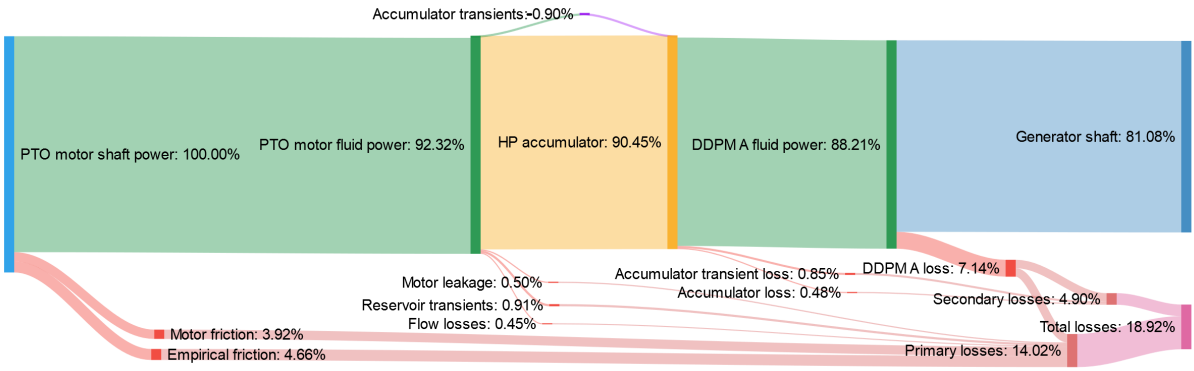

Figure 8.22 *Model results of quantised* 200 bar *case with an average input power of* 30.6 kW

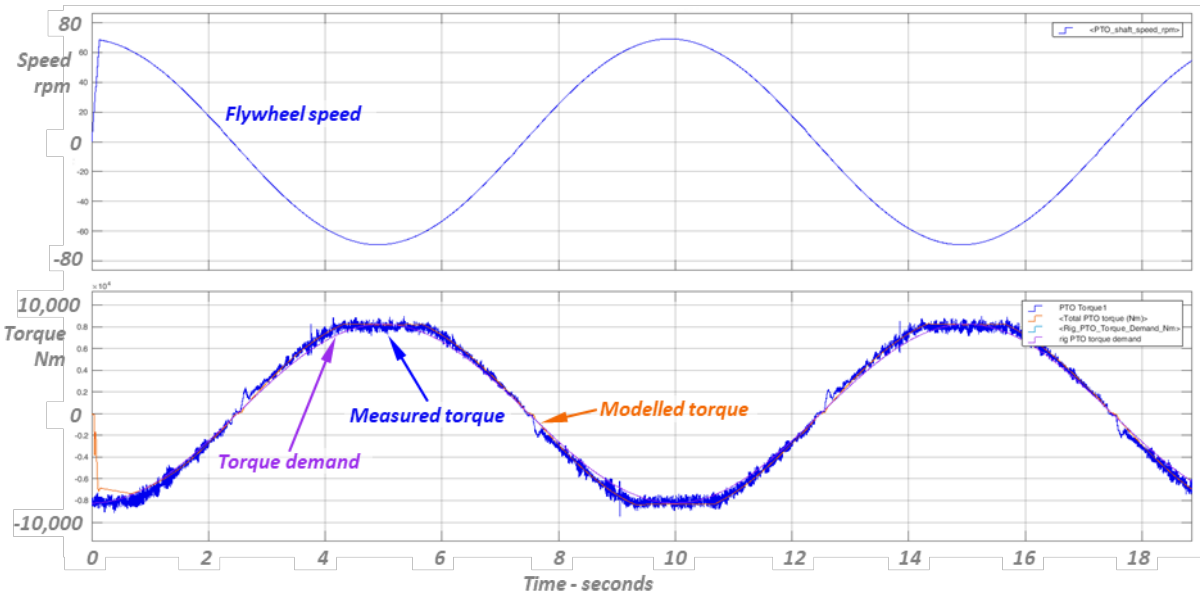

Figure 8.23 *Model screenshot for flywheel speed (top) and PTO torque(demand, modelled and measured) (bottom) for the Quantor mode 4 case at* 31 kW.

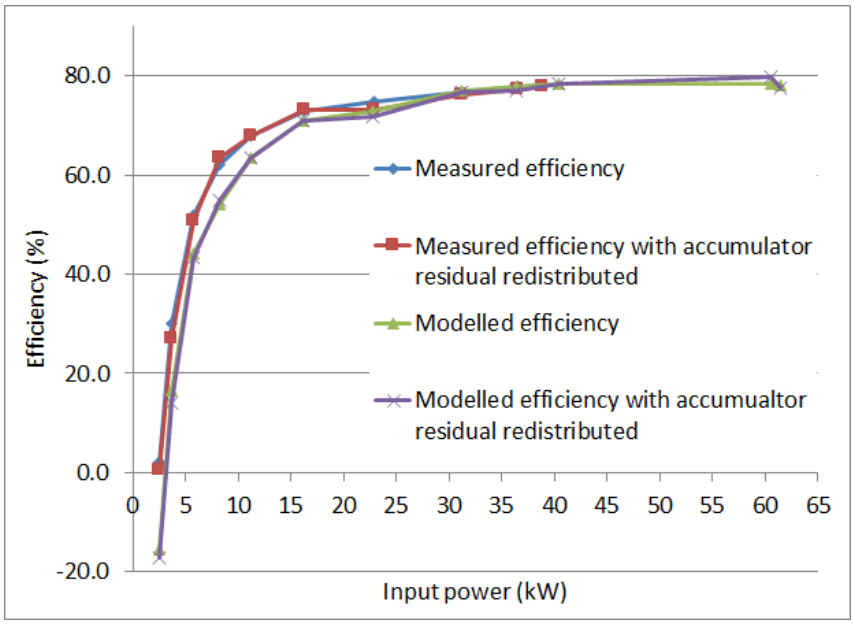

Figure 8.24 *Comparison of measured and modelled efficiency for Quantor mode 4 cases across the range of input power*

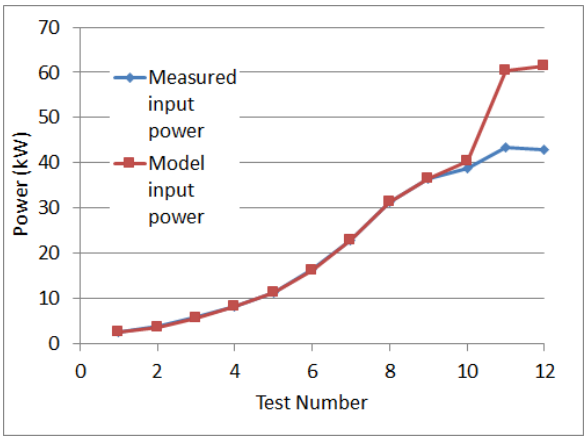

(a) *Comparison of measured and model Quantor mode 4 input power for twelve different tests.*

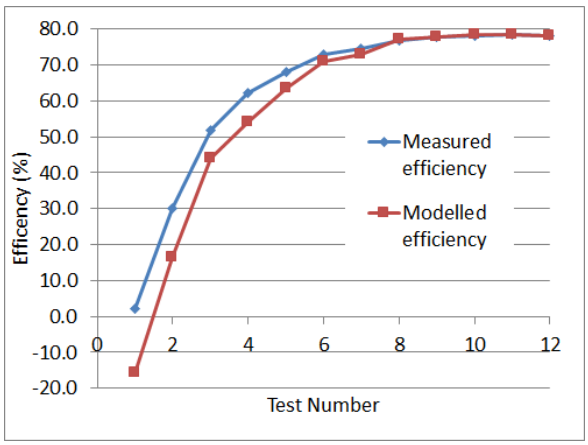

(b) *Comparison of measured and model Quantor mode 4 efficiency for twelve different tests.*

Figure 8.25 *Separated comparison of measured and modelled power and efficiency for each Quantor mode 4 case.*

Figure 8.24 compares the efficiency/power curve for the modelled and measured cases of Quantor mode 4. Figure 8.25 provides more detail on these results by showing the input shaft power and efficiency separately for each test case. The shaft power agreement (and hence PTO torque) is very good up to test 10, where, it wildly diverges. This is because this is where DDPM B was saturated on flow and was overdriving into the HP accumulator in the test. It seems that this behaviour is not being correctly represented by the model, which could be fixed in future work. However this is not part of the normal operation of the Quantor lab system which the Simscape model represents, so it is not a particularly important feature to correct. The efficiency in the modelled cases is about 7% lower in the low power cases, but the match improves once the input power is above around 15 kW.

Figure 8.12 and Figure 8.26 are respectively the Sankey diagrams for the Quantor mode 4 case from test data and model data. Again it can be seen that the loss breakdown is very similar in both cases and the difference in the final efficiency is only 0.4%.

8.4.4 Quantor Mode 1

Figure 8.27 shows a model screenshot of the torque output from both the model and measured data. The agreement is very good. The small torque artefacts from the quantised transitions are present in the model at the same points as in the data, but they have different shapes and slightly different magnitudes. Possibly this could be resolved with a higher fidelity model of the valves and relevant compliances, but that was not judged to be necessary to fulfil the demands of the project at the time.

Figure 8.28 compares the measured and modelled efficiency for the Quantor mode 1 case at 300 bar with slug only control. The model slightly overestimates the efficiency at higher powers but still shows good agreement across the range. The comparison of the loss breakdown in the Sankey diagrams in Figure 8.29 and Figure 8.13b also shows good agreement, although the efficiency is slightly overestimated by 1.2%.

Figure 8.30 shows the torque match between the model and the measured data for the Quantor mode 1 300 bar slug and X case at 30.2 kW. To achieve this, some of the control parameters relating to feature X had to be adjusted from the values used in the test rig.

The efficiency and loss breakdown for Quantor mode 1 test and modelled cases with 'slug and X control' are shown in Figure 8.31, Figure 8.32 and Figure 8.13d. Again, the efficiency is slightly overestimated by the model (by 1.6%), but the match in the loss breakdown is still very good.

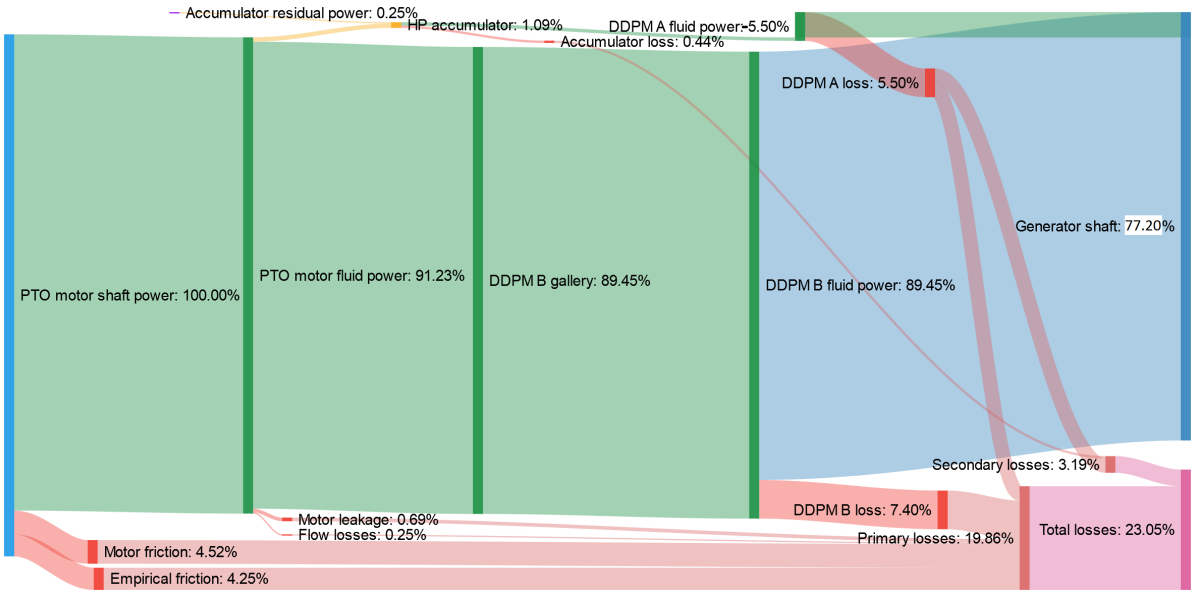

Figure 8.26 *Sankey diagram for a model run of Quantor mode 4 at accumulator pressure of* 250 bar *with losses normalised. The input shaft power was* 31.2 kW.

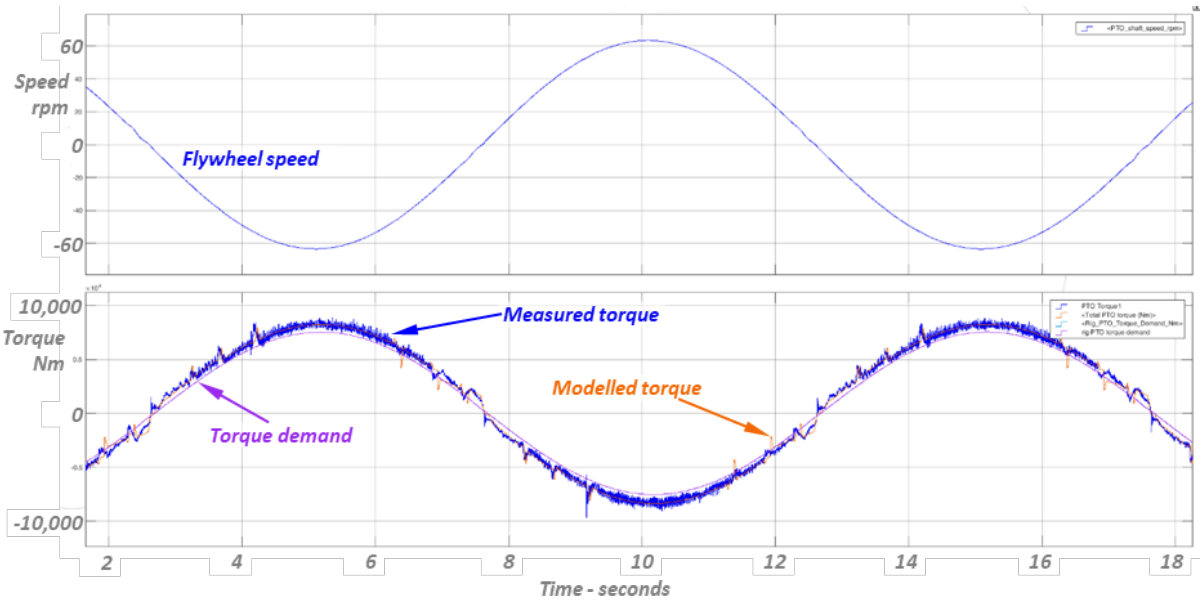

Figure 8.27 *Model screenshot of PTO shaft speed (top) and PTO torque demand, measured torque and model torque (bottom) for Quantor mode 1* 300 bar *case with slug only at an average input power of 27kW.*

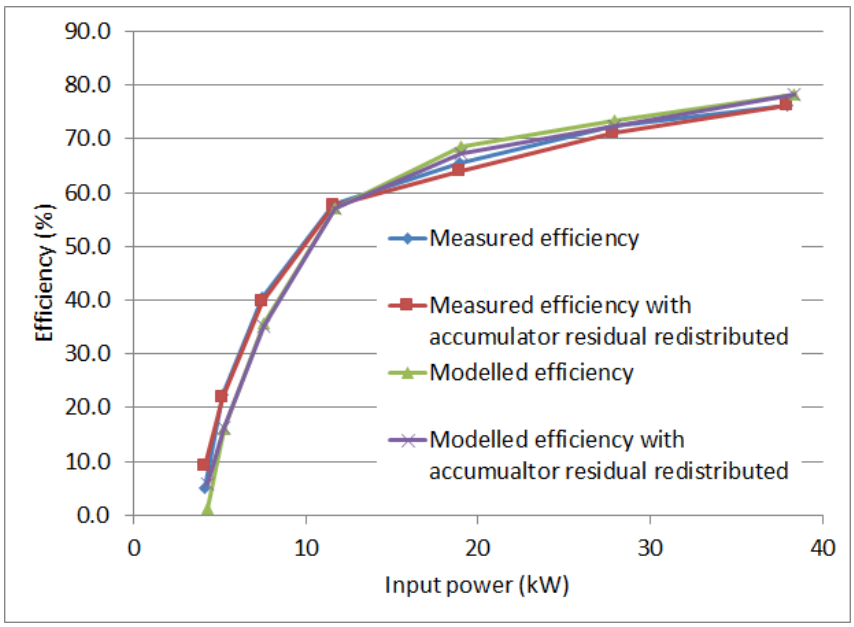

Figure 8.28 *Comparison of measured and modelled efficiency for Quantor mode 1 at* 300 bar *with slug only control*

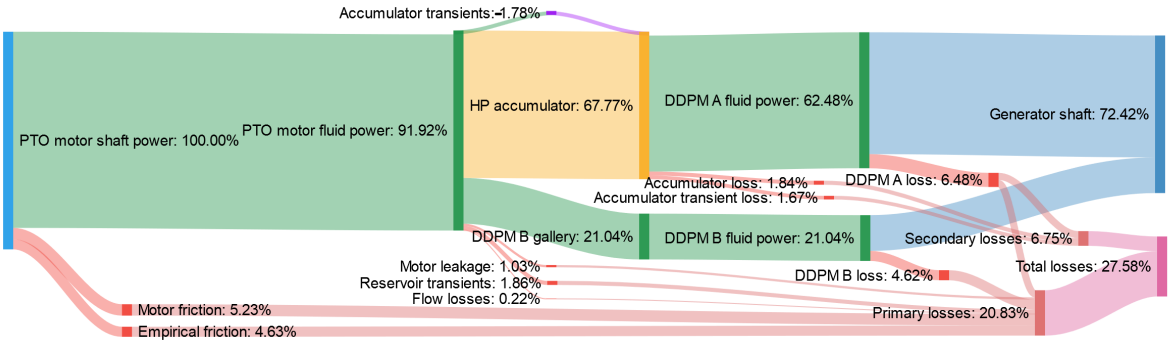

Figure 8.29 *Sankey for a model case of Quantor mode 1 at* 300 bar *with slug only control. Input shaft power was* 27.9 kW*.*

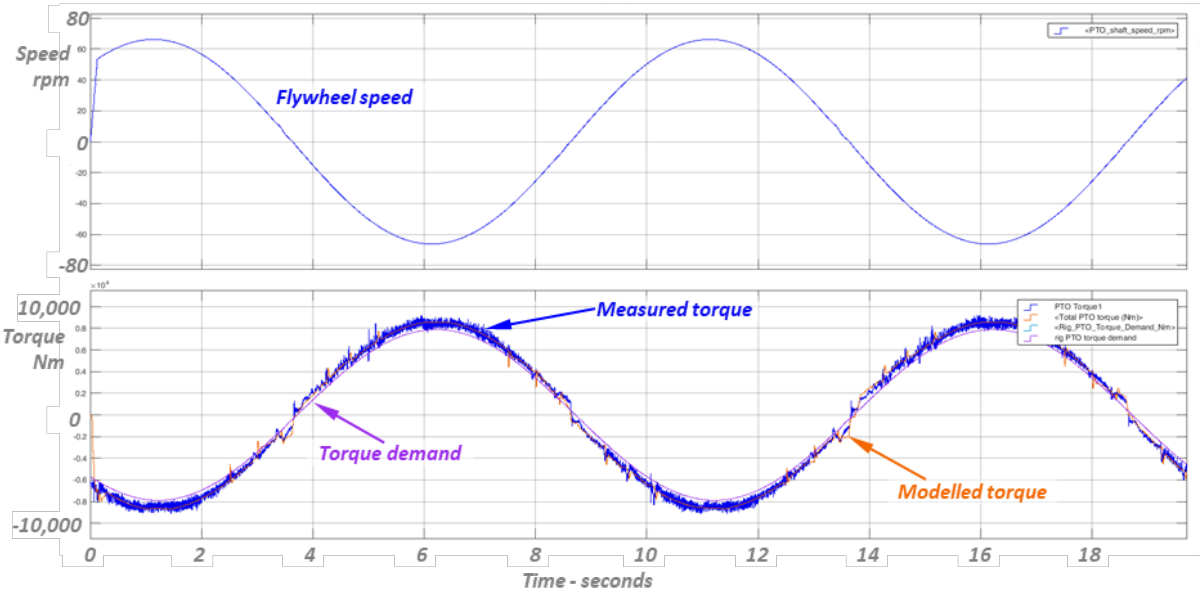

Figure 8.30 *Model screenshot showing flywheel speed (top) and PTO torque(demand, modelled and measured) (bottom) for Quantor mode 1,* 300 bar *slug and X control*

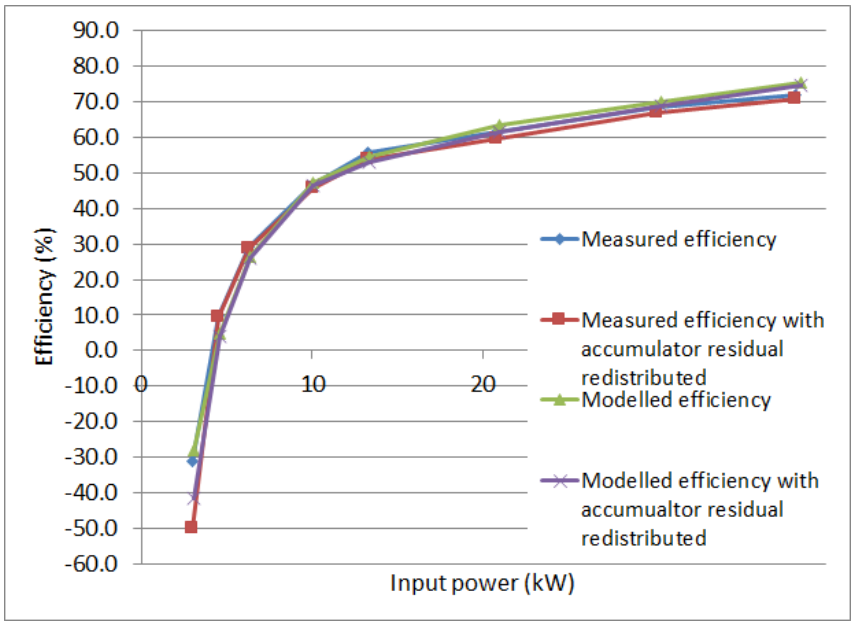

Figure 8.31 *Comparison of measured and modelled efficiency for Quantor mode 1* 300 bar *with slug and X control*

This broad range of power levels and control modes shows that the Simscape model can accurately replicate the torque and losses of the tested Quantor system (apart from the accumulator losses). Since the model is slow and unwieldy (like many Simscape models), running a full irregular case for comparison to the tested results would have required more computing power than was easily available. The purpose of this model is more for looking at detailed behaviour of the hydraulic circuit and designing control, so the validation carried out for the regular cases was judged to be adequate. The simplified model was developed as a tool for broader efficiency and architecture studies, removing most of the intricacies of the hydraulic circuit.

For all control modes described above the Simscape model was able to replicate the measured efficiency within 5% when the absorbed power was over 10 kW. It is more difficult at very low input powers because a small absolute difference in a particular loss has a large proportional impact. However, representing the efficiency well in waves above the Quantor's cut-in power is probably more useful.

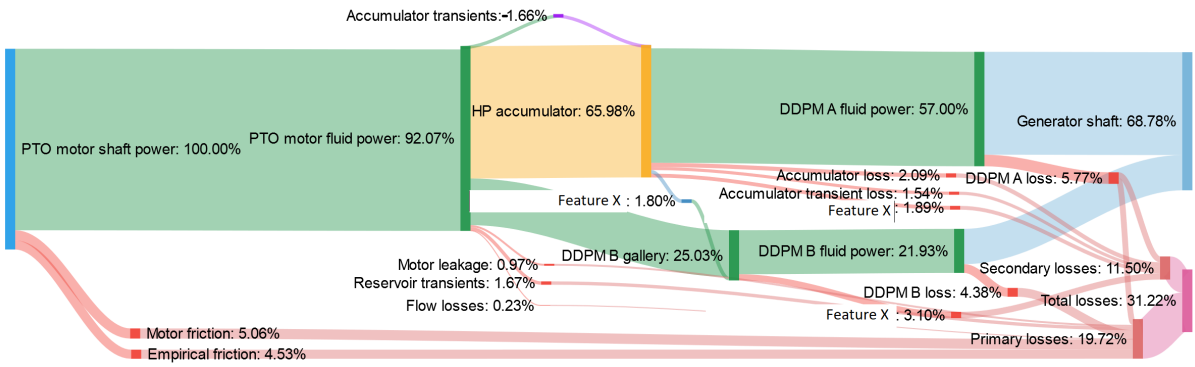

Figure 8.32 *Sankey for a Quantor mode 1 model case at* 300 bar *with 'slug and X' control (input shaft power of* 30.4 kW*).*

8.5 Model Simplification and Extension

Appendix A contains excerpts from the confidential Milestone 8 Report which was written by AIP and Quoceant for WES. These summarise the work carried out during the Stage 3 PTO project in producing a simplified Simulink model which could represent Quantor torque and losses for alternative future Quantor architectures for full-scale WEC applications. This development of a simple validated model would not have been possible without the loss breakdown analysis and Simscape model validation work described above. The simplified model was a natural development of work already carried out, in that it allowed the learning from testing and loss analysis to be applied to Quantor systems of

realistic scale in a computationally efficient way.

8.6 Summary

A full loss breakdown analysis for Quantor was carried out, using a combination of measured data, manufacturer data and model calculations. All major losses and components were included, and although this was not completely exhaustive, the remaining losses are relatively insignificant compared to those examined. The loss breakdown was carried out for a broad range of cases and control modes, and the residual errors were within 5% of the measured losses (above a minimum input power). Loss analysis was carried out on a node-by-node basis so that detailed Sankey diagrams could be produced and comparisons between cases drawn. The loss analysis means that efficiency improvements could be targeted to the most significant losses in the system, and that the impact of various control modes on the efficiency could be understood. This means that informed decisions about how to best control the Quantor under particular conditions can be made.

Once this was complete the Simscape model was validated against the test data and found to agree well with experiment in a broad range of cases. The model was validated in terms of applied PTO torque, efficiency and loss breakdown. There was slight underestimation of the efficiency in the quantised cases and overestimation some Quantor cases but this remained within 5% for all examples with an absorbed power of more than 10 kW. The loss breakdown for the model results also compared well with the measured results.

A simplified Simulink model for performance prediction of alternative Quantor architectures, based on the testing and loss analysis carried out, was then produced. This means that torque control and efficiency of different Quantor architectures can be predicted with much greater confidence as the results are based on real test data. This would greatly improve the WEC system design process, as the impact of design choices on the system losses and torque response could be properly evaluated.

Chapter 9

Conclusions

9.1 Summary

The design of PTOs for WEC applications has been a key challenge for the sector, with the key technical difficulties including:

- Production of smooth PTO torque in response to control algorithms, requiring four-quadrant capability and a rapid response rate from the system.
- Ability to handle loads with extreme ratios of the peak to mean power, whilst generating smooth electrical output.
- Ability to generate electricity efficiently across the broad load range.

The Quantor PTO has been designed as a system which overcomes these difficulties, and is both scalable and versatile enough to apply to a broad range of WEC architectures at many various rated powers. The hypothesis of this research was that the Quantor is a highly controllable and efficient PTO system for wave energy conversion that can be representatively tested at laboratory scale to understand full-scale deployments. The aims of this project were to demonstrate that the Quantor can smoothly follow a four-quadrant torque demand in representative test conditions, to quantify its efficiency and losses, and to estimate the performance of full-scale Quantor architectures.

To the above ends, a detailed physical model of the Quantor was constructed in Simscape, of the desired laboratory Quantor system which included a WEC emulator rated to 304 kW and a Quantor PTO which featured four fixed-displacement ($255\,\mathrm{cm}^3/\,\mathrm{rev}$) pump motors

and two M96 type DDPMs. Design work and control system development, as well as initial efficiency modelling, was carried out using this model. Once the feasibility of the Quantor laboratory system was verified in simulation, construction of the physical system was carried out. This was done in several stages to ensure the functionality of all components, especially the manifold blocks, before building the final test rig. Extensive testing was carried out on this final system to evaluate different control modes. The system was tested under prescribed motion conditions, and with a WEC HIL model in regular and irregular seas. The data gathered was analysed to produce a loss breakdown of the Quantor PTO in various operating conditions. This data was used to validate the efficiency and losses of the physical model. Once this was complete, a simplified and flexible Quantor model was produced which could be used to examine to PTO torque, efficiency and losses of alternative architectures to the system constructed in the laboratory.

9.2 Outcomes of Research

The initial simulation work confirmed the essential functionality of the Quantor hydraulic circuit, informed the control system design and provided initial estimates of the system efficiency and losses.

The testing carried out unambiguously confirmed that the Quantor system is capable of smooth full four-quadrant torque control of a variable load. This is significant because, as discussed in Chapter 2, many sophisticated control strategies for WECs have been proposed but there is a distinct lack of proven hardware which can perform in the manner needed for these control strategies to be practically feasible. Even Pelamis, which demonstrated full four-quadrant control at scale in the sea, had quantised output torque which limited the options for control. The Quantor was able to generate electricity at a synchronous speed of 1500 rpm which will greatly simplify the process of grid integration.

The data gathered on the test rig gave superb insight into the possible operation of Quantor in real conditions, allowing inferences to be made about the scalability and potential optimal operating modes for different conditions. For example, it was established that Quantor mode 4 was the most efficient mode for low absorbed power levels.

The design and construction of a test rig which can represent realistic WEC operating conditions at scale in a laboratory is also a major achievement. Whilst a few previous examples exist, the inclusion of a representative inertia is novel and means that the control stability of the PTO is tested in a more meaningful way. Whilst only speed control of the WEC emulator was used in Quantor testing, the capability for torque control also exists

and would provide opportunities for even more useful testing.

The efficiency of Quantor for a broad range of power levels (up to what was practically feasible on the test rig), control modes and damping and spring coefficients is now well known from measured test data, and the associated losses are understood. Apart from the detailed loss breakdown done for Pelamis [49], no equivalent study has been carried out on a wave PTO to a similar level of detail using measured data (to the best of the author's knowledge at the time of writing).

The data gathered was used to validate the physical model, so that a detailed model of the hydraulic circuit of the laboratory system with realistic losses was produced. Whilst the model is not a perfect representation of the laboratory system, particularly when coming to fine control details such as the timing of specific valves, it can replicate the torque and efficiency of the rig within 5% and shows a similar distribution of losses. The existence of this model means that physical changes to the laboratory implementation of the Quantor or new control features could be tested in simulation in great detail.

A simplified model was then developed, based on the loss breakdown analysis and possible future designs of the Quantor in higher power regimes explored. The existence of a scalable and validated model comprising both the torque and losses of a wave PTO is a highly novel step, as the majority of developers do not possess validated PTO models which are applicable beyond the scale of their existing WEC designs. This model will allow WEC design and PTO design to happen together in an iterative way, such that the most efficient PTO for the WEC scale and deployment location can be chosen with the confidence that the simulated results have a basis in experimental data.

9.3 Further Work

There are many possible avenues for further work on the Quantor PTO. The research presented here has focused on demonstrating the fundamental feasibility of this type of system and on understanding the system losses with a view to possible future applications. Medium-term goals could include:

- Improving the validation of the Simscape physical model of the Quantor lab system by including a validated accumulator model and adding further detail around individual valve characteristics.
- Further testing and control system development of the PTO on the test rig, for example by using other WEC models, or attempting to further refine control

features.

- Testing the Quantor by using the WEC emulator in torque control mode.
- Testing the Quantor in more challenging conditions by adding compliance to the test rig to represent the behaviour of a real cable.
- Focused individual motoring efficiency testing of the DDPMs to establish whether the assumptions made in the current loss model are valid in this operating mode.
- More extensive modelling of full-scale Quantor architectures using the simplified model.
- Modelling of the Quantor with different types of generator using detailed generator models to analyse electrical output performance.

Beyond the above immediate steps, the ultimate goal would be to continue the engineering design of the Quantor so that it could be deployed in a real WEC. This would require a great deal of further simulation, design and testing, from mechanical, electrical and control perspectives. Other aspects such as reliability of the components would need to be examined as well. There may also be the possibility of using the Quantor in other non-WEC application where the need for smooth torque control over a wildly varying input power range is required, such as heave compensation systems.

Appendix A

Milestone 8 Report Excerpt: Model Simplification and Projection to Other Architectures

This appendix contains excerpts from the confidential Milestone 8 Report which was written by AIP and Quoceant for WES. This appendix has been removed for reasons of confidentiality.

Appendix B

Quantor Commissioning

B.1 Prototype Block Tests with Small Flywheel

B.1.1 Aims

It was decided to order and test a prototype Quantor manifold on a small dedicated test rig, to confirm the design of the block and the valve selection, before ordering the full set of four, as this was a very technically risky component. This also gave an opportunity to do some initial tests of the control system using the Speedgoat, which would aid commissioning the main rig later on.

B.1.2 Setup

As these tests only involved a single block, the combination of quantised and continuous control could not be proven in this context. Rather this test was to demonstrate the functionality of the block as designed in either a quantised or a continuous control mode. The control system allowed either of these control modes to be selected for this block. A prescribed torque demand was given by the controller. Usually in Quantor operation when power is being extracted from a shaft, the torque demand is calculated from damping and spring terms respectively applied to the measured shaft speed and position. However, the flywheel and motor shaft here are not transmitting power from some external wave-operated source; they simply provide a load for the pressure in the Quantor ports to act on.

The schematic of the first iteration of the prototype block testing is shown in Figure B.1.

In this setup, an 11 kW power pack supplies the flow for both the HP gallery and the DDPM gallery. The intention for the HP gallery was that the HP accumulator could be pumped up to a chosen pressure and the HP isolate valve could then be closed, so that the block ports would be supplied from the accumulator. As the DDPMs for the Quantor hadn't been built by this stage, the rapidly varying pressure signal of the stiff service was provided by using a proportional pressure reducer reliever valve (PRRV), which varied the pressure in the DDPM gallery (shown by the green line) according to a voltage control signal from the Speedgoat, and relieved any excess from the desired setpoint to tank.

There are three accumulators in the system: HP, LP and pilot. The precharge of the 10 l HP accumulator is 110 bar, that of the 25 l LP accumulator is 2.5 bar and that of the 0.5 l pilot accumulator is 100 bar. The purpose of the LP accumulator is to provide a constant 'tank' pressure to the system. In the final Quantor test rig, a very large LP accumulator was used to keep the low pressure as constant as possible. The HP accumulator here acted as a supply and also allowed us to assess the need for accumulation as shock absorption in the abrupt pressurising and depressurising that occur in the quantised service. The pilot accumulator was to provide acceptable pilot pressure for the duration of the tests, so that any valves operated by the controller would open in time.

A Parker 19 cm^3/ rev fixed displacement motor was connected to the output ports of the manifold block, instead of the Poclain motors chosen for the final test rig. This was connected to a small flywheel of approximately 400 mm diameter. In this round of testing, it should be noted that the Quantor block was not extracting power from the flywheel; rather the flywheel was an energy sink for the output of the Quantor block, which came ultimately from the 11 kW power pack. The flywheel was used to give a load for the block pressure to act on and to physically observe certain capabilities such as directional switching. It also meant that the correct behaviour of the valves in both static (conditions without flow) and dynamic (conditions with flow) could be verified. In the early stage of testing, the fixed displacement motor and flywheel were not connected to the manifold block, as it was considered desirable to confirm correct operation of the manifold block and control software by observing pressurisation of the appropriate motor port, without supplying flow. To this end, the two motor ports were initially connected with a needle valve as a safe bypass of the motor (shown in Figure B.4). This meant the first tests could be done without the pressure in the ports applying torque to the small flywheel.

The pressure transducers used in almost all cases were Kyowa PGS-50KA which have a range of 0 to 50 bar. The low pressure accumulator pressure was measured with a Hydac HDA 8400 0 to 40 bar transducer. There was a SICK DFS60A-S4CC65536 encoder mounted on the flywheel shaft. Torque on the flywheel was not measured but

was calculated from the pressure on the motor ports and motor displacement, ignoring mechanical losses. This was felt to be adequate as these tests are qualitative rather than quantitative and this particular motor was not part of the final Quantor rig system.

B.1.3 Static Test Procedures

The tests of each specific function were carried out as briefly described below. Before these specific tests general checks of the hydraulic circuit and control system were carried out (for example checking for leaks, ensuring every solenoid valve could be controlled as demanded, connecting encoder correctly to data acquisition system and calibrating voltage control of the PRRV which represented the DDPM. The safety systems, E-stop and auxiliary systems such as the low pressure circuitry were also tested beforehand. Initial tests of basic hydraulic integrity of the manifold were carried out, mainly by pressurising different ports and observing that pressure was not raised in any unexpected part of the block, and checking that pressure held within the manifold for a reasonable length of time. All tests were first carried out in the static configuration, i.e. with the fixed displacement motor disconnected and the needle valve between the motor ports (M1 and M2) on the manifold closed.

Failsafe System

The aim of this test was to confirm that the pilot lines were pressurised only when the failsafe pilot enable valve was engaged, and that oil flowed through the failsafe relief valve via the port drain valve when the failsafe pilot enable valve was not engaged.

- Pressurise the HP gallery from the power pack, observing the pressure increase.
- Energise the failsafe pilot enable valve and check that the pilot lines pressurise.
- De-energise the failsafe pilot enable valve and check that the pilot lines depressurise.
- Switch off the power pack and depressurise the system.
- With the failsafe pilot enable valve de-energised, connect the power pack supply directly to the motor port M1 and remove the connection to the HP gallery. Isolate M2 using the needle valve.
- Run the power pack and check that flow goes through the failsafe relief valve. Adjust the failsafe relief pressure if needed.

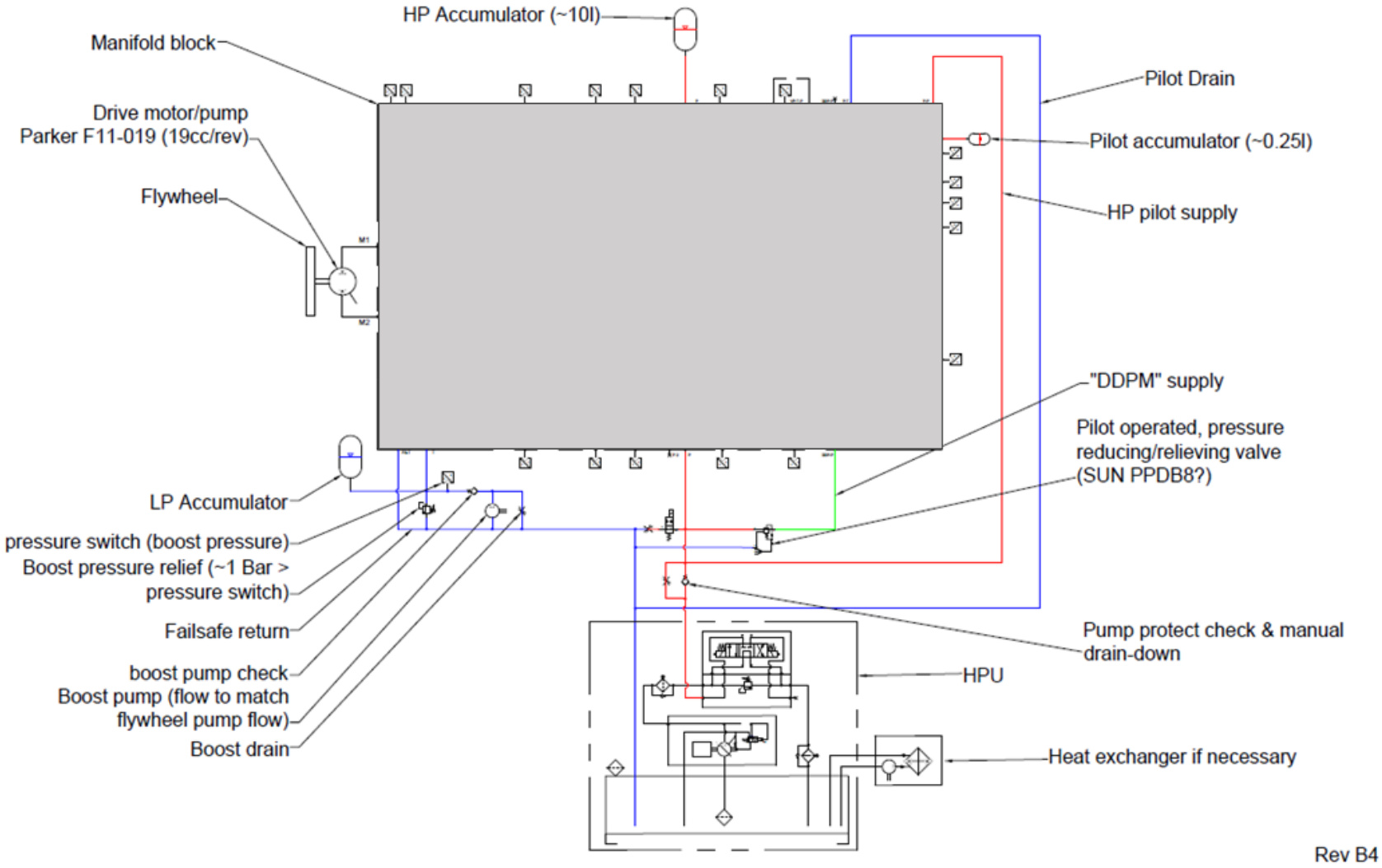

Figure B.1 *Schematic of the original hydraulic circuit of prototype block test setup. (Drawing by Carn Gibson, manifold block redacted)*

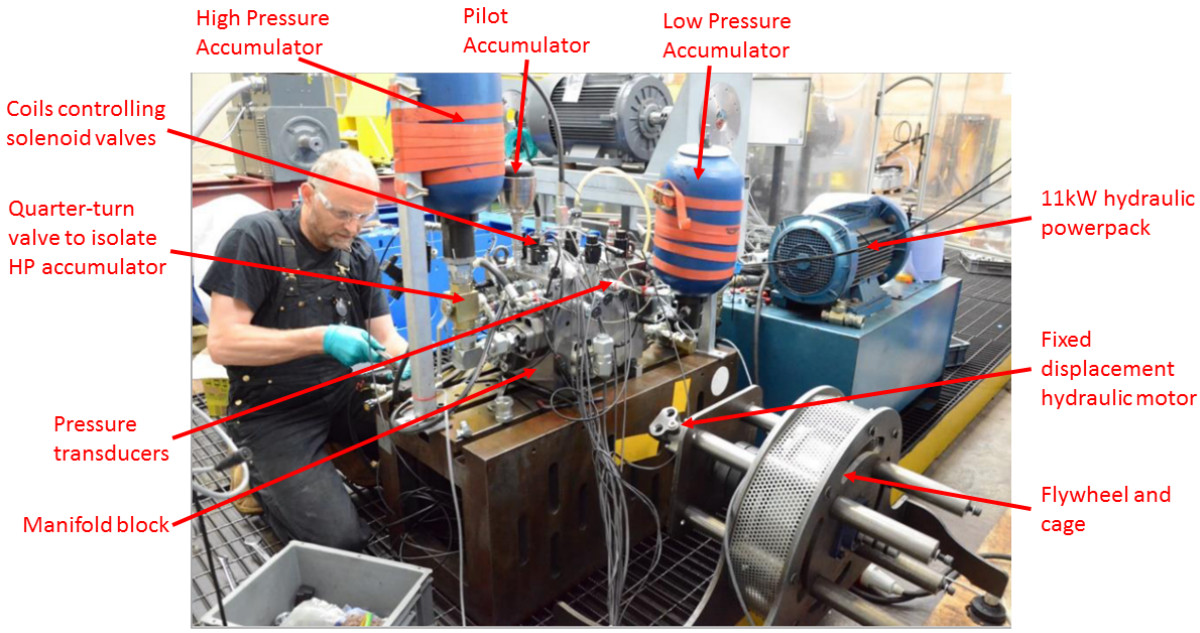

Figure B.2 *Annotated photograph of the prototype block test setup from the control cabin side. (Photo credit: Jamie Taylor)*

Figure B.3 *Photograph of the prototype block test setup from the test rig side. (Photo credit: Jamie Taylor)*

Table B.1 *Example of manual test order of quantised transient valves. The corresponding main flow valves would be tested in the same way.*

Valve	Action	Expected Result
Transient Flow HP A+	ON	Port M1 (A+) pressurises
Transient Flow HP A+	OFF	Port M1 (A+) remains pressurised
Transient Flow LP A+	ON	Port M1 (A+) depressurises
Transient Flow LP A+	OFF	Port M1 (A+) remains depressurised
Transient Flow HP B-	ON	Port M2 (B-) pressurises
Transient Flow HP B-	OFF	Port M2 (B-) remains pressurised
Transient Flow LP B-	ON	Port M2 (B-) depressurises
Transient Flow LP B-	OFF	Port M2 (B-) remains depressurised

- Energise the failsafe relief valve and confirm that the motor port pressurises and the pressure in the HP accumulator increases, with the pressure in the LP gallery remaining low. This verifies the flow path through the check valves and DDPM engaged valve.
- Repeat for M2.

Quantised Valve Testing

The aim of this was to confirm the function of the eight quantised valves. This also allowed initial tuning of the control parameters of the quantising process, such as the delay between opening the transient and main flow valves. This was not a final setting for these values, as the incarnation of Quantor on the full test rig would have many differences to this setup, including the compliance on the motor ports, but provided useful experience in sweeping the available parameters.

- Close the motor port needle valve.
- Pressurise the HP gallery and pilot gallery using the power pack and failsafe pilot enable valve.
- Manually fire the quantised valves to pressurise and depressurise both M1 and M2 motor ports. A suggested order is given in Appendix B.1.3. Observe that the DDPM gallery pressure is not affected and any transient behaviour on the HP and LP galleries.

Real Time Transient Flow Valve Testing

This stage involved testing the transient valve control from the Speedgoat software and meant that pressurisation curves of the transient valves could be characterised and adjusted using the throttle valves.

- Override the main flow valves to off.
- Enable the real-time control of the transient valves from the Speedgoat.
- Using a prescribed torque demand of sufficient amplitude to cause the quantiser to trigger the prototype block into a positive and negative quantised state alternately.
- Adjust the needle valves such that the pressurisation and depressurisation of both ports transitions take a nominal 50 ms (which is estimated to be the fastest transition time which DDPM B can adequately respond to with pressure control).

Cross-Pilot Valve Tests

- Close the motor port needle valve.
- Manually pressurise port A using the transient flow valve.
- Leaving port A pressurised, open the transient flow HP valve for port B.
- See that port B cannot pressurise and that port A depressurises.
- Set the cross pilot cracking pressure by pressurising port A using a transient valve and using the DDPM emulation valve to gradually raise the pressure on port B until the cross-pilot opens, depressurising both ports. Adjust the setting until the cracking pressure is set at a nominal 30 bar (to protect the Poclain motors which cannot tolerate having both ports pressurised simultaneously).
- Open the motor port needle valve slightly so that some flow can pass between the ports.
- Pressurise port A manually using the transient valve and see the resulting flow pass to tank via the cross-piloted LP valve.
- Repeat the above steps for port B.

- Apply the real-time quantiser control sequence to alternate the pressurised ports and check that there are no transient effects on the cross pilots, and that the opposing LP valve of each active quantised port is opened at the correct time, meaning that in normal quantised operation the cross pilots are superfluous.

The original cross-pilot valves in the manifold block did not perform this function correctly; they were substituted later with the valves shown in pink in Figure B.4.

DDPM Enable Test

The purpose of this valve is to isolate the motor ports from the HP gallery when the DDPM is controlling the pressure in these ports. This is because the DDPM pressure changes over the full range of systems pressures from boost pressure to 350 bar, whereas the pressure in the HP gallery is set by the HP accumulator and should vary over a much smaller and lower range as the HP accumulator smoothes the absorbed power, roughly 175 to 250 bar.

- Pressurise the HP gallery using the power pack. Leave the DDPM enable valve off (open).
- Turn off and drain the HP supply and see that the gallery drains only through the HP supply line and not through the DDPM gallery.
- Pressurise the HP gallery using the power pack. Energise the DDPM enable valve (close it).
- Turn off and drain the HP supply and see that the HP gallery remains pressurised in this case.

Directional Valves Test

The PRRV is a substitute for DDPM B in the final Quantor. It allows continuous pressure control. There is a normally open valve which can be used to isolate the HP and DDPM galleries so they can be at different pressures. The directional valves connect either motor port to this continually variable pressure.

- With the motor port needle valve closed, pressurise the HP gallery to 100 bar, which is below the HP accumulator precharge.
- Close the DDPM enable valve.

- Set the DDPM emulation valve to an intermediate pressure of 70 bar.
- Open the directional valve to port A and observe the port pressure increasing to match the PRRV setting, without any other ports or galleries changing pressure.
- Vary the PRRV setting and check that the port pressure follows the DDPM gallery pressure.
- Close the directional valve and open the LP quantised valve to drain the port.
- Repeat for the opposing port.

DDPM Overdrive Test

This test was to check that the DDPM overdrive relief valve correctly relieved pressure from the DDPM gallery to the HP gallery above a certain threshold. In the final Quantor design, the DDPM must be able to reach a higher maximum pressure than the quantised service to enable it to control pressure over a broad enough range to smooth out the quantised transitions. Having a relief valve from the DDPM gallery to the HP gallery means that not all the energy is lost from relieving, as it would be if the pressure were relieved to tank, so this reduces the losses of the system.

- Charge the HP accumulator to 130 bar.
- Set the PRRV to output 70 bar into the DDPM gallery.
- Close the NO shutoff valve, isolating the HP gallery.
- Increase the supply from the power pack to a higher pressure than that of the HP accumulator.
- Energise the DDPM enable valve, isolating the accumulator from the motor port galleries.
- Open a directional valve to one of the ports.
- Control the PRRV to vary the pressure in the DDPM gallery, seeing the overdrive relief valve crack and flow moving into the accumulator from the DDPM gallery above a threshold.
- Iteratively adjust the cracking pressure of the overdrive relief valve to a nominal 70 bar.

The original overdrive relief valve was found to have its ports incorrectly oriented in the galleries of the manifold block. As a result, it relieved from the HP gallery into the DDPM gallery but not in the other direction. To resolve this, a plug was purchased to fill the original cavity and the valve connected correctly to the manifold galleries using an external line body and hoses.

B.1.4 Dynamic Test Procedures

Dynamic tests were carried out with the corrections to the hardware made as shown in Figure B.4. All the necessary valve changes had been made and the fixed displacement motor and flywheel were connected to the manifold motor ports. These tests allowed testing of valve-switching and control under dynamic flow, with an inertial load, in all four speed and torque quadrants. The block could be selected to be in either quantised or continuous mode and a prescribed PTO torque demand was provided by the controller.

An encoder mounted on the flywheel measured the shaft speed. In some tests, it was necessary to feed a virtual damping term back into the controller, based on multiplying the measured speed by a control gain to artificially increase the load of the flywheel. This also meant the phase of the torque applied could be shifted relative to the flywheel speed. The feedback torque has the effect of limiting the flywheel speed in both the quantised and continuous control modes.

Emulation of DDPM B Pressure Control

Having tuned the pressure control loop for the PRRV in the static tests, it was then trialled in dynamic tests. A prescribed torque demand was provided so that the controller would alternately pressurise the two motor ports, with varying pressure. However, the initial pressure control range of the PRRV was 35 to 300 bar, which meant that the corresponding gap in the torque was too large, making it impossible to demonstrate smooth control of the torque on the continuous service around zero. Data from a test with this valve is shown in Figure B.5. This PRRV was swapped with another one which had a range of 3 to 50 bar, which allowed the directional switchover with variable pressure to be demonstrated, as shown in Figure B.6.

There will always be a residual gap in around zero torque in the DDPM control, as the DDPM cannot perfectly control pressure right down to boost pressure. The greater this residual gap, the less smooth the PTO torque around zero will be, which could severely affect the efficiency of the Quantor, especially in low energy sea states where zero crossings are more frequent. Therefore, establishing the minimum practically controllable pressure

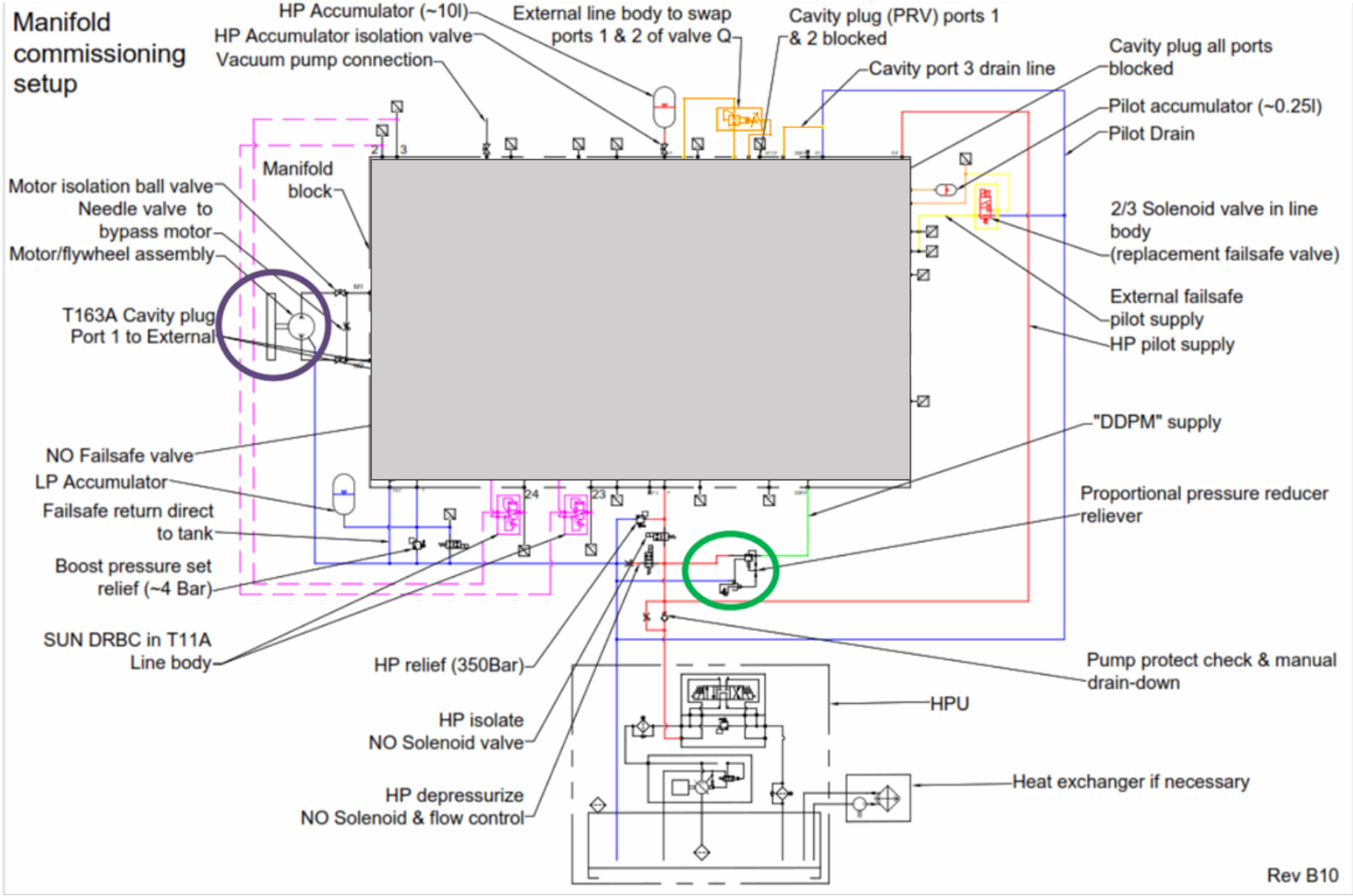

Figure B.4 *Schematic of final hydraulic circuit of prototype block test setup, with line bodies to correct block design errors.(Drawing by Carn Gibson, manifold block redacted)*

on the continuous service with the DDPM is a key outcome of this project.

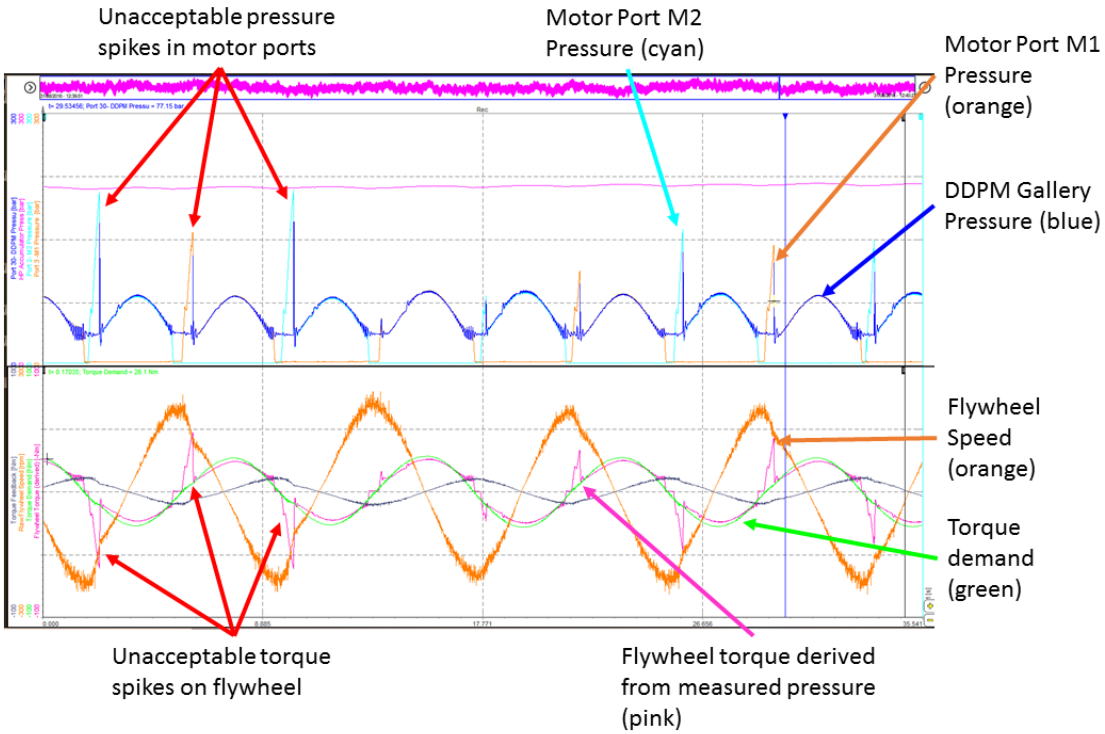

Figure B.5 *Screenshot of pressure and torque data showing unacceptably large pressure and torque spikes around zero with PRRV of range* 35 *to* 300 bar.

Quantised Control Testing

In this test, the prototype block was controlled as if it were one of four wheel motors under quantised control. This is why there is a difference between the green torque demand and the pink contribution from the single motor. A prescribed torque demand was given to the real-time controller which would use all four quantised states were they available. The quantiser state trace shows how the quantiser would be switching the additional three motors if they were physically available. The alternating pressurisation of the motor ports M1 and M2 corresponds to the positive and negative quantised torque output of the flywheel.

During the test, the pressure in the HP gallery rises from approximately 200 bar to 220 bar because of the power pack supply. In Quantor in a WEC the accumulator pressure would vary according to the power absorbed from the waves.

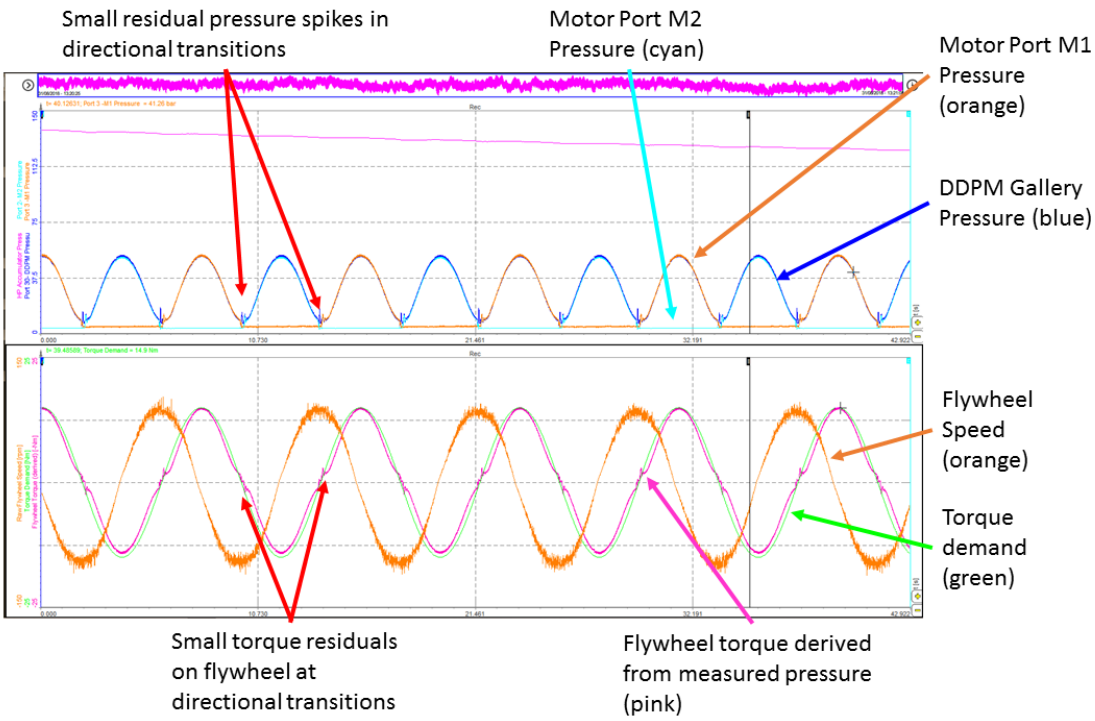

Figure B.6 *Screenshot of pressure and torque data showing greatly reduced pressure and torque spikes around zero with PRRV of range* 3 *to* 50 bar.

B.1.5 Summary

Figure B.4 shows the hydraulic schematic of the prototype block test circuit after the corrections to the failsafe pilot valve, the cross-pilot valves and the overdrive relief valve. The original failsafe cavity was blocked with a plug and an external line body added to the block with a solenoid-operated valve which would carry out the failsafe function correctly. In the original design, the port drain valve would have been closed with the failsafe pilot enable valve in its default position (i.e. not energised and not supplying pilot pressure to the valves), so the manifold block would pump passively. Also, when the failsafe valve was energised, the port drain valve would have been open, resulting in the Quantor pumping against the failsafe relief valve, causing significant losses. This was corrected so that, with the failsafe pilot enable valve energised, pilot supply pressure was available to the control valves and the port drain valve was closed, and with it de-energised, the port drain valve was open and the pilot supply to the control valves was cut off, so they could not act.

In the course of testing, it was found that the cross-pilot valves tended to open at points when it was not desirable, causing any pressure in the motor port galleries to be lost to tank. An alternative valve architecture (shown in the line bodies in pink) was chosen which functioned as desired.

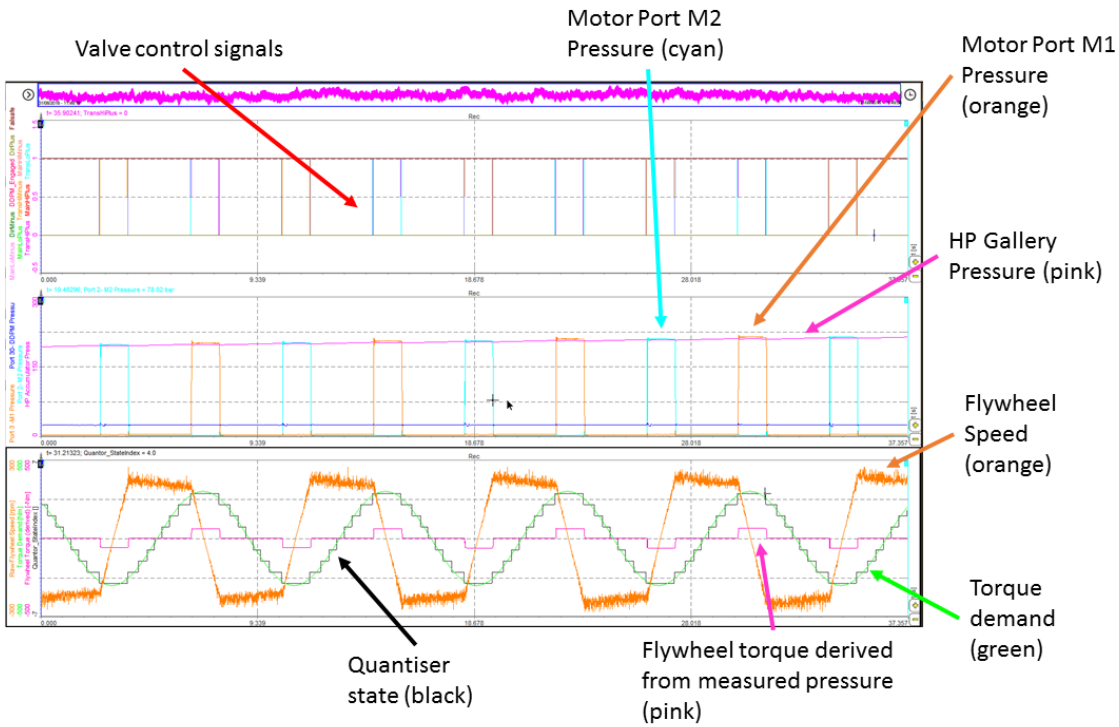

Figure B.7 *Screenshot of pressure and torque data showing quantised control with flywheel connected.*

The DDPM overdrive relief valve was found to be oriented the wrong way in the manifold block, in that it didn't relieve pressure from the DDPM gallery to the HP gallery above a certain threshold. The original cavity was plugged and the same valve mounted externally with hose connections to the correct galleries, which fixed this issue.

For the final Quantor test rig, four blocks were needed. It was decided to redesign the manifold block so that these changes were included, rather than ordering three more of the prototype design and making the same changes with external line bodies. So four new manifold blocks were designed according to the schematic shown in Figure B.8.

There were many aspects of the Quantor control software which could not be tested on this experimental setup because the hardware was missing, such as the DDPMs. There were also several features which were developed specifically for this test rig and not necessary in later additions, such as the control of the PRRV for emulating the DDPM.

However, the fundamental control of valves, including sequencing and timing could be checked, as well as the Quantor's ability to respond to a prescribed torque demand. The majority of control refinements that were carried out during these tests were to do with interfacing with real hardware, and small alterations such as adjusting valve timings and delays.

Figure B.8 *Schematic of redesigned manifold block.(Drawing by Carn Gibson, redacted)*

B.2 WEC Emulator with Prototype Manifold Block

Whilst waiting for the delivery of the four redesigned manifold blocks, the prototype block with modifications was connected to the WEC emulator, Poclain PTO motor and DDPMs for further commissioning of the hardware and control systems.

Figure B.9 shows a hydraulic schematic of the setup, with the prototype manifold block (with modifications) connected to the Poclain fixed displacement motor, DDPMs, final test rig galleries and auxiliary systems (such as the boost pump) of the final test rig. Figure B.10 shows how this setup was physically enacted on the test rig. There were quarter-turn valves installed between the manifold and the Poclain motor so that the manifold block could be tested statically if desired. This setup meant that apart from the four final manifold blocks and the connections between them, the rig hardware was essentially complete.

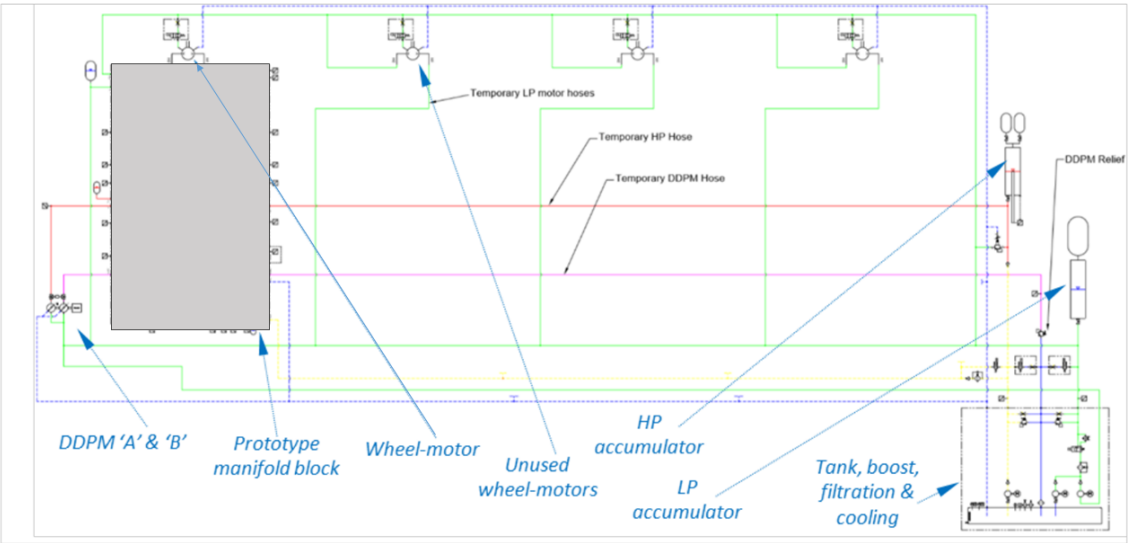

Figure B.9 *Schematic of the prototype block with WEC emulator and DDPM. The prototype blocks had the modifications shown in Figure B.4 but the block is redacted. (Drawing by Carn Gibson)*

The tests carried out were almost the same as those carried out on the prototype block with the small flywheel; verifying the functions already checked had not been lost in the course of the transition to the new test rig. Initially, static tests in which the flywheel was held still by the inverter and the motor ports pressurised at zero speed were carried out, followed by dynamic tests which meant controlling the flywheel speed simultaneously with the Quantor functions on the block. The other major new addition was the real

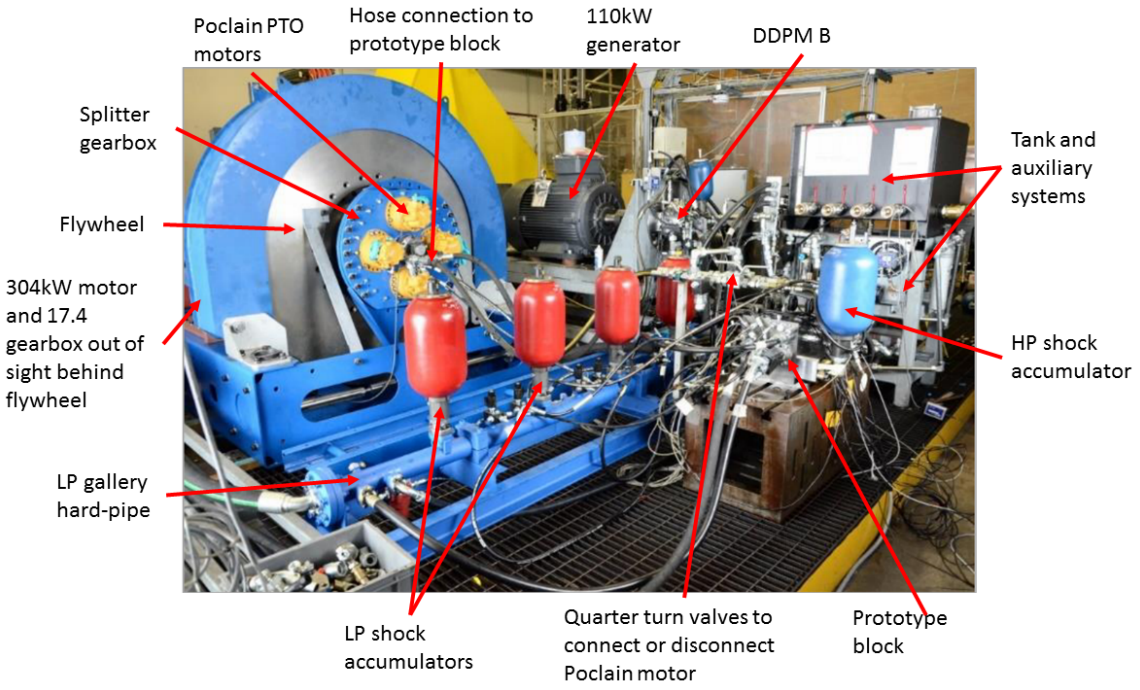

Figure B.10 *Annotated photograph of prototype block with WEC emulator and DDPM.[24]*

DDPMs, so the pressure control for DDPM B could be tested in its final implementation without using the substitute PRRV. The boost system for the final Quantor could also be commissioned through this process.

Carrying out this procedure meant that the commissioning of the final Quantor test rig was much more straightforward, having removed many of the initial hardware/software interface issues and tested almost all components of the real-time control. The commissioning of the final Quantor rig was still a long and involved process, but these initial tests gave us increased confidence that the final system would perform in experiment as well as in simulation.

Appendix C

European Wave and Tidal Energy Conference 2019

The following pages contain a paper submitted for European Wave and Tidal Energy Conference (EWTEC) in September 2019 in Napoli, Italy. This overlaps with much of the material presented in Chapter 4.

Simulation of Digital Displacement Hydraulic Power Take-Off for Wave Energy Converters (February 2019)

Sarah Acheson, Ross Henderson and Daniil Dumnov

Abstract—**Designing a power take-off (PTO) for a wave energy converter (WEC) is a a serious technical challenge. Ideally a PTO would have smooth four-quadrant controllability, with high instantaneous power absorption across a broad range of incident wave periods and amplitudes, and efficient conversion to electricity. The Pelamis hydraulic PTO demonstrated many of these features, but the quantised nature of the applied PTO torque meant that the WEC response was not smooth and that instantaneous power absorption was reduced. Artemis Intelligent Power (AIP) have developed highly controllable and efficient hydraulic Digital Displacement®Pump Motors (DDPMs) which could be combined with the quantising features of the Pelamis PTO to give efficient, broad-band and smooth control. This concept is known as the Quantor PTO, and this paper presents the results of modelling the Quantor efficiency prior to testing. Across a range of four different input wave sets (including irregular seas) the simulated Quantor had an efficiency performance of between 64.7% and 70.9%. Primary conversion efficiencies were between 73.6% and 79.8%, and secondary conversion efficiencies were between 91 and 91.1%. Simulation results will subsequently be experimentally validated.**

Index Terms—**Power take-off, hydraulic, wave energy**

I. Introduction

DESPITE the availability of a large potential global wave energy resource (estimated at 2.11 ± 0.05 TW [1]), wave energy conversion has not yet been deployed on a large commercial scale, although many different types and designs of WEC have been proposed [2]. This is due to the many technical challenges involved in converting energy from a random, reversing, high force, low speed resource with very high peak to mean power ratios to synchronous, grid quality electricity [3]. The subsystem of a WEC which performs this conversion from mechanical motion of the device to electricity is the PTO.

PTO design is a core challenge of wave energy, as many of the technical difficulties of constructing a WEC culminate in this single subsystem. The desirable characteristics of a PTO include;

- Efficient instantaneous power absorption over a very broad range of wave amplitudes and periods
- Efficient conversion of variable instantaneous mechanical power to steady output electrical power
- Ability to efficiently handle power transferred at low speeds with high forces
- Responsive four-quadrant controllability of force and speed

This is not a full list of requirements as robustness to the marine environment, ease of assembly and maintenance, reliability and storm survivability and acceptable cost are also necessary to produce a commercially successful PTO [4], [5]. Hydraulic systems are a good candidate for meeting these requirements, as they are inherently well-suited to applications with high forces and torques at low speeds. In contrast, electrical systems struggle in this regime. They are capable of providing energy storage in the form of gas pressure accumulators, which enables the smoothing of peaks and troughs in the input power [3]. However the need for broad-band efficiency and precise four-quadrant controllability is not met by conventional hydraulics and novel approaches must be used to tackle these challenges. Conventional hydraulic transmissions can provide the variable load and flow required, but would need to be sized according to the maximum instantaneous power, which would mean that the average exported power would be in a very inefficient operating regime of the transmission [6]. For further detail on the challenges of WEC PTO design and the potential use of hydraulics, please see [7].

To maximise power extraction, an ideal PTO should be capable of control forces in a way which optimises the responses of the WEC in varying incident waves [8]. This generally means that the PTO should be able to both absorb and return energy to the WEC over the wave cycle to keep the system in resonance with the waves, so that the maximum power can be extracted and converted to electricity. Control of such reactive power flows was successfully demonstrated with full conversion efficiencies of 70% for a hydraulic PTO in Pelamis [9], but the 'quantised' PTO response meant that achieving continuous optimum PTO torque, as described in [8], was not possible.

Following the end of the Pelamis project, a proposal was put forward to combine the quantised PTO proven on Pelamis with a smaller continuously variable transmission of sufficient bandwidth to achieve the ideal continuous force control. The highly efficient, high bandwidth, hydraulic Digital Displacement pump motors (DDPMs) of AIP have the ability to act in combination with the quantised system to continually

This is paper ID 1283 submitted to the thematic track of grid integration, power and control. This work was supported in part by Wave Energy Scotland and by the EPSRC via the Industrial Doctoral Centre for Offshore Renewable Energy (IDCORE).

S. Acheson (an IDCORE student) and D. Dumnov work for Artemis Intelligent Power Ltd, Unit 3, Edgefield Industrial Estate, Loanhead EH20 9TB (e-mail: s.acheson@artemisip.com). R. Henderson works for Quoceant Ltd, Bonnington Bond, 2 Anderson Place, Edinburgh, EH6 5NP.

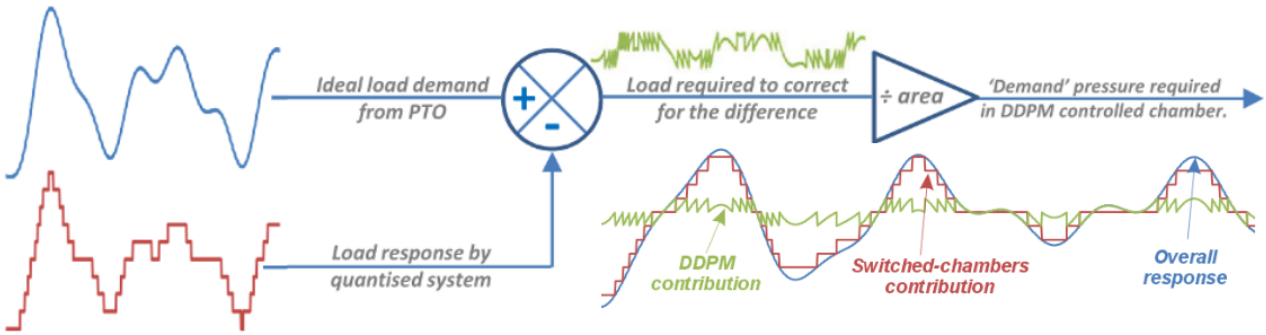

Fig. 1. Idealised Quantor concept taken from [4]. The error between the ideal load demand from the PTO (blue) and the load response from the quantised system (red) can be corrected using a DDPM capable of producing a rapidly changing load (green).

deliver the optimum continuous PTO force. (see [10] and [11] for an explanation of DD technology). This PTO concept is known as 'Quantor'.

Quoceant Ltd and AIP are working to develop and test the Quantor as part of a Wave Energy Scotland (WES) Stage 3 PTO project. A key deliverable of this project is the construction of a representative test rig, on which the Quantor can be experimentally tested. The test rig will have a 300kW motor which drives a flywheel with inertia of up to $973\,\mathrm{kg/m^2}$, which will provide a load representative of a WEC in irregular seas from which the Quantor will extract power. This project also involves building models of the Quantor, both for control strategy development and for efficiency modelling, the latter of which is presented here. For a discussion of the LCOE of Quantor, please see [4].

II. Description of Technology

The Quantor can be considered as an evolution of the Pelamis PTO. The Pelamis PTO used a novel digital approach to provide discrete set of net loads from pressurising or not pressurising individual piston areas. This 'quantised' system could approximate continuous control by choosing the number of discrete load steps which were enabled (pressurised) at any one time [6]. This system meant that absorbed power was transferred directly to (and from) the energy storage accumulators, so that instantaneous power absorption could be very high and absorbed power was decoupled from average exported power [12].

However, a disadvantage of this discretised system was that the PTO could only provide a quantised approximation to a continuous load, which limited the power absorption [6] and made the system inapplicable to low inertia WEC types where the quantised resolution would have been too coarse. A compromise is required between the WEC mass, the quantised step size, and the resulting distortion in control. Control strategies which could yield power or reliability performance improvements rely on continuously variable PTO force to achieve optimal power capture.

Adding a continuously controlled load of the same range as one or more of the quantised load steps would make it possible to achieve continuous control across the full load and power range. For this to work, the control of the continuously variable load must be fast enough to compensate for the step changes in the underlying quantised load [6]. Fig.1 shows the idealised Quantor concept combining a quantised system with a continuously controlled load, producing a smooth PTO load which can follow the ideal demand from the controller.

Fig. 2 shows a simple schematic of the Quantor PTO with a single degree-of-freedom WEC with linear hydraulic actuators (cylinders). These cylinders have multiple chambers, like those used in Pelamis. As the WEC moves in heave, the Quantor PTO system must provide the required PTO load for extracting power, consisting of both resistive and reactive components. The quantised chambers are connected via the digitally controlled chamber switching valves (housed in manifold blocks) to either the accumulator or to tank. This means they provide steps of force or torque as shown by the red line in Fig. 1. Hydraulic energy collected by these quantised chambers is buffered by the accumulator (a compliant energy store). Meanwhile, the continuously controlled chamber is connected to DDPM B, which provides the smoothing contribution (green line in Fig. 1) by controlling the chamber pressure at high bandwidth. This rapidly varying pressure signal from DDPM B results in an irregular torque on the common fixed-speed shaft, which is connected to generator and the opposing DDPM machine (DDPM A). The role of DDPM A is both to counteract this irregular torque, smoothing the output to the generator shaft; and to extract energy from the accumulator to provide a net power export.

III. Description of Model

A. Model Overview

Whilst the Quantor PTO could function with either linear (multi-chambered cylinders as in Pelamis) or rotary (fixed displacement pump-motors) actuators, rotary actuators were chosen for the Quantor test rig, as they were more appropriate for both the space available and the current WEC market. Whilst Fig. 2 shows a WEC with a linear system as an example, the modelling work treated a rotary system as this will be available for validation on the test rig. Fig.3 shows an overview of the energy flow through the system, characterised by key components, energy stores and

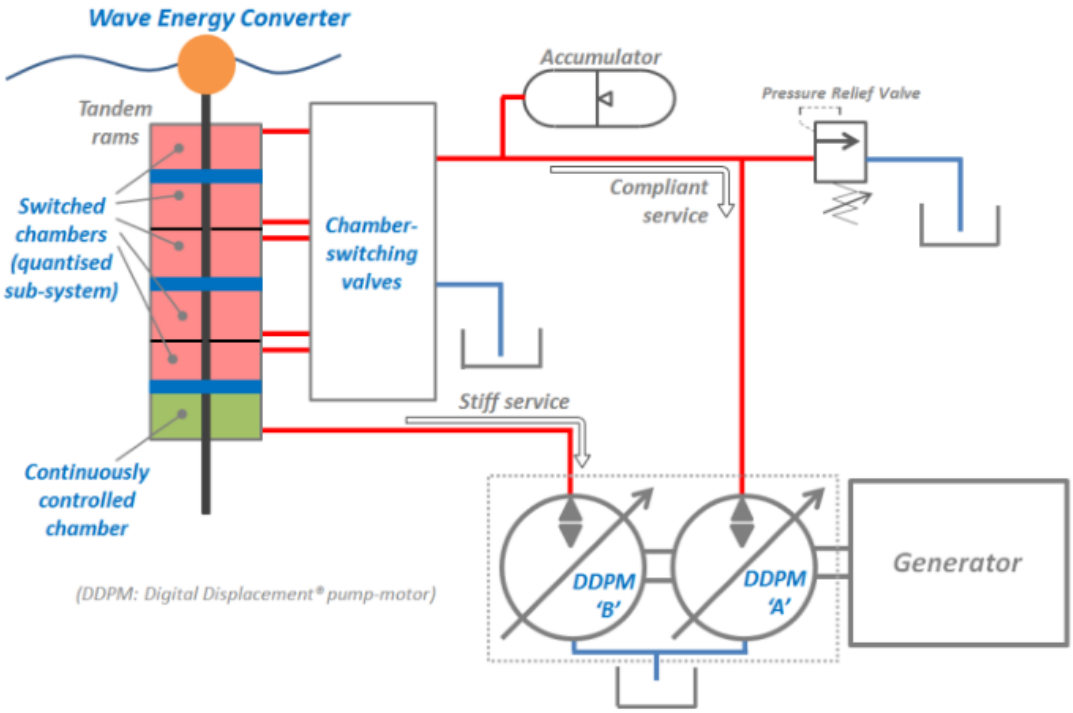

Fig. 2. Schematic of Quantor with linear actuator with single degree-of-freedom WEC. It should be noted that there is a manifold block containing switching valves connected to each chamber including the continuously controlled one, but it is omitted above to show the direct pressure control which DDPM B has over this chamber. [4]

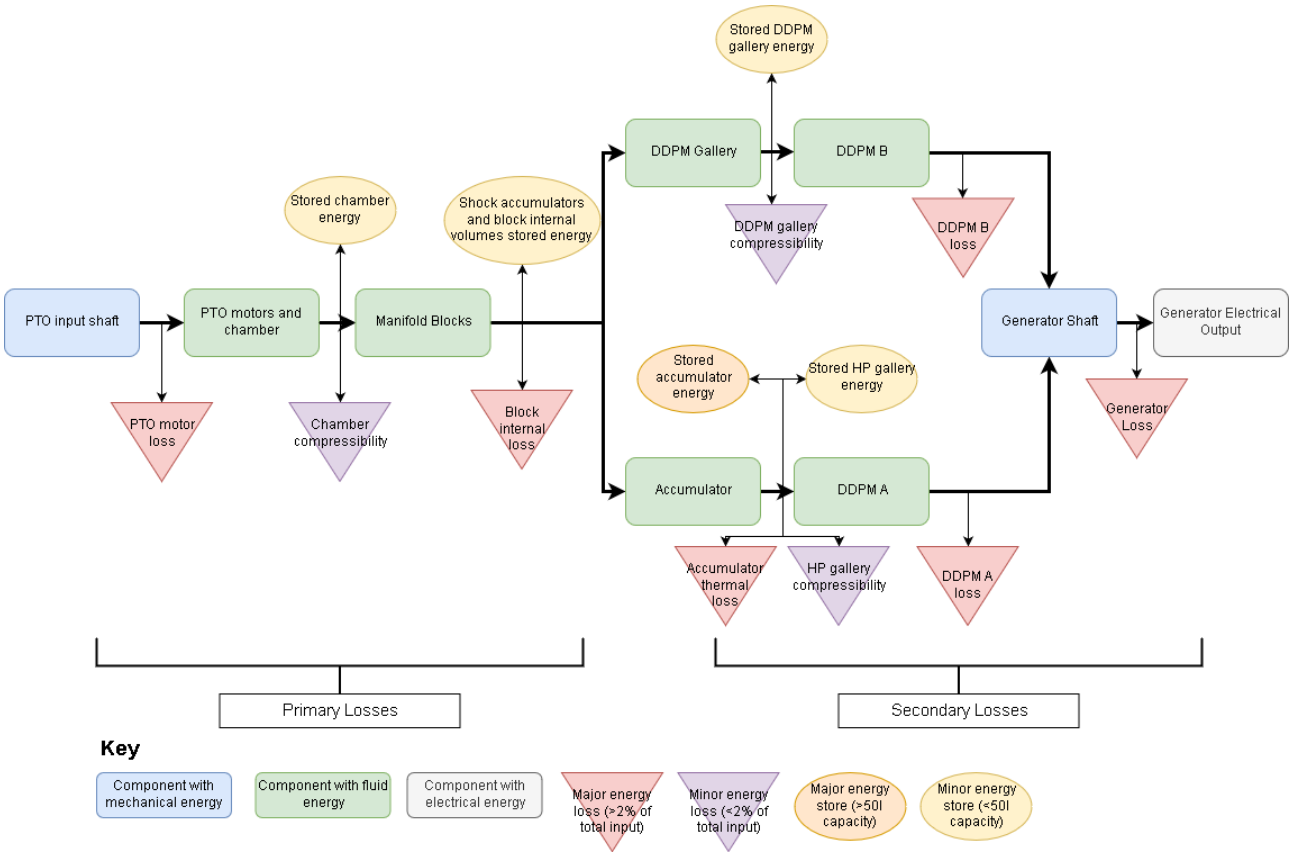

Fig. 3. Schematic of Quantor model structure, showing the flow of energy through key components, as well as the positions of energy stores and the energy losses measured at each stage in the model. The 'minor energy stores' are included in this figure because they are included in the model, but the energy stored in them is proportionally very small (0.4% or less) so it is assumed that any stored energy from these components is distributed pro rata to the remaining nodes.

248

measured losses in the model. The input to the system is the mechanical power on the PTO input shaft, which

is mechanically driven by the relevant WEC system (in this case, by a winch and ring gear). Losses in the specific WEC systems prior to the PTO are not included in this model. This input PTO shaft connects to the multiple (in this example, four) PTO motors which, as they convert mechanical energy to fluid energy, will give rise to the first major losses of the system, due to leakage and friction as explained in III-G. Rotating machines introduce substantial additional losses over hydraulic cylinders but offer flexibility for different WEC designs (e.g. winches and hinges). The chamber refers to the volume of fluid via which the motors connect to the manifold blocks, the pressure of which dictates the applied load of the actuator. For rotating motors this volume is dominated by connecting pipework; in the equivalent linear system, this would be dominated by the volume of the chamber inside the cylinder. Volumetric losses can result from energy used to pressurise the oil in the chambers then being vented to tank as part of the control process. Energy is then transferred to the manifold blocks, where it can be lost internally via flow losses, valve pressure drops and valve leakages. Due to the shock accumulators mounted on the blocks' HP galleries and the internal fluid volumes of the block, some energy may be stored in the blocks or even extracted from the energy stores in the blocks, for example if the charge of the shock accumulators is lower at the end of the simulation than at the start. Depending on the control of the valves in the manifold blocks, the oil may then flow into the DDPM gallery (the 'stiff service') or into the accumulator (called the compliant service because the quantised chambers are connected to an accumulator). In both of these galleries, energy may be stored or lost to hose compliance. The system to be tested on the rig has a precharge pressure of 150bar with an oil volume of up to 74l and gas back-up bottles of a further 75l. This is scalable to much larger storage volumes in line with the PTO as a whole. The two DDPMs then convert the stored hydraulic energy back into mechanical energy applied to the generator shaft, on which they are both mounted. This conversion incurs energy losses to the system as well, which are defined by the loss model described in III-F. In converting the received mechanical energy to electrical energy the generator is not perfectly efficient as explained in III-H.

The losses are divided into primary and secondary losses according to the method proposed in [12], where the main HP accumulator divides the system. The primary losses are those incurred in delivering energy from the PTO input to the accumulator and the secondary losses are those incurred in delivering energy from the accumulator to the generator. However since there are two services, only one of which has an accumulator, this definition is less obvious than in the Pelamis system. Particularly this is because DDPM A is carrying the transforming function of counteracting the irregular torque output of DDPM B by exchanging energy with the accumulator, whilst simultaneously extracting energy from the accumulator to drive the generator. The transforming function can be considered a primary conversion process, whilst exporting to the generator is a secondary conversion process. It is not possible to distinguish the primary and secondary DDPM A losses using this model, so an equal split is assumed. Therefore the PTO motor losses, valve block losses, hydraulic hose losses, DDPM B losses and half of the DDPM A losses make up the primary losses, and the remaining half of the DDPM A losses, and the generator losses make up the secondary losses.

It should be noted that energy does not necessarily always flow in the directions shown; all the hydraulic machines involved can transfer power in either direction. However the arrows in Fig.3 represent the primary direction of energy flow for electricity generation. Total PTO efficiency is defined as the ratio of the electrical energy generated to total mechanical energy available to the PTO from the wave induced WEC motion. This PTO efficiency does not include hydrodynamic or other losses in the WECs primary absorption mechanism.

The hydraulic system is simulated using Simscape, which is a physical modelling package within the Matlab/Simulink environment. The AIP DDPM loss models are built in Simulink.

B. PTO Control Strategy

The PTO control strategy chosen was reactive control with a spring term, as described in [7] by 1 where τ_{PTO} is the demanded PTO torque, c_{PTO} is the damping coefficient, ω is the rotational speed of the PTO shaft, k_{PTO} is the spring coefficient and θ is the angular position of the PTO shaft. The addition of the spring term means that the frequency response of the WEC can be shifted towards resonance in non-resonant conditions, improving net power absorption. The Quantor tested in the laboratory will have a maximum PTO torque of 1.4kNm but this could be easily increased by adding more fixed displacement motors to the system.

$$\tau_{PTO} = c_{PTO}\omega + k_{PTO}\theta \tag{1}$$

C. Wave and WEC model

The model was used to simulate a WEC with a Quantor PTO in both regular and irregular waves, of two different scales each. For the regular waves the simulation was 300s long and for irregular seas it was 512s long. The difference was because it was necessary to allow the regular simulation to reach a steady state, whereas for the irregular sea, 512s is a reasonable minimum length of time required for a representative range of waves from the chosen sea spectrum. The irregular waves were modelled using a JONSWAP spectrum with a gamma factor of 1 and timeseries were produced using the WAFO Matlab toolbox [13]. The details of each set of waves are given in Table III-C. The power per unit crest length (or wave energy flux per unit crest length in the case of irregular waves) is given by (2) for regular waves [14] and by (3) for irregular waves [15]. These were chosen such that there was both a low and high energy example of regular and irregular waves. R1 and I2 were very similar in terms of the wave energy density, and the four different wave sets

TABLE I
CHARACTERISTICS OF DIFFERENT INPUT WAVES USED FOR SIMULATION

Input Waves	T	T_p(s)	T_e (s)	H_s (m)	Wave power per unit crest length (kW/m)
Regular 1 (R1)	7.5			2.5	45.9
Regular 2 (R2)	8.5			3.5	102.1
Irregular 1 (I1)		7.7	6.6	2.5	20.2
Irregular 2 (I2)		9.1	7.8	3.5	46.9

provide a broad spread of input power per unit crest length.

$$P = \frac{\rho g^2}{32\pi} H_s^2 T \tag{2}$$

$$P = \frac{\rho g^2}{64\pi} H_s^2 T_e \tag{3}$$

The WEC was modelled using a one-dimensional linear hydrodynamic equation of motion. The WEC modelled was a simple heaving sphere of 4.5m diameter. The modelled architecture was a winch PTO system, attached to a ring gear, with the fixed displacement motors of the Quantor mounted on its circumference. This means the fixed displacement motors on the test rig to run at the same speed as they would on the simulated WEC, grounding the hardware-in-the-loop system in the reality of a sea deployment.

D. Valve Block Model

The manifold block has many functions within the Quantor, but the main purpose is that it connects the appropriate motor ports to either the HP gallery, DDPM gallery or LP gallery according to the real-time control algorithm. Each fixed displacement motor has its own corresponding manifold block to control its port connections. Each manifold block contains approximately forty valves, twelve of which are solenoid-operated and seven of which have tunable settings, such as adjustable needle valves.

The control valves were modelled as Simscape two-way directional valves controlled by two-position valve actuators, characterised by maximum area and opening. This assumes that the valve passage area is linearly dependent on control member displacement [16]. The Simscape valve models include important loss characteristics and have a user-specified transit time to simulate their dynamic behaviour. Dynamic behaviour due to spring loading and spool characteristics are omitted to keep complexity and simulation time manageable, given the large number of valve components in this system.

Experiments have been carried out on each valve type to characterise its performance in terms of opening time and pressurisation curves for the chambers connected to that valve. These experiments were used to tune the model parameters and match the model to test data. Fig 4 gives an example comparison between valve test data and the model. This valve block model will be further refined with data from the full test rig.

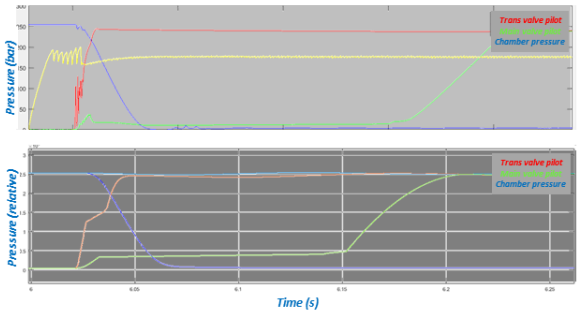

Fig. 4. Top: pressure data gathered showing two-stage depressurisation of a Quantor chamber, Bottom: model data of the same event after validation, with same time axis. The key comparisons are between the 'Trans valve pilot', 'Main valve pilot' and 'chamber pressure' curves.

E. Auxiliary Systems

The simulation of the hydraulic circuit includes all of the major hoses and piping connections between the hydraulic machines, manifold blocks and accumulators. The oil volumes within the galleries of the manifold blocks are also included, based on approximations derived from the manifold block design. The simulated hydraulic connections account for the bulk modulus of the oil volume in those connections (compliance), pressure drop due to the length and diameter of the connections, and in the case of hydraulic hoses, the additional compliance due to the expansion under pressure of the hose itself. Fluid inertia is omitted from this model since the purpose of this model is to study the performance and efficiency of the Quantor PTO, and the addition of fluid inertia to the hydraulic connections significantly increases the higher frequency dynamics of the system, and hence greatly slows down the simulation solution time without changing the overall system efficiency or performance. These higher order effects will of course be present on the test rig, and if they are significant then will need to be addressed. Since the hydraulic connections are fairly short it is not expected that inertial effects will present significant issues in practice. A single run in an irregular sea was carried out with and without fluid inertia and the results in terms of average power transferred at various key points in the model differed by a maximum of $0.02\,\mathrm{kW}$. Hydraulic accumulators are simulated using the standard polytropic gas model. A constant thermal efficiency value of 95% is used, assuming a foam-filled accumulator as described in [17].

The low pressure supply was modelled as reservoir of volume $2\,\mathrm{m}^3$ with a constant pressure of 5 bar. On the test rig the low pressure may vary more due to changing volumes of oil as chambers are depressurised but the low pressure accumulator is so large ($75\,\mathrm{l}$ accumulator with $975\,\mathrm{l}$ of gas back-up bottles) that this effect should be minor.

F. DDPM Model

The DDPMs were modelled using existing AIP Simulink models of their pumps, which are based on the loss model proposed by [10]. These are semi-empirical models based on test data collected from real

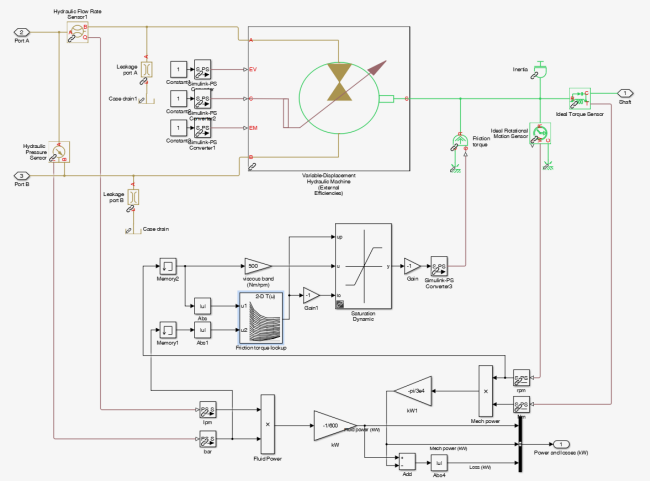

Fig. 5. Model of Poclain pump-motor, showing inclusion of leakage, friction torque and mechanical inertia.

machines at AIP. The loss models are based on data collected from machines operating as pumps, and it is assumed that the same losses apply for a machine acting as a motor. This is because all of the physical mechanisms of loss in the machine (leakage and friction) remain the same in motoring as in pumping and the duration of pressurisation of each cylinder in the machine is roughly the same in both cases. The model does account for the difference in effective displacement in pumping and motoring, since this is does have an impact on the overall ability to transmit power.

G. PTO Motor Model

The fixed displacement pump-motor selected for the test rig was a Poclain MS02 of $255\,\mathrm{cm}^3/\mathrm{rev}$. The manufacturer provided performance data which was used to model the friction torque and leakage, as shown in Fig. 5. It should be noted that any fixed displacement motor could be used in a rotary system. The system can be scaled up using much larger motors with similar efficiency characteristics. This particular model was chosen for its suitability to the rig-scale torques, speeds and flows, and for a real WEC of a different scale a different pump-motor may be more suitable.

The Simscape variable-displacement hydraulic machine block was chosen as this operates in both directions as a pump and a motor. However it was decided not to use its inbuilt 'external efficiencies' feature as efficiency curves often have very steep gradients at the corners of the map, causing problems with extrapolation and interpolation. Given we had measured data for output torque and leakage, it was a more direct approach to apply these to the shaft and the ports respectively. Hence the volumetric and mechanical efficiency of the motor were set to one, as was the displacement, as this is a fixed-displacement machine. For the leakage, a linear hydraulic resistance was used with a leakage corresponding to the manufacturer-supplied data. From the calculated friction torque, a lookup table was generated which was applied to the output shaft so that it reduced the output torque in both directions. The motor's internal inertia was also represented.

H. Generator

The electric generator on which the DDPMs are through-shafted was modelled very simply in Simulink, according to 4, where η is the provided motor manufacturer's estimated efficiency of 94.3%, ω is a constant generator speed of 1500rpm and τ is the total shaft torque, which is calculated by summing the torques of both DDPMs.

$$P = \eta\tau\omega \tag{4}$$

The reason this was simplified is that on the test rig to be used to validate the model, the measurement of output power will be the speed and torque on the generator shaft; not the electrical power generated. This is because the generator chosen for the test rig is not sized to the Quantor power regime but to give sufficient shaft diameter for the two DDPMs operating 'back-to-back' as a pump-motor test rig, making its electrical output unrepresentative of the intended WEC system. An induction motor has been used here so that testing can be carried out at different speeds if required, whereas a real WEC deployment would more likely use a synchronous generator. There is little doubt over the established efficiency of electrical generators operating at fixed speed, so this does not undermine the model validation.

IV. Model Results

The modelled Quantor showed the ability to perform in all four quadrants of force and speed, and smooth overall output torque could be achieved with careful tuning of the control parameters. Fig. 6 shows a Sankey diagram of the results from modelling sea state I2. The results are shown in percentages of the total input energy on the PTO shaft. The nodes correspond to those shown in Fig. 3, but those where the percentage of the total energy reaching them is less than 0.1% are omitted for clarity. The accumulator starts and finishes the model run at the same pressure, so there is no net change in its stored energy. Any residual energy in the minor energy stores is assumed to be used 'pro-rata' by the following nodes.

The model result for total electrical energy output is 68.6% of the input energy, with 22.5% going to primary losses and 8.9% going to secondary losses.

From Fig. 6 it is clear that the greatest energy loss in the system is the PTO motors at 8.4%, followed closely by the primary control losses at 8.0%. These elements handle most of the power and therefore are expected to induce a substantial proportion of the losses. As previously mentioned, the PTO motors were chosen for the test rig and may not be the best choice for any given WEC, so this loss could be changed by selecting PTO motors of appropriate specification for the application. Larger motors for higher power applications also offer higher efficiency. The option of using linear actuators instead of motors would also greatly improve the efficiency of this step. The primary control losses

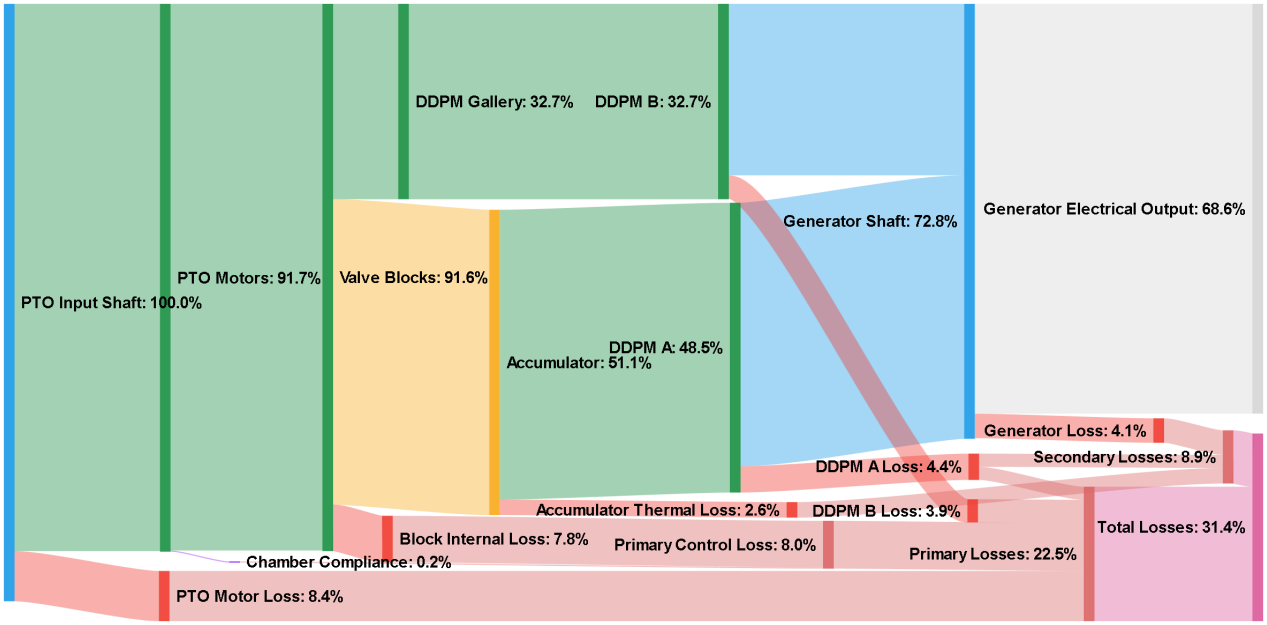

Fig. 6. Sankey diagram of model results of sea state I2, with energy flow going from left to right.

TABLE II
RESULTS OF MODELLING FOR DIFFERENT INPUT WAVES, IN TERMS OF AVERAGE INPUT POWER INCLUDING PRO-RATA ALLOCATION OF STORED ENERGY IN EFFICIENCY CALCULATION.

Input Waves	Average Model Input Power (kW)	Average Generated Power (kW)	Average Stored Power (kW)	Average Lost Power (kW)	Quantor Efficiency (%)
R1	40.3	28.4	0	11.9	70.5
R2	53.5	37.9	0.1	15.6	70.9
I1	25.9	16.8	0	9.2	64.7
I2	37.5	25.8	0.5	11.2	68.6

comprise the loss caused by depressurising chambers and venting to tank, chamber compliance and losses within the valve block. The block internal losses could possibly be reduced by choosing different valves with lower pressure drops and by redesigning some internal galleries. Data from the test rig (e.g. pressure measurements along the flow paths) will allow refinement of the flow loss coefficients for the valves.

The DDPM losses are the next most significant losses at 4.4% of the total on machine A and 3.9% on machine B. These are significantly impacted by the operating point of each machine in the chosen input waves. Depending on the operating point, DDPMs have shown efficiencies at 1500rpm (the chosen speed for the DDPMs on the test rig) ranging from 91% to 97% [10]. Generally the higher the displacement, the more efficiently the machine operates. The average efficiency over this simulation run for DDPM A was 90.9% and for DDPM B was 87.9%. This is because the machines are operating at a lower average power than the optimum, particularly DDPM B. DDPM B has to operate at very low pressures and displacements due to the need for torque exerted by the stiff service to regularly pass through zero, which means the stiff service pressure must go as close to the LP system pressure as possible.

Table IV shows the key model results for all four wave sets in terms of average power input, stored, generated and lost, as well as the percentage efficiency. This percentage assumes that the stored power displayed in the table would be extracted through the generator 'pro-rata', were it to be used. Despite the large variation in the power density of the input waves (between 20 and 100 kW/m), the Quantor efficiency varies by only approximately 6%, with 64.7% being the minimum and 70.9% being the maximum.

The results for R1 and R2 are very similar in terms of efficiency and loss breakdown (see Fig. 7). This is because both wave sets are using the full range of the Quantor system, and in R2, which is the higher energy wave set, the PTO load is fully saturated at the peak where the PTO motors cannot exert any more torque. It is encouraging to note that once the full load range of the Quantor is exercised, saturation did not lead to excessive losses, which suggests that the Quantor could operate in saturation conditions in the sea. The PTO motor losses are higher in R2 than R1, due to flow losses and also due to partially bypassing of the DDPM while saturated and hence shedding a proportion of the bypassed energy as the

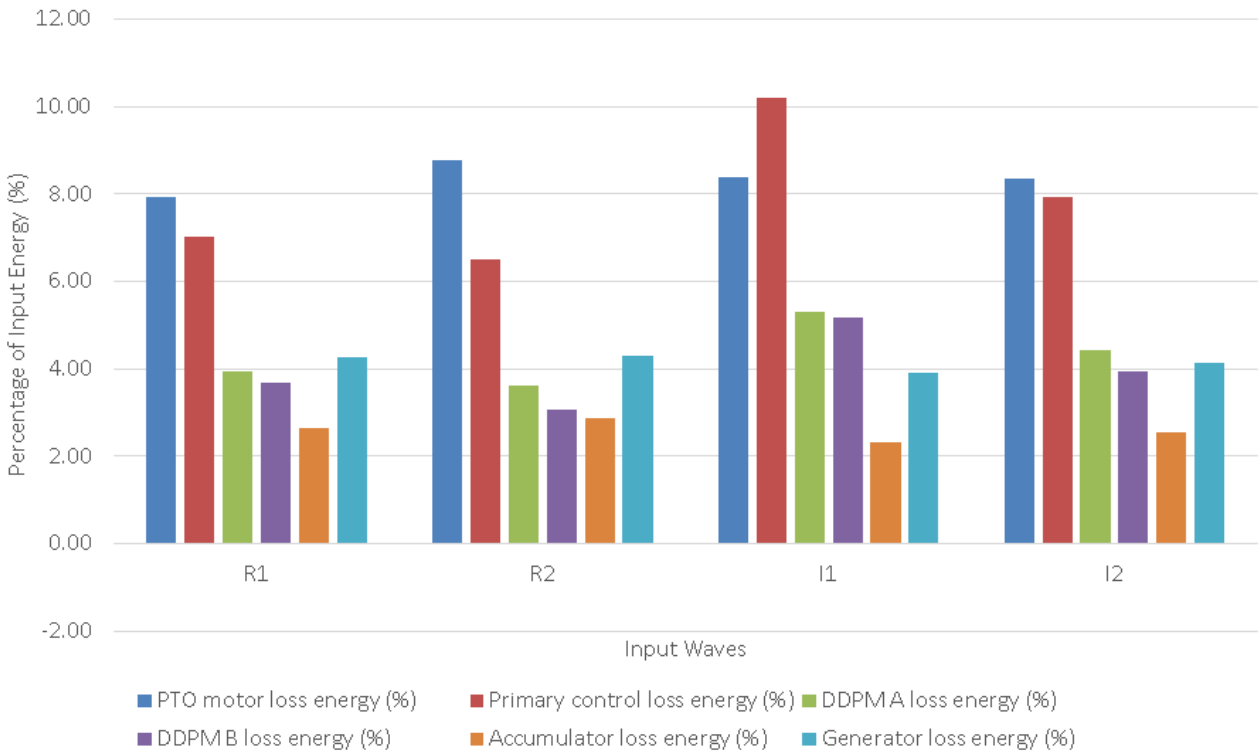

Fig. 7. Bar chart showing breakdown of energy lost for each wave input as a percentage of the total input shaft energy

pressure drops from the DDPM 'overdrive' pressure to the accumulator pressure. However the block losses and DDPM losses are slightly lower proportionally in this case. For the DDPMs this is because they are able to reach a more efficient operating point as they work with higher displacement.

I1 and I2 results show more variation, despite being closer in power density than R1 and R2. The efficiency of the Quantor in I2 is approximately 3.9% higher than I1. From Fig. 7 it is clear that the block internal losses are the major contributor to this difference, as they are proportionally much higher for I1. This is because a lower energy sea state involves more zero-crossings in the applied PTO torque, relative to the power extracted. In the case of the Quantor, this means that more valve transitions are involved as the direction of the PTO torque changes. In the quantised service a loss occurs every time a chamber is vented from high pressure to low pressure, which is every time the applied quantised moment is stepped down in magnitude. A similar loss occurs in the continuous service because during load reversals the continuously controlled chambers must vent any residual pressure between the minimum DDPM pressure and the tank pressure. During this simulation, the DDPM was assumed to be able to reliably control pressure to a minimum of 30bar, which must be verified in the lab. The DDPM losses reduce in I2 as they deliver higher average flows.

An interesting comparison is between R1 and I2, which have similar wave power densities (45.9 and 46.9 kW/m of crest length respectively). The Quantor is only 1.9% less efficient in I2 than in R1, which demonstrates that it can cope well with the varying loads without prior knowledge of the incoming waves. Again, this difference is likely caused by the requirement for more zero-crossings and valve transitions in the irregular sea state. The primary and secondary conversion efficiencies of the Quantor in each set of input waves are shown in Fig. PTO 8. In all cases the secondary conversion efficiency is higher than the primary conversion efficiency, and varies very little between sea states, remaining around 91.1%. The primary conversion efficiencies for the regular waves are both over 79%, whereas they are 73.6% and 77.6% for I1 and I2 respectively. As discussed above, a different choice of PTO motor and lowering the minimum pressure on the stiff service may improve the primary conversion efficiency. The peak value of primary conversion efficiency of 79.9% is lower than that of 91.5% reported in [18] in irregular waves for a discrete displacement cylinder (DDC) system which was tested experimentally. The efficiency impact of rotary actuators compared to linear actuators may explain this difference.

[12] reports primary conversion efficiencies of over 80% which is higher than the results for the Quantor. The total wave-to-wire efficiency for Pelamis was over 70% [9], with a secondary conversion efficiency of approximately 90% for the P2 Pelamis. The primary conversion efficiency of the Quantor PTO cannot feasibly be as high as that of the Pelamis because the continuously controlled service inherently has higher losses than the quantised service. However the continuous control should benefit the instantaneous power absorption and WEC control over the pure quantised control.

Fig. 9 shows the percentage of input energy which is delivered through the quantised (A) and continuous

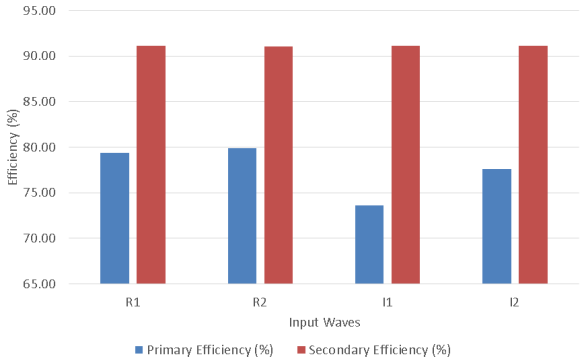

Fig. 8. Bar chart showing efficiency of primary and secondary conversion for each set of input waves.

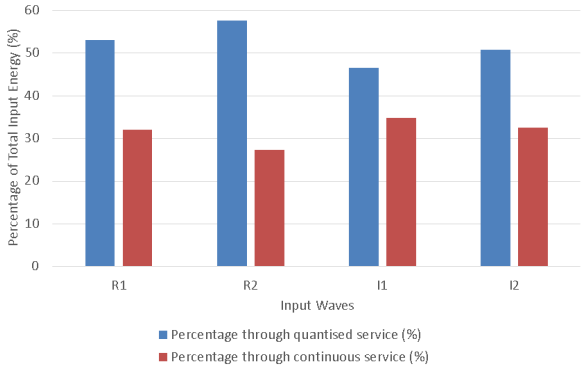

Fig. 9. Bar chart showing proportion of total input energy delivered through A (quantised) service and B (continuous) service.

(B) services. The more energy that passes through the quantised service and the less through the continuous service, the higher the primary conversion efficiency. This is because DDPM B is generally at a less efficient operating point than DDPM A because it must go to lower displacements. The accumulator also acts as an energy store for the quantised service, but DDPM B must either instantaneously absorb the power available from the continuous service or lose it, as this service is very stiff. This result suggests that it is desirable for the quantised service to handle as much of the load as possible, with the continuous service only smoothing the response.

In addition to the detailed models described above, a simplified model was constructed to explore the power curve of the Quantor in irregular seas in a more computationally efficient way. This was identical to the previous model except that the pipe and hose connections (except for those to the chambers where the compliance is critical) were removed to improve the speed of the model. Fig. 10 shows the results from this model, and a comparison with the above-mentioned results of the detailed model. It is clear that the simple model predicts slightly higher efficiencies than the detailed model. It seems that the efficiency drops off steeply below 10 kW. The simple model predicts an efficiency of nearly 80% with an average input power of 59 kW. It is possible that once the PTO is saturated, DDPM B need only provide a constant high pressure, rather than a rapidly varying pressure control signal, which is a more efficient operating point. However

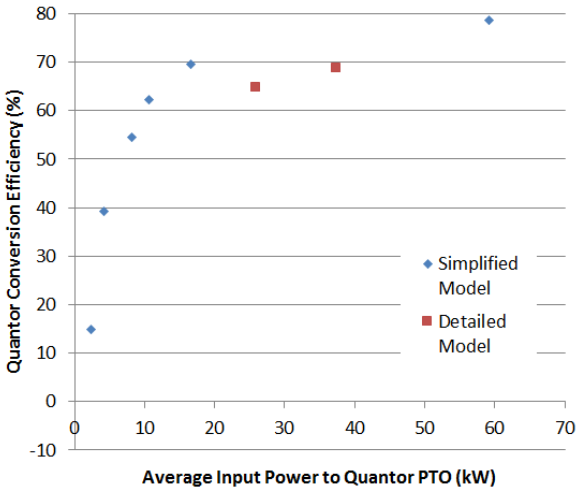

Fig. 10. Graph of modelled Quantor conversion efficiency against average input power in irregular seas from two models: one detailed and one simplified.

the discrepancy between the results of the simple and detailed model, and the need for validation means that this result must be treated with caution, until the model can be validated using the test rig.

V. Model Evaluation

Valve opening times and pressurisation curves have already been validated with experimental data from a prototype manifold block. The PTO motor model is based on measured data from the manufacturers. The DDPM loss models are well-validated for pumping, and it is assumed that the motoring losses are the same since the loss mechanisms in this mode are the same. The auxiliary systems are difficult to model realistically, but every effort was made to accurately represent the physical dimensions and compliance of hydraulic connections. Fluid inertia was ignored as it would have been very computationally expensive to include, so this means that some transient effects may be missing. This was justified by carrying out a single model run in irregular seas with and without fluid inertia, which showed that the effect of fluid inertia on the average power transferred by key model components was very small. Whilst reasonable effort has been made to accurately model the hydraulic detail of the Quantor PTO, the true test of the model accuracy will be experimental validation on the test rig. The model may then be confidently extrapolated to larger rated powers and loads, and to different architectures. It is also anticipated that a validated simplified model of the PTO will allow rapid integration into third party WEC models for development of detailed WEC designs and control strategies.

VI. Conclusions and Further Work

A Simulink model of the Quantor PTO was constructed, which combines the quantising principle of the Pelamis PTO with AIP's DDPM machines. This combination should allow fully reactive WEC control, with the applied PTO torque smoothly matching

the demand, while power is transmitted and converted with an efficiency similar to that of the quantised system. Reactive control and smooth PTO torque were shown in the detailed model, although obtaining smooth PTO torque required careful tuning of the control parameters. The detailed modelling of the hydraulics and mechanical systems allowed the various losses to be quantified at each stage of the power transmission. The Quantor PTO was simulated in a range of input waves, both regular and irregular, covering a wide range of power densities. The overall efficiency of the Quantor varies between 64.7% and 70.9%, which is very stable considering the variety in the input wave conditions. The Quantor performs well in irregular waves, with efficiency decreasing by only 2% between a regular and irregular wave set of similar power density. The largest sources of loss are the primary motors and the manifold blocks controlling flow to and from these motors, with the DDPM machines next. The easiest of these to improve is the primary motors where flow losses may be reduced with alternative choices. A system using linear actuators would have substantially lower primary losses, but would introduce end-stops and pressure shocks due to the larger chamber volume.

The Quantor performs more efficiently if a greater proportion of the energy is transferred through the quantised service and a smaller proportion is transferred through the continuous service. The Quantor system modelled here, and about to be physically tested, uses only 4 motors altogether, whereas an applied WEC system could use a larger number of motors with a commensurately larger proportion of energy being transmitted by the quantised service, which would offer increased efficiency. The primary conversion efficiency is slightly lower than that measured in previous studies of linear actuators, whilst the secondary conversion efficiency seems comparable to that of Pelamis.

An experimental study of a Quantor prototype which will allow model refinement and validation is the most important piece of further work. A test rig is currently being commissioned on AIP's premises to enable this. A flywheel of significant inertia will be driven by an electric motor to emulate the hydrodynamic excitation and dynamic response of a WEC in regular and irregular waves. A Quantor PTO, matching that modelled, will be tested on this rig, extracting power from the emulated WEC and demonstrating combined quantised and continuous control. The data gathered will be invaluable for confirming the viability and efficiency of the Quantor PTO, and therefore its potential usefulness for WEC applications. There is also the possibility of simulating different fixed-displacement PTO motors, as well as simulating linear primary actuators. Different power ratings and architectures may also be extrapolated using the validated model elements. Control is another avenue for further work; once the model is fully validated new control features can be developed in the model environment.

ACKNOWLEDGEMENT

The authors gratefully acknowledge the support of Wave Energy Scotland and the EPSRC via the IDCORE programme.

REFERENCES

[1] K. Gunn and C. Stock-Williams, "Quantifying the global wave power resource," *Renewable Energy*, vol. 44, pp. 296–304, 2012. [Online]. Available: http://dx.doi.org/10.1016/j.renene.2012.01.101

[2] H. L. Bailey, "The effect of a nonlinear Power Take Off on a Wave Energy Converter," Ph.D. dissertation, University of Edinburgh, 2009. [Online]. Available: http://hdl.handle.net/1842/5741

[3] S. H. Salter, J. R. M. Taylor, and N. J. Caldwell, "Power conversion mechanisms for wave energy," *Proceedings of the I MECH E Part M*, vol. 216, no. 1, pp. 1–27, 2002. [Online]. Available: http://www.ingentaselect.com/rpsv/cgi-bin/cgi?ini=xref{\&}body=linker{\&}reqdoi=10.1243/147509002320382112

[4] Artemis Intelligent Power Ltd, "Hybrid Digital Displacement ® hydraulic PTO for wave energy WES Power Take Off Public Report," Tech. Rep., 2017. [Online]. Available: https://library.waveenergyscotland.co.uk/development-programmes/power-take-off/stage-2/pt21{_}art/

[5] R. Henderson, J. Macpherson, and J. Taylor, "Wave Energy Power Take-Off Competition Milestone 2 report " Hybrid Digital Displacement ® hydraulic PTO for wave energy "," Tech. Rep. January, 2016.

[6] J. Taylor and R. Henderson, "Wave Energy Power Take-Off Competition Milestone 1 report " Hybrid Digital Displacement ® hydraulic PTO for wave energy "," Tech. Rep. December, 2015.

[7] R. H. Hansen, *Aalborg Universitet Design and Control of the PowerTake-Off System for a Wave Energy Converter with Multiple Absorbers Hansen , Rico Hjerm Publication date :*, 2013.

[8] W. Sheng, R. Alcorn, and A. Lewis, "On improving wave energy conversion, part I: Optimal and control technologies," *Renewable Energy*, vol. 75, pp. 922–934, 2015. [Online]. Available: http://dx.doi.org/10.1016/j.renene.2014.09.048

[9] R. Yemm, D. Pizer, C. Retzler, and R. Henderson, "Pelamis: experience from concept to connection," *Philosophical Transactions of the Royal Society A: Mathematical, Physical and Engineering Sciences*, vol. 370, pp. 365–380, 2012.

[10] N. J. Caldwell, "Digital Displacement Hydrostatic Transmission Systems," Ph.D. dissertation, University of Edinburgh, 2007.

[11] W. H. S. Rampen, "The Digital Displacement Hydraulic Piston Pump," Ph.D. dissertation, University of Edinburgh, 1992.

[12] R. Henderson, "Design, simulation, and testing of a novel hydraulic power take-off system for the Pelamis wave energy converter," *Renewable Energy*, vol. 31, no. 2, pp. 271–283, 2006.

[13] E. No TitBrodtkorb, P.A., Johannesson, P., Lindgren, G., Rychlik, I., Rydén, J. and Sjö, "WAFO - a Matlab toolbox for analysis of random waves and loads," in *Proceedings of the 10th International Offshore and Polar Engineering Conference*, Seattle, 2000, pp. 343–350.

[14] J. Falnes, "A review of wave-energy extraction," *Marine Structures*, vol. 20, no. 4, pp. 185–201, 2007.

[15] A. F. Falcão and J. C. Henriques, "Effect of non-ideal power take-off efficiency on performance of single- and two-body reactively controlled wave energy converters," *Journal of Ocean Engineering and Marine Energy*, vol. 1, no. 3, pp. 273–286, 2015.

[16] Matlab, "2-way Directional Valve." [Online]. Available: https://uk.mathworks.com/help/releases/R2015b/physmod/hydro/ref/2waydirectionalvalve.html?searchHighlight=2waydirectionalvalve

[17] A. Pourmovahed, S. Baum, F. Fronczak, and N. Beachley, "Experimental evaluation of hydraulic accumulator efficiency with andwithout elastomeric foam," *Journal of Propulsion and Power*, vol. 4, no. 2, pp. 185–192, 1988.

[18] R. H. Hansen, T. O. Andersen, H. C. Pedersen, and A. H. Hansen, "Control of a 420kN Discrete Displacement Cylinder drive for the Wavestar energy converter," in *Proceedings of the ASME/BATH 2014 Symposium on Fluid Power & Motion Control*, Bath, UK, sep 2014, pp. 1–10. [Online]. Available: http://proceedings.asmedigitalcollection.asme.org/pdfaccess.ashx?url=/data/conferences/asmep/81754/

References

[1] R. Henderson, "Design, simulation, and testing of a novel hydraulic power take-off system for the Pelamis wave energy converter," *Renewable Energy*, vol. 31, no. 2, pp. 271–283, 2006.

[2] Artemis Intelligent Power Ltd, "Hybrid Digital Displacement ® hydraulic PTO for wave energy WES Power Take Off Public Report," Wave Energy Scotland, Tech. Rep., 2017. [Online]. Available: https://library.waveenergyscotland.co.uk/development-programmes/power-take-off/stage-2/pt21{_}art/

[3] Artemis Intelligent Power Ltd and Quoceant Ltd, "Quantor hybrid hydraulic PTO Stage 3 Milestone M1 Report," Wave Energy Scotland, Tech. Rep. July, 2017.

[4] T. Heath, "The Development and Installation of the Limpet Wave Energy Converter," in *World Renewable Energy Congress VI*, A. Sayigh, Ed., Brighton, UK, jul 2000, pp. 1619–1622. [Online]. Available: http://www.sciencedirect.com/science/article/pii/B9780080438658505183

[5] N. Johnson and E. Olson, "Wells Turbine Demonstration," 2010. [Online]. Available: https://owcwaveenergy.weebly.com/our-demonstrations.html

[6] M. Prado and H. Polinder, "Case study of the Archimedes Wave Swing (AWS) direct drive wave energy pilot plant," in *Electrical Drives for Direct Drive Renewable Energy Systems*. Woodhead Publishing Limited, 2013, pp. 195–218. [Online]. Available: http://dx.doi.org/10.1533/9780857097491.2.195

[7] R. Hart, "A Goodbye to the P2 Pelamis," 2016. [Online]. Available: https://www.quoceant.com/single-post/2016/03/18/A-Goodbye-to-the-P2-Pelamis

[8] Quoceant Ltd, "Power Take-Off: Non Confidential Summary Report," Wave Energy Scotland, Tech. Rep. April, 2016. [Online]. Available: https://library.waveenergyscotland.co.uk/knowledge-capture/se01{_}quo/se01{_}quo{_}er-wp2-pto/

[9] R. Yemm, D. Pizer, C. Retzler, and R. Henderson, "Pelamis: experience from concept to connection," *Philosophical Transactions of the Royal Society A: Mathematical, Physical and Engineering Sciences*, vol. 370, pp. 365–380, 2012.

[10] M. M. Kramer, L. Marquis, and P. Frigaard, "Performance Evaluation of the Wavestar Prototype," in *9th European Wave and Tidal Energy Conference*, Southampton, UK, September 2011.

[11] R. H. Hansen, T. O. Andersen, H. C. Pedersen, and A. H. Hansen, "Control of a 420kN Discrete Displacement Cylinder drive for the Wavestar energy converter," in *Proceedings of the ASME/BATH 2014 Symposium on Fluid Power & Motion Control*, Bath, UK, September 2014, pp. 1–10. [Online]. Available: http://proceedings.asmedigitalcollection.asme.org/pdfaccess.ashx?url=/data/conferences/asmep/81754/

[12] R. H. Hansen, "Aalborg Universitet Design and Control of the PowerTake-Off System for a Wave Energy Converter with Multiple Absorbers Hansen , Rico Hjerm Publication date :," Ph.D. dissertation, 2013.

[13] N. J. Caldwell, "Digital Displacement Hydrostatic Transmission Systems," Ph.D. dissertation, University of Edinburgh, 2007.

[14] R. E. Dorey, "Modelling of losses in pumps and motors," in *First Bath International Fluid Power Workshop: Design, Modelling and Control of Pumps*, Bath, UK, September 1988, pp. 71–97.

[15] K. L. De Koker, G. Crevecoeur, B. Meersman, M. Vantorre, and L. Vandevelde, "A wave emulator for ocean wave energy, a Froude-scaled dry power take-off test setup," *Renewable Energy*, vol. 105, pp. 712–721, 2017. [Online]. Available: http://dx.doi.org/10.1016/j.renene.2016.12.080

[16] UMBRA Group, "Reciprocating Ball Screw Generator (ReBaS) WES Power Take Off," 2017.

[17] R. Henderson, A. Latham, J. Macpherson, R. Yemm, and J. Taylor, "Wave Energy Power Take-Off Competition Milestone 5 Report," Wave Energy Scotland, Tech. Rep. June, 2016.

[18] R. Henderson, J. Macpherson, and J. Taylor, "Wave Energy Power Take-Off Competition Milestone 2 report " Hybrid Digital Displacement ® hydraulic PTO for wave energy "," Wave Energy Scotland, Tech. Rep. January, 2016.

[19] R. Henderson, J. Macpherson, D. Pizer, R. Yemm, and J. Taylor, "Wave Energy Power Take-Off Competition Milestone 4 report," Wave Energy Scotland, Tech. Rep. May, 2016.

[20] A. Dole, C. Gibson, R. Henderson, A. Latham, J. Macpherson, R. Yemm, and J. Taylor, "Wave Energy Power Take-Off Competition Milestone Report 6 (final) The Quantor hybrid Digital Displacement ® hydraulic PTO for wave energy," Wave Energy Scotland, Tech. Rep. November, 2016.

[21] Artemis Intelligent Power Ltd and Quoceant Ltd, "Quantor hybrid hydraulic PTO Stage 3 Milestone M6 Report," Wave Energy Scotland, Tech. Rep. March, 2019.

[22] Artemis Intelligent Power Ltd and Quoceant Ltd, "Quantor hybrid hydraulic PTO Stage 3 Milestone M4-B Report," Wave Energy Scotland, Tech. Rep. August, 2018.

[23] Artemis Intelligent Power Ltd and Quoceant Ltd, "Quantor hybrid hydraulic PTO Stage 3 Milestone M4-C Report," Wave Energy Scotland, Tech. Rep. March, 2019.

[24] Artemis Intelligent Power Ltd and Quoceant Ltd, "Quantor hybrid hydraulic PTO Stage 3 Milestone M5 Report," Wave Energy Scotland, Tech. Rep. January, 2019.

[25] E. S. Arrhenius, Svante; Holden, "On the Influence of Carbonic Acid in the Air Upon the Temperature of the Earth," *Publications of the Astronomical Society of the Pacific*, vol. 9, no. 54, pp. 14–24, 1897.

[26] G. S. Callendar, "The Artificial Production of Carbon Dioxide and its Influence on Temperature," *Quarterly Journal of the Royal Meteorological Society*, pp. 223–240, 1938.

[27] C. Parmesan and G. Yohe, "A globally coherent fingerprint of climate change impacts across natural systems," *Nature*, vol. 421, pp. 37–42, 2003.

[28] M. T. Taye, E. Dyer, F. Hirpa, and K. Charles, "Climate change impact on water resources in the Awash basin , Ethiopia," *Water*, vol. 20, p. 4491, 2018.

[29] A. G. Koutroulis, I. K. Tsanis, I. N. Daliakopoulos, and D. Jacob, "Impact of climate change on water resources status: A case study for Crete Island, Greece," *Journal of Hydrology*, vol. 479, pp. 146–158, 2013. [Online]. Available: http://dx.doi.org/10.1016/j.jhydrol.2012.11.055

[30] J. Fuhrer and P. J. Gregory, *Climate Change Impact and Adaptation in Agricultural Systems: Soil Ecosystem Management in Sustainable Agriculture*, 2014. [Online]. Available: http://books.google.co.zw/books?id=FseWBAAAQBAJ

[31] International Energy Agency, "World Balance 2017," 2017. [Online]. Available: https://www.iea.org/Sankey/{\#}?c=World{\&}s=Balance

[32] K. Gunn and C. Stock-Williams, "Quantifying the global wave power resource," *Renewable Energy*, vol. 44, pp. 296–304, 2012. [Online]. Available: http://dx.doi.org/10.1016/j.renene.2012.01.101

[33] Carbon Trust and AMEC Environment & Infrastructure UK Limited, "UK Wave Energy Resource," Tech. Rep., 2012. [Online]. Available: https://www.carbontrust.com/media/202649/ctc816-uk-wave-energy-resource.pdf

[34] Department for Transport, "The Road to Zero: Next steps towards cleaner road transport and delivering our Industrial Strategy," Tech. Rep. July, 2018.

[35] G. Strbac, D. Pudjianto, R. Sansom, P. Djapic, H. Ameli, N. Shah, and A. Hawkes, "Analysis of Alternative UK Heat Decarbonisation Pathways For the Committee on Climate Change," Tech. Rep. June, 2018.

[36] J. Leijon and C. Boström, "Freshwater production from the motion of ocean waves – A review," *Desalination*, vol. 435, no. October 2017, pp. 161–171, 2018. [Online]. Available: https://doi.org/10.1016/j.desal.2017.10.049

[37] J. Falnes, "A review of wave-energy extraction," *Marine Structures*, vol. 20, no. 4, pp. 185–201, 2007.

[38] J. Cruz, *Ocean Wave Energy: Current Status and Future Perspectives*. Berlin: Springer, 2008.

[39] H. L. Bailey, "The effect of a nonlinear Power Take Off on a Wave Energy Converter," Ph.D. dissertation, University of Edinburgh, 2009. [Online]. Available: http://hdl.handle.net/1842/5741

[40] S. Salter, J. Taylor, and N. J. Caldwell, "Power conversion mechanisms for wave energy," *Proceedings of the I MECH E Part M*, vol. 216, no. 1, pp. 1–27, 2002. [Online]. Available: http://www.ingentaselect.com/rpsv/cgi-bin/cgi?ini=xref{\&}body=linker{\&}reqdoi=10.1243/147509002320382112

[41] S. Salter, "Wave energy: Nostalgic Ramblings, future hopes and heretical suggestions," *Journal of Ocean Engineering and Marine Energy*, vol. 2, no. 4, pp. 399–428, 2016. [Online]. Available: http://link.springer.com/10.1007/s40722-016-0057-3

[42] J. Taylor and R. Henderson, "Wave Energy Power Take-Off Competition Milestone 1 report " Hybrid Digital Displacement ® hydraulic PTO for wave energy "," Wave Energy Scotland, Tech. Rep. December, 2015.

[43] W. Sheng, R. Alcorn, and A. Lewis, "On improving wave energy conversion, part I: Optimal and control technologies," *Renewable Energy*, vol. 75, pp. 922–934, 2015. [Online]. Available: http://dx.doi.org/10.1016/j.renene.2014.09.048

[44] Artemis Intelligent Power Ltd and Quoceant Ltd, "Quantor hybrid hydraulic PTO WES PTO Stage 3 Public Report," Wave Energy Scotland, Tech. Rep., 2019. [Online]. Available: https://library.waveenergyscotland.co.uk/media/1319/pt32{_}art{_}wes-public-report.pdf

[45] Artemis Intelligent Power Ltd and Quoceant Ltd, "Quantor hybrid hydraulic PTO – Stage 3 Milestone ' M0 0 ' Report," Wave Energy Scotland, Tech. Rep. July, 2017.

[46] Artemis Intelligent Power Ltd, "Artemis Company History," 2018. [Online]. Available: http://www.artemisip.com/company/history/

[47] Artemis Intelligent Power Ltd and Danfoss, "Danfoss to build low-carbon global manufacturing facility for Artemis technology," 2018. [Online]. Available: http://www.artemisip.com/danfoss-to-build-low-carbon-global-manufacturing-facility-for-artemis-technology/

[48] Quoceant Ltd, "Our Projects," 2018. [Online]. Available: https://www.quoceant.com/projects

[49] B. Dickens, R. Yemm, and R. Henderson, "System Performance & Reliability of the P2 PTO," Wave Energy Scotland, Tech. Rep. April, 2016.

[50] B. Drew, A. Plummer, and M. N. Sahinkaya, "A review of wave energy converter technology," *Journal of Power and Energy*, vol. 223, pp. 887–902, 2009. [Online]. Available: http://dx.doi.org/10.1243/09576509JPE782

[51] A. F. Falcão and J. C. Henriques, "Oscillating-water-column wave energy converters and air turbines: A review," *Renewable Energy*, vol. 85, pp. 1391–1424, 2016.

[52] M. Mueller, "Electrical generators for direct drive wave energy converters," *IEE Proceedings - Generation, Transmission and Distribution*, vol. 149, no. 4, p. 446, 2002.

[53] R. Alcorn and D. O'Sullivan, *Electrical design for ocean wave and tidal energy systems*. London: The Institution of Engineering and Technology, 2013. [Online]. Available: http://cds.cern.ch/record/1641804

[54] EMEC Ltd, "Pelamis Wave Power." [Online]. Available: http://www.emec.org.uk/about-us/wave-clients/pelamis-wave-power/

[55] Quoceant Ltd, "Non-Confidential Summary of Modelling WECs," Wave Energy Scotland, Tech. Rep. April, 2016.

[56] R. H. Hansen, T. O. Andersen, and H. C. Perdersen, "Analysis of discrete pressure level systems for Wave Energy Converters," *Proceedings of 2011 International Conference on Fluid Power and Mechatronics*, pp. 552–558, 2011.

[57] R. H. Hansen, M. M. Kramer, and E. Vidal, "Discrete displacement hydraulic power take-off system for the Wavestar wave energy converter," *Energies*, vol. 6, no. 8, pp. 4001–4044, 2013.

[58] A. Price, "New Perspectives on Wave Energy Converter Control," Ph.D. dissertation, Edinburgh, 2009.

[59] J. Hals, J. Falnes, and T. Moan, "A Comparison of Selected Strategies for Adaptive Control of Wave Energy Converters," *Journal of Offshore Mechanics and Arctic Engineering*, vol. 133, no. 3, pp. 031 101–01–031 101–12, 2011.

[60] J. Falnes, "Optimum control of oscillation of wave-energy converters," *International Journal of Offshore and Polar Engineering*, vol. 12, no. 2, pp. 147–155, 2002.

[61] S. Salter, "Power Conversion Systems for Ducks," in *IEE Future Energy Concepts Conference*, feb 1979.

[62] J. Hals, J. Falnes, and T. Moan, "Constrained Optimal Control of a Heaving Buoy Wave-Energy Converter," *Journal of Offshore Mechanics and Arctic Engineering*, vol. 133, no. 1, pp. 011 401–01–011 401–15, 2010.

[63] J. Falnes, "Wave-Energy Absorption by Oscillating Bodies," *Ocean Waves and Oscillating Systems*, pp. 196–224, 2010.

[64] P. Nebel, "Maximising the efficiency of wave-energy plant using complex-conjugate control," *Proceedings of the Institution of Mechanical Engineers, Part I: Journal of Systems and Control Engineering*, vol. 206, no. 4, pp. 225–236, 1992. [Online]. Available: https://doi-org.ezproxy.is.ed.ac.uk/10.1243{\%}2FPIME{_}PROC{_}1992{_}206{_}338{_}02

[65] K. Budal, J. Falnes, L. C. Iversen, P. M. Lillebekken, G. Oltedal, T. Hals, and T. Onshus, "The Norwegian wave-power buoy," pp. 323–344, 1982.

[66] E. A. Amon, T. K. Brekken, and A. A. Schacher, "Maximum power point tracking for ocean wave energy conversion," *IEEE Transactions on Industry Applications*, vol. 48, no. 3, pp. 1079–1086, 2012.

[67] S. R. Nielsen, Q. Zhou, B. Basu, M. T. Sichani, and M. M. Kramer, "Optimal control of an array of non-linear wave energy point converters," *Ocean Engineering*, vol. 88, pp. 242–254, 2014. [Online]. Available: http://dx.doi.org/10.1016/j.oceaneng.2014.06.027

[68] G. Li and M. R. Belmont, "Model predictive control of sea wave energy converters – Part II: The case of an array of devices," *Renewable Energy*, vol. 68, pp. 540–549, 2014. [Online]. Available: http://dx.doi.org/10.1016/j.renene.2014.02.028

[69] P. Stansell, A. Price, A. Hagruller, and M. Ginsberg, "Cost of Energy Optimised by Reinforcement Learning," Tech. Rep., 2017. [Online]. Available: https://library.waveenergyscotland.co.uk/development-programmes/control-systems/stage-1/cs11{_}mxs/control-systems-stage-1-public-report-maxsim-ltd/

[70] Corpower Ocean AB, "The CorPower Wave Energy Converter." [Online]. Available: http://www.corpowerocean.com/corpower-technology/corpower-wave-energy-converter/

[71] W. H. S. Rampen, "The Digital Displacement Hydraulic Piston Pump," Ph.D. dissertation, University of Edinburgh, 1992.

[72] M. Ehsan, W. H. S. Rampen, and S. Salter, "Modeling of Digital-Displacement Pump-Motors and Their Application as Hydraulic Drives for Nonuniform Loads," *J. Dynamic Systems, Measurement, and Control*, vol. 122, no. 1, pp. 210–215, 2000.

[73] D. Dießel, G. Bryans, L. Verdegem, and H. Murrenhoff, "Wavepod a transmission for wave energy converters - Set-up and testing," *International Journal of Fluid Power*, vol. 16, no. 2, pp. 75–82, 2015. [Online]. Available: http://dx.doi.org/10.1080/14399776.2015.1055990

[74] D. Dießel, G. Bryans, L. Verdegem, R. Payne, and H. Murrenhoff, "Component Analysis for Hydrostatic Transmission for Wave Energy Application: Simulation and Validation," in *Proceedings of the ASME/BATH 2015 Symposium on Fluid Power and Motion Control*, Chicago, Illinois, October 2015.

[75] N. J. Baker, M. A. Mueller, L. Ran, P. J. Tavner, and S. McDonald, "Development of a linear test rig for electrical power take off from waves," *Proceedings of the Institute of Marine Engineering, Science and Technology Part A: Journal of Marine Engineering and Technology*, vol. 4177, no. 10, pp. 3–15, 2007.

[76] Artemis Intelligent Power Ltd and Quoceant Ltd, "Quantor hybrid hydraulic PTO – Stage 3 Milestone M02 Report," Wave Energy Scotland, Tech. Rep. February, 2018.

[77] M. Holland and E. Bannon, "WES NW11 – Standardised Sea States and Testing Requirements Section 1 – Methodology for Mandatory Testing in Standardised Sea States," Wave Energy Scotland, Tech. Rep. April, 2016.

[78] P. Brodtkorb, P.A. Johannesson, G. Lindgren, I. Rychlik, J. Rydén, and E. Sjö, "WAFO - a Matlab toolbox for analysis of random waves and loads," in *Proceedings of the 10th International Offshore and Polar Engineering Conference*, Seattle, 2000, pp. 343–350.

[79] A. F. Falcão and J. C. Henriques, "Effect of non-ideal power take-off efficiency on performance of single- and two-body reactively controlled wave energy converters," *Journal of Ocean Engineering and Marine Energy*, vol. 1, no. 3, pp. 273–286, 2015.

[80] Matlab, "2-way Directional Valve." [Online]. Available: https://uk.mathworks.com/help/releases/R2015b/physmod/hydro/ref/2waydirectionalvalve.html?searchHighlight=2waydirectionalvalve

[81] S. K. Thirumalai and S. Chenniappan, "Performance analysis of wind driven generators supplying an isolated load," *Journal of Computational and Theoretical Nanoscience*, vol. 14, no. 12, pp. 6014–6019, 2017.

[82] A. Pourmovahed, S. Baum, F. Fronczak, and N. Beachley, "Experimental evaluation of hydraulic accumulator efficiency with andwithout elastomeric foam," *Journal of Propulsion and Power*, vol. 4, no. 2, pp. 185–192, 1988.

[83] Matlab, "Gas-Charged Accumulator," 2019. [Online]. Available: https://uk.mathworks.com/help/physmod/hydro/ref/gaschargedaccumulator.html

[84] Vascat, "MAC QI Series," 2019. [Online]. Available: https://vascat.es/products/motors-for-industrial-applications/asynchronous-servomotors/mac-qi-series/

[85] Poclain Hydraulics, "MS02-MSE02 Hydraulic Motors," 2017. [Online]. Available: https://www.poclain-hydraulics.com/{_}upload/ressources/media/pdf/A36314W.pdf

[86] AWS Ocean Energy Ltd, "Archimedes Waveswing MK IV – WES Novel Wave Energy Converter – Stage 1 Project Public Report," pp. 1–12, 2017.

[87] Sun Hydraulics, "DKFS Normally closed, balanced poppet, logic element -pilot-to-open," 2019. [Online]. Available: https://www.sunhydraulics.com/model/DKFS

[88] Matlab, "2-Position Valve Actuator," 2019. [Online]. Available: https://uk.mathworks.com/help/physmod/hydro/ref/2positionvalveactuator.html

[89] Sun Hydraulics, "DKJS Normally closed, balanced poppet, logic element - pilot-to-open," 2019. [Online]. Available: https://www.sunhydraulics.com/model/DKJS

[90] A. Pourmovahed, N. H. Beachley, and F. J. Fronczak, "Modeling of a hydraulic energy regeneration system-Part II: Experimental program," *Journal of Dynamic Systems, Measurement and Control, Transactions of the ASME*, vol. 114, no. 1, pp. 160–165, 1992.

[91] Harvard University, "A Summary of Error Propagation," 2007. [Online]. Available: http://ipl.physics.harvard.edu/wp-uploads/2013/03/PS3{_}Error{_}Propagation{_}sp13.pdf

[92] D. LeTran, "The Ideal Gas Law," 2020. [Online]. Available: https://chem.libretexts.org/Bookshelves/Physical{_}and{_}Theoretical{_}Chemistry{_}Textbook{_}Maps/Supplemental{_}Modules{_}{\%}28Physical{_}and{_}Theoretical{_}Chemistry{\%}29/Physical{_}Properties{_}of{_}Matter/States{_}of{_}Matter/Properties{_}of{_}Gases/Gas{_}Laws/The{_}Ideal{_}Gas{_}Law

[93] J. C. Dutton and R. E. Coverdill, "Experiments to study the gaseous discharge and filling of vessels," *International Journal of Engineering Education*, vol. 13, no. 2, pp. 123–134, 1997.

[94] P. Puddu and M. Paderi, "Hydro-pneumatic accumulators for vehicles kinetic energy storage: Influence of gas compressibility and thermal losses on storage capability," *Energy*, vol. 57, pp. 326–335, 2013. [Online]. Available: http://dx.doi.org/10.1016/j.energy.2013.04.072

[95] G. Thorncroft, J. S. Patton, and R. Gordon, "Modeling compressible air flow in a charging or discharging vessel and assessment of polytropic exponent," *ASEE Annual Conference and Exposition, Conference Proceedings*, 2007.